THÈSE

Pour obtenir le diplôme de

DOCTORAT DE L'UNIVERSITÉ GRENOBLE ALPES

École doctorale : CSV- Chimie et Sciences du Vivant
Spécialité : Biologie cellulaire
Unité de recherche : IAB : Institute for Advanced Biosciences (UGA / Inserm U1209 / CNRS UMR 5309)

Exploration de la dynamique de la chromatine des spores de levure

Exploring chromatin dynamics in yeast spores

Présentée par :

Anna Maria ALAZZI

Direction de thèse :

Jérome GOVIN DIRECTEUR DE RECHERCHE, INSERM Auvergne Rhône Alpes	Directeur de thèse
Thierry GAUTIER MAITRE DE CONFERENCES HDR, Université Grenoble Alpes	Co-directeur de thèse

Rapporteurs :

Armelle CORPET
MAITRESSE DE CONFERENCES HDR, Université Lyon 1 - Claude Bernard
Antoine MOLARO
CHARGE DE RECHERCHE HDR, INSERM Délégation Auvergne-Rhône-Alpes

Thèse soutenue publiquement le **26 juin 2026**, devant le jury composé de :

Christel CARLES, PROFESSEURE DES UNIVERSITES, Université Grenoble Alpes	Présidente
Jérôme GOVIN, DIRECTEUR DE RECHERCHE, INSERM Auvergne Rhône Alpes	Directeur de thèse
Armelle CORPET, MAITRESSE DE CONFERENCES HDR, Université Lyon 1 - Claude Bernard	Rapporteure
Antoine MOLARO, CHARGE DE RECHERCHE HDR, INSERM Délégation Auvergne-Rhône-Alpes	Rapporteur
Sandra DUHARCOURT, DIRECTRICE DE RECHERCHE, CNRS Délégation Ile-de-France Villejuif	Examinatrice
Dominique HELMLINGER, DIRECTEUR DE RECHERCHE, CNRS Délégation Occitanie Est	Examinateur

Behind every page of this thesis stand many hands, hearts, and voices, to whom I owe my deepest gratitude…

First and foremost, I would like to express my sincere gratitude to the members of my thesis jury, Dr. Christel CARLES, Dr. Armelle CORPET, Dr. Antoine MOLARO, Dr. Sandra DUHARCOURT, and Dr. Dominique HELMLINGER, for their time, their interest in my research, and for accepting the responsibility of evaluating this work.

I would like to express my sincere gratitude to the members of my CSI, Dr. Saadi Khochbin, Dr. Dominique Helmlinger, and Dr. Gabrielle Tichitnsky, for their continuous scientific guidance, constructive feedback, and unwavering support throughout these three years of research.

I would like to thank the collaborators who contributed to the completion of this work: Mahmmood MOHAMMED ALI, Lisa GERMAIN, Eve MOUTAUX, Guillermo ORSI, Dimitrios SKOUFIAS, Carlo PETOSA, CIQLE Platform in Lyon: Elisabeth ERRAZURIZ-CERDA and Christel CASSIN for their valuable support and expertise.

I feel incredibly fortunate to have carried out this work within the "Translational Epigenetics" team, an exceptional group where every member felt like family. I would like to express my sincere gratitude to all members of the team for their support, collaboration, and the stimulating environment they created throughout my research. Their willingness to share ideas, provide feedback, and offer help, both in and out of the lab, made this experience not only productive but also genuinely enjoyable.

I would like to express my deepest gratitude to my supervisors, Dr. Jérôme GOVIN and Dr. Thierry GAUTIER. I am truly thankful for the opportunity they gave me to embark on this PhD journey and for their continuous support throughout these years. This path was not always easy and, at times, was particularly challenging; however, I am proud that we persevered together and brought this project to completion. Thank you for your guidance and for believing in this work until the very end even when I lost faith. It was a pleasure working by your side and learning from you. I promise to always start my figures from left to right and take a step backwards when things are tough.

I would like to thank Dr. Anouk EMADALI, a true role model who shows that everything is possible. You embody the balance between kindness, dedication, and excellence. Being both a devoted mother and a brilliant researcher and mentor, you are an inspiration to many, and your students are truly fortunate to benefit from your support.

Dr. Camille SAYOU, you have been a constant source of support and encouragement. The impact of your kindness and presence is far greater than you may realize. You are not only a brilliant researcher but also an exceptional mentor. Thank you for your guidance during my first year of PhD, I will always be deeply grateful. I truly admire the person and the scientist you are.

Marie ARLOTTO, thank you for all the help you provided throughout my thesis. Your organization and sense of responsibility made everyday life in the lab smoother and more enjoyable. A special thanks as well for your kind (and patient!) messages whenever I managed to incorrectly fill out the attendance sheet.

Sieme HAMAIDIA, ma petite Sieme, it has been a real pleasure getting to know you. I will always cherish our conversations and our shared sense of humor. To the strong and independent woman who may not love hugs but graciously tolerates mine, you have a heart of gold. One day, you will finally teach me cell culture, and I will become as skilled as you!

Dr. Andrea GARCIA SANDOVAL, notre Péruvienne, thank you for being by my side throughout these three years. Your support, your presence, and your attentive listening meant more than words can express. You were always there when I needed it most.

To Héloïse, Syrine, and Victoria, thank you for all the laughter and the good moments we shared. I wish you all the very best for what lies ahead, everything will work out.

A special thank you to the PhD committee. Being involved in its activities was one of the most rewarding aspects of my time at the institute. I truly enjoyed contributing to the organization of events, working alongside such dedicated colleagues, and helping create opportunities for doctoral students to connect and share experiences. Beyond the meetings and responsibilities, I will especially remember the many fun moments, celebrations, and friendships that made these years so enjoyable. Thank you for making the PhD journey feel like more than just research.

To everyone who crossed my path in this team and left a lasting mark:

Oriane, I am so grateful for you. You were our little protégé, and thankfully Jordan was there to keep things balanced with me!

Speaking of my bench partner, Jordan, thank you for your patience and for that memorable note that ensured I would never again confuse concentration with quantity.

Alexia, it was a pleasure working with you on yeast and introducing you to our little world. I am so proud of you and of what you have achieved.

And Emily… where do I even begin? You were a true light during the most difficult moments, bringing warmth and positivity when it was needed most. Thank you for simply being you and for our Imagine Dragons office dates.

I owe a special thanks to William. As fellow yeast enthusiasts, we share an appreciation for the beauty of our favorite organism, particularly during fermentation. I cherish all the wonderful moments we've shared. Take good care of Albert (and keep Xavier safe from him!). Thank you for being the perfect 'oil to my salad' throughout this journey.

Marie-Léa, thank you for our PSM rituals, singing La Marseillaise and rehearsing for the "entretien d'assimilation", which brought both laughter and strength during intense times. I am incredibly proud of everything you have accomplished, both personally and professionally. Never forget ta machine a optimization sur pattes will always be there for you.

To my close friends,

Dr. Momo HABIBI, *ya mamhoun*, you were always there when I needed you, whether it was teaching me how to mount a coverslip on a slide or reminding me to persevere and stay patient to achieve what I want. Khaye, I will always support you and be there for you. You are a truly great person. Our late-night talks and funny jokes will always stay in my heart. And even though you are in Strasbourg, you never fail to make my day through your funny and thoughtful reels.

Thomas, *le pilote*, thank you for every hug, every joke, and every moment of support. Thank you as well for always taking the time to teach me how to analyze microscopy images, and for constantly reminding me that Zhu et al. had already published my work :p. Thank you for standing by me and pushing me forward. See, I did not forget you! I wish you all the very best as you complete your own journey. I cannot wait to call you Dr. I will always be there for you.

Bastien, *ya mal3oun*, one day you will speak Lebanese like a native… but until then, I will keep traumatizing you with "nehna b lebnennn". You, our structural biology enthusiast, kept telling me my manuscript lacked interesting structural figures… well, now they are all there just for you :p. Every time

you cook your ragout or listen to your ringard music, just know I will be there in the background, judging you and telling you to add ba2dounes everywhere.

Mahmmfood, I am so grateful for the AI geek that you are, for the person who taught himself everything from A to Z to build pipelines and analyze -seq data. I am truly proud of you. One day, we will open a farm somewhere in Switzerland, laughing together with a drink in hand and a cigarette in the other. And I am sure your famous quote will go viral one day: “A man needs a good drink and a cigarette on a cold rainy day.”

Lisa, Eve, Guillaume, Maelle, Marie, thank you for every laugh, every complaint, and every night out. I wish you all the very best. And Eve, please give baby Abel a big kiss for me.

Rakan, Carmen, Ahmad, Samer, Jenny, Quentin, Amani, Rita, Sirar, Lea, Imad my Lebanese gang. Thank you for all the memorable game/shisha nights were we made “lougaroud” our emblem. You truly made Grenoble feel like home.

To my best friends,

Khaldoun, six years ago, we met at Jean Roget, and you thought I was corny, well... it turns out you were the corny one. Six years of nonstop arguments, dramatic calls, but also unforgettable cooking nights and Elissa shows that became some of the highlights of my life. You never fail to remind me that friendship is not defined by how long we have known each other, but by how deeply someone impacts us and becomes part of who we are.Thank you for always being there, in your own unique way, for the chaos, the laughter, and the unwavering presence. I would not trade it for anything.

Nour, my “silent” (though not always so silent) best friend, you have always had my back no matter what I placed on your shoulders. You are a truly beautiful person, affectionate, thoughtful, and full of love. Thank you for your constant support and for never letting me down. We have been through many difficult phases together, and I want you to know that I will always be there for you. Thank you for being my everyday reminder, always putting me back in the right place at the right time. Your support means more to me than words can ever fully express.

Karen, bestie, you were my first home away from home, my refuge, and my safe place. From Lebanon to France, you never left my side, even if you sometimes “cheated” on me with others, sharing Macdo and Burger King meals (though I blame that on distance). Thank you for our singing routines, our dinner dates, and your never-ending support. You are truly a bundle of joy, always finding a way to make me laugh whenever you can. I am deeply grateful for you. Montpellier is lucky to have an incredible person like you.

To my family, one sentence says it all: I would never have come this far without your support. This thesis is for you. I hope I have made you proud. Six years ago, I left home to follow my dreams, carrying with me everything you had given me. You never held me back, you became the wind beneath my wings, always pushing me forward, even when distance stood between us. I still remember, Dad, your words: “You’ll do everything to make me call you Doctor.” At the time, I had not yet signed my doctoral contract, and those words felt like a distant promise written in the future. Today, I dedicate this thesis to you, to Mom, to my brother, and to Micha. You are the quiet architects of who I have become. You never stopped believing, never stopped telling me that the sky was never the limit, only the beginning. For six years, I have lived away from a family made of gold, one that distance has never diminished and time will never erase. Auntie Cizo, Auntie Théa, I am sorry for every birthday I missed, and endlessly grateful for every embrace, every kiss, every return that feels like home. I will never be able to repay what you have given me. I carry you all with me. I love you.

À mon amour, mon fiancé, mon avenir, tu as été à mes côtés à chaque instant, dans les sommets qui m'ont porté comme dans les épreuves. Je me demande souvent ce que j'aurais fait sans toi près de moi. Tu es cette force silencieuse qui me fait avancer, cette présence constante qui transforme le doute en possible. Avec toi, chaque rêve semble à portée de main. Je te dédie également cette thèse. Un jour, mon cœur, nous prendrons notre envol ensemble et nous réaliserons tous nos rêves. Merci d'être ma famille et de m'avoir donné tout ce que j'ai aujourd'hui.

Table of Contents

List of Figures 9
Abbreviations 11
Chapter 1: Introduction 14
I. Chromatin Structure 14
I.1. Nucleosomes 14
I.1.1 Core Histones 16
I.1.2. Linker Histone 19
I.2. Functional organization of the chromatin 20
I.3. Conclusion 21
II. Dynamics of the epigenome 22
II.1. What is the epigenome? 22
II.2. DNA methylation 23
II.2.1. DNA methylation during replication 24
II.3. Histone variants 25
II.3.1. H2A variants family 26
II.3.2. H2B variants family 27
II.3.3. H3 variants family 28
II.3.4. H4 variants family 28
II.3.5. Linker H1 variants family 29
II.4. Post-translational modifications (PTMs) 30
II.4.1. Histone Acetylation 30
II.4.2. Histone Methylation 31
II.4.3. Histone Phosphorylation 31
II.4.4. Histone Ubiquitination 32
II.4.5. Histone SUMOylation 32
II.4.6. Histone Crotonylation, Butyrylation 33
II.5. Epigenetic machinery: writers, erasers, remodelers, and readers 33
II.5.1. Epigenetic writers. 34
II.5.1.1. Histone methyltransferases (HMTs) 34
II.5.1.2. Histone acetyltransferases (HATs) 35
II.5.1.3. Histone kinases: writers of phosphorylation 36
II.5.2. Epigenetic erasers 37
II.5.2.1. Lysine demethylases (KDMs) 37
II.5.2.2. Histone deacetylases (HDACs) 38

II.5.3. Chromatin remodelers 39
II.5.4. Epigenetic readers 40
II.5.5. Conclusion 41
III. Bromodomain (BRD) family 42
III.1. Overview of Bromodomain and extra-terminal proteins (BET) proteins family 43
III.2. Functional role of BET proteins 43
III.2.1. Functions of BRD2 43
III.2.2. Functions of BRD3 44
III.2.3. Functions of BRD4 44
III.2.4. Functions of BRDT 45
III.3. Overview: Bdf1 and Bdf2 in yeast 45
III.3.1. Structural characteristics of Bdf1 and Bdf2 46
III.3.2. Conservation of Bdf1 through fungal evolution 47
III.3.3. Functions of Bdf1 47
III.3.3.1. Bdf1 regulates gene transcription 47
III.3.3.2. Bdf1 mediates chromatin remodeling 48
III.3.3.3. Bdf1 in DNA damage and stress responses 49
III.3.3.4. Bdf1 as a potential antifungal target 49
III.3.3.5. Bdf1 and Bdf2 distinct roles 49
III.3.3.6. Bdf1 essential for gametogenesis 50
IV. Spores and quiescence 50
IV.1. Yeast importance in science 50
IV.2. Yeast cellular life cycle 51
IV.3. Survival: response to stress 52
IV.3.1. Sporulation: a survival pathway conserved through species 53
IV.3.1.1. Sporulation in bacteria 53
IV.3.1.2. Sporulation in plants 54
IV.3.1.3. Sporulation in yeast 55
IV.3.1.3.1. Sporulation repression in vegetative growth 56
IV.3.1.3.2. Sporulation repression in haploid cells 58
IV.3.1.4. Biology of spores 59
IV.3.1.5. Sporulation and autophagy 60
IV.3.1.6. Spore chromatin 61
IV.3.1.7. Spore chromatin in other fungi 62
V. Sporulation exit: Germination 63
V.1. Optimal conditions: what happens? 63

V.1.1. Activation and commitment 64
V.1.2. Spore wall un-coating and swelling 64
V.1.3. Outgrowth and polarity 65
V.1.4. Cell-cycle re-entry and budding 65
V.1.5. Post-germination growth 66
VI.1. Objectives 68
VI. State of the art: Exploring chromatin dynamics in quiescent yeast spores 68
Chapter 2: Materials and Methods 72
Chapter 3: Results 91
I. Chromatin organization and compaction in yeast spores 91
II. Chromatin accessibility and histone acetylation landscapes in spores 98
III. Histone acetylation and chromatin compaction in spores 101
IV. Functional analysis of BET bromodomain biology across species 106
V. Bromodomain-dependent regulation of chromatin binding dynamics 111
VI. Functional consequences of BET bromodomain humanization in yeast 115
VII. Distinct BET bromodomains differentially sustain transcriptional program execution 120
VIII. Functional interplay between Bdf1 and Bdf2 in regulating chromatin acetylation 130
IX. Ethanol exposure reveals a metabolic vulnerability of BET-humanized strains during sporulation 137
X. Summary and concluding remarks of the Results 147
Chapter 4: Discussion 150
II. Nuclear size and chromatin compaction 151
III. H4 hyperacetylation in spores 152
IV. The biology of the bromodomains differs from yeast to human 153
V. Functions of Bdf1 bromodomains in sporulation 154
VI. Bdf1 and chromatin integrity 155
VII. Bromodomain specificity and chromatin boundaries 156
VIII. H4 acetylation genomic pattern 156
IX. Coordination of Bdf1 in DNA damage response (DDR) 157
X. Possible effect of Bdf1 on mating 159
XI. The humanization of bromodomains increase sensibility to ethanol 160
XII. Homodimerization of Bdf1 is essential for sporulation entry 161
Bibliographic References 164
Abstract 228
Résumé 229

List of Figures

Introduction:

Figure 1: Structural evidence of DNA and nucleosome core. 15
Figure 2: Histone gene regulation, synthesis, and replication-coupled assembly during G1/S transition. 17
Figure 3: Structure of the histones. 18
Figure 4: Structure of linker histone. 20
Figure 5: Levels of DNA packaging. 21
Figure 6: DNA Methylation and its impact on gene expression. 24
Figure 7: Summary of core and variant histones and their role in cellular processes. 29
Figure 8: Epigenetic machinery. 34
Figure 9: Classification of human bromodomain family. 42
Figure 10: Conservation through evolution between Bdf1 and Bdf2 and human BET factors. 46
Figure 11: Schematic alignment of TFIID (TAFII250) and TAF145/Bdf1 48
Figure 12: Phylogenetic tree of sequenced Candida and Saccharomyces clade species. 50
Figure 13: Budding yeast life cycle. 52
Figure 14: Sporulation progression of S. cerevisiae overview. 56
Figure 15: Sporulation repression in vegetative growth. 57
Figure 16: Sporulation repression in haploid cells. 58
Figure 17: Spore wall architecture in Saccharomyces cerevisiae. 60
Figure 18: Spore germination. 63

Material and Methods:

Figure 19: CRISPR Cas9 technique. 75

Results:

Figure 20: Quantitative assessment of nuclear compaction in yeast spores. 94
Figure 21: Comparative spatial organization and compaction of the yeast genome. 97
Figure 22: Assessment of chromatin accessibility in spores (n=1). 100
Figure 23: Distribution of H4ac in yeast spores. 102
Figure 24: Genome-wide Profiling of Histone H4 Acetylation via CUT&Tag-seq. 105
Figure 25: Structural conservation and chimerization of BET bromodomains. 108
Figure 26: Comparative structural and electrostatic analysis of yeast and human BET bromodomains. 110
Figure 27: Bromodomain-dependent mobility of BET proteins. 114
Figure 28: Impact of BD humanization on growth, mating, and genome stability. 118
Figure 29: Impact of BD humanization on sporulation and spores. 120
Figure 30: Impact of Bdf1 BD humanization on the kinetics of meiotic divisions. 121
Figure 31: Global transcriptional landscape of meiotic progression. 123
Figure 32: Transcript levels of canonical genes defining early, middle, and late developmental stages. 125
Figure 33: Dynamics of the WT meiotic program. 126
Figure 34: Comparative transcriptomic analysis of BRD4- and BRDT-humanized strains during sporulation. 128
Figure 35: Comparative Gene Ontology (GO) enrichment. 129

Figure 36: BDF2 deletion as a strategy to unmask Bdf1 bromodomain function and enable BET inhibitor sensitivity. 131
Figure 37: Bdf2-loss induces H4ac spatial redistribution. 133
Figure 38: Genome-wide H4ac profiling via CUT&Tag in vegetative cells and spores. 136
Figure 39: Ethanol hypersensitivity reveals a hidden functional vulnerability in BET-humanized strains. 138
Figure 40: Impact of ethanol on the temporal dynamics of the sporulation transcriptome. 140
Figure 41: Quantitative assessment of meiotic progression and the ethanol-induced transcriptional delay. 142
Figure 42: Transcriptional deregulation of the acetate pathway by ethanol reveals a metabolic-epigenetic vulnerability in humanized strains. 146

Discussion:

Figure 43: Bdf1 essential for DNA damage response. 159

Abbreviations

A: Adenine

Ac: Acetylation

aDMA: Asymmetric dimethyl arginine

ASF1: Anti-silencing function 1

ATAC-seq: Assay for transposase-accessible chromatin with high-throughput sequencing

ATP: Adenosine triphosphate

BET: Bromodomain and extra-terminal proteins

Bp: Base pairs

BRD: Bromodomain

Bu: Butyrylation

C: Cytosine

cAMP: Cyclic AMP-independent

CD: Chromodomain

CDKs: Cyclin-dependent kinases

CDs: Chromatin domains

CpG: Cytosinephosphateguanine

CHD: Chromodomain helicase DNA-binding

CK2: Casein kinase II

CPT: Camptothecin

Cr: Crotonylation

CUT&Tag-seq: Cleavage under targets and tagmentation with high-throughput sequencing

D: Aspartate

DDR: DNA Damage Response

DEGs: Differentially expressed genes

DNMTs: DNA methyltransferases

DSBs: DNA double-strand breaks

FAD: Flavin adenine dinucleotide - dependent Amine Oxidases family

G: Guanine

G: Glycine

G1 phase: Gap 1

G2 phase: Gap 2

GNAT: GCN5-related N -acetyltransferases group

GO: Gene ontology

HDACs: Histone deacetylases

HMTs: Histone methyltransferases

HP1: Heterochromatin Protein 1

HU: Hydroxyurea

IAB: Institute for advanced biosciences

IBS: Institut de biologie structurale

IGV: Integrative genomics viewer

ISWI: Imitation switch family

JmjC Family: Jumonji C-domain-containing Oxygenases

K: Lysine

KMTs: Lysine methyltransferases

M phase: Mitosis

MBD: Methyl-CpG Binding Domain

MBT: Malignant Brain Tumor

Me: Methylation

MMA: Monomethylarginine

MMS: Methyl Methanesulfonate

MNase: Micrococcal Nuclease

mRNPs: Messenger ribonucleoprotein particles

MSE: Middle Sporulation Elements

NAP1: Nucleosome assembly protein

NASP: Nuclear autoantigenic sperm protein

NFR: Nucleosome-free regions

Nm: Nanometer

NMC: NUT midline carcinoma

NPAT: Nuclear Protein Ataxia-Telangiectasia Locus

NuRD: Nucleosome Remodeling and Deacetylase

P: Phosphorylation

PCA: Principal component analysis

PcG: Polycomb group

PDD: Phosphorylation-dependent dimerization domain

PHD: Plant homeodomain

PIC: Preinitiation complex

PKA: Protein kinase A

PRMTs: Protein arginine methyltransferases

PSM: Prospore Membrane

PTMs: Post-translational modifications

R: Arginine

S phase: Synthesis

S: Serine

SAM: S-adenosyl methionine

sDMA: Symmetric dimethyl arginine

SLBP: Stem-loop binding protein

SPB: Spindle Pore Bodies

SRA: SET and RING Associated proteins

SUMO: Small ubiquitin-like modifier

T: Threonine

T: Thymine

TFIID: Transcription factor II D

TSA: Trichostatin A

TSS: Transcription start sites

TTD: Tandem tudor domain

Ub: Ubiquitination

UCS3: Upstream Control Region 3

UCS4: Upstream Control Region 4

UHRF1: Ubiquitin-like with PHD and RING finger domains 1

W: Tryptophan

WT: Wild-type

Y: Tyrosine

Chapter 1: Introduction

Chapter 1: Introduction

I. Chromatin Structure

I.1. Nucleosomes

Known to be the blueprint of life, deoxyribonucleic acid (DNA) is found in each cell of every living organism. It carries the genetic information and instructions that determine the development and functioning of the organism. This hereditary material was first discovered in 1869 by the 25-year-old Swiss biochemist Friedrich Miescher by isolating a phosphorus-rich substance that he called "nuclein" from pus cells and salmon sperm. With time, "nuclein" was then recognized as DNA and started intriguing scientists. Although it was discovered in the 18th century, its structure was only visualized 83 years later in 1952 by Rosalind Franklin and her PhD student, Raymond Gosling. Using high-resolution X-ray diffraction, they successfully captured the famous Photograph 51 after numerous attempts and failed experiments, revealing for the first time the helical and repeating structure of DNA (Figure 1A) (R. E. Franklin & Gosling, 1953). Photograph 51 served as evidence needed for James Watson and Francis Crick to model the exact structural representation and propose the double helix model in 1953 (Figure 1B) (R. E. Franklin & Gosling, 1953; Lamm et al., 2020). The double helix consists of two antiparallel polynucleotide strands of opposite directions. Each nucleotide is formed of three components: a phosphate group, a deoxyribose sugar, and one of four nitrogenous bases: adenine (A), thymine (T), cytosine (C), and guanine (G) that pair in a specific way. Adenine pairs with thymine, and cytosine pairs with guanine through hydrogen bonding, which maintains the stability of the molecule during replication. This well-organized, double-stranded, and twisted ladder is compacted by wrapping 146-147 base pairs (bp) around nucleosomes in a left-handed helix to form a dense chromatin structure packaged in the nucleus. The nucleosome plays a central role in DNA packaging, gene regulation, and genome stability. Although it is the building block for higher chromatin orders, it also acts as a barrier for several DNA-templated processes such as DNA replication, transcription, and repair, emphasizing the importance of constantly assembling and dis-assembling it. Each nucleosome is formed of an octamer of core histone proteins: two molecules of each H2A, H2B, H3, and H4 histones (Figure 1C) (Caron et al., 2005; Ozonov & Nimwegen, 2013; Feng et al., 2021). Histones account for approximately half the weight of chromatin, highlighting their importance for organizing our genetic material (Felsenfeld et al., 1976).

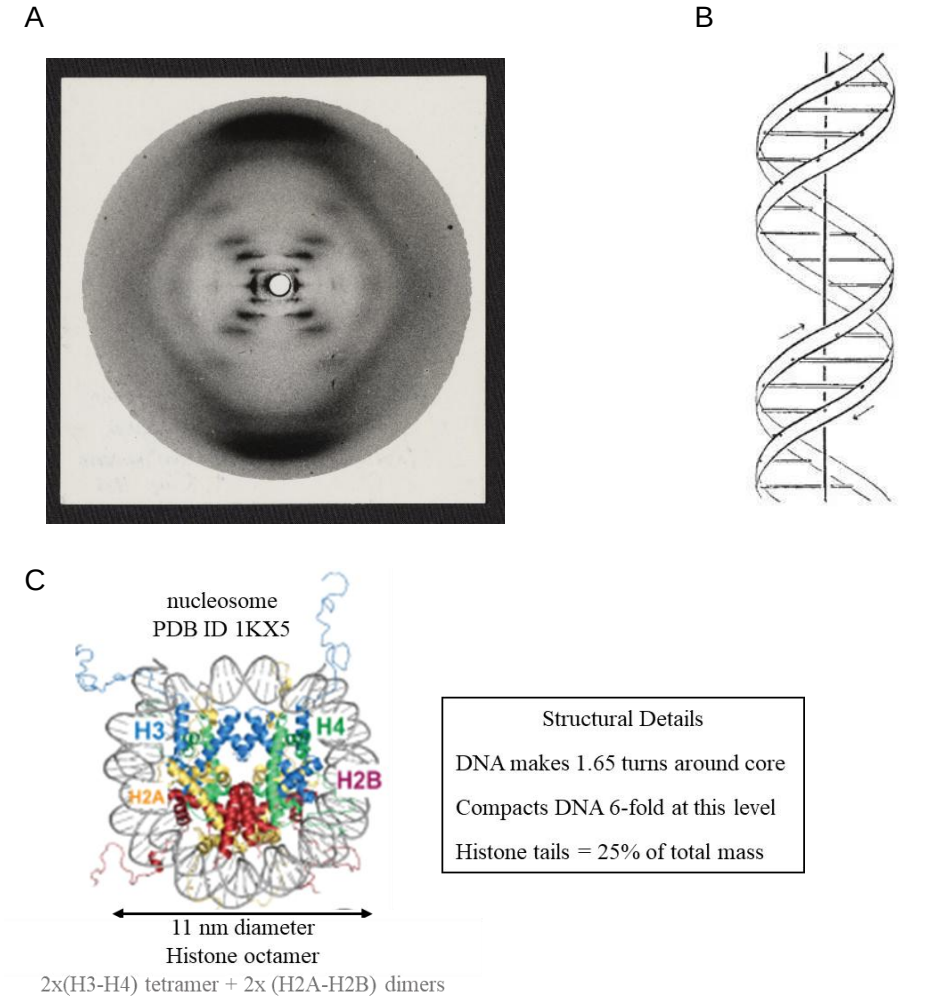

Figure 1: **Structural evidence of DNA and nucleosome core.** (A) Photograph 51: First photographic print of a DNA high-resolution X-ray pattern Structure B. The "X" is the signature of double-helix viewed from the side. The layer line (the arranged dots across the "X") spacing was measured 3.4nm (34Å) revealing the distance of 10bp for one full helical turn and the strong meridional arcs show 3.4Å spacing between consecutive nucleotides (Figure from R. E. Franklin & Gosling, 1953). (B) Sketched model of the DNA double helix by James Watson and Francis Crick (Figure from R. E. Franklin & Gosling, 1953). (C) Cartoon representation of the structure of the nucleosome with the positioning of the core histones (PDB ID 1KX5). Histone polypeptides are demonstrated in yellow for H2A, red for H2B, blue for H3, green for H4, and grey for DNA. The nucleosome has a diameter of 11nm and can compact the DNA 6x. The histone tails form 25% of the total mass of the nucleosome and the 147 bp of DNA makes 1.65 turns around the core (Figure adapted from Bernardes NE, et al.2020).

I.1.1 Core Histones

As mentioned earlier, the core histone proteins (H2A, H2B, H3, and H4) form the nucleosome core particle, and their N-terminal tails serve as accessible sites for covalent modifications influencing chromatin compaction and transcription activity (Biterge & Schneider, 2014; H. Huang et al., 2015; Y. Feng et al., 2021).

Histone genes are extremely regulated and sharply expressed at the G1/S transition phase of the cell cycle (Stein et al., 1996; Kurat et al., 2014). Upon the activation of the G1 phase and the release of the transcription factor E2F, the expression of the nuclear protein ataxia-telangiectasia locus (NPAT) increases leading to the recruitment of RNA Pol II to the genes cluster and transcription activation (Gao et al., 2003; DeRan et al., 2008). Stem-loop mRNAs lacking polyA tails are subsequently produced and undergo 3' processing by the stem-loop binding protein (SLBP), forming messenger ribonucleoprotein particles (mRNPs). These particles, responsible for the protection of non-polyadenylated mRNAs, are exported from the nucleus to the cytoplasm and translated by polysomes into histone monomers. The monomers are then shuttled by importins to the nucleus and undergo dimerization and tetramerization with the help of chaperones while maintaining epigenetic fidelity (ERKMANN et al., 2005; J. Zhang et al., 2014).

The newly synthesized proteins are first folded by the chaperone nuclear autoantigenic sperm protein (NASP) ensuring their stability (Cook et al., 2011) and are then assisted and aided along with the parental histones, by histone chaperones such as the heat shock proteins HSC70, HSP90 for their folding and association into dimers: H2A-H2B and H3-H4 (Hammond et al., 2017; Pardal et al., 2019). H3-H4 dimers are then handed off to anti-silencing function 1 (ASF1) chaperone (Horard et al., 2018; Mendiratta et al., 2024), and H2A-H2B dimers to nucleosome assembly protein (NAP1) chaperone which forms a soluble complex preventing their aggregation (Akishina et al., 2020).

During replication, the newly synthesized histones are integrated and deposited on the newly replicated nuclear DNA after recycling the parental histones ahead of the fork. The recycled parental nucleosomes are disrupted into structurally stable units, and $(H3\text{-}H4)_2$ tetramers are randomly transferred to daughter strands via chaperones while maintaining epigenetic marks crucial for epigenetic inheritance (Z. Li et al., 2020; Mühlen et al., 2023; Nagae et al., 2024; Bi, 2025). Moreover, available evidence indicates that H3–H4 may initially be handed off as dimers

(Dalal et al., 2007; Tagami et al., 2004; Corpet & Almouzni, 2009). On the other hand, H2A-H2B dimers are recycled separately and symmetrically, allowing their modifications to be preserved and diluted as needed (Flury et al., 2023). This helps re-establish the correct post-replicative chromatin state through the action of chromatin-modifying enzymes before transcription resumes (Figure 2) (Marzluff & Duronio, 2002; J. M. Nicholson et al., 2004; Corpet & Almouzni, 2009; Q. Li et al., 2012; R. J. Burgess & Zhang, 2013; Doenecke, 2014; Pardal et al., 2019).

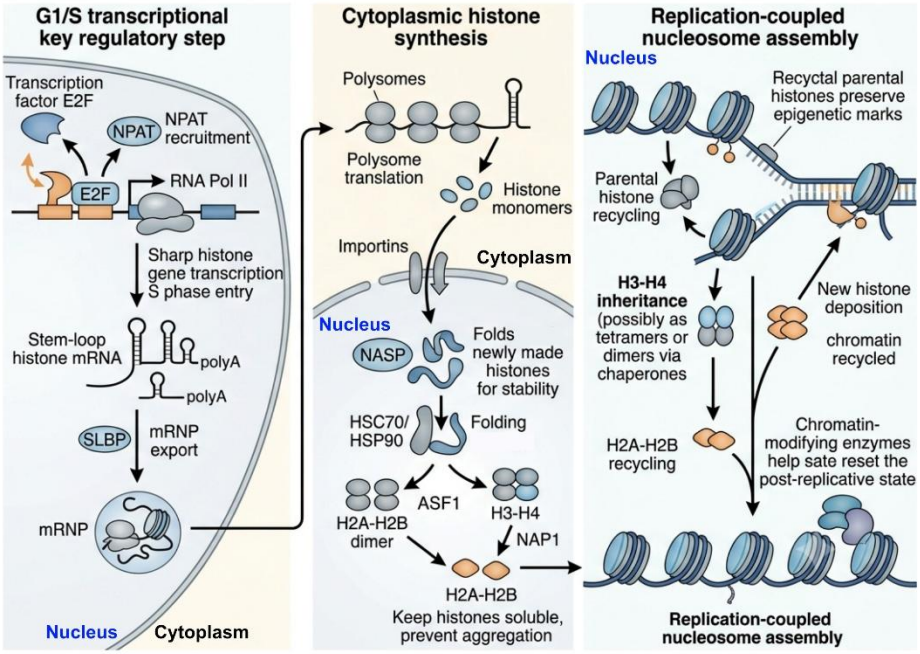

Figure 2: **Histone gene regulation, synthesis, and replication-coupled assembly during G1/S transition.** Schematic representation of the histone biosynthesis and assembly in the cell. As detailed in the above paragraph, the activation of E2F factor by the growth factors, results in the transcription and accumulation of NPAT that recruits RNA Pol II to the clustered histone genes. This leads to the formation of stem-loop mRNP bound and cleaved by SLBP, exported to the cytoplasm where they are translated into histone monomers by polysomes and imported back to the nucleus where they are dimerized and tetramerized by the help of chaperones such as NAP1 and ASF1. Finally, the tetramers are deposited on the newly synthesized nuclear DNA with the recycling of parental histones (The figure was generated with the help of Gemini AI).

As for their structural aspect, each core histone is formed of a structured central domain and an unstructured basic amino-terminal tail that extends outward from the nucleosome (mainly N-terminal except for H2A C-terminal). The central domain of each of the four core histones has a characteristic structure consisting of three α-helices (α1, α2, α3) separated by short loops (Arents & Moudrianakis, 1995). This structured core mediates histone-histone folds, driving the formation of two stable heterodimers, H3-H4 and H2A-H2B dimers and histone-DNA contacts (further elaborated throughout the paragraph). As for the amino-terminal tails, their size varies depending on the core histones and carries mostly post-translational modifications, allowing the regulation of the chromatin structure (Figure 3).

Moreover, they are enriched in lysine and arginine residues, favoring their contact with DNA and neighboring nucleosomes (Y. Peng et al., 2021; Ohtomo et al., 2021).

As mentioned earlier, the core histones mediate a histone-DNA interaction determined by the electrostatic charges between the positively charged histone surface, generated by the enrichment of lysine and arginine residues, and the negatively charged phosphodiester DNA backbone. This leads to the bending of the phosphate backbone around the nucleosome core in a specific orientation, creating contact on periodic positions (~10 bp) where the minor groove faces the octamer. This conformation forms the regular pattern of DNA bend of 3 to 6 hydrogen bonds matching one helical turn of DNA, and creates the fundamental repeating unit of the chromatin (Burton et al., 1978; Kerrigan & Kadonaga, 1992).

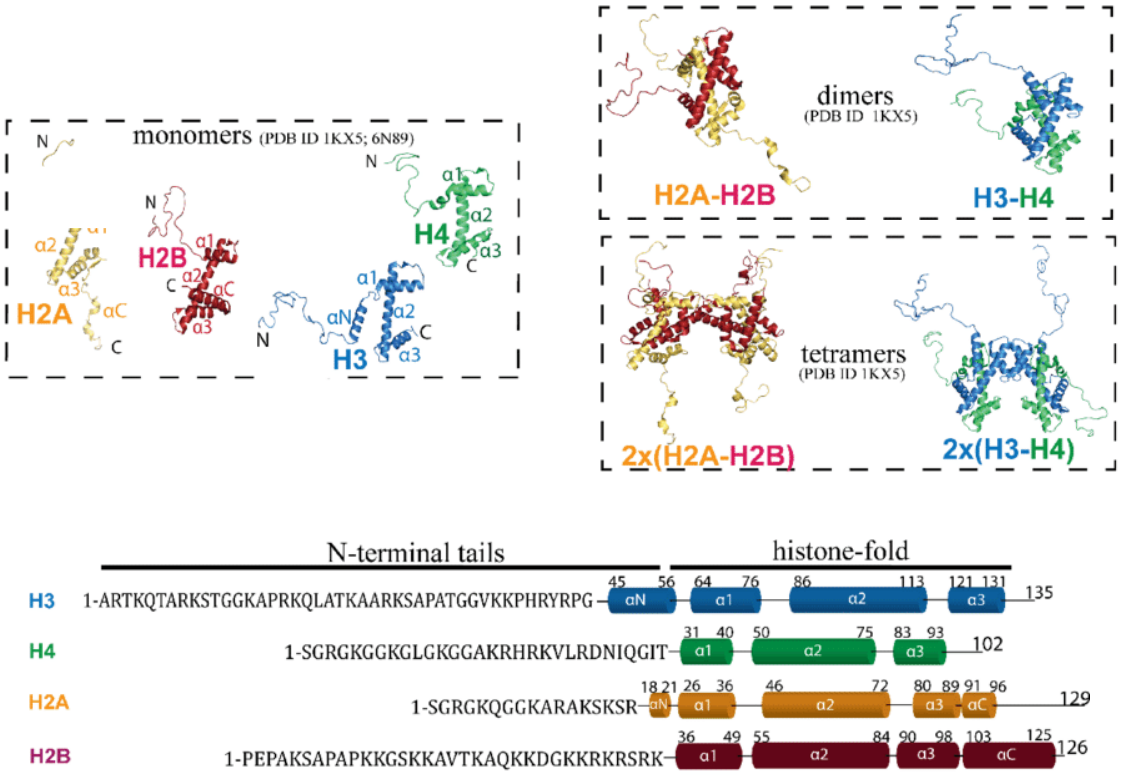

Figure 3: **Structure of the histones.** Cartoon representation of the structures of core histones (PDB ID 1KX5 and 6N89). Individual histone polypeptides are represented in yellow for H2A, red for H2B, blue for H3, and green for H4. The left panel shows single polypeptide chains of the histone proteins, top right panel shows the H3–H4 and H2A–H2B and the bottom right panel shows the H3–H4 and H2A–H2B tetramers as found in the nucleosome. Under the panels the domain organization of canonical human core histones H3, H4, H2A, and H2B. Sequences of the N-terminal tails and secondary structures of the histone-fold domains are shown (Figure adapted from Bernardes & Chook, 2020).

I.1.2. Linker Histone

After histone dimerization and nucleosomes formation and positioning on the DNA backbone, many are then linked together by a small fragment of 20 to 50 bp linker DNA. This fragment is stabilized by a linker histone, H1, helping to compact the chromatin into higher-order structures. This fifth histone is very rich in lysine residues and stabilizes nearly two superhelical turns of DNA at the nucleosomal entry and exit sites by binding at the surface of the nucleosome core. Thus, engaging with approximately 20 additional bp of linker DNA beyond the canonical 147 bp associated with the nucleosome core particle. This configuration results in a chromatosome, a structure that consists of 167 nucleotide pairs of DNA, the core histone octamer, and one molecule of H1 (Figure 4) (Simpson, 1978).

In humans, the H1 histone has a three-domain structure: a short N-terminal domain of ~45 majorly basic amino acids rendering it quite flexible, a central globular domain of ~75 highly conserved amino acids folded into a globular conformation known as “wing-helices”, and the intrinsically disordered C-terminal domain of ~100 amino acids enriched in lysine, serine, and proline unstructured in aqueous solution and organized into a specific polyelectrolyte-like conformation when bound to DNA (Roque et al., 2005; Bernardes & Chook, 2020; Hao et al., 2021; Yuan et al., 2026). The functions of the two domains are essential for chromatin compaction, as the globular domain is responsible for specific nucleosome binding with high specificity, while the C-terminal binding domain mediates chromatin compaction by neutralizing the linker DNA charge, reducing the repulsion between nucleosomes, and initiating inter-nucleosomal contacts.

In other words, H1 is involved in multiple interconnected roles in chromatin organization, gene regulation, along with maintaining genome stability (Kilichowska & Kotliński, 2022), and participates in non-nuclear functions, such as immune signaling and cellular organization (Hergeth & Schneider, 2015; Kilichowska & Kotliński, 2022; S. He et al., 2024; Żukowska & Perła-Kaján, 2024).

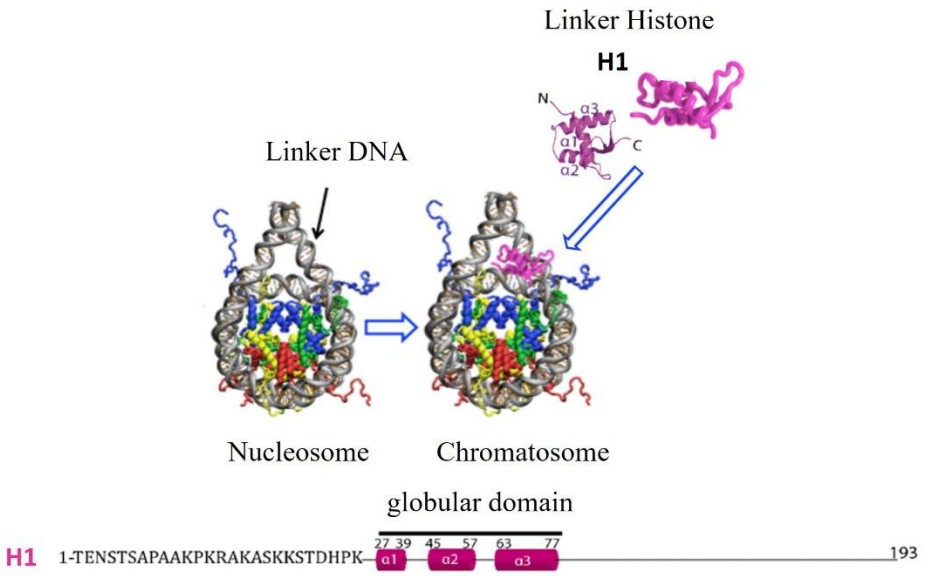

Figure 4: **Structure of linker histone.** Representation of the structures of nucleosome and chromatosome with the representation of the linker DNA and the linker histone H1 in pink. Sequence of the N-terminal tail and secondary structure of the histone-fold domains of the linker histone H1 is shown below. (Figure adapted from Bernardes & Chook, 2020 and histone DB 2.0)

On the other hand, *Saccharomyces cerevisiae* lacks a canonical linker histone and instead has an H1-like nuclear protein, Hho1p, that serves as the distant homolog with yeast-specific adaptations. Knowing that in yeast the linker DNA is shorter than in mammals (20-25 bp instead of 40-60 bp in mammals), Hho1p adapted its structure with the unique features of having an N- and a C-terminal globular domains (GI/GII). Both globular domains adapted the canonical winged helix folds: GI is more stable, while GII remains more dynamic (Landsman, 1996; Ushinsky et al., 1997; Patterton et al., 1998; Ono et al., 2003; Georgieva et al., 2012; Panday & Grove, 2016).

I.2. Functional organization of the chromatin

Packaging genomic DNA with core and linker histones safeguards the genome against various DNA-damaging agents, thereby maintaining genomic integrity. The fundamental repeating unit of chromatin is the nucleosome, which folds into a hierarchical nucleofilament structure that regulates both genome compaction and functional accessibility (Luger et al., 2012). Chromatin organization spans multiple levels of structural compaction, beginning with the primary "beads-on-a-string" fiber. In vitro, this fiber can fold into higher-order architectures, such as regular solenoids, which further condense into irregular chromatin loops. These loops coalesce

into chains of interlinked chromatin domains (CDs), ultimately forming the fully condensed chromosome (Figure 5) (Miron et al., 2020; Vinayak et al., 2026).

Depending on the packaging level of compaction, the chromatin is said to be in a transcription activating and relaxed form, also known as the euchromatin, or in a repressive compacted form, heterochromatin (Luger et al., 2012). The 3D spatial organization of the chromatin is actively dynamic rendering the different chromatin states reversible and providing adapted accessibility in distinct regions. This allows the regulation of several key processes such as transcription activation, DNA repair, and replication processes (Moindrot, 2012).

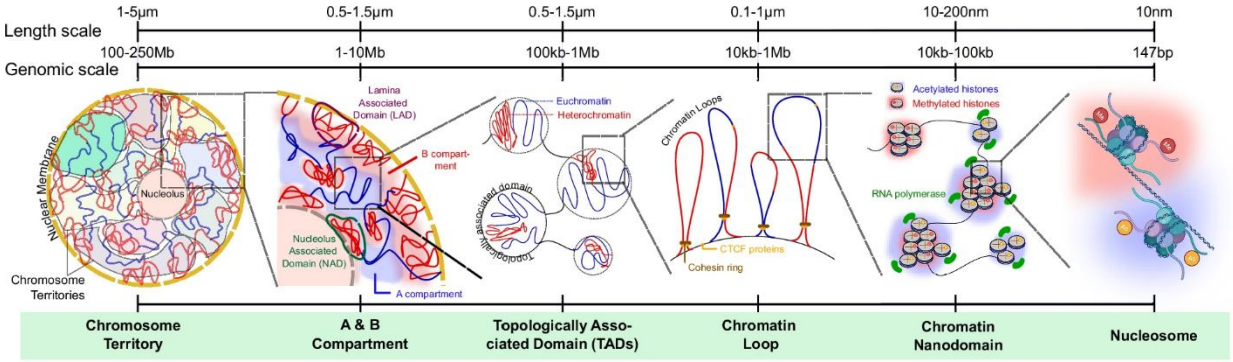

Figure 5: **Levels of DNA packaging.** Schematic depicting the main architectural levels (chromosome territories, compartments, TADs, loops, nanodomains, and nucleosomes. Chromatin nanodomains (~50–200 nm) represent a recently identified layer of organization, enriched in specific histone modifications and transcriptional regulators, yet invisible to diffraction-limited microscopy. This illustration provides an approximate overview of the length scales associated with chromatin organization across a structural continuum. The drawing is not to scale with respect to nucleosome number and does not imply a strict hierarchy. The sizes of TADs (typically a few hundred nanometers to several micrometers) and loops (from tens to hundreds of nanometers), as well as those of nanoscopic chromatin domains, cover broad ranges and are shown here as conceptual models. The depiction of “nanodomains” as clusters of a few nucleosomes is purely schematic and does not reflect their actual nucleosome content, which can range from tens to hundreds depending on genomic span and compaction state (Figure from Vinayak et al., 2026).

I.3. Conclusion

In summary, the genetic material is highly ordered and organized in the nucleus. The DNA is wrapped around the nucleosome, a key component for genome organization and regulation, composed of an octamer of canonical histone proteins (H2A, H2B, H3, H4). With the help of the linker histones, the DNA fibers are further compacted to higher order structures creating the chromosome. This functional organization of the chromatin not only helps organize the genome and store the DNA from damaging agents and degradation, but also remains dynamic and reversible when needed. Dynamicity balances the need for DNA compaction with the

requirement for a controlled access to the genetic information while laying the foundation for epigenetic mechanisms that control gene expression without changing the DNA code itself.

II. Dynamics of the epigenome

II.1. What is the epigenome?

Epigenome derives from the Greek prefix *epi-*, meaning "above" or "on top of" the genome. It involves a repertoire of mitotically and/or meiotically heritable chemical modifications on the DNA and histone proteins as well as specific associated proteins. Altogether, they act as a dynamic "instruction manual" altering the gene expression without modifying the genetic sequence. This regulatory framework is transiently modulated by environmental factors, metabolic states, and cellular context in a reversible manner, highlighting its adaptability and plasticity along with its importance in determining the chromatin structure. Upon modulating the chromatin organization, an imminent alteration of function is recorded with a direct influence on gene expression throughout the cellular life cycle (C. -t. Wu & Morris, 2001; Marabita et al., 2015; Singla et al., 2023).

Emphasizing its dynamic nature, the concept of epigenetics has evolved over several decades through multiple conceptual refinements to reach its modern concept, mirroring the continuous advancement of our understanding of the field. The term was first introduced by Conrad Waddington in the 1950s to describe poorly understood developmental processes, addressing the question of how a single fertilized egg develops into a complex multicellular organism with diverse phenotypes. By the late 20th century, the current definition began to take shape with the recognition of a heritable regulatory layer beyond the DNA sequence. Subsequently, the term "epigenome" became widely used following the discovery and genome-wide mapping of chemical marks, referring to the genome-wide pattern of epigenetic modifications and often described as a "second genetic code"(Felsenfeld et al., 1976; Berger et al., 2009; Felsenfeld, 2014).

Thus, it was clear that DNA methylation, histone chaperones, histone variants, post-translational modifications, and epigenetic tools (writers, readers, and erasers) form the epigenome implicated in the chromatin (Maunakea et al., 2010; Khochbin, 2011; Ganesan, 2018). The next sections present a comprehensive and detailed characterization of these key epigenetic components.

II.2. DNA methylation

DNA methylation is a well-characterized epigenetic modification that plays a crucial role in maintaining cellular identity and regulating gene expression. It involves the addition of a methyl group to the 5′ position of cytosine residues, predominantly at CpG dinucleotides in mammals, but also at non-CpG contexts such as CHG and CHH in plants and embryonic stem cells. This modification is associated with transcriptional silencing, stable gene repression, and the maintenance of chromosomal integrity. (Marabita et al., 2015; Stepanić et al., 2014). DNA methylation is a major epigenetic mechanism in animals and plants, but appears to play a minor role in the budding yeast Saccharomyces cerevisiae, where it occurs at extremely low levels and is therefore considered insignificant. The organism lacks the enzymatic machinery required for DNA methylation as well as methylation-specific reader domains (Duan et al., 2010; Y. Tang et al., 2012; Capuano et al., 2014; Morselli et al., 2015; Buitrago et al., 2021). The epigenetic mark is catalyzed and mediated via DNA methyltransferases (DNMTs) that transfer the methyl group from S-adenosyl methionine (SAM) to the cytosine, thus transforming it into 5-methyl-cytosine (5mC) (Robertson, 2005; Omari et al., 2025). The DNMT family is composed of four proteins: DNMT1, DNMT3A, DNMT3B, and the inactive DNMT3L. DNMT1 primarily maintains existing methylation patterns (Sundrani et al., 2016; Yan et al., 2023), while DNMT3A and DNMT3B also known as *de novo* methyltransferases are responsible for establishing new methylation marks during development and cellular differentiation (Tóth et al., 2025). After deposition, methylation is interpreted and read by proteins known as DNA methylation readers that are divided in several major families such as: methyl-CpG Binding Domain (MBD) proteins, identified in mammals and bind strongly to methylated CpGs (Mahmood & Rabbani, 2019; Contreras et al., 2025), and SET and RING Associated (SRA) domain proteins, identified in plants and bind methylated CG and non-CG sites (Figure 6) (Grimanelli & Ingouff, 2020; Cahn et al., 2023). Depending on the environmental factors, the DNA is said to be either hypomethylated, leading to less methyl groups allowing transcription, or hypermethylated, repressing transcription and found in heterochromatin regions (Biermann & Steger, 2007; Rajender et al., 2011; Rizzo et al., 2024).

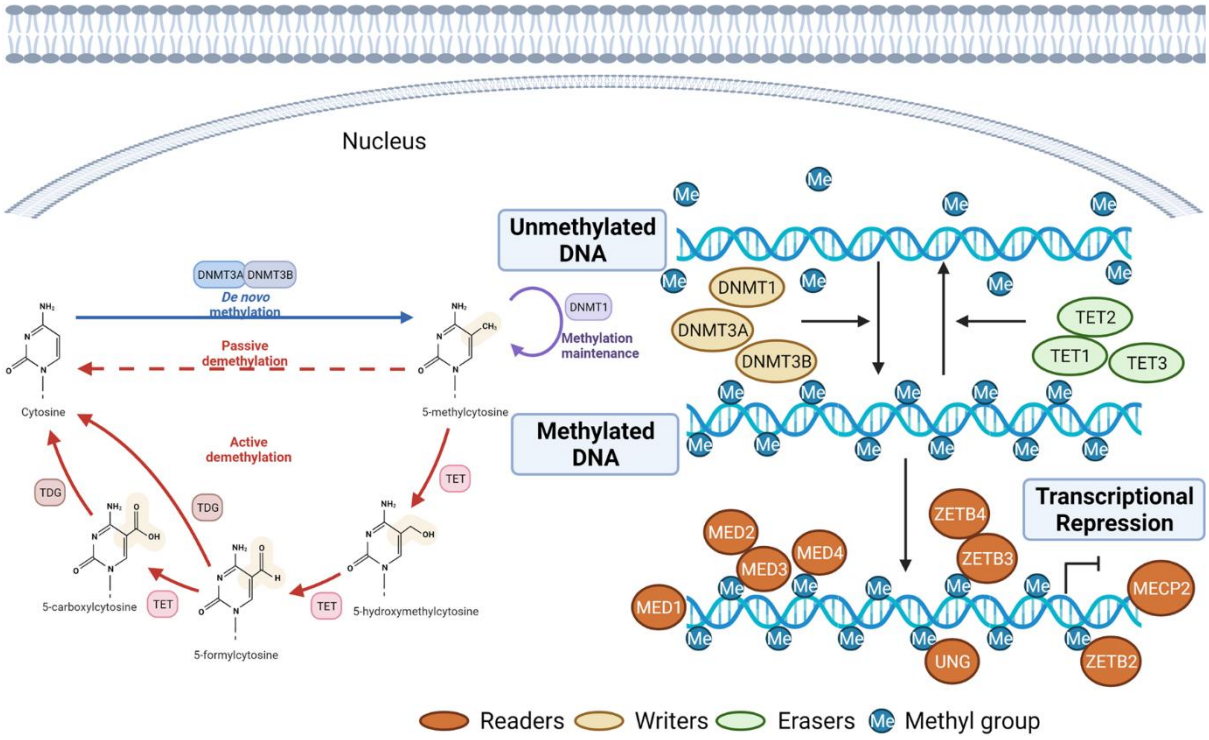

Figure 6: **DNA Methylation and its impact on gene expression.** This model represents the DNA methylation occurring majorly in the islands of CpG gene promoter region. This reversible process is mediated by different sets of proteins either responsible for the deposition of this mark on cytosine residues, known as writers (represented in yellow), or responsible for the removal of these deposited methyl groups, known as erasers (represented in green). The last category of proteins implicated in this process, known as readers (represented in orange) is responsible for the reading of these added marks and affect gene expression (Figure from Shi et al., 2022).

II.2.1. DNA methylation during replication

During replication, DNA methylation serves as an important process to ensure the propagation of epigenetic patterns and epigenetic memory from a mother cell to its daughter cell. A symmetrical restoration of CpG methylation on the daughter strands involves the functions of ubiquitin-like with PHD and RING finger domains 1 (UHRF1), a multi-domain protein, and DNMT1 through a replication-coupled mechanism. Prior to replication, UHRF1 accumulates at early replication foci and primes the heterochromatin sites with its tandem tudor (TTD) domain and mono-ubiquitinates with its RING domain H3K18/K23 or PAF15, a small PCNA-interacting protein, thus creating DNMT1-binding sites post MCM helicase unwinding, replication forks incorporate unmethylated dCTP into the daughter strands forming hemi-methylated CpGs (methylated on the parental strand). By generating hemi-methylated DNA, the cell risks losing the mark due to the dilution by half with every cellular division. Fortunately, a dedicated correction machinery repairs this state immediately after the replication fork. UHRF1 binds to these hemi-methylated CpGs via its SRA domain (identified as the thumb) CpG and flips 5mC

out of the helix into a hydrophobic pocket, and its TTD domain reinforces its binding to H3K9me2/3 on the recycled parental histones. This locks UHFR1 in an open conformation allowing it to recruit DNMT1 and allosterically activate its catalytic loop enabling it to copy the methylation pattern from the parental strand to the daughter strand (Moore et al., 2013; Fang et al., 2016; Xue et al., 2019; Yamaguchi et al., 2024).

Unlike mammals and plants, *S. cerevisiae* has no detectable 5mC in its genomic DNA (<0.03%) therefore, as the DNA remains a blank slate throughout the replication process, the yeast maintains its epigenetic memory through histone methylation. As the replication fork passes, the old histones carrying specific methylation marks, such as H3K4me3 and H3K79me3, are recycled and then redistributed to the daughter strands. But how does the budding yeast fix replication errors? Instead of methylating adenine for replication fidelity and mismatch repair as E. coli, the yeast uses structural signals and nick-directed mechanisms. During replication, the newly synthesized DNA strand is built differently from the leading strand. The first is built by pieces called Okazaki fragments leaving “nicks”, unsealed gaps in the backbone, while the second consists of temporary nicks created by the removal of mis-incorporated ribonucleotides. Moreover, the sliding clamp protein (PCNA) is loaded onto the DNA in a specific orientation serving as a directional and physical signal identifying the newly synthesized strand. Along with the presence of nicks, they guide the mismatch repair machinery Mlh1-Pms1 complex recruited by Msh2-Msh6 to identify and correct replication errors on the nascent strand. The machinery is activated upon the contact with the “front” face of the PCNA ring ensuring the specific cutting and erasing of the error-prone strand leaving the original intact (Xiao et al., 1996; Cejka & Jiricny, 2008; Rizzardi et al., 2012; Tang et al., 2012; Capuano et al., 2014; O’Kane & Hyland, 2019).

II.3. Histone variants

Beyond DNA methylation, which regulates gene expression by altering the genome itself, the incorporation of histone variants into nucleosomes represents a distinct epigenetic mechanism that reshapes chromatin architecture by replacing canonical histones. This replacement can affect chromatin compaction, nucleosome positioning and stability, and DNA accessibility to the transcriptional machinery (Borg et al., 2021; Catoni et al., 2025; Hegazy et al., 2025). Histone variants are structural variants and paralogs of the core histones (H2A, H2B, H3, and H4), encoded by distinct genes and distinguished by sequence differences in regions such as

the N- or C-terminal tails and docking domains. Unlike canonical histones, which are typically produced in a replication-dependent manner to support bulk genome packaging, many variants are expressed throughout the cell cycle and can be incorporated independently of DNA replication. These non-canonical histones have evolved specialized features that enable functions beyond those of canonical histones, including roles in DNA repair, transcription initiation, and centromere specification (Skene & Henikoff, 2013).

Histone variant deposition is mediated by dedicated chaperones, and this replication-independent incorporation influences gene expression, DNA repair, and chromosome stability throughout the cell cycle (Figure 7) (Ragusa & Vagnarelli, 2023; Kirkiz et al., 2023; Lai et al., 2024; Lai & Chan, 2024). Several chaperones are known to promote variant-specific nucleosome assembly or histone exchange, including HIRA and DAXX, as well as Chz1 and ANP32E (Mattiroli et al., 2015; Hammond et al., 2017; Pardal et al., 2019; Kirkiz et al., 2023). Due to their diversity, histone variants are classified into distinct families according to their structural and functional properties. By contrast, canonical histone isoforms are the major histone forms responsible for bulk chromatin packaging. They are encoded by multiple gene copies to ensure high-level production during DNA replication, and even subtle sequence differences among isoforms can influence post-translational modification patterns (Ausió, 2006; P. Chen et al., 2013; Skene & Henikoff, 2013; Talbert & Henikoff, 2021; Joseph & Young, 2023).

II.3.1. H2A variants family

The canonical histone H2A has two isoforms: H2A.1 and H2A.2 that are known to be homomorphous and differs from the canonical H2A by only few amino acids (West & Bonner, 1980). In *S. cerevisiae* for example, HTA1 and HTA2 are two genes that produce isoforms that differ by only two amino acids (Tsui et al., 1997; House et al., 2019). As for H2A variants family, it consists of the largest and most diverse family, with 19 known mammalian variants (Monteiro et al., 2014; Lai & Chan, 2024; X. Yin et al., 2024). There are different heteromorphous variants that form this family: the ultimate epigenetic silencer and the structural “dead bolt” macroH2A (mH2A) (Oberdoerffer & Miller, 2023), the metabolic lock mH2A1, (isoforms mH2A1.1, mH2A1.2) (House et al., 2019), and its sibling the developmental lock mH2A2 (Monteiro et al., 2014). The master of nucleosome mobility H2A.Z (isoforms H2A.Z.1, H2A.Z.2 with three amino acids difference) and the primate-specific splice variant H2A.Z.2.2 considered as the extreme

version of H2A.Z that produces structurally unstable nucleosomes and known as the super-opener (Corujo & Buschbeck, 2018). H2A.X involved in DNA repair (Corujo & Buschbeck, 2018; Oberdoerffer & Miller, 2023), H2A.B (formerly H2A.Bbd) (isoforms H2A.B.1.1, H2A.B.1.2) the high-speed and most radical variant (Molaro et al., 2020), H2A.W mediates heterochromatin condensation in plants (Lei & Berger, 2020). H2A.L (isoforms H2A.L.1, H2A.L.2, H2A.L.3), H2A.P, and H2A.Q are specialized variants found during spermiogenesis and helps with the DNA histone/protamine transition (Govin et al., 2007; Boussouar et al., 2008; Barral et al., 2017; Molaro et al., 2018). H2A.J known as the senescence marker (Talbert & Henikoff, 2021; Oberdoerffer & Miller, 2023), and finally the primate specific H2A.R (isoforms H2A.R.3, H2A.R.2) associated with early embryonic reprogramming.

The variants have additional domains on either the N- or the C- terminal resulting in different and distinct structures from the canonical histone (West & Bonner, 1980; Ausió, 2006). They are mainly involved in chromatin dynamics and stability, transcription regulation, genome organization, and DNA damage response (Ferguson et al., 2009; Barral et al., 2017; Molaro et al., 2018; Hoghoughi et al., 2018; Khadka et al., 2020; Lei & Berger, 2020; Molaro et al., 2020; Lai & Chan, 2024).

II.3.2. H2B variants family

The canonical histone H2B is encoded by a multigene family in humans, including several highly similar genes such as HIST1H2BB, HIST1H2BD, and HIST1H2BJ located on chromosome 6, which encode proteins with nearly identical amino acid sequences (Voss & Korb, 2025). In *S. cerevisiae, by contrast*, H2B is encoded by only two genes, HTB1 and HTB2, each paired with H2A genes and serving as core structural components of nucleosomes (Libuda & Winston, 2006; Jiang et al., 2017). As canonical histones, these isoforms provide the primary framework for chromatin organization and help regulate the deposition and interpretation of key histone modifications.

The H2B variant family is considerably more diverse in metazoans and includes several specialized variants with distinct biological functions. For example, H2B.W is enriched in sub-telomeric regions and has been linked to telomere protection, whereas H2B.K has been associated with telomere maintenance in germ cells. H2B.E has been proposed as a neuronal aging-associated variant, and its accumulation has been linked to neuronal dysfunction and turnover (Raman et al., 2022; Feierman et al., 2024; Louzon et al., 2025; Santoro & Dulac,

2012). The testis-specific H2B.t variant, formerly referred to as H2B.1, is associated with chromatin reorganization during spermatogenesis and contributes to the formation of highly open nucleosomal states (Raman et al., 2022). Additional niche variants such as H2B.L and H2B.N are found in oocytes and early embryos, where they are thought to help maintain permissive chromatin states (Raman et al., 2022). H2B.O, an oocyte-specific variant, is implicated in the rapid reorganization of paternal chromatin after fertilization, facilitating the replacement of protamines and the re-establishment of nucleosomal packaging (McLay & Clarke, 2003; Jullien et al., 2014; Shinagawa et al., 2014; Raman et al., 2022). These H2B variants are subject to relatively rapid gene turnover and evolutionary divergence compared with canonical H2B genes (Raman et al., 2022). Collectively, they contribute to chromatin architecture and function by influencing gene expression, genome stability, and cellular identity (Montellier et al., 2013; Skene & Henikoff, 2013; Shinagawa et al., 2014; Khadka et al., 2020; Lai et al., 2024; Saintilnord et al., 2024; Voss & Korb, 2025).

II.3.3. H3 variants family

As for the H3 variants family, it consists of H3.1, H3.2, H3.3, testis-specific H3T, H3.5, primate -specific H3.X and H3.Y, tissue-specific H3.6, H3.7, H3.8, and centromeric protein A (cenH3) with H3.1 H3.2, and H3.3 as the most abundant (Xiong et al., 2016; Taguchi et al., 2017). Each of these variants have unique and distinct roles in transcription and replication (Tachiwana et al., 2011; Delaney et al., 2023). For example, H3.3, enriched in post-translational modifications, and CENP-A play a crucial role in the stability of the chromosome and their loss leads to chromosomal instability and aneuploidy (Giunta et al., 2021; Ragusa & Vagnarelli, 2023).

II.3.4. H4 variants family

H4 is the most conserved histone compared to other core histones, thus, H4 variants are extremely rare and thought to be non-existent. In 2018 and 2024, two novel variants H4G, Hominidae-specific variant, and H4E, ascomycetes-specific enigmatic variant, were identified by Mengping Long and Michel Flipphi respectively revolutionizing this era. The H4G variant was shown to have a unique amino acid sequence with a truncated C-terminus. Positioned in the nucleoli, this variant is implicated in rDNA transcription and its overexpression is associated with breast and colon cancer (Long et al., 2019; Ding et al., 2020). On the other hand, H4E was shown to have shorter N- and C-terminal tails than the canonical histone with less Lys and Arg

residues. This enigmatic variant, localized in the nucleus, is expressed specifically in nitrogen deprivation and high temperature (37°C) conditions, but its function remains a mystery (Flipphi et al., 2024).

II.3.5. Linker H1 variants family

Finally, H1 variants family plays a crucial and important role in chromatin organization and gene regulation in somatic cells. There are up to eleven main somatic variants separated into two distinct groups: the replication-dependent variants (H1.1, H1.2, H1.3, H1.4, and H1.5), and the replication-independent variants with differential expression profiles in somatic cells (H1.0, H1t/ testis, H1oo/oocyte, and H1*x*). They paly diverse and distinct functions in nuclear architecture and RNA processing (Happel & Doenecke, 2009; Pascal et al., 2023). These variants are differentially distributed, forming distinct patterns: H1.2, H1.3, and H1.5 are enriched at the nuclear periphery, where they co-localize with compacted DNA, highlighting their roles in chromatin organization and compaction; in contrast, H1X is present throughout the nucleus and is particularly abundant in nucleoli, suggesting a role in ribosomal DNA transcription and nucleolar activity (Salinas-Pena et al., 2024).

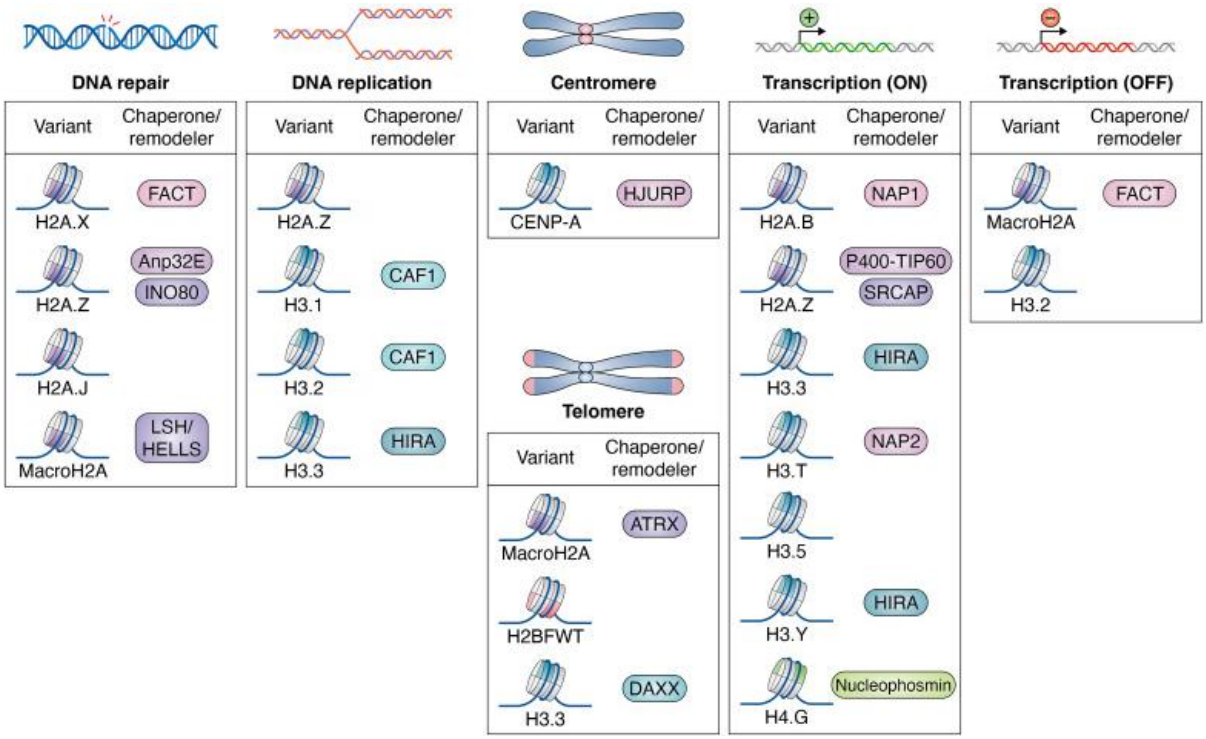

Figure 7: **Summary of core and variant histones and their role in cellular processes.** Scheme representing the different core and variant histones with their associated chaperones and remodelers separated based on their function in cellular processes. (Figure from Hegazy et al., 2025)

II.4. Post-translational modifications (PTMs)

Beside the incorporation of histone variants to the chromatin, post-translational modifications (PTMs) on histone proteins play another crucial layer of chromatin structure and gene regulation by altering and influencing nucleosome dynamics, histone interactions, and signaling the recruitment of transcriptional machinery and regulatory complexes. Post-translational modifications are enzyme-mediated chemical and covalent alterations of proteins after translation, influencing their structure and thus modifying their activity, stability, interactions, and function (Delaney et al., 2021; Pienkowski et al., 2023; G. Li, 2024). These modifications occur mainly on amino acids at the N-terminal histone tails, but some can occur within the core domain. Along with the information provided from these modifications, they constitute a complex known as "histone code" which serves as a regulatory system influencing chromatin accessibility and gene expression proposed by David Allis and Thomas Jenuwein in the year 2000 (Y. Wang et al., 2004; Lennartsson & Ekwall, 2009; Shahid et al., 2026). There are different post-translational modifications such as the classical acetylation (Ac), methylation (Me), phosphorylation (P), ubiquitination (Ub), and the novel ADP-ribosylation, citrullination, butyrylation (Bu), crotonylation (Cr), glcNAcylation, SUMOylation, and fatty acylation (Figure 8) (Mariño-Ramírez et al., 2005; R. Liu et al., 2023; Yao et al., 2024). They can also serve as biomarkers for diseases such as cancer and metabolic disorders. The combination of several post-translational marks on one histone establishes local and global pattern of chromatin modifications (X. Li & Li, 2021; R. Liu et al., 2023).

II.4.1. Histone Acetylation

Histone acetylation, the first epigenetic modification discovered, is a dynamic modification where an acetyl group ($-C=O-CH_3$) is transferred to lysine residues on the N-terminal tails of core histones particularly on histones H3 and H4, but also on H2A and H2B (Gujral et al., 2020; Y. Chen et al., 2024). The position of the acetyl group reduces the positive charge on histones and weakens their interaction with DNA (negatively charged). This reversible modification reflects a balance that modulates chromatin structure and gene expression and is generally associated with active transcription, DNA replication, DNA repair, and accessible chromatin (Zentner & Henikoff, 2013; Filippakopoulos & Knapp, 2014; Fan et al., 2016; Shin et al., 2024). Although this mark recognized for its role in chromatin accessibility and gene activation, some research suggest that it might be also implicated in gene repression and other mechanisms. For example, histone 3 on the SNR6 gene was observed under stress conditions and repression

to be acetylated on lysine 9 suggesting a regulatory role of acetylation in stress response (Arimbasseri et al., 2024). Moreover, in human cells, the acetylation of lysine 20 on histone 4 was shown to be highly expressed around the transcription start sites of minimally expressed genes. This suggested that H4K20ac forms a unique mark for gene repression in human cells (Kaimori et al., 2016). Finally, a hyperacetylation wave on histone 4 lysine 4, 8, and 12 was shown to be essential to the transition of histones with protamines leading to genome compaction (Govin et al., 2006; Goudarzi et al., 2014; Barral et al., 2017; Dong et al., 2017). This indicates a multifaceted nature of this epigenetic modification in cellular biology.

II.4.2. Histone Methylation

Histone methylation is a dynamic, reversible, and crucial post translation modification that significantly influences gene expression by altering the chromatin structure. It is characterized by the addition of methyl groups to histone proteins either activating or repressing gene transcription (Dimitrova et al., 2015; Hong et al., 2022; Kales & Simeonov, 2024). The methyl group is deposited on specific lysine (K) and arginine (R) residues on histone tails modifying gene expression. The most common histone methylation marks occur on H3K4 (me1, me2, me3), H3K36 (me1, me2, me3), H3K79 (me1, me2, me3) associated with active transcription, H3K9 (me1, me2, me3), H3K27 (me1, me2, me3) associated with gene repression, Polycomb repression, and gene silencing, as well as on H4K20 associated to DNA replication, damage, and heterochromatin. The latter occurrence is less common on H2AK9 associated to gene activation, and H2BK5 associated to transcription regulation (Strahl et al., 1999; Cui et al., 2019; Y. Li et al., 2021).

II.4.3. Histone Phosphorylation

The phosphorylation of histones play an essential role in regulating the chromatin structure and function due to their implication in several cellular processes such as DNA repair, gene expression, and cell cycle progression (B. Zhang et al., 2014; R. Liu et al., 2023). Histone phosphorylation occurs usually at serine (S), threonine (T), tyrosine (Y), and histidine (H) residues (Carlberg & Molnár, 2018). The phosphorylation on S10 of histone H3 (H3S1ph) leads to transcription activation and gene expression while phosphorylation on the histone variant H2AX as response to DNA double-strand breaks results in chromosome compaction and transcription arrest (Berger, 2002; Lacoste & Côté, 2003; Rossetto et al., 2012; B. Zhang et al., 2014). Moreover, the crosstalk of phosphorylation with other post-translational modifications

such as methylation and acetylation, can affect their influence creating a complex regulatory network (R. Liu et al., 2023).

II.4.4. Histone Ubiquitination

As for ubiquitination, it is a critical gatekeeper modification crucial in chromatin regulation. Ubiquitin unlike small molecules such as methylation and acetylation, is a ~8.5kDa protein causing the physical remodeling of the nucleosome and acts as a significant signal for other proteins. It primarily occurs on lysine residues provoking degradation or alters chromatin dynamics, impacting gene expression and cellular processes. The ubiquitination on the canonical histone H2A forms a bulky speed bump preventing the transcription machinery of reading the DNA. Thus, it is associated with transcription repression modulating cellular signals and is essential for maintaining the inactive X chromosome in females. While ubiquitination on histone H2B in both yeast and mammals acts a prerequisite for the methylation on histone H3 leading to transcription activation and transcriptional machinery recruitment. Moreover, the ubiquitination of H2A.X acts as a guide when DNA breaks, directing the repair proteins to fix these breaks and prevent genomic instability and cancer (Zhou et al., 2008; Weake & Workman, 2010; Lopes et al., 2024).

II.4.5. Histone SUMOylation

SUMO (Small ubiquitin-like modifier) is a 10kDa protein covalently bound to lysine residues either on histone tails or on the cores. They are present on all core histones and some variants such as H2A.Z; and peak during transcription activation preventing over-elongation. In both yeast and mammals, SUMOylation is primarily found at the promoter regions resulting in transcription repression and gene silencing. They are normally attached to the same lysine residues that would be otherwise acetylated creating a competition between the two marks. By blocking these sites, sumo prevents the deposition of acetylation marks keeping the gene in a “closed” state. Once the N-terminal tails of H2A and H2B are sumoylated, this is linked to a major mechanism for repressing “noise” from non-coding regions of the genome in yeast, while once sumoylated on the H4 tail it is mainly associated with a potent signal for long-term silencing helping maintain heterochromatin. Finally, it is less common to be present on H3 tail and is associated to the regulation of specific developmental genes. Not only does sumo induce silencing, but it also plays a structural role during high-stress events: such as maintaining centromere stability while promoting proper chromosome segregation during mitosis and

stabilizing the chromatin environment post DNA damaging events (Shiio & Eisenman, 2003; Iñiguez-Lluhí, 2006; Nathan et al., 2006; Heideker et al., 2009; Ullmann et al., 2012; Ohkuni et al., 2018; Keiten-Schmitz et al., 2020; Ryu et al., 2020; Bradley et al., 2021).

II.4.6. Histone Crotonylation, Butyrylation

Crotonylation (cr) and butyrylation (bu) of histones are recently discovered epigenetic modifications of the broader group of lysine acylations. They are involved in various biological processes playing a significant role in gene regulation, DNA damage responses, spermatogenesis nucleoprotamin transition, HIV latency, and stem-cell biology. Both modifications occur on lysines by either adding a crotyl group (4-carbon unsaturated chain: -CO-CH=CH-CH_3), or a butyl group (4-carbon chain: -CO-CH_2-CH_2-CH_3) and are associated with transcription activation. The deposition of these epigenetic marks is influenced by cellular metabolic status, with competition for modification sites between crotonylation, butyrylation, and acetylation (Sabari et al., 2017; Simithy et al., 2017). The crotonylation on histone H3 is associated to active promoter regions facilitating transcription (K. Li & Wang, 2021; Sun et al., 2023). Moreover, crotonylation was shown to destabilize the nucleosome structure and be part of a compensatory mechanism during chromatin to nucleoprotamin transition during spermatogenesis (Y. Chen et al., 2007; Montellier et al., 2012; Ntorla & Burgoyne, 2021). The butyrylation on the histone H4 acts as a hallmark for active gene and transcription activation (Z. Xie et al., 2016; Z. Wang et al., 2025).

II.5. Epigenetic machinery: writers, erasers, remodelers, and readers

The regulation of gene expression through the highly dynamic epigenetic mechanisms relies on a tripartite system of specialized proteins. These proteins are known as writers, readers, and erasers, and manage to add, recognize, and remove epigenetic marks such as post-translational modifications to histone proteins or DNA. They are crucial in different cellular processes and disease mechanisms, and their coordinated function regulates chromatin architecture and gene expression by rendering the chromatin either more or less accessible to the transcription machinery (Figure 8) (Arrowsmith et al., 2012; González et al., 2022; R. Ren et al., 2022).

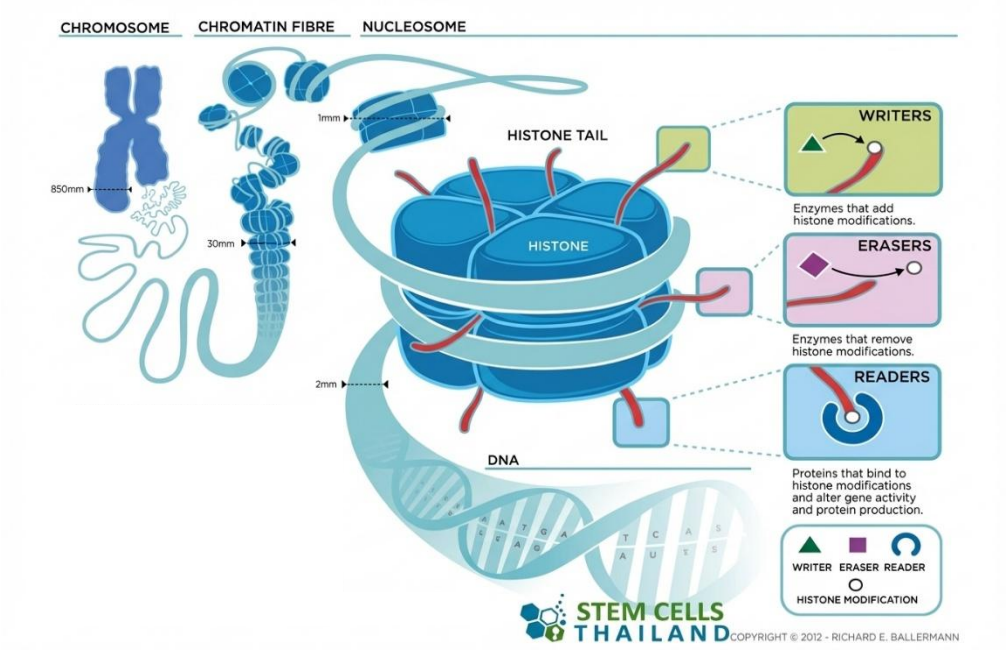

Figure 8: **Epigenetic machinery**. A representation of epigenetic factors acting on histone tails: writers (in green), erasers (in pink), and readers (in blue) with their functions of either adding, removing, or reading the histone modifications (Figure adapted from stem cells Thailand).

II.5.1. Epigenetic writers.

Epigenetic writers are enzymes capable of adding specific chemical epigenetic marks (PTMs) to the DNA and histones without modifying the DNA sequence. Their primary role is to establish and maintain these chemical groups that influence chromatin structure and gene activity. Moreover, they are crucial for several biological processes such as development, cellular differentiation, and response to environmental stimuli (Honer et al., 2024; T. B. Nicholson et al., 2015). Epigenetic writers include three large families:

II.5.1.1. Histone methyltransferases (HMTs)

HMTs are crucial enzymes known to add methyl groups to lysine and arginine residues on histones leading to either the activation or the repression of gene expression. They are categorized according to the amino acids they methylate and the structural domains they contain. Thus, they are divided into two main families: Lysine methyltransferases (KMTs) characterized by the addition of the methyl group on lysine residues. This family is formed of two major subfamilies: starting with the SET domain-containing family which is characterized by a conserved Su(var)3-9, Enhancer of Zeste, Trithorax domain of ~130 amino acids responsible for their catalytic function. The group is composed of several enzymes interacting

with histone tails such as SUV39, EZH, SET1, SET2, MLL/KMT2, SET7/9, G9a/EHMT2, SMYD2, and SMYD3 (B. Xiao et al., 2003; Mazur et al., 2014). Then, the non-SET Domain-containing family which is characterized by the lack of this domain with DOT1L as the sole well-known enzyme at that time. DOT1L possesses a unique catalytic domain with a seven-beta-strand (7βS) fold and specifically methylates the lysine 79 on the globular domain of histone 3. This enzyme was shown to play important roles in transcriptional regulation, DNA damage response, and development (Hu, 2025; Ishiguro et al., 2025; J. Liu et al., 2025). Protein arginine methyltransferases (PRMTs) family is characterized by enzymes catalyzing the transfer of methyl groups from S-adenosyl methionine (SAM) to arginine residues. This subfamily is further categorized into groups according to the type of arginine methylation they produce: Type I PRMTs group composed of PRMT1, PRMT2, PRMT3, PRMT4, PRMT6, and PRMT8 enzymes forms monomethylarginine (MMA) and asymmetric dimethylarginine (aDMA) by positioning two methyl groups on the same nitrogen atom of the guanidino group. Type II PRMTs composed of PRMT5, and PRMT9 generate MMA but with a symmetric dimethyl arginine (sDMA) by positioning one methyl group on each of the two terminal nitrogens. Finally type III PRMTs composed of PRMT7, only produces MMA with no further demethylation (X. Zhang et al., 2000; Tewary et al., 2019; vanLieshout et al., 2019; Halabelian & Barsyte-Lovejoy, 2021; Hwang et al., 2021).

II.5.1.2. Histone acetyltransferases (HATs)

HATs are responsible for the addition of acetylation marks on lysine residues on histones leading to the neutralization of their positive charge and the loosening of the chromatin structure. This facilitates the access of the transcription machinery and activates transcription. This family includes 5 different groups of enzymes: GCN5-related N -acetyltransferases (GNAT) group (GCN5, PCAF, Hat1, Elp3, Hpa2-Hpa3, ATF-2, NUT1) primarily acetylate lysine residues on histone H3 (mainly H3K9 and H3K14) thus responsible for transcription activation. Some members are important factors in gene regulation, stress response, and development while others act in the cytoplasm and are responsible for acetylating the newly synthesized nucleosomes prior to their incorporation into the chromatin (Sanchez et al., 2025; Weber et al., 2025). p300/CBP group acts as broad transcription co-activators involved in acetylating all core histones and non-histone proteins including transcription factors. They are crucial for cellular growth, differentiation, and response to environmental stimuli (Reynoird et al., 2010; Y. Wang et al., 2021; Z. Ibrahim et al., 2022). MYST group (MOZ, MORF, HBO1, MOF, TIP60),

most MYST HATs are responsible for acetylating histone H4 (mainly H4K16), and specific others are involved in several processes such as DNA repair, development, and apoptosis (Gordon et al., 2025; Mousavi & Yang, 2025; L. Wang et al., 2025). Type B HATs (cytoplasmic) (HAT1, HAT4) are known to acetylate free histones in the cytoplasm (mainly H4) prior to their incorporation into nucleosomes. Thus, their primary role is in histone processing and not in gene regulation like the other groups (Nagarajan et al., 2013; Varga et al., 2019; Ortega et al., 2023). Finally, associated co-activators (TAF1, TIFIIC90, SRC1, SRC3/AIB1/ACTR, p600, CLOCK) where TAF1 a component of general transcription factor TFIID is involved in promoter recognition and plays a significant role in histone acetylation and gene expression regulation. TAF1 is not a major HAT in *Saccharomyces cerevisiae,* with Gcn5 and Esa1 being the core contributors to histone acetylation and gene expression (Hilton et al., 2005; Durant & Pugh, 2006; H. Peng et al., 2021a). As for SRC1 and SRC3, they act as nuclear receptor co-activators, regulating hormone-dependent transcription (X. Li et al., 2024; W. Zhang et al., 2024). Moreover, CLOCK acetylates for circadian rhythm regulation (Cal-Kayitmazbatir et al., 2023; Aguillon et al., 2024; L. Liu et al., 2024). These proteins often function as multi-protein complexes and regulate specific transcriptional programs (Roth et al., 2001; Demetriadou & Kirmizis, 2017; R. He et al., 2021)

II.5.1.3. Histone kinases: writers of phosphorylation

Histone kinases are enzymes known to deposit phosphate groups derived from ATP on serine (S), threonine (T), and tyrosine (Y) on histone tails. They play a crucial role in regulating transcription, DNA replication, and cell division by modifying histones and influencing the chromatin structure and function. There are two different types of kinases: Cyclic AMP-independent (cAMP) kinases which are linked to cell proliferation and activated to phosphorylate serine and threonine residues in the non-globular domains of histone H1 or non-histone chromosomal proteins promoting chromosome condensation (Matthews & Huebner, 1984). Cyclic AMP-dependent kinases or protein kinase A (PKA) are enzymes that phosphorylate preferentially free and unbound histone proteins in a process regulated by cAMP and play a crucial role in transcriptional regulation influencing chromatin structure and gene expression (Sweet & Allis, 1993). Moreover, the kinases can also be categorized according to their biological functions forming three groups: Mitotic kinases known to be mediators of chromosome condensation and genome compaction. One example is Aurora B or Ipl1 in yeast; as cells enter mitosis, aurora B floods the chromatin with phosphate marks on H3S10 leading to the drop of HP1 bound on methylated H3K9. The drop is due to the repulsive and bulky

negatively charged phosphorylation mark, thus allowing the reconfiguration of the chromatin for cellular division. The second group consists of the DNA damage kinases also known as the "first responders" that scan the genome constantly for breaks and phosphorylate histones as a help signal to initiate the damage-response mechanism upon the break recognition. As an example, ATM, ATR, and DNA-PK (Tel1/Mec1 in yeast) are kinases continuously screening the DNA and marking H2A.X S139 rapidly from the break site creating a scaffold for repair proteins. Finally, the third group known as transcriptional kinases uses the phosphorylation marks for transcription activation by shocking genes at specific promoters. As example, MSK1 and MSK2 kinases are activated prior to stress signals and activate by its turn "the nucleosomal response" mediate by the phosphorylation of H3S10 and H3S28 on the promoters of "immediate-early genes". The phosphorylation acts as a cue required for the recruitment of HATs, such as p300 or GCN5, that acetylates the neighbouring lysine residue H3K14 and creates a "hyper-active" promoter state and activates transcription. Another example is Casein kinase 2 (CK2) which is identified as the "architect" of the genome and responsible for maintaining its structural integrity. This kinase is constitutively active phosphorylating H4S1 that serves as a negative regulator in *S. cerevisiae.* CK2' s phosphorylating function serves as a "binary switch" turning "off" and "on" transcription through the phosphorylation or dephosphorylation (by phosphatase) of H4S1. In other words, upon the phosphorylation of this serine, the mark acts as a blocking agent ejecting the histone reader protein from the acetylated neighbouring lysine residues and prevent the formation of "active" chromatin structures (Soloaga et al., 2003; W. L. Cheung et al., 2005; Utley et al., 2005; Keogh et al., 2006; Marmorstein & Trievel, 2009; Altaf et al., 2010; Baek, 2011; Rossetto et al., 2012; Watson & Higgins, 2016).

II.5.2. Epigenetic erasers

Epigenetic erasers are enzymes that remove post translational modification marks from DNA and histone proteins. They maintain cellular homeostasis by allowing the reversibility of gene activation or repression and are implicated in gene expression and cellular functions (Nicholson et al., 2015; Yang et al., 2015.; Honer et al., 2024). The primary families of epigenetic erasers are:

II.5.2.1. Lysine demethylases (KDMs)

KDMs are enzymes responsible for the removal of methyl groups from lysine residues on histones leading to either the activation or repression of transcription. These enzymes reverse

the methylation marks added by histone methyltransferases and influence cellular processes such as transcription, DNA repair, cell cycle progression, and development. They are divided mainly into: Flavin adenine dinucleotide (FAD)-dependent Amine Oxidases (LSD family) composed of LSD1/KDM1A and LSD2, that uses FAD as a cofactor and catalyzes the oxidation of mono- and di- methylated lysine. This oxidation forms an imine intermediate which will be hydrolyzed resulting in demethylated lysine and release of formaldehyde. For example, LSD1 demethylates H3K4me1/2 repressing transcription and impacting gene regulation (Zheng et al., 2016; Yu et al., 2021; González et al., 2022). Jumonji C-domain-containing Oxygenases (JmjC Family) is composed of KDM2A, KDM2B, KDM3A, KDM3B, KDM3C, KDM4A-D, KDM4E, KDM4F, KDM5A-D, KDM6A, KDM6B, UTY, JMJD6, JMJD5, JMJD7, PHF2, PHF8, FBXL10, RIOX1, RIOX2. These enzymes use Fe^{2+} and α-ketoglutarate as cofactors to hydroxylate methyl groups on mono-, di-, tri-methylated lysine residues. This hydroxylation produces a hydroxymethyl lysine released as formaldehyde. For example, KDM2A and KDM2B are known to demethylate H3K36me1/2 regulating gene expression at CpG islands. Moreover, some of these enzymes (JMJD6, JMJD7) can also modify non-histone proteins (Z. Chen et al., 2007; Markolovic et al., 2018; Chowdhury et al., 2022; Islam et al., 2022; F. Yin et al., 2024; S. Feng et al., 2024; Y. Liu et al., 2025).

II.5.2.2. Histone deacetylases (HDACs)

HDACs counteract the activity of HATs, which add acetyl groups leading to chromatin opening. HDACs are enzymes known to erase acetyl groups from histone and non-histone proteins. They play a crucial role in transcription regulation and influences various biological processes. These enzymes facilitate chromatin compaction by increasing the positive charge of histone tails strengthening their interaction with DNA, thus silencing gene expression vital for cellular function and differentiation. HDACs are divided into four classes based on the sequence homology and structure: Class I consists of the nuclear HDAC1, HDAC2, HDAC3, and HDAC8 that primarily deacetylate histones and affect cell cycle regulation. Class IIa and IIb consist of nuclear and cytoplasmic shuttling HDAC4, HDAC5, HDAC6, HDAC7, HDAC9, and HDAC10 that can influence both histone and non-histone proteins. Class III consist of NAD^+-dependent Sirtuins SIRT1, and SIRT 7 structurally distinct from other HDACs and target only non-histone proteins playing roles in metabolism, stress responses, and aging. . Class IV is composed of HDAC11, which displays unique features and shares characteristics with both Class I and Class II. Most classes of HDACs, except Class III that requires NAD^+, uses Zn^{2+} as a cofactor for their

catalytic mechanism (Milazzo et al., 2020; Puttalingaiah et al., 2022; S. Zheng et al., 2024; S. Y. Ibrahim et al., 2025).

II.5.3. Chromatin remodelers

Chromatin remodelers are a group of proteins bound together forming complexes that can modify and alter the chromatin structure to regulate the accessibility of the DNA without changing its sequence. They act as molecular machines that reshape the chromatin architecture by dynamically repositioning or restructuring nucleosomes using ATP as a source of energy to control gene expression, DNA repair, replication, and other cellular processes (Handy et al., 2011; Becker & Workman, 2013). Epigenetic remodelers are divided into four main families of ATP-dependent chromatin remodeling complexes: SWI/SNF complex is conserved in eukaryotes and play a crucial role in regulating gene expression by altering the chromatin structure. The complex disrupts the nucleosome positioning by repositioning, sliding, or ejecting nucleosomes thereby increasing the chromatin accessibility and promoting gene activation crucial for DNA repair pathways (L. Tang et al., 2010; Z. He et al., 2021; Bieluszewski et al., 2023; Church & Workman, 2024). ISWI (Imitation switch family) is a group of chromatin remodeling complexes that regulate nucleosome positioning and spacing by translocating the DNA on nucleosomes and creating evenly spaced arrays moving the nucleosomes along the DNA fiber. Along with preserving the nucleosome integrity, these remodelers are important for chromatin assembly after replication and for the maintenance of higher-order chromatin structure (Erdel et al., 2010; Bartholomew, 2014; Yan et al., 2019). Nucleosome Remodeling and Deacetylase (NuRD)/CHD3 and CHD4 (Mi-2 proteins)/Chromodomain helicase DNA-binding (CHD) complex is a multi-subunit chromatin remodeling complex that combines remodeling and histone deacetylase activities. This complex remodels the chromatin to more compact and transcriptionally repressive state (W. Xie et al., 2012; Torchy et al., 2015). INO80 remodeling complex plays an important role in gene expression regulation, DNA double-strand break repair and nucleotide excision repair, and DNA replication by modulating the chromatin at replication forks and activating DNA damage tolerance pathways. Moreover, it is implicated in maintaining the genome stability by regulating the centromere chromatin and preventing faulty chromosome segregation. This versatile complex can remodel the chromatin by sliding the nucleosomes, exchanging histone variants, and positioning nucleosomes at regulatory regions (Chambers et al., 2012; Watanabe et al., 2015; Eustermann et al., 2018).

II.5.4. Epigenetic readers

Epigenetic readers are proteins that recognize and read specific chemical modifications (epigenetic marks) on DNA or histone proteins. They interpret and transduce the "epigenetic code" and recruit other complexes to regulate chromatin structure, gene expression, and DNA repair. Epigenetic readers contain specialized domains that recognize specific modified amino acids on histones or methylated DNA with high substrate specificity. These domains form binding pockets that enable selective interaction with particular epigenetic marks. Epigenetic readers include different key families: Chromodomain (CD) family consists of conserved protein domain (~40 -50 amino acids) and serves as key readers of methylated lysine residues on histones such as H3K9me3 or H3K27me3 present in the Polycomb group (PcG) proteins and Heterochromatin Protein 1 (HP1), and H3K4me3. The recognition of these marks leads to the recruitment of protein complexes, such as CHD remodelers, that can modulate chromatin accessibility, influence nucleosome positioning, and drive heterochromatin formation, stem cell maintenance, development, and DNA repair processes (*Chromodomain - an Overview | ScienceDirect Topics*; Franklin et al., 2022; Hou et al., 2023). Plant Homeodomain (PHD) finger family is a group of zinc finger proteins that bind methylated as well as unmodified lysine residues including H3K4me3. They are characterized by a conserved Cys4-His-Cys3 binding motif and play crucial roles in plant growth, development, and responses to environmental stresses (Jain et al., 2020; Quan et al., 2023; M. Liu et al., 2024). Tudor domain family composed of a 60 amino acid conserved protein domain structurally folded like SH3 domain. These proteins recognize methylated lysine and arginine residues on histone tails and other proteins recruiting other factors that can either activate or repress transcription. They are present in a range of chromatin regulatory proteins that are involved in silencing transposable elements, RNA metabolism, transcription regulation, and chromatin organization (Lu & Wang, 2013; R. Ren et al., 2014; Gan et al., 2019). Malignant Brain Tumor (MBT) domain family consists of 100 amino acid conserved protein domains that act as chromatin readers and bind specifically to mono- and di-methylated lysine residues on histone H3 and H4 tails. They are implicated in transcriptional repression by recruiting and stabilizing interactions with other protein complexes involved in gene silencing (Bonasio et al., 2010; M. Tang et al., 2013). PWWP domain family is a group of protein domains (~100-130 amino acids) with dual functionality recognizing both DNA and histone methylated lysine residues. They can read weakly but specifically H3K36me3, H3K79me3, and H4K20me3 marks and with their combined ability to bind

methylated histones and DNA, position their host protein at particular chromatin regions essential to regulate transcription, epigenetic modification, and DNA repair (H. Wu et al., 2011; Qin & Min, 2014; Rona et al., 2016). YEATS domain family consists of evolutionarily conserved protein domains characterized by a unique structural fold and their specific binding to acylated lysine residues on histones including acetylation and crotonylation marks. Through this binding, they recruit chromatin modifying complexes to specific genomic loci on the chromatin influencing transcription regulation, histone variant deposition (H2A.Z), DNA repair, and gene expression (A. Y. Wang et al., 2009; Erb, 2023). Methyl-CpG Binding Domain (MBD) family consists of a protein domain (~70 amino acids) that specifically recognizes and binds symmetrically methylated CpG dinucleotides DNA rather than histone marks. Through this binding, they recruit various chromatin-modifying complexes leading to chromatin compaction and transcriptional repression acting as a bridge connecting DNA methylation to downstream repressive chromatin state (Skalnik, 2004; K. Liu et al., 2018; Lee & Skalnik, 2021). Bromodomain (BRD) family consists of protein domains of about 110 amino acids recognizing acetylated lysine residues on histone tails and facilitating the recruitment of chromatin remodeling complexes and transcription machinery. A well-studied example is the Bromodomain and Extra-Terminal (BET) family of proteins. (Ladurner et al., 2003; Ferri et al., 2016; Filippakopoulos & Knapp, 2014). This section will be further elaborated in detail in the following chapter.

II.5.5. Conclusion

In conclusion, the epigenome is a highly dynamic regulatory system that manages and control gene expression through the addition and removal of chemical tags on histones known as histone post-translational modifications. These modifications such as histone acetylation, methylation, phosphorylation, SUMOylation, ubiquitination, crotonylation, and butyrylation act as versatile switches, deposited by dedicated writers, and interpreted by specific proteins called readers. By their turn, readers recruit different downstream response machineries in response to the read signal creating a feedback loop and maintaining the stability of the chromatin state through cellular division. On the other hand, to ensure the reversibility and adaptability of the chromatin, specific proteins known as erasers remove these added signals, PTMs, and act as switches of the chromatin state.

Finally, this symbiosis between writers, erasers, and readers makes the epigenome essential for balancing genome stability with flexible responses during differential cellular processes.

III. Bromodomain (BRD) family

The BRD family is composed of protein domains known as bromodomains (BDs) that specifically bind and assess acetylated lysine residues on histone tails. Their function is essential for the transduction of the acetylation signal into chromatin remodeling and transcription regulation. The human genome encodes for 61 BDs across 46 proteins that can co-occur with either other chromatin reader domains such as PHD fingers, PWWP domains, or with enzymatic domains such as histone acetyltransferases. Bromodomains adopt a four α-helix bundle structure (α_Z, α_A, α_B, α_C), with variable loop regions: a ZA loop connecting α_A and α_Z, and a BC loop, with a highly conserved asparagine, connecting α_B and α_C forming a hydrophobic pocket that specifically recognizes acetylated lysine residues of histone proteins (Smith & Zhou, 2016). Moreover, some proteins can contain multiple BDs such as ASH1L which contains 6 BDs, and the BET family members which contains 2 BDs (Figure 9) (Z. Chen et al., 2007; Ferri et al., 2016; Z.-Q. Wang et al., 2023).

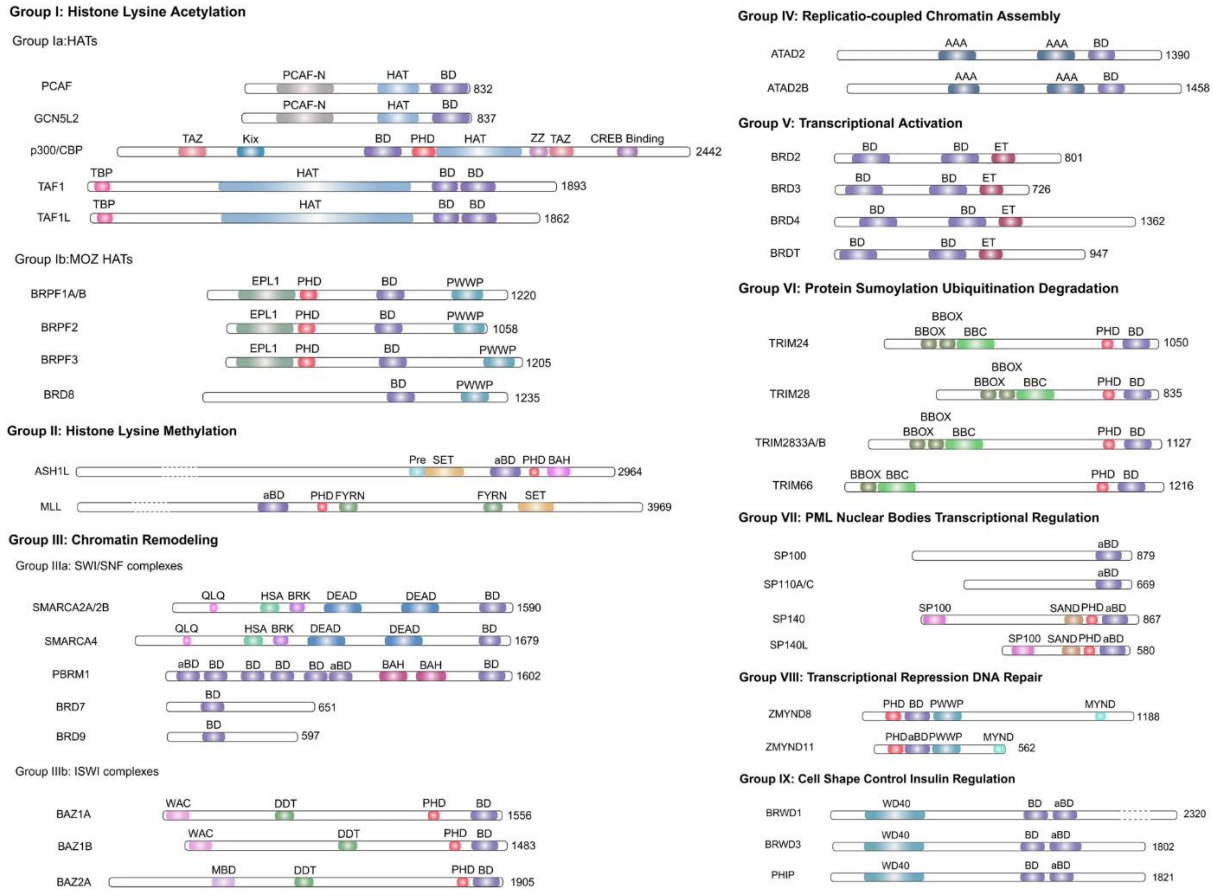

Figure 9: **Classification of human bromodomain family.** Representation of the different subfamilies of human BRD family classified according to their structure and function. (Figure from Wang et al., 2023)

III.1. Overview of Bromodomain and extra-terminal proteins (BET) proteins family

The BET family of bromodomain-containing reader proteins are known to be highly studied. They are key epigenetic readers capable of interpreting histone acetylation marks to regulate chromatin dynamics and gene transcription. In humans, the family is composed of four proteins: BRD2, BRD3, BRD4 that are ubiquitously expressed, and BRDT which is largely restricted to the testis. They possess two specialized and highly conserved N-terminal bromodomains named bromodomain 1 (BD1) and bromodomain 2 (BD2) responsible for the reading of the histone acetylation code, along with a C-terminal extra-terminal (ET) domain, of ~80 amino acids, that mediates protein-protein interactions and recruits transcription cofactors along with chromatin remodelers (Taniguchi, 2016; Ali et al., 2022). The bromodomains BD1 and BD2 are homologous within each BET member with more than 75% of identity, however, they show low similarity when compared within the same protein indicating separate and independent functions (Matangkasombut & Buratowski, 2003a; Vollmuth et al., 2009). As for the ET domain, it varies slightly between the BET family members but is evolutionary conserved across the family. Moreover, the BET family of proteins evolved from a repeated gene duplications and conserved some structural similarities to yeast's Bdf1 and Bdf2 and Drosophila's FSH protein (Taniguchi, 2016). They serve as a scaffold by recruiting transcription cofactors and recognizing short peptide motifs on partner proteins. Finally, only BRD4 and BRDT possess a C-terminal motif (CTM) that facilitates the recruitment of positive transcription elongation factor (P-TEFb) to promote transcriptional elongation.

III.2. Functional role of BET proteins

III.2.1. Functions of BRD2

BRD2 is a multifunctional chromatin-associated protein. It recognizes acetylated lysine residues on histone tails, specifically H4K5ac and H4K12ac, and has different crucial roles in coordinating chromatin structure and gene expression. BRD2 recruits some key transcription factors such as E2F and RNA polymerase II to the promoters of cell cycle genes. It promotes chromatin opening and facilitates the passage of RNA polymerase II through nucleosomes acting as its chaperone during cell cycle progression and transcription (K. L. Cheung et al., 2021; Cribbs et al., 2021). Furthermore, it modulates alternative splicing of several genes creating a diversity of gene products within the cell in addition to its involvement in DNA damage responses by collaborating with several chromatin remodeling complexes (Swi/Snf, HATs, HDACs) influencing the chromatin accessibility and structure, thus modifying transcription and

DNA repair processes (Gothwal et al., 2024). Finally, the dysregulation of BRD2 is linked to cancer, inflammation, and neurological disorders highlighting its important role in cell proliferation, embryonic neural development, immune responses, and metabolic signaling (Lin et al., 2022; Ji et al., 2024).

III.2.2. Functions of BRD3

Structurally, BRD3 resembles BRD2 and shares overlapping cellular functions, such as binding to acetylated lysine residues on histone tails, recruiting to acetylated chromatin, repositioning nucleosomes, and activating transcription (Werner et al., 2020). This nuclear protein is also involved in RNA biology by interacting with RNA molecules forming protein-RNA aggregates, it promotes the transcription of the interferon-beta (IFN-β) gene by interacting with IRF3 and the acetyltransferase p300 (W. Ren et al., 2017). Moreover, BRD3 was linked to cancer either by acting as a tumor suppressor in colorectal cancer (M. Hashimoto et al., 2024), or by its involvement in the chromosomal translocations fused to the nuclear protein in testis (NUT) gene causing NUT midline carcinoma (NMC) (Aryal et al., 2022).

III.2.3. Functions of BRD4

BRD4 is a key member of the BET protein family that binds to acetylated lysine residues on histones H3 and H4 tails and is involved in various transcriptional regulation and chromatin remodeling processes. It acts as a mitotic biomarker by helping to reactivate early G1 genes during mitosis after cellular division. BRD4 can act as a recruiter, an atypical kinase, and a HAT promoting chromatin decompaction, facilitating transcription elongation, and maintaining higher-order chromatin structure (Nihozeko, 2023; Devaiah et al., 2024). It undergoes phosphorylation by CK2, a modification that regulates its activity essential for transcriptional activation. Additionally, CK2-mediated phosphorylation modulates its dimerization via a phosphorylation-dependent dimerization domain (PDD), which is required for chromatin remodeling (Malvezzi et al., 2021). In addition to its role in coordinating the chromatin's accessibility along with the transcriptional process in normal cases, it mediates the transcription of oncogenes such as c-MYC, and inflammatory genes rendering it a promising target for cancer and inflammatory diseases (F. Huang et al., 2018; Mann et al., 2023). Moreover, chromosomal translocations involving BRD4 fused with NUT lead to aberrant NUT expression and disruption of BRD4 function, resulting in an aggressive form of NUT midline carcinoma (NMC) (French et al., 2003; Rousseaux et al., 2022).

III.2.4. Functions of BRDT

BRDT is a testis-specific member of the BET protein family that plays a crucial role in male germ cell development, particularly during meiosis and spermatogenesis. The latter binds acetylated lysine residues K5 and K8 on the histone H4 tail and regulates the chromatin organization during meiosis, spermatogenesis, silencing of sex chromosomes, chromatin reprogramming, and histone modification regulation in addition to its chromatin remodeling activity (Pivot-Pajot et al., 2003; Dhar et al., 2012; Manterola et al., 2018). Moreover, it can regulate transcription by binding to active promoter and enhancer regions in cooperation with other factors, such as ΔNp63 in cancer cells (X. Wang et al., 2021),. In addition, its loss of function results in male sterility characterized by defects in both meiotic progression and post-meiotic differentiation (Gaucher et al., 2012).

III.3. Overview: Bdf1 and Bdf2 in yeast

The BET family of proteins emerged from a series of gene duplication events, leading to paralogous genes in mammals. Throughout evolution, these proteins retained key structural features, including tandem bromodomains an extra-terminal domain and a coiled-coil domain, that are also present in the yeast homologs bromodomain factor 1 (Bdf1) and bromodomain factor 2 (Bdf2), reflecting their shared ancestry and conserved molecular architecture (Figure 10). As their mammal homologs, they bind to acetylated lysine residues, particularly on histone H4, and play a key role in transcription regulation, chromatin structure, and stress responses (Donczew & Hahn, 2021a). Bdf1 and Bdf2 also originated from a gene duplication event, resulting in approximately 48% overall sequence similarity between these paralogs in both S. cerevisiae and S. pombe (Garabedian et al., 2012a).

Although Bdf1 exhibits broader genome-wide occupancy and higher expression, and preferably binds hyperacetylated histone H4, whereas Bdf2 interacts with both acetylated and non-acetylated forms, Bdf2 can partially substitute for Bdf1's function in its absence by relocating to sites previously occupied by Bdf1. This redundancy is critical, as the simultaneous loss of both Bdf1 and Bdf2 causes synthetic lethality in yeast, resulting in a global collapse of nascent mRNA synthesis (Matangkasombut & Buratowski, 2003). Both factors share extensive overlap in chromatin binding, contribute to histone H4 acetylation, and interact strongly with the SWR1 chromatin remodeling complex (homologous to Swi/Snf in mammals) implicated in

H2A.Z histone variant incorporation and anti-silencing functions at the heterochromatin boundaries (Mizuguchi et al., 2004). Furthermore, they facilitate preinitiation complex (PIC) formation and support transcription initiation and early elongation, mirroring the roles of their human BET protein counterparts (García-Oliver et al., 2017; Donczew & Hahn, 2021a).

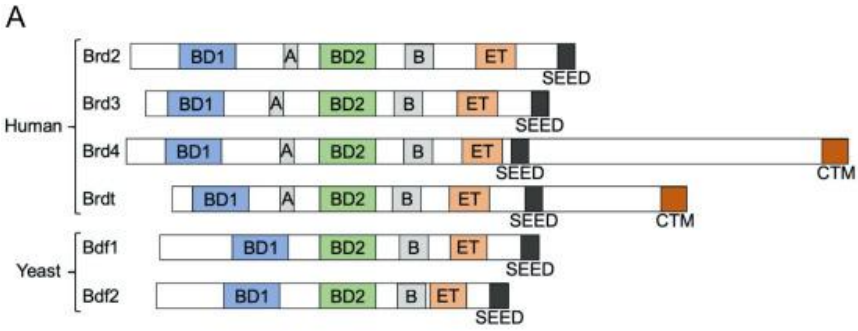

B

Common	Human specific
DNA repair	NF-kappaB signaling pathway
cell cycle	mitochondrion organization
TOR signaling pathway	Pol II transcription
autophagy	
RNA processing	
cellular transport	
protein modification	

Figure 10: **Conservation through evolution between Bdf1 and Bdf2 and human BET factors.** (A) Conserved domain organization of human and yeast BET family members (B) Major functions conserved between yeast and human BET proteins (Figure adapted from Donczew & Hahn, 2021).

III.3.1. Structural characteristics of Bdf1 and Bdf2

Bdf1 and Bdf2, localized exclusively in the nucleus, share the conserved BET family architecture characterized by two tandem bromodomains, BD1 and BD2, that bind tetra-acetylated histone H4 peptides with higher affinity (Kd 8.4 µM) than tetra-acetylated histone H3 peptides. They also contain an ET domain responsible for mediating protein-protein interactions, and a coiled-coil domain likely involved in dimerization and complex formation. The high-resolution crystal structures of Bdf1 bromodomains from *C. albicans* and *C. glabrata* revealed the canonical bromodomain fold consisting of a four-helix bundle and an acetyl-lysine binding pocket defined by the ZA and BC loops. Moreover, this analysis identified key tyrosine residues, Tyr187 in BD1 and Tyr354 in BD2, as essential for recognizing acetylated lysine residues which was then validated by in-vitro and functional assays (Ladurner et al., 2003; Mietton et al., 2017).

Although the crystallographic structures of Bdf1 bromodomains in *S. cerevisiae* are not yet publicly available, its conserved modular architecture is well established, and the critical role

of key tyrosine residues in acetyl-lysine recognition is preserved across species (García-Oliver et al., 2017).

III.3.2. Conservation of Bdf1 through fungal evolution

The Bdf1 protein sequence is highly conserved among fungal species, with particularly strong conservation in its two bromodomains. This conservation reflects their essential role in recognizing acetylated histone tails and modulating chromatin structure. Key functional motifs, including the bromodomain fold and crucial ligand-binding residues, are maintained across fungi, underscoring Bdf1's vital function in transcription regulation and cell differentiation. Sequence analyses and functional studies in organisms such as *C. glabrata* and *S. cerevisiae* demonstrate that mutations impairing bromodomain function significantly reduce growth or viability, highlighting the evolutionary pressure to preserve this protein's structure and function (Wei et al., 2025).

III.3.3. Functions of Bdf1

III.3.3.1. Bdf1 regulates gene transcription

Bdf1 serves as an essential epigenetic regulator in yeast, binding acetylated lysine residues on histone H4 through its bromodomains to facilitate transcription initiation and elongation. It operates across the genome with a higher specificity for TFIID-dependent loci, where it promotes the recruitment of essential transcriptional coactivators and facilitates the assembly of the PIC. Specifically, some researchers claims that Bdf1 corresponds to the C-terminal region of the Taf1 subunit within the TFIID complex compensating for the lack of bromodomains in Taf1 (Figure 11) (Matangkasombut & Buratowski, 2003). Importantly, Bdf1 is indispensable for small nuclear RNA (snRNA) gene transcription, ensuring proper generation and assembly of snRNP complexes vital for splicing. This conserved function of Bdf1 and BRDT links Bdf1 to global gene expression regulation, affecting both protein-coding and non-coding RNA genes (Lygerou et al., 1994; Albulescu et al., 2012; Berkovits et al., 2012; Donczew & Hahn, 2021a).

Moreover, as its human ortholog Brd4, Bdf1 is shown to be phosphorylated by CK2 at two specific regions which is indispensable for Bdf1's activity without affecting its binding to the TFIID complex (Sawa et al., 2004).

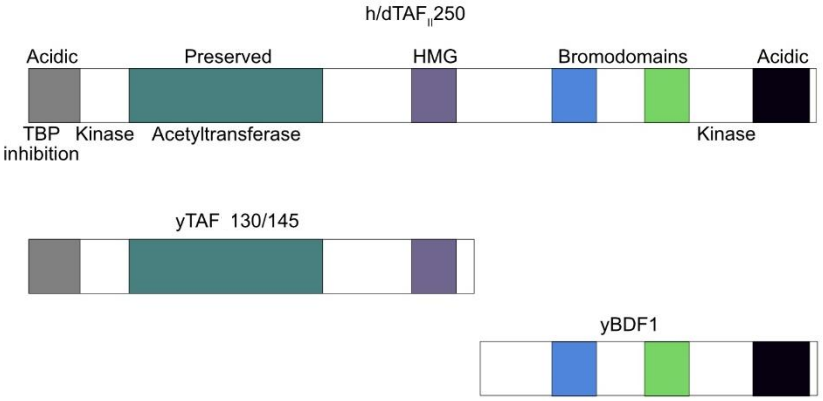

Figure 11: **Schematic alignment of TFIID (TAFII250) and TAF145/Bdf1** indicating that Bdf1 is a subunit of TFIID complex.(Figure adapted from Matangkasombut & Buratowski, 2003)

III.3.3.2. Bdf1 mediates chromatin remodeling

Beyond its role in transcription regulation, Bdf1 contributes to chromatin remodeling by recognizing acetylated histone H4 tails through its bromodomains and serving as a subunit of the SWR1 remodeling complex. SWR1 is functionally and physically connected to the NuA4 histone acetyltransferase complex, which acetylates histones H4 and H2A in vivo and orchestrates the replacement of histone H2A with the H2A.Z variant. In higher eukaryotes, these complexes correspond to the TIP60/p400 complex, highlighting an evolutionarily conserved mechanism. Together with Yaf9, another acetylation reader, Bdf1 targets SWR1 to nucleosomes adjacent to nucleosome-free regions (+1 nucleosomes), promoting effective deposition of H2A.Z. Although a loss of Bdf1 reduces the kinetic binding of SWR1 to chromatin, it does not impair H2A.Z incorporation, reflecting Bdf1's specific role in enhancing SWR1 activity in a NuA4-dependent manner (Raisner et al., 2005; Altaf et al., 2010; Ranjan et al., 2025).

Additionally, Bdf1 plays an anti-silencing role at heterochromatin boundaries by preventing the spread of silent chromatin mediated by Sir proteins, thus safeguarding euchromatin integrity and genome stability. This positions Bdf1 as a key link between chromatin remodeling and transcriptional regulation of gene expression programs (Ladurner et al., 2003).

III.3.3.3. Bdf1 in DNA damage and stress responses

Bdf1 has been shown to be important for cellular viability in S. cerevisiae, but it is not essential due to the presence of its paralog, Bdf2, which shares partially redundant functions with Bdf1 (Matangkasombut & Buratowski, 2003). However, loss of Bdf1 results in mitochondrial dysfunction, apoptosis, and altered regulation of certain stress-response genes under conditions like salt and ethanol stress (Kubota et al., 2004; X. Liu et al., 2009; L. Chen et al., 2014; Simpson-Lavy & Kupiec, 2019; Kong et al., 2022).

Moreover, Bdf1 plays a key role in resistance to DNA-damaging agents and is required for efficient repair of DNA double-strand breaks. It likely acts in the same pathway as its human homolog TAF1 to maintain genome stability under genotoxic stress (Lygerou et al., 1994; Chua & Roeder, 1995; Peng et al., 2021).

III.3.3.4. Bdf1 as a potential antifungal target

Two decades ago, Bdf1 emerged as a highly promising antifungal drug in pathogenic yeast such as *C. albicans* and *C. glabrata* as it is crucial for their viability and virulence (since they lack Bdf2). Antifungal compounds were developed to selectively inhibit both Bdf1 bromodomains over the human orthologs leading to the loss of viability of the Candida species through blocking the bromodomain interaction with acetylated chromatin. This approach reveals an innovative antifungal strategy against the increasing antifungal-resistant strains (Filippakopoulos & Knapp, 2014; Mietton et al., 2017; Wei et al., 2025).

III.3.3.5. Bdf1 and Bdf2 distinct roles

In a healthy yeast cell, Bdf2 serves as the primary architect at heterochromatin boundaries. It is recruited by Epe1 to specific DNA elements (IRC elements), where its dual bromodomains binds onto multi-acetylated H4 tails, particularly H4K16ac. This interaction acts like a physical anchor or a mechanical blockade (Trewick et al., 2008; J. Wang et al., 2013). By shielding these acetylated histones from deacetylation by Sir2, Bdf2 prevents the spread of silencing marks that would otherwise "invade" and shut down neighboring active genes. While Bdf1 is crucial for meiotic entry and general transcription at promoters through its association with the TFIID complex, it does not possess the same architectural specialized role as Bdf2 (Matangkasombut et al., 2000; Donczew & Hahn, 2021).

III.3.3.6. Bdf1 essential for gametogenesis

Bdf1 as its mammalian successor BRDT was shown to be crucial for sporulation in *S. cerevisiae*. Sporulation is a multi-step developmental process comprising two meiotic divisions, heavily regulated by the chromatin factor Bdf1. Functional Bdf1 bromodomains are required for meiotic progression, as their mutation or deletion arrests cellular development at the pachytene-to-meiotic-division transition (Chua & Roeder, 1995; García-Oliver et al., 2017).

IV. Spores and quiescence

IV.1. Yeast importance in science

Fungi constitute a diverse kingdom of eukaryotic organisms thriving in varied ecological niches and playing pivotal roles in environmental systems, industry, and medicine. Among fungi, yeasts present as unicellular organisms with distinct biological attributes that make them invaluable both as tools for fundamental research and in practical applications (Figure 12). Their straightforward cellular structure, coupled with complex and conserved molecular processes, places yeasts at the forefront as model organisms for molecular and cellular biology (Hakim, 2018; Mbuyane et al., 2021).

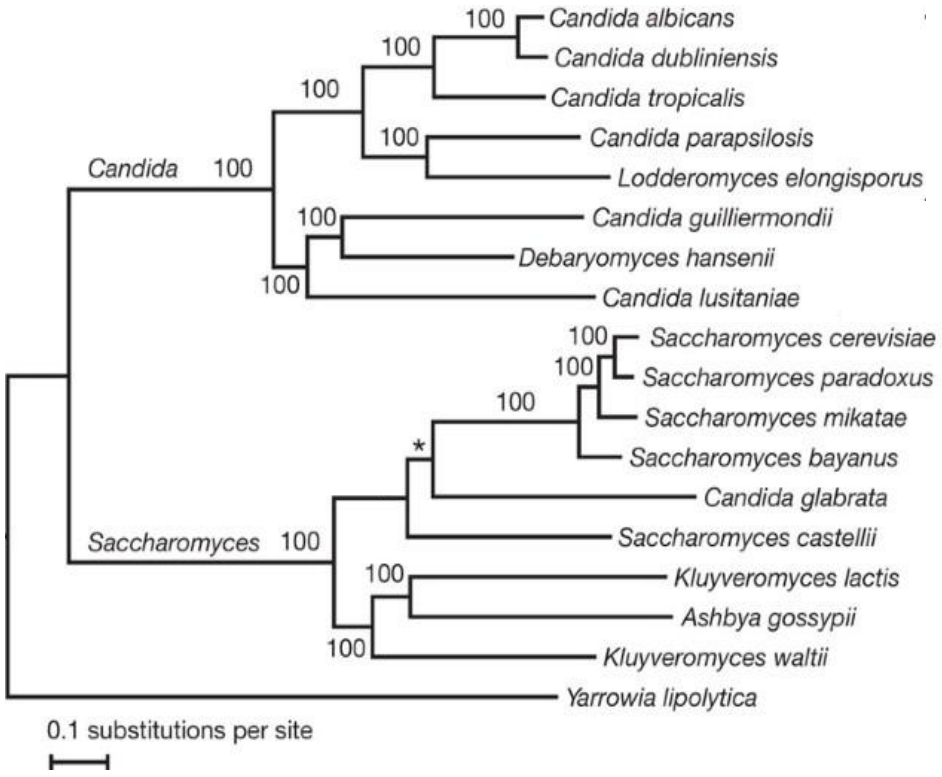

Figure 12: **Phylogenetic tree of sequenced Candida and Saccharomyces clade species.** (Figure from Butler et al., 2009)

Saccharomyces cerevisiae, also known as budding yeast, is the most prominent yeast species, historically used in fermentation for bread, beer, and wine production. Its rapid growth, fully sequenced and manipulatable genome of 6000 genes across 16 chromosomes, and ability to exist as both haploid and diploid cells make it an essential model for studying processes such as cell division, mating, and sporulation (Hakim, 2018; Parapouli et al., 2020).

The biological importance of S. cerevisiae extends beyond yeast biology, as many cellular pathways, including those governing DNA replication, transcription, chromatin remodeling, and cell cycle regulation,are conserved from yeast to humans. This conservation enables findings in yeast to shed light on complex mechanisms in higher organisms and has contributed significantly to our understanding of epigenetics, stress response, and cell signaling relevant to health and disease states.

IV.2. Yeast cellular life cycle

The eukaryotic cell cycle of Saccharomyces cerevisiae is categorized into four distinct phases that coordinate cell growth, DNA replication, and division (Gap1-G1 phase, Synthesis-S phase, Gap2-G2 phase, and Mitosis-M phase).

During the G1 phase, the cell accumulates essential biosynthetic resources and duplicate organelles in preparation for DNA replication. A critical checkpoint in this phase, known as START, assesses nutrient availability and overall cellular status controlling whether the cell proceeds to the next stage. Once past the START, the cell enters the S phase initiating and completing DNA replication. This is then proceeded by the G2 phase, where the cell further grows and ensures the integrity and the successful replication of the DNA prior progressing into the next stage. In the M phase, the replicated chromosomes are separated into the two daughter nuclei, a process called segregation, followed by cytokinesis, leading to physically dividing the cell to form two genetically identical daughter cells. Progression through these phases is governed by cyclin-dependent kinases (CDKs), particularly Cdc28 in yeast, which interacts with phase-specific cyclins (CLNs during G1 and CLBs during S, G2, and M). Checkpoint mechanisms monitor DNA integrity, DNA replication, repair, and chromosome alignment. A hallmark of the budding yeast cycle is the initiation of bud emergence during S phase, which enables asymmetric division as the daughter cell develops while the mother cell prepares for mitosis, reflecting the organism's specialized reproductive strategy (Spencer & Spencer, 1997; Mell & Burgess, 2003; Jiménez et al., 2015; Bast et al., 2019; Fischer et al., 2021).

IV.3. Survival: response to stress

Saccharomyces cerevisiae exhibits both haploid (MATa or MATα) and diploid (MATa/α) states, with the capacity to reproduce asexually or sexually depending on environmental conditions. In nutrient-rich environments, propagation occurs predominantly via asexual reproduction through budding, a process in which a daughter cell emerges from the parent cell, facilitating rapid population expansion. Under nutrient limitation or adverse conditions, cells preferentially initiate sexual reproduction. Haploid cells are capable of mating-type switching and conjugation, thereby generating diploid cells. These diploids can proliferate mitotically under favorable conditions or, when stress persists, undergo meiosis to produce tetrads containing four haploid ascospores encased within a stress-resistant ascus. Upon restoration of favorable environmental conditions, the spores germinate to produce vegetative haploid cells, which can subsequently mate to restore diploidy and thus complete the yeast life cycle (Figure 13) (Mell & Burgess, 2003; N, 2016; S. M. Burgess et al., 2017; Karki, 2017; Bast et al., 2019).

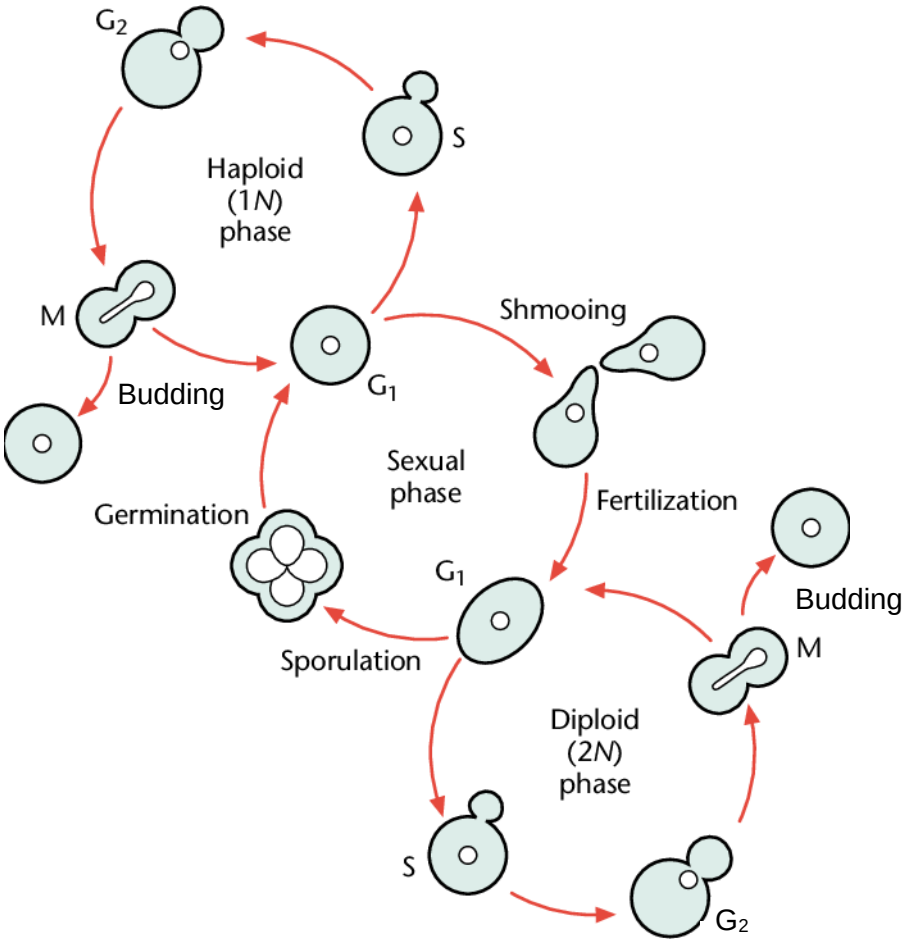

Figure 13: **Budding yeast life cycle.** The sexual pathways Saccharomyces cerevisiae can undergo are represented either as budding reproduction, sexual reproduction, and sporulation along with their life cycle progression through G1, G2, M phase, and sporulation exit through germination. (Figure adapted from Mell & Burgess, 2003)

IV.3.1. Sporulation: a survival pathway conserved through species

Sporulation is a complex and specialized developmental process employed by various bacteria and yeasts. It is triggered in response to nutrient deprivation, particularly the lack of nitrogen and fermentable carbon sources. This survival mechanism allows the cells to exit vegetative growth and enter a differentiation pathway, producing four haploid nuclei. These dormant nuclei are then packaged into highly stress-resistant spores within the cytoplasm of the parent cell, which becomes the ascus.

Progression through this process is tightly controlled and depends on multiple factors prior the commitment of the cell through the process. These complex genetic and metabolic regulatory pathways vary among the different organisms.

IV.3.1.1. Sporulation in bacteria

Bacterial sporulation, particularly in endospore-forming bacteria such as *Bacillus* and *Clostridium*, is initiated by nutrient limitation and mediated through regulatory cascades involving the master transcriptional regulator Spo0A (Hutchison et al., 2014). The process begins with the phosphorylation of the master regulator which will be then activated, thus regulating more than 100 genes including those necessary for early and late sporulation events. The cell is then committed for sporulation and DNA replication is initiated and tightly regulated by Spo0A ensuring the replication of only two chromosome copies: one for the mother cell and the other for the daughter cell called the forespore (Stragier & Losick, 1996). Post replication, the organization of the two nucleoids into an axial filament is formed and the asymmetric septation formed near one pole then partitions the cell into a mother cell and a smaller forespore (also called prespore), establishing the two distinct compartments, each containing a complete chromosome, crucial for differential gene exression and spore development (Piggot & Hilbert, 2004). The forespore is subsequently engulfed by the mother cell membrane, forming a double-membrane structure (inner and outer forespore membranes). Between these membranes, a specialized peptidoglycan cortex is developed, promoting dehydration of the spore core, increasing its resistance to heat and desiccation (Popham, 2002). Simultaneously, protective proteinaceous coats are assembled around the forespore, with some species forming an additional exosporium, enhancing protection against enzymes, chemicals, and ultraviolet radiation (Driks & Eichenberger, 2016). During maturation, the spore core accumulates dipicolinic acid and calcium ions, which stabilize DNA and proteins,

further dehydrate the spore, and enhance its durability, while the mother cell undergoes a programmed autolysis to release the mature endospore (Setlow, 2006). Ultimately, the mature endospore enters a metabolically dormant yet highly resistant state. Upon restoration of favorable conditions, the endospore undergoes germination through activation, cortex hydrolysis and degradation, water uptake, and metabolic reinitiation, culminating in outgrowth into a vegetative cell (Setlow, 2014). This intricate program of sporulation is essential for bacterial persistence, ecological fitness, and the transmission of both pathogenic and industrially relevant species.

IV.3.1.2. Sporulation in plants

As for plants, sporulation is a form of sexual reproduction where the diploid sporophyte is capable to give rise to a new haploid individual called sporangia, through meiosis, without the need to fuse with another cell. This process is crucial for the plant life cycle allowing the alternation of generations in land plants and many algae.

The process begins by the formation of sporophyte, a multicellular diploid phase, where the development of organs like stems, leaves, and more importantly, sporangia - tissues in which spores are produced is initiated. Within these sporangia, sporogenous cells, also known as sporocytes, undergo meiosis resulting in genetically unique spores, encased in a tetrad durable, resistant wall made of sporopollenin, a highly durable polymer that protects them from desiccation, UV radiation, and microbial attack. Once mature, the sporangium releases dormant spores into the environment, which, under favorable moisture and temperature conditions, germinate and develop into haploid gametophytes. This gametophyte matures and generates gametes for fertilization, ultimately creating a new sporophyte, thus completing the life cycle. In seed plants like angiosperms and gymnosperms, sporulation is highly specialized, with separate structures producing male microspores (pollen grains) and female megaspores (in ovules), both crucial in genetic recombination, species dispersal, and adaptation.Thus, sporulation confers resilience, promotes genetic diversity, and facilitates wide dispersal, ensuring plant survival and adaptation across diverse ecosystems (H. Wang et al., 2016; Kaitera et al., 2017; Ajmal et al., 2023).

IV.3.1.3. Sporulation in yeast

In yeast, the initiation of sporulation relies on a combination of environmental and physiological factors such as the diploidy of the cell and their mating type heterozygosity determined by the presence of both MATA and MATα mating type alleles, along with the nutrient deprivation signaling with the lack of fermentable carbon sources such as glucose, and the nitrogen starvation. This triggers complex signaling cascades that arrest the mitotic cell cycle in G1 and induce respiratory metabolism. Only under these restrictive conditions do diploid, mating type heterozygous cells commit to meiosis and sporulation, a developmental pathway where more than 1,000 genes are transcriptionally regulated to support stress resistance, survival, and future reproduction. These genes are repartitioned in 10 well defined clusters of genes repressed during vegetative growth and expressed at specific timepoints throughout sporulation. Post the exit of the mitotic cycle, the cell is induced by the early expressed genes, regulated by the master regulator Ime1, into a premeiotic S phase where the DNA starts to replicate, and progress into meiotic prophase with homologous chromosome pairing and recombination to increase genetic diversity. After the completion of the initiation, early phase with an alteration in the cell cycle machinery and modifications in RNA processing, the cell enters the middle phase of sporulation with the induction of the middle-expressed genes at the pachytene checkpoint with Ndt80 as the master regulator with an autoactivated expression. Thus, promoting complex proteins and factors involved in the meiotic cell division M phase and producing four haploid nuclei packaged into daughter cells. This packaging is mediated by the remodeling of the spindle pore bodies (SPBs) that are formed during the meiosis II into meiotic plates serving as nucleation sites for prospore membrane (PSM) assembly. These PSMs encapsulates progressively each of the four nuclei, along with organelles such as the mitochondria and the fusion of their edges leads to the segregation of the four daughter cells from their mother by a process called cytokenesis. Finally, the cells enter the late phase of sporulation marked by the synthesis and maturation of a multi-layered, robust, and resistant spore wall rich in chitosan and glucan initiated by the expression of specific genes known as late genes (Figure 14) (Piekarska et al., 1970; Chu et al., 1998; Primig et al., 2000; Deng et al., 2008; Govin & Berger, 2009; Neiman, 2011; Y. Liu et al., 2020).

In conclusion, the entire sporulation program is interconnected through a highly regulatory cascade of extrinsic nutrient-sensing signals and intrinsic signals of cell-type pathways such as diploidy and transcription factors such as Ime1, Ime2, and Ndt80 coordinating stage-specific gene expression, along with intense chromatin and cellular remodelling processes ensuring the restriction of sporulation to the correct context.

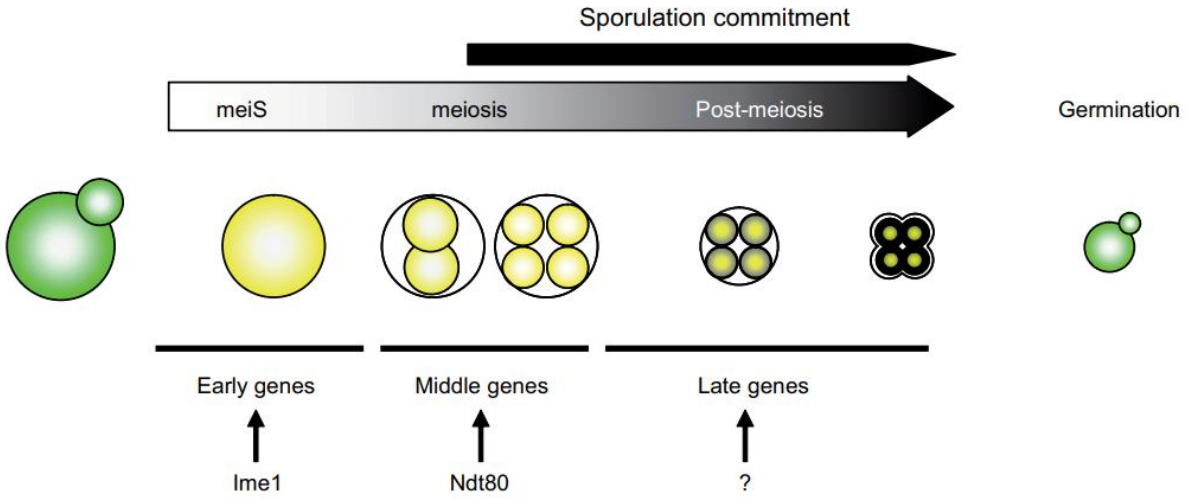

Figure 14: **Sporulation progression of S. cerevisiae overview.** Along nutrient deprivation, diploid yeast cells halt mitotic growth (green) and initiate sporulation (yellow). During the meiotic S phase (meiS), the genome is duplicated and prepared for meiosis, leading to the formation of four haploid nuclei that further differentiate into spores through nuclear compaction and spore wall assembly. Upon nutrient availability, spores germinate and re-enter the vegetative cycle. Commitment marks the phase during sporulation where cells need to finalize the sporulation process before returning to vegetative growth, even if nutrients become available. The three main classes of genes expressed and responsible for each sporulation checkpoint progression are annotated as early genes, middle genes, late genes, with their master regulators (Ime1 and Ndt80). (Figure from Govin & Berger, 2009)

IV.3.1.3.1. Sporulation repression in vegetative growth

Sporulation is a highly regulated pathway, and its repression is crucial for the survival and replication of vegetative cells when conditions favor mitotic proliferation. As well as its entry, its repression is tightly controlled involving multiple pathways and complexes to ensure sporulation genes remain silent.

At a master regulatory level, the zinc finger protein Rme1p blocks expression of IME1 in haploid and diploid cells with inappropriate mating types, by binding to its promoter and recruiting the Mediator complex subunits (Rgr1p and Sin4p) to maintain repressive chromatin structure. On the other hand, nutrient-rich conditions reinforce repression through cAMP-PKA and Ras signaling pathways, which diminish IME1 and IME2 expression, as well as glucose sensing pathways involving multiple sensors and transporters.While on a sporulation progression level, each group of genes is stringently governed by a transcriptional repressor specific to each phase in sporulation. For example, the early meiotic genes are repressed by the transcriptional

repressor Ume6p, a C6 zinc cluster DNA binding protein. The latter binds to the promoters of the genes and recruits the HDAC complex Sin3p-Rpd3p and chromatin remodeler Isw2 to maintain a closed and inactive chromatin structure. As for the middle sporulation genes, they are repressed by the Sum1-Rfm1-Hst1 complex maintained by Set1, an HMT, and H3K4 methylation. The DNA-binding transcriptional regulator Sum1p binds to a specific region in the promoters of the genes called the middle sporulation elements (MSEs), recruiting Hst1p, an NAD+-dependent HDAC, which maintains histone deacetylation at these loci and represses transcription (Figure 15) (Anderson et al., 1995; Strich et al.; Xie et al., 1999; McCord et al., 2003; Bungard et al., 2004; Robert et al., 2004; Deng et al., 2008; Jaiswal et al., 2017; Liu et al., 2020).

Overall, sporulation repression is a sophisticated network of chromatin remodeling, histone modification, transcriptional repression, and nutrient sensing. It is a multidisciplinary process that ensures tight regulation of sporulation, preventing premature or inappropriate entry into meiosis and spore formation during vegetative growth.

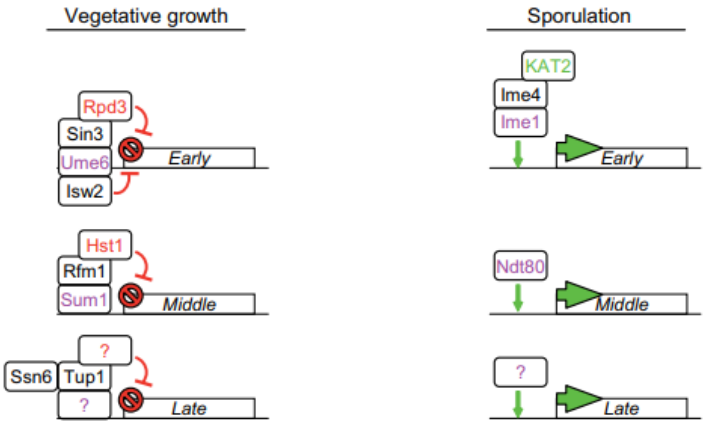

Figure 15: **Sporulation repression in vegetative growth.** During vegetative growth (represented on the left) Ume6, a transcriptional repressor, recognizes a specific sequence on the promoters of early, middle, and late sporulation genes forcing their silencing. In early genes, the repression is implemented by the recruitment of Ume6 to different repressor complexes such as Rpd3, a histone deacetylase, and Isw2, an ATP-dependent remodeling enzyme. However, during sporulation (represented on the right) Ime1, the master meiotic regulator, binds to the promoter of early meiotic genes activating their transcription through the interaction with Ume6p and recruiting Ime4, an mRNA N6-adenosine methyltransferase, and KAT2/Gcn5¸ histone acetyltransferase, for proper activation. In middle genes, the transcriptional repressor Sum1 binds to the promoters during vegetative growth blocking transcription and recruits Rfm1 and Hst1, a histone deacetylase repressing completely their transcription. On the other hand, during sporulation, the master regulator Ndt80 binds to their promoter inducing their expression and regulating the meiotic progression. Finally, the repression of late genes during vegetative growth and their activation during sporulation remains unclear with a possible involvement of Ssn6 and Tup1 for the repression (Figure from Govin & Berger, 2009).

IV.3.1.3.2. Sporulation repression in haploid cells

To maintain its viability and prevent a disastrous entry into meiosis, the haploid cell needs to ensure the stringent repression of sporulation with the help of the master regulator Rme1p. The zinc finger protein is highly expressed in haploid as well as in artificial diploids with inappropriate homozygous mating type (MATA/MATA or MATα/MATα) leading to the repression of meiosis entry through the inhibition of Ime1 expression. Rme1p binds to two regulatory elements known as Upstream Control Regions 3 and 4 (UCS3 and UCS4) of the IME1 promoter, modifying its chromatin structure and preventing the binding of any activator. Moreover, Rme1p recruits Mediator subunits Sin4 and Rgr1 to further maintain the repressive chromatin environment at this locus even under starvation. However, the MAT A1–α2 heterodimer, present only in standard diploids, represses the expression of RME1, allowing IME1 induction and sporulation, and its absence in haploid cells ensures constitutive RME1 expression and strong sporulation block (Figure 16) (Kassir & Simchen, 1976; Shimizu et al., 1997, 1998; Govin & Berger, 2009).

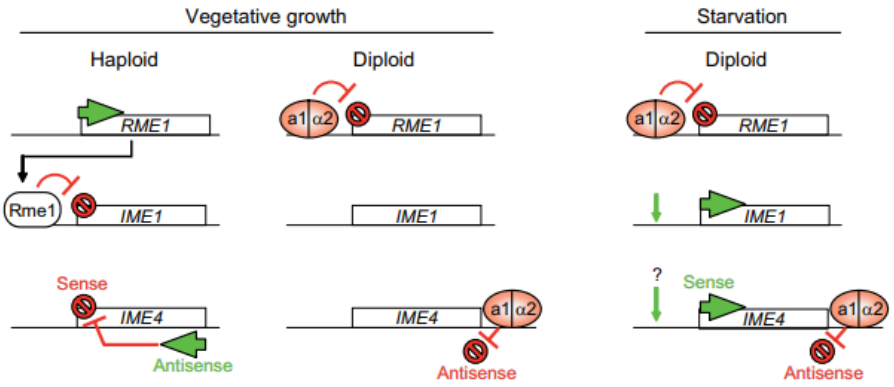

Figure 16: **Sporulation repression in haploid cells.** Sporulation is tightly regulated in haploid yeast by the expression of Rme1 a major repressor of Ime1. It recognizes specific elements on the promoter of Ime1 binds to it and inhibits the expression of this master regulator of early meiotic genes. On the other hand, in diploid cells, the product of the mating type genes MATa1/MATα2 forms a heterodimer that binds to the promoter of major repressor Rme1 preventing its expression, and derepressing the master regulator gene Ime1 during vegetative growth. The latter can be further activated upon starvation and promote sporulation. As for Ime4, the gene is regulated by a competition between a sense and an antisense transcript. In haploid cells, an antisense transcript is favoured due to its stronger promoter, leading to the silencing of the Ime4 genes. Moreover, in diploid cells, the a1α2 heterodimer product binds downstream Ime4 gene inhibiting antisense transcription leading to its derepression during vegetative growth and activation upon starvation/sporulation (Figure from Govin & Berger, 2009).

IV.3.1.4. Biology of spores

Yeast spores are an essential adaptive form of Saccharomyces cerevisiae, allowing the survival of the species during long environmental stress. After meiosis, each haploid nucleus is enveloped by a prospore membrane, resulting in four discrete compartments within the ascus. These stress-resistant, dormant spores are considered "bunkerized" due to their robust and multilayered extracellular wall, composed of four distinct layers specifically assembled during sporulation. The innermost layer, near the plasma membrane, mainly contains mannan (mannosylated proteins), presenting core structural integrity. This is followed by a β-1,3-glucan-rich layer that enhances strength and resistance. However, while these mannan and glucan layers are also found in vegetative cells, their sequential arrangement is reversed in spores. The third layer consists of chitosan, a glucosamine-based polymer that imparts both structural rigidity and a positive charge to the spore wall, playing a crucial role in spore protection. Chitosan is produced via the enzymatic deacetylation of chitin, by the chitin deacetylase enzymes CDA1 and CDA2. Finally, the last and outermost layer is composed of a polymer containing crossed linked dityrosine molecules assembled by Dit1 and Dit2 enzymes and additional outer wall factors such as OSW. This layer provides important chemical resistance, such as protection from high temperatures, digestive enzymes, and toxic compounds (Figure 17) (Moens, 1971; Neiman, 1998; Coluccio et al., 2004; Okumura et al., 2015; Zhang et al., 2017; Basiony et al., 2020; Plante et al., 2023; Durant et al., 2024).

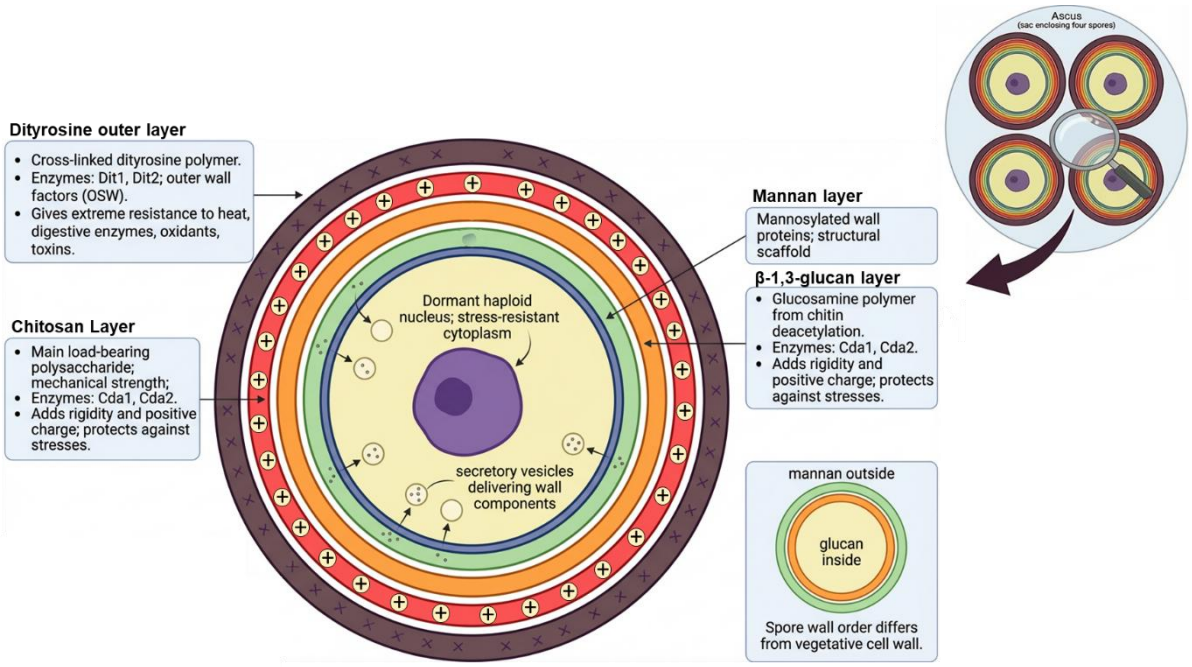

Figure 17: **Spore wall architecture in Saccharomyces cerevisiae.** A scheme representing the four different layers of the spore wall. The dark-violet outer ring represents the dityrosine outer layer with the cross-linked dityrosine polymers represented as crosses throughout the ring layer. Followed by the red ring that corresponds to the chitosan layer covered with "+" sign representing the positive charge addition. An orange ring representing the β-1,3-glucan layer, and finally, the green ring representing the mannan layer. On the bottom right, an illustration indicating the switching of the mannan and glucan layers position in vegetative cells. This scheme was generated with the help of FigureLabs AI.

IV.3.1.5. Sporulation and autophagy

A recent review suggested a fundamental cross talk between autophagy and sporulation as both processes are induced by nitrogen starvation and share several common transcription factors and novo formation of double-layered structures. Moreover, the authors further suggested that autophagy not only is active during sporulation but is also required to support the cells' integration into the developmental program (Barve & Manjithaya, 2021).

Sporulation represents a profound metabolic transformation. Under the stress of nitrogen starvation, the cell is forced to synthesize new prospore membranes and protective walls using only its existing internal resources. This transition is powered by resource recycling, where autophagy degrades misfolded proteins and damaged organelles into essential building blocks, such as amino acids and lipids, required for meiotic differentiation (Barve & Manjithaya, 2021). This recycling program is initiated by the inactivation of the TORC1 (Target of Rapamycin Complex 1) kinase, a master nutrient sensor. In the absence of nitrogen, TORC1 inhibition leads

to the dephosphorylation of Atg13, which in turn triggers the assembly and activation of the Atg1 complex. This molecular switch drives the bulk autophagy necessary to meet the heavy biosynthetic demands of prospore membrane formation and eventual maturation into a resilient ascospore.

IV.3.1.6. Spore chromatin

In this highly preserved and resistant bunker lies the well-organized and highly compacted genetic material exhibiting specialized features reflecting the dormant state of the spore. How is that possible? The extreme compaction of the chromatin is associated to a series of chromatin remodeling and epigenetic modifications leading to a tight packaging of the nucleosomes thus, reducing the accessibility and protecting the genome by restricting DNA damage and transcription. This tight packaging is mediated on one hand by an enrichment of the histone variant H2A.Z on meiotic chromosomes promoting proper formation of chromosome axis, the assembly of synaptonemal complex, and the regulation of recombination as well as an enrichment of the histone linker Hho1, which facilitates the higher-order chromatin folding during sporulation and spore maturation. On the other hand, a series of epigenetic changes mark the repression of critical regions in the meiotic process and long-term gene silencing. For example, the methylation of histone H3 on lysine K4 by the KMT Set1 was shown to be involved in the meiotic gene regulation, and the phosphorylation of the histone H4 serine S1 correlated with the transition between open and closed chromatin. Followed by a hyperacetylation wave on the histone H4 K5, K8, and K12 lysine residues, that enables the complete repression and reinforcement of the dormant protective state of the spore chromatin with an extreme decrease in global transcription. H4S1ph and H4Kac marks coexist on the promoter sites genome-wide with distinct functions: The first responsible for the structural compaction reinforcing the repression while the second potentially serves as a stored “hyperacetylated” epigenetic signature exploited for rapid transcription reactivation upon germination.

All these genomic and epigenomic repressive events allow a metabolic dormancy and resistance to environmental stresses characterized by their dynamic reversibility upon favorable conditions. The reader BET protein Bdf1 connects the two aspects responsible for this compaction by interacting with SWR1 and TFIID responsible for the H2A.Z variant deposition, enabling the efficient activation of NDT80 regulon along with many middle/late

genes, and directly binding to the H4 acetylated lysine residues where it probably maintains promoter architecture within the compacted genome (Krishnamoorthy et al., 2006; Govin et al., 2010; Bryant et al., 2012; González-Arranz et al., 2018; McCullough et al., 2015; Chigweshe et al., 2022; Movilla Miangolarra et al., 2024).

IV.3.1.7. Spore chromatin in other fungi

This highly compacted and silenced chromatin is not only reported in *S. cerevisiae* spores but is also shown to be conserved across other fungi species with a strong implementation of heterochromatic domains. These domains mediate genome stability and transcription silencing. However, the molecular mechanisms leading to this closed chromatin remain different from the H4S1ph, H4Kac, and Bdf1 mediated compaction in S. cerevisiae.

For example, in Neurospora crassa, the orange/red bread mold, constitutive heterochromatin is characterized by the H3K9me3 mark, its canonical reader HP1, and 5-methylcytosine, which is tightly coupled to H3K9me3 and reinforces transcriptional repression.

What happens? DIM-5, a histone lysine methyltransferase, methylates H3K9 over repetitive AT-rich regions which will be then read by HP1 through its chromodomains and recruit both DIM-2, the unique DNA methyltransferase, that will, by its turn, methylate cytosines in the underlying DNA and the DMM-1/DMM-2 complex sharpening heterochromatin boundaries to prevent the spreading of these “lock down” marks into neighboring euchromatin.

In conclusion, these events lead to the formation of large and compact blocks acting as structural anchors to maintain genome stability through sexual reproduction and spore formation (Kouzminova & Selker, 2001; Selker et al., 2002; Freitag et al., 2004; Honda & Selker, 2008; Rountree & Selker, 2010; Shao et al., 2024).

In *Arabidopsis thaliana,* and more specifically in male spores also known as pollen and sperm cells, the DNA and nuclei compaction is mediated by the male-germline-specific histone variant H2B.8. As in yeast, the chromatin remains histone-based, thus the tight compaction is not due to the replacement of histones by protamines such as in higher eukaryotes. The histone variant H2B.8 disordered N-terminal region drives the aggregation at AT-rich euchromatin chromatin into phase-separated condensates thus remodeling the genome architecture. Although, this architectural reorganization restricts spatially transcriptionally active regions, the sperm chromatin remains not fully silent, thus balancing genome protection/packaging with the

necessity of expressing necessary/specific genes in the male gamete (Borg & Berger, 2015; Buttress et al., 2021, 2022; Méteignier, 2022).

Finally, in *Schizosaccharomyces pombe* or fission yeast, the genome is initially pre-compacted in vegetative state and this heterochromatin persists through meiosis into spores. How is that possible? Actually, in vegetative cells, ~40% of the genome is highly occupied by H3K9me2/3 at centromeres, telomeres, and mating-type loci. This mark deposition is mediated by several enzymes such as Clr4 methylase, Swi6/Chp2 HP1 homologs, and Stc1 SHREC complex. Upon nitrogen starvation and meiosis induction, the centromeric heterochromatin expands while the RNAi machinery remains active reinforcing heterochromatin boundary defense. Clr6, a H3K9 specific HDAC, is upregulated resulting in a global loss of H3 acetylation marks and leading to gene silencing. Not much is known about the chromatin state with some speculations of meiosis-specific histone variants and chaperones involved in the compaction but till now, this remains a black box (Krapp et al., 2006; Allshire & Ekwall, 2015).

V. Sporulation exit: Germination

V.1. Optimal conditions: what happens?

After meiosis and spore formation, the "bunkerized" cell remains poised conserving its genome integrity, its energy saving mode, and its epigenetic primed state until the restoration of favorable conditions. Within 2 to 6h these stress-resistant spores are committed to transform back into growing vegetative haploid cells. As simple as it may seem, the process is well elaborated and consists of several steps (Figure 18):

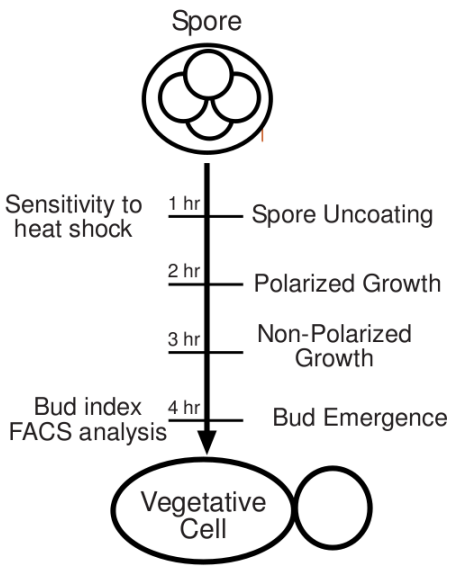

Figure 18: **Spore germination.** Schematic representation of S. cerevisiae spore germination phases with time points. (Figure from Joseph-Strauss et al., 2007)

V.1.1. Activation and commitment

The revival story initiates with sensing the availability of fermentable carbon sources, such as glucose, by its binding to the Gpr1/Gpa2 plasma membrane receptors. This leads to the activation of the Ras2 GTPases which will bind and activate by its turn adenylate cyclase, Cyr1, to convert ATP to cAMP. The latter will bind to Bcy1, the regulatory subunit of protein kinase A, release the catalytic subunit Tpk1/2/3 and activate it leading to the phosphorylation of several targets. This promotes cellular growth and promotion through stimulating the ribosomal biogenesis, the repression of stress resistance responses by inhibiting the stress transcription factors Msn2/4, and the inhibition of autophagy through the elevated Ras/PKA signaling. Resulting in a 10-folds increase of protein synthesis coordinating metabolic and transcriptional "quickening" with a poised DNA replication and a repression of TCA, respiration, genes (Herman & Rine, 1997; Sáenz et al., 1997; Budovskaya et al., 2004; Joseph-Strauss et al., 2007; Stewart-Ornstein et al., 2017; Tamanoi, 2011; Kayikci & Magwene, 2018; Plante et al., 2023).

V.1.2. Spore wall un-coating and swelling

Following the nutrient sensing and commitment phase, the breakdown of the spore wall starts through the selective weakening and rupture of the Dit1/2 and Cda1/2 coats by dityrosinases and chitin deacetylases wall-modifying enzymes, respectively. In parallel trehalose, a compatible osmolyte produced in high amounts to protect the integrity of the cells, is rapidly degraded and spores start losing heat resistance. With this drop in resistance, the water influx begins with the appearance of a large vacuole to help accommodate volume changes leading to the localized rupture of the outer coat. Then comes the swelling of the small and round cells to larger, and more ovoid along with a cytoplasm shift from glass-like to fluidified. This shift results due to an increased proteome solubility, mainly for metabolic enzymes and chaperones, thus dissolving protein assembly initially formed in spores with the help of Hsp42 heat-shock protein. At the metabolic level and through the activation of the gene expression wave 1, spores deploy a coordinated transcriptional program that initiates by the strong activation of time-course transcription factors of the heat shock factor protein 1, Hsf1. It secures the proteins quality throughout the trehalose degradation and cytoplasm re-liquefaction. A downstream network is then activated and headed by Sok2/Yap6/Phd1, responsible for the repression of IME1, re-establish glucose-driven growth metabolism along with ribosome production and nutrient uptake (Hashimoto et al., 1958; Panek & Bernardes,

1983; Kloimwieder & Winston, 2011; Joseph-Strauss et al., 2007; Geijer et al., 2012; Plante et al., 2023).

V.1.3. Outgrowth and polarity

The first gene expression wave proceeds with the induction of mating-related genes and the cell continues to increase in size and the cytoplasm evolute into a vegetative-like cytosol. Spores are said to be "born pre-polarized" carrying a complete polarity landmark from sporulation essential to identify pre-marked sites for cellular outgrowth. Knowing that S. cerevisiae spores are in contact within the ascus, the pre-polarization is oriented so that the outgrowth and budding occurs away from the neighboring sibling contact points. Each mature spore has one stable cortical polarity site that can be marked either by the protein Bud8, a distal budding landmark, Bud5, the guanine-nucleotide-exchange factor (GEF) for Rsr1p, or the septin ring component, Cdc10. These proteins serve as long-lived marks throughout sporulation able to recruit and guide Cdc42, master polarity regulator, during germination and initiate polarized growth (Pringle et al., 1995; Kozminski et al., 2000; Pruyne et al., 2004; Iwase et al., 2006; Joseph-Strauss et al., 2007b; Bonazzi et al., 2014a; Chiou et al., 2017; Heasley et al., 2021).

V.1.4. Cell-cycle re-entry and budding

Vegetative growth starts with DNA replication and bud neck formation the bud then emerges in G1/S transition where it requires the phosphorylation and subsequent degradation of Sic1, cyclin-dependent kinase inhibitor. On the other hand, in germinating spores, a growth delay is marked prior to entering the S phase. Sic1's expression is retained blocking premature Clb5/6 involved in DNA synthesis initiation and replication while Cln3 cyclin expression lag involved in cell cycle progression and G1 to S phase transition. This delay is mainly characterized by the doubling and tripling of the cellular volume through isotropic expansion and polarized secretion at the pre-marked sites. The cytoplasm is completely liquified and the ribosomes are fully assembled. Post completely restoring cytoplasmic integrity and ribosome assembly with scarce resources, Clb2 cyclin, involved in G2/M transition, accumulates promoting DNA replication and bud formation (Spellman et al., 1998; Donaldson, 2000; Breeden, 2003; Joseph-Strauss et al., 2007; Veis et al., 2007; Bonazzi et al., 2014).

V.1.5. Post-germination growth

During the first spore mitotic division, Clb2's expression is increased leading to the activation of Cdc28/CDK and the phosphorylation of Pds1 securin, multiple spindle assembly proteins, and APC/C inhibitor. This drives metaphase arrest and induce anaphase. The bud emerges and the spindle pole body is duplicated and forms the short spindle along with the migration of the nuclei to the mother and the bud. The FEAR network composed of Spo12, Slk19, Cdc14, and Cfi1 is activated assisting in the partial release of Cdc14, the master mitotic phosphatase required for mitosis exit. Pds1 is degraded leading to the sister chromatid separation followed by the activation of the Mitotic Exit Network (MEN) at the daughter spindle body. Several downstream proteins are activated or downregulated fully releasing Cdc14 which by its turn dephosphorylates more than 50 targets involved in disactivating and blocking Cln/CDK and allowing mitotic exit.

A hetero-octameric septin ring composed of Cdc3, Cdc10, Cdc12, and Cdc11 assembles in an hourglass-like form at the bud neck that splits into double ring during cytokinesis. Actomyosin rings forms then the chitin primary septum followed by the secondary ensuring mother-bud separation. The nitrogen sensing network is activated and allows amino acid biosynthesis. At this stage, TORC1 is fully reactivated, and the cell is in maximum growth rate. The bud scar becomes new polarity cue, and the growth site shifts from spore landmark to axial/distal pattern. Finally, daughter cells remain competent for mating ~6–12h prior second division commitment, thus opposite mating type form shmoo, a projection that reaches out to the nearby yeast, before mitosis II (Schwab et al., 1997; Donaldson, 2000; Deutschbauer et al., 2002; Iwase et al., 2006; Joseph-Strauss et al., 2007; Veis et al., 2007; Bonazzi et al., 2014; Tamborrini & Piatti, n.d.).

Thesis Objectives

VI.1. Objectives

VI. State of the art: Exploring chromatin dynamics in quiescent yeast spores

Numerous plants and fungi, including *S. cerevisiae*, respond to sudden environmental stress by entering a highly regulated meiotic program that ensures genome preservation. During this program, the genome is meticulously and swiftly packaged within a highly protected, stress-resistant cellular structure known as a spore. Sporulation is accompanied by extreme chromatin reorganization, a global transcriptional shutdown, and the establishment of an ultracompact chromatin state, that remains fully reversible upon germination. These transitions are meticulously regulated by key epigenetic regulators and metabolic cues, allowing spores to remain quiescent while retaining the capacity for rapid reactivation upon restoration of favorable conditions. Despite its fundamental significance, the molecular mechanisms that facilitate yeast spores' achievement and maintain this rapid transition remain poorly elucidated.

The team has previously demonstrated that spore chromatin is both highly compacted and hyperacetylated on the histone H4 tail, and that this acetylation is essential for spore viability. This observation is counterintuitive, as H4 acetylation is typically associated with transcriptionally active, open chromatin. We therefore hypothesize that, in spores, H4 acetylation triggers a cascade of molecular events that paradoxically promotes chromatin compaction and transcriptional repression during quiescence. A key player in this cascade is Bdf1, which has been shown to be essential for entry into sporulation through the binding of its bromodomains to acetylated lysine residues on histone H4. In mammalian systems, BET proteins have been shown to actively reorganize acetylated chromatin and to promote histone replacement by protamines during differentiation. In yeast, the bromodomains of Bdf1 specifically recognize acetylated lysine residues on histone H4 (K5, K8, and K12) and are essential for sporulation through activation of NDT80, the master regulator of the meiotic transcriptional program. Notably, at later stages of sporulation, Bdf1 protein levels increase and Bdf1 becomes enriched on mature spore chromatin, suggesting an additional, yet unexplored role beyond meiotic entry. Altogether, this led us to hypothesize that the functions of the bromodomains of Bdf1 are essential to this organized packaging.

Therefore, my thesis project was focused on elucidating the mechanism by which H4ac and Bdf1 ensures genome packaging during the post-meiotic phase and how they prime the genome for compaction exit and germination. Thus, the objectives of this thesis are:

1. Explore chromatin organization in spores

To address the challenge of imaging the highly compacted spore nucleus, which measures approximately 1 µm in diameter, we will collaborate with Guillermo Orsi's team at IAB to establish an optimized protocol for two-color DNA imaging using Stochastic Optical Reconstruction Microscopy (STORM). This super-resolution approach will enable detailed visualization of spore chromatin organization.

By employing this approach, we will be able to visualize the nuclear envelope and DNA, facilitating quantitative measurements of nuclear volume. This analysis will reveal the significant reduction in volume between vegetative cells and spores, consistent with extensive chromatin compaction and spatial reorganization. To precisely define nuclear boundaries, we will tag the nucleopore protein Nup84 with GFP, enabling visualization of the nuclear envelope.

In parallel, we will collaborate with the Epinomics platform at IAB to assess chromatin accessibility through ATAC-seq experiments in both vegetative cells and spores. The integration of these orthogonal datasets will provide a comprehensive view of chromatin organization and accessibility in yeast spores.

2. Decipher H4ac distribution in spores

We will then utilize super-resolution microscopy to visualize the spatial distribution of H4ac on spore chromatin in comparison to vegetative cells. Simultaneously, we will map the genomic distribution of H4ac through CUT&Tag experiments. These spatial and genomic datasets will enable a deeper understanding of the link between H4 acetylation and chromatin compaction during sporulation.

3. Understand the functions of Bdf1 bromodomains in spores, along with their impact on chromatin organization and compaction

Given that BDF1 and its bromodomains are essential for sporulation and meiotic progression, the complete deletion of BDF1 results in a blockage of sporulation. Consequently, we are seeking to modulate the binding affinity of BDF1 bromodomains for H4 acetylation by

engineering a humanized version of these domains. To achieve this, we will introduce the humanized bromodomains directly into the endogenous BDF1 locus using markerless CRISPR–Cas9 genome editing.

The resulting strains will facilitate functional dissection of BDF1 bromodomain activity by evaluating cell viability, sporulation, and germination efficiency, as well as other established BDF1-dependent processes, including double-strand break repair, mating efficiency, and transcriptional regulation throughout meiotic progression. Simultaneously, we will employ super-resolution microscopy and CUT&Tag to map the spatial and genomic organization of H4 acetylation in vegetative cells, thereby determining whether this organization is altered by bromodomain humanization.

During my thesis, I had the opportunity to participate in several side projects that provided me with authorships.

a. **Project in collaboration with Dr. Cyrille Botté on PCS60 in yeast.**

Charital, S., Shunmugam, S., Dass, S., **Alazzi, A. M.**, Arnold, C.-S., Katris, N. J., Duley, S., Quansah, N. A., Pierrel, F., Govin, J., Yamaryo-Botté, Y., & Botté, C. Y. (2024). The acyl-CoA synthetase TgACS1 allows neutral lipid metabolism and extracellular motility in Toxoplasma gondii through relocation via its peroxisomal targeting sequence (PTS) under low nutrient conditions. mBio, 15(4), e0042724. https://doi.org/10.1128/mbio.00427-24

In this project I demonstrated that TgACS1 is capable of rescuing yeast strain defective of the peroxisomal bubble gum acyl-CoA synthase function linked to β-oxidation but cannot complement any other ACS functions.

b. **Project in collaboration with Dr. Cyrille Botté on Flp12 in yeast.**

Arnold, C. S**., Alazzi, A. M.**, Shunmugam, S., Janouškovec, J., Berry, L., Charital, S., Gautier, T., Duley, S., Jublot, D., Lemaire-Vieille, C., Cesbron-Delauw, M. F., Cavailles, P., Govin, J., Katris, N. J., Yamaryo-Botté, Y., & Botté, C. Y. (2025). A P5-ATPase, TgFLP12, diverging from plant chloroplast lipid transporters mediates apicoplast fatty export in Toxoplasma. Nature communications, 16(1), 5538. https://doi.org/10.1038/s41467-025-61155-9

Chapter 2: Materials and Methods

Chapter 2: Materials and Methods

Antibodies- Antibodies used are listed in Table 1. Anti-Bdf1 was previously developed in -house (García-Oliver et al., 2017).

Antibody	Target	Reference	Concentration for IF	Concentration for WB
GFP Booster Alexa Fluor 647	Goat/Rabbit	Fischer scientific, 17393333	1:1000	
Goat anti-Rabbit IgG (H+L) Cross-Adsorbed Alexa 488	Rabbit	Thermo, A-11008	1:1000	
Goat anti-Rabbit IgG (H+L) Cross-Adsorbed Alexa 647	Rabbit	Thermo, A-21244	1:10000	
Bdf1	Rabbit	Covalab		1:1000
GAPDH	Mouse	Cell Signaling, 97166		1:1000
Goat Anti-rabbit IgG peroxidase	Rabbit	Merck, #A91629		1:5000
Rabbit Anti-mouse IgG peroxidase	Mouse	Agilent, #P026002-2		1:5000
Histone 4	Rabbit	Milipore		1:1000
H4ac (pan-acetyl)	Rabbit	Active Motif, AB_2793201	1:500	1:1000

Table 1: List of antibodies used in this study.

Yeast culture media- *S.cerevisiae* strains were cultured and selected on solid and liquid media. For solid media, 9 cm diameter plastic Petri dishes were filled with either YPD-agar (1% Bacto Yeast Extract, 2% Bacto Peptone, 2% D-glucose, 2% Difco agar granulated), SC-agar (0.17% YNB 0.5% Ammonium sulfate(Euromedex), 2% D-glucose, 0.2% w/v amino acid mix (Sigma), 2% Difco agar granulated), SC-min agar (0.17% YNB 0.5% Ammonium sulfate(Euromedex), 2% D-glucose, 2% Difco agar granulated), SC-5FOA (0.17% YNB 0.5% Ammonium sulfate(Euromedex), 2% D-glucose, 0.2% w/v amino acid mix (Sigma), 0.1% w/v 5FOA, 2% Difco agar granulated), SC-LEU agar (0.17% YNB 0.5% Ammonium sulfate(Euromedex), 2% D-glucose, 0.2% w/v SC-LEU amino acid drop-out mix (Bufferad), 2% Difco agar granulated), SC-URA agar (0.17% YNB 0.5% Ammonium sulfate(Euromedex), 2% D-glucose, 0.2% w/v SC-URA amino acid drop-out mix (USBiological), 2% Difco agar granulated), and SC-TRP (0.17% YNB 0.5% Ammonium sulfate(Euromedex), 2% D-glucose, 0.2% w/v SC-TRP amino acid drop-out mix

(Bufferad), 2% Difco agar granulated). As for the liquid media used in this study, the compositions are the following: YPD (1% Bacto Yeast Extract, 2% Bacto Peptone, 2% D-glucose), YPA (1% Yeast Extract, 2% Bacto Peptone, 2% Acetate), YPAE (1% Yeast Extract, 2% Bacto Peptone, 2% Acetate, 0.8% Ethanol), Kac (2% Potassium Acetate), and KacEth (2% Potassium Acetate, Ethanol 0.8%). Solid and liquid media were either autoclaved or filter sterilized. Liquid YPA-based media and Kac-based media were freshly prepared while YPD media was autoclaved and stored at RT.

Yeast strains- Yeast strains generated and used in this study are listed in Table 2. The genotypes/expression profiles of all deletion mutants and tagged strains were confirmed by PCR analysis, DNA sequencing and/or western blot analysis and RT-qPCR.

Table 2: List of yeast strains used in this study

Yeast	Description	Mating Type	Genotype	Background	Source
yJG2	WT	Haploid	leu2::hisG trp1::hisG lys2-SK1 his4-N ura3-SK1 ho::LYS2	SK1	Winter Ed
yJG791	hBdf1(Brd4)	Haploid	Bdf1::hBdf1(Brd4)	SK1	This study
yJG816	NUP84-GFP//dit1 Δ	Haploid	NUP84::NUP84-GFP_HIS3 dit1::TRP1	SK1	This study
yJG824	hBdf1(Brdt)	Haploid	Bdf1::hBdf1(Brdt)	SK1	This study
yJG836	bdf2Δ	Haploid	Bdf2::LEU2	SK1	This study
yJG837	hBdf1(Brd4) //bdf2Δ	Haploid	Bdf1::hBdf1(Brd4) Bdf2::LEU2	SK1	This study
yJG838	hBdf1(Brdt) //bdf2Δ	Haploid	Bdf1::hBdf1(Brdt) Bdf2::LEU2	SK1	This study
yJG839	bdf2Δ//dit1Δ	Haploid	Bdf2::LEU2 dit1::TRP1	SK1	This study
yJG840	hBdf1(Brd4) //bdf2Δ//dit1Δ	Haploid	Bdf1::hBdf1(Brd4) Bdf2::LEU2 dit1::TRP1	SK1	This study
yJG841	hBdf1(Brdt) //bdf2Δ//dit1Δ	Haploid	Bdf1::hBdf1(Brdt) Bdf2::LEU2 dit1::TRP1	SK1	This study
yJG66	WT//dit1Δ	Diploid	dit1::TRP1//dit1::TRP1	SK1	Govin Lab
yJG727	WT	Diploid	leu2::hisG/leu2::hisG trp1::hisG/trp1::hisG lys2-SK1/lys2-SK1 his4-N/his4-G ura3-SK1/ura3-SK1 ho::LYS2/ho::LYS2	SK1	Winter Ed
yJG796	hBdf1(Brd4)	Diploid	Bdf1::hBdf1(Brd4)/ Bdf1::hBdf1(Brd4) Bdf2::LEU2/ Bdf2::LEU2	SK1	This study
yJG817	NUP84-GFP//dit1 Δ	Diploid	NUP84::NUP84-GFP_HIS3/ NUP84::NUP84-GFP_HIS3	SK1	This study
yJG825	hBdf1(Brdt)	Diploid	Bdf1::hBdf1(Brdt)/ Bdf1::hBdf1(Brdt) Bdf2::LEU2/ Bdf2::LEU2	SK1	This study
yJG842	bdf2Δ	Diploid	Bdf2::LEU2/Bdf2::LEU2 dit1::TRP1/ dit1::TRP1	SK1	This study
yJG843	hBdf1(Brd4)// bdf2Δ//dit1Δ	Diploid	Bdf1::hBdf1(Brd4)/ Bdf1::hBdf1(Brd4) Bdf2::LEU2/ Bdf2::LEU2 dit1::TRP1/dit1::TRP1	SK1	This study

yJG844	hBdf1(Brdt)//bdf2Δ// dit1Δ	Diploid	Bdf1::hBdf1(Brdt)/ Bdf1::hBdf1(Brdt) Bdf2::LEU2/ Bdf2::LEU2 dit1::TRP1/dit1::TRP1	SK1	This study

Yeast background choice- Several *Saccharomyces cerevisiae* strain backgrounds are commonly used in laboratory settings, including SK1, BY4741 (derived from S288C), W303, and Σ1278b. These strains display distinct sporulation phenotypes, reflecting natural genetic variation that influences meiotic progression, recombination rates, and spore viability. For instance, BY4741 exhibits low sporulation efficiency (approximately 1–10% asci), largely due to polymorphisms in key regulatory genes, whereas W303 and Σ1278b show intermediate sporulation efficiencies. Given our objective to investigate post-meiotic stages and chromatin dynamics during sporulation, we selected the most suitable strain background, characterized by its high sporulation efficiency, with over 90% asci formation (Ben-Ari et al., 2006; Song et al., 2014).

Strain construction- The humanization of Bdf1 bromodomains was performed by CRISPR Cas9 adapted from Ellis Lab (Shaw et al., 2019) sgRNAs targeting each bromodomain were designed using Benchling CRISPR guide RNA design tool platform (benchling.com). The sgRNA sequences are listed in Table *3*. The 5'-end of each oligo was phosphorylated and annealed by PNK (NEB). The annealed oligos were then ligated and assembled in the sgRNA entry vector (pWS082) by golden gate assembly with a ratio insert:vector of 15:1. The assembled plasmid was then transformed in DH5α bacteria that were then selected on LB-amp plates and no-GFP expression (since the insert would ligate at the GFP site of the plasmid).The plasmid was purified using a midi-prep kit (Macherey-Nagel) following the manufacturers recommendations and validated by sanger sequencing and plasmid digestion with the digestion enzyme EcoRV (New England BioLabs). In parallel, the Cas9-sgRNA repair vector-Ura3 (pWS158) was linearized using Esp3I (New England BioLabs) enzyme and stored at -20°C until use. The repair template was assembled: the humanized bromodomains BD1 and BD2 (hBrd4 and hBrdt) were ordered as gBlocks separately with 60 bp of flanking regions on each side from IDT DNA technologies and amplified by PCR with using Phire direct PCR mix (Thermo) (for oligonucleotides see Table 3). The amplified BD1 and BD2 sequences were then assembled in a PRS316 plasmid by Gibson assembly (NEB HiFi Assembly master mix) respecting a 1: 5 backbone: insert ratio at 50°C for 1h. The assembled plasmids were the transformed in DH5α bacteria, selected on LB-amp plates, and purified using a midi-prep kit as previously described.

The assembled BD sequences were finally amplified by PCR including the upstream and downstream flanking regions and purified using the PCR clean-up kit (Macherey-Nagel) (Figure 19A). Finally, the cells were transformed using LiAc transformation method as described in August, 2003 with 10^7 cells, 100 µg sheared salmon sperm DNA, 2.5µg of repair template, 100ng of linearized Cas9 vector, and 200 ng of the digested sgRNA vector. The clones were selected on SC-URA and 5-FOA plates (for composition see paragraph yeast culture media) then validated by PCR and sanger sequencing. For other modifications such as GFP-tag addition and gene deletions, the inserts were amplified by PCR with 60 bp of homology and transformations were performed using LiAc transformation methods (Gietz & Schiestl, 2007) (Figure 19B).The clones were selected on the corresponding selective media and validated by PCR and sanger sequencing(for oligonucleotides see Table 3).

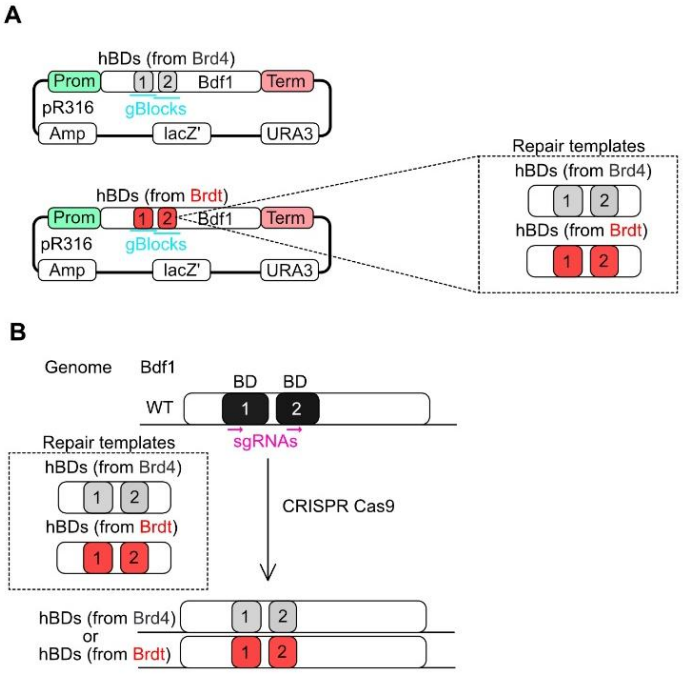

Figure 19: **CRISPR Cas9 technique. (A)** schematic representation of the repair template assembly. The human bromodomains (BD1 and BD2) of BRD4 and BRDT were assembled by Gibson in PRS316 plasmid. The assembled sequence was then amplified by PCR and purified resulting in the repair template used in B. **(B)** CRISPR Cas9 performed on *S.cerevisiae* Bdf1 ith sgRNAs targeting each BD. The system was complemented with the repair template (generated in AI) resulting in two humanized strains : hBdf1(Brd4) and hBdf1(Brdt).

Table 3: List of oligonucleotides used to generate and validate (by PCR screening, DNA sequencing, and qPCR) the strains used in this study.

Oligonucleotides	Alias	Sequence	Tm
prJG210sc	TRP1 Int Fwd	GCAAGAATACCAAGAGTTCCTCG	64.1°C
prJG211sc	TRP1 Int Rev	CGAGGAACTCTTGGTATTCTTGC	64.1°C
prJG212sc	LEU2 Int Fwd	GAACAATACACCGTTCCAGAAGTG	64.7°C
prJG213sc	LEU2 Int Rev	CACTTCTGGAACGGTGTATTGTTC	64.7°C
prJG243sc	MAT_test	AGTCACATCAAGATCGTTTATGG	62°C
prJG244sc	MAT_alpha	GCACGGAATATGGGACTACTTCG	70°C
prJG245sc	MAT_A	ACTCCACTTCAAGTAAGAGTTTG	62°C
prJG605	NDT80_F_qPCR	GGAAGAGGATACGCCTGTTATC	63°C
prJG606	NDT80_R_qPCR	GAGGTCCCACTTTGAACTGTAG	63°.3C
prJG1257	screen_sgRNA_vector	TACAAGGGCATGTCCAGCTACC	58.2°C
prJG1325	ACT1 F_qPCR	GAAATGCAAACCGCTGCTCA	65°C
prJG1326	ACT1 R_qPCR	TACCGGCAGATTCCAAACCC	65.3°C
prJG1961	screen_Bdf1	TGATAAACGTACGTAATGACCG	61.2˚C
prJG2008	sgRNA_Bdf1_BD1_F	GACTTTAGTTCCGGAGCAAATCACGG	68.4˚C
prJG2009	sgRNA_Bdf1_BD1_R	AAACCCGTGATTTGCTCCGGAACTAA	69.6˚C
prJG2010	sgRNA_Bdf1_BD2_F	GACTTTCTGGCAGTATCAAACAATGG	65.4˚C
prJG2011	sgRNA_Bdf1_BD2_R	AAACCCATTGTTTGATACTGCCAGAA	66.4˚C
prJG2014	Bdf1_hBrd4_BD_F	CTCAAAACAAGAACTTCCGAT	59.6˚C
prJG2015	Bdf1_hBrd4_BD_R	CAGATTCATAATCGTCGTAGTC	59.2°C
prJG2016	screen_Bdf1_hBrd4_BD2_F	AGAATTTGGTGCTGATGTTAG	59.5˚C
prJG2017	Bdf1_hBrd4_BD1_R	AATTGGGGCATCCTCTTG	60.3°C
prJG2018	Bdf1_hBrd4_BD2_F	GAATCGAAGAAACCGAAATCC	60.3°C
prJG2021	screen_Bdf1_hBdr4_BD1_R	CAGATTCATAATCGTCGTAGTC	60.4°C
prJG2040	NUP84_screening_Up_F	ATGGCATCTGTCATACTAGA	58.6°C
prJG2041	NUP84_Up_F	GTTGATAAGTCCAAGCTCAT	58.4°C
prJG2042	NUP84_Down_R	TTCCTCTTGGAATGACGATA	59.1°C
prJG2093	Bdf1_qPCR_F	TCGAATGGACTCGCAGAAGA	61.6°C
prJG2094	Bdf1_qPCR_R	GCGCCTTCAATACCGTTCTC	64.2°C
prJG2145	Bdf1_Brdt_BD1_F	AGAACGGTATTGAAGGCG	60.2°C
prJG2146	Bdf1_Brdt_BD1_R	GGATTTCGGTTTCTTCGATT	59.3°C
prJG2147	Bdf1_Brdt_BD2_F	CACCTGTAATAGCCAAGGG	60.5°C
prJG2148	Bdf1_Brdt_BD2_R	TTAATTGTTGCAACTCCACT	58.8°C
prJG2160	Bdf2_qPCR_F	CACGCCCACCAAACTTTGT	63.7°C
prJG2161	Bdf2_qPCR_R	TCCGCTTCCATTTCAGCTTC	64.4°C
prJG2178	Brdt_BD1_R	GTTCAGATCCATCGGGTTTTTA	61.6°C
prJG2180	dit1_F	TGATTGCATTGCTTTCAGTG	60.3°C
prJG2181	dit1_R	ACATCTATCCTCTTAGACAACT	59°C
prJG2182	screening_dit1_F	ACAATTTGTCTAATTTACTCA	54.2°C
prJG2183	screening_dit1_R	TATTTAATCACTTGTTACTCCG	56.9°C
prJG2205	Bdf2_Promoter_F	ATATACCATTGTTATATACGG	53.3°C
prJG2206	Bdf2_Terminator_R	TTGCGTAAATCATAGTACA	54.7°C
prJG2215	Bdf2_LEU2_F	CCAGAAAAGAGCGAAAAAGAGAGAACGCGGAAA AACTGAAACAAACAATTGAGCGAAATAAACCTCG GCGGCTCGGATCCCCGGGTTAATTAA	62.5°C
prJG2216	Bdf2_LEU2_R	TTTATCCCCATTCTTCCCAATTTTTTTTTTCTTTTC TTTTTTTCCTTAATT ACATGAAGCCCATTTCGATTGGCATAGGCCACT AGTGGATC	62.8°C
prJG2217	Bdf2_P_F	TAAATGCGCGATGATATTGG	59.5°C
prJG2218	Bdf2_T_R	TTTATTGGTTACCTGAAATTACT	57.1°C
prJG2219	Sequencing_F	CTCGTGCACAGTGACACG	63.6°C
prJG2221	LEU2_F	AGATACCACCAACCAATTCT	59.7°C
prJG2222	LEU2_R	ACGAAGCTATTAAGGTCTTGAA	60.5°C

prJG2229	Bdf1_F	CTGGAGTTCGTGACCGCCGCCGGGATCACTCTCGGCATGGACGAGCTGTACAAGATGACCGATATCACACCCGTAC	64.3°C
prJG2230	Bdf1_R	TAGGGATAGGCTTCCCGTTATCAACCACTTTGTACAAGAAAGCTGGGTCTAGATATTCACTCTTCTTCACTTTCGCTG	63.5°C
prJG2237	BRD4_GFP_Backbone_F	ATATCTAGACCCAGCTTTCTTG	60.4°C
prJG2238	BRD4_GFP_Backbone _R	CTTGTACAGCTCGTCCATG	60.9°C
prJG2239	Seq_Backbone_F	GTGGACTCTTGTTCCAAACTGG	64.3°C
prJG2240	Seq_LNCX_F	AGCTCGTTTAGTGAACCGTCAGATC	67.3°C

Growth assessment- Vegetative cells of *S. cerevisiae* were inoculated into liquid YPD at a 1/5 liquid to air volume ratio in an Erlenmeyer flask. The culture was incubated in an agitator at 30°C at 180 rpm. After 6 h, the cells were retrieved, washed (RT 4,000 g for 3min), and diluted in a sterile 96-well plate to an OD_{595} of 0.1 in SC (Synthetic Complete) medium. The plate was sealed with transparent PCR film and placed in a Multiskan™ spectrophotometer set at 30°C. OD_{600} readings were programmed every 15 min for 24 h, without shaking, to monitor the growth kinetics of the yeast cells. The data was retrieved and normalized to the corresponding blanks then plotted using graphpad prsim.

Sporulation- Diploid yeast in the SK1 background was grown to an OD_{600} of 0.5 in YPD. Cells were washed and primed by being resuspended in YPA (1% Yeast Extract, 2% Bacto Peptone, 2% Acetate) at an OD_{600} of 0.015. After 16 h cells were washed and induced into meiosis upon their transfer into sporulation media (K acetate 2%) supplemented with auxotrophic amino acids respecting a 1/10 liquid to air ratio. Sporulation efficiency was assessed after 72 h and is defined by the number of cells which formed tetrads.

Sporulation with Ethanol -Diploid yeast in the SK1 background was grown to an OD600 of 0.5 in YPD. Cells were washed and resuspended in YPAE at an OD_{600} of 0.015. After 16 h cells were washed and transferred into KacEth supplemented with auxotrophic amino acids. Sporulation efficiency was assessed after 72 h and is defined by the number of cells which formed tetrads.

Germination- Spores of *S. cerevisiae* were washed (4000g RT 3min) and diluted to a final OD_{600} of 0.1 in SC medium in a 96-well plate. The plate was sealed with transparent qPCR film and placed in a Multiskan™ spectrophotometer at 30°C without shaking to monitor OD every 15 min for 24h.

Spore viability assay- Tetrads were prepared for dissection by a Zymolyase digestion (MP Biomedicals, Zymolyase-100T, 100,000 U/g, Cat # 320931, Lot # 6948H). 1250 µg of Zymolyase 250 U/mL was added to 6×10^6 spores and incubated for 10 min at RT to fragilize the spore wall. The tetrad dissection was then performed using a SporePlay+ tetrad dissection microscope (Singer Instruments, Roadwater, UK) on YPD-agar plates. The plates were incubated for 48h at 30°C and scanned using a scanner (Epson Perfec on V550 Photo). Images were processed using Fiji.

Mating efficiency- Cells were inoculated in liquid YPD medium and incubated for 17 h at 30 °C with shaking at 180 rpm. The following day, cultures were diluted to an OD_{600} of 0.000025, mixed with the appropriate mating type, and incubated overnight at 30 °C with shaking at 180 rpm. On the next day, 100 µL of the mated cultures were diluted to an OD_{600} of 0.1 and plated as serial dilutions using a frogger onto YPD and SC-min selective plates for 48h.

DNA damaging assay- Cells were inoculated in liquid YPD medium and incubated for 17 h at 30 °C with shaking at 180 rpm. The following day, cultures were diluted to an OD_{600} of 0.2 in H_2O with a 3-fold dilution series in a 96-well plate while YPD, YPD+ CPT (8µg/mL) (Fisher, J62523.MD), YPD+ HU (120mM) (Sigma, H8627), and YPD+MMS (0.009%) (Fisher, H55120.14) were preheated at 30°C. Cells were then spotted on the consecutive agar plates and incubated at 30°C 24h before imaging (48h for HU). Images were then taken using the MultiSkan FC microplate reader (Thermo Scientific).

Protein Extraction and Western-Blot- Proteins were extracted from 50 mL YPD cultures harvested at $OD_{595} \approx 0.5$ or from 50 mL KAc sporulated cultures at $OD_{600} \approx 2$ with 500 µL of TENG-300 lysis buffer (50 mM Tris-HCl pH 7.4, 1 mM EDTA pH 8, 0.5% NP-40, 10% glycerol, 300 mM NaCl), supplemented with 1× PMSF, 1× Complete protease inhibitor cocktail, and 1× DTT. Cells were lysed by bead beating with 1 mL of glass beads using a FastPrep®-24 Classic bead beating grinder and lysis system (MPbio) for 45 s at 6.5 m/s, that was pre-cooled with dry ice. Whole cell extracts were collected and sonicated at 30% amplitude for a total of 1 min (20 s ON, 10 s OFF). Lysates were then centrifuged at 16000g for 10 min at 4 °C to remove insoluble material. Protein concentrations were determined using the Bradford protein assay (Bio-Rad). Equal amounts of protein (15 µg) were loaded on NuPAGE 4–12% Bis-Tris gradient gels (1 mm;

Invitrogen) and electrophoresed in MES running buffer (Invitrogen). Proteins were transferred onto nitrocellulose membranes using Tris–glycine transfer buffer containing 10% ethanol for 1 h at 100 V and 4 °C. Membranes were blocked for 1 h at room temperature in 5% non-fat dry milk prepared in PBS containing 0.1% Tween-20 (PBST), followed by overnight incubation at 4 °C with primary antibodies (listed in Table 1) under gentle agitation. The next day, membranes were washed three times with PBST and incubated with the appropriate secondary antibodies (Table 1) for 1 h at room temperature. After three additional washes with PBST, proteins were detected using Clarity Western ECL substrate (Bio-Rad). Chemiluminescent signals were acquired using a Vilber imaging system.

RNA extraction and RT-qPCR -Yeast cells (wild-type, hBdf1 (Brd4), and hBdf1(Brdt)) were grown in 20 mL YPD to reach mid-logarithmic phase (OD_{600} ~0.5). The cells were then washed and primed in either YPA or YPA + EtOH 0.8% media for 16h with shaking at 180rm. They were finally washed and induced in the sporulation media either supplemented or not with EtOH 0.8%. Samples were collected at 0, 4, and 8 h during meiosis, washed twice with cold H_2O, and stored at −80 °C. Total RNA was extracted from three independent biological replicates using the Macherey-Nagel NucleoSpin RNA extraction kit (ref. 740955.250), following the manufacturer's instructions. An additional initial bead-beating step was included, consisting of two rounds of beating with 300 µL of glass beads using the FastPrep®-24 Classic bead beating grinder and lysis system (MPbio) at 6.5 m/s for 45 s, with cooling on ice between cycles. The purity of RNA was monitored by nanodrop analysis using the ratios A260/A280 and A260/A230. Reverse transcription was performed using IScript Ready-to-Use cDNA Supermix (BioRad) and following the manufacturers recommendations. Target genes amplified represents the master regulators of the different stages of meiosis: Ime1/Ime2, NDT80 and Bdf1 with the housekeeping gene ACT1 (for oligonucleotide sequence see Table 3). The amplification was quantified by qPCR on the thermocycler CF384 Touch Real-Time PCR (Bio-Rad). The raw threshold cycle (Cq) data from qPCR runs were first processed in Bio-Rad's CFX Manager to calculate mean Cq values across technical replicates, then normalized by subtracting ACT1 Cq values (ΔCq method) to account for loading/input variations before comparative analysis

Yeast preparation for microscopy- Yeast preparation was performed as described in Ruault et al., 2011. Yeast cells were grown in 50 mL YPD to reach mid-logarithmic phase (OD_{600} ~0.5)

and washed twice with PBS and fixed in 4% Paraformaldehyde (biovalley ref # 15714) diluted in PBS for 20 min. The cells are then washed (RT 4000xg for 3min) and incubated in a pre-incubation solution (0.1M EDTA-KOH (Thermofisher, 15575020) pH8 + 10mM DTT) at 30°C with gentle agitation for 10 min. The cells were cultivated at RT 800g for 5min and spheroplasted in 2 mL YPD + 1.2M sorbitol (Euromedex) with Zymolyase (16-24 µL Zymolyase 100T (Roth, 9329.1) at 5 mg/mL) at 30°C for 15 min (vegetative cells) and 35 min (spores). The spheroplasting reaction was stopped by adding 40 mL YPD-Sorbitol solution. The cells were washed twice, and the pellet was re-suspended in 1mL YPD-Sorbitol. The cells were then dropped for 10 min on 22 mm coverslips previously treated for 10 min with Poly-L-Lysine (sigma) and air dried for 45 min. The coverslips are then washed with PBS and put in methanol at -20°C for 6 min, then transferred to acetone at -20°C for 30 s. Finally, the coverslips are air-dried for 2 min and stained with Hoechst (Thermo) for 10 min at 1:10000 dilution in PBS.

Immunofluorescence microscopy- Yeast cells and coverslips were prepared as previously described in the paragraph above. The coverslips were blocked with 1% Bovine Serum Albumin (BSA, Sigma) in PBS- 0.1% TritonX-100 (Sigma) (PBST) for 20 min at RT and then incubated with primary antibody (see Table 1) diluted in 1% BSA-PBST overnight at 4°C with gentle agitation. The next day, 3 washes with PBST were performed, and the cells were incubated with anti-rabbit secondary antibody coupled with AlexaFluor 488 (1:1000, Thermo) for 1h at 37°C. The coverslips are finally washed 3X with PBST and mounted using Dako fluorescent mounting medium (Merck) on a cover slide. The images were taken using the Zeiss AxioImager M2 (Zeiss) using the Plan- Apochromat 100x/1.4 Oil lens and Dynascope, microscope confocal multiparametrique LSM710 NLO - LIVE7 - Confocor3, using the Plan-Apochromat 63x/1,4 Oil DICIII, WD 190 lens. Images were deconvoluted using PSF Generator Fiji plugin.

Super-resolution microscopy- The protocole for super-resolution miscrocopy was implemented as previosuly published in (Orsi et al., 2023). The coverslips were prepared as previously described. The coverslips were blocked with 1% Bovine Serum Albumin (BSA, Sigma) in PBS- 0.1% TritonX-100 (Sigma) (PBST) for 20 min at RT and then incubated with anti-H4kac pan diluted in 1% BSA-PBST overnight at 4°C with gentle agitation. All antibodies are found in Table 1. The next day, 3X washes with PBST were performed, and the cells were incubated with secondary antibody diluted 1:10000 for 1h at 37°C. The coverslips are finally washed 3X with

PBST. For nanobodies: An additional permeabilization step was performed by incubating the coverslips in PBS containing 0.5% Triton X-100 for 5mins at RT. The coverslips were washed twice by PBS and the blocked with 4% BSA for 10 min at RT. The GFP-Booster nanobody was diluted 1:1000 in the blocking buffer and incubated for 1h at RT. The coverslips were then washed 3X with PBS. Finally, the coverslips were incubated with 1nM Hoechst (JF549, Lavis Lab) for 1h at RT with agitation and mounted into concave slides with Abbelight mounting medium (Abbelight Smart Kit dSTORM Super Resolution buffer ready-to-use). We immediately proceeded with imaging using SAFe360 microscope from Abbelight and Olympus (SR-M4D) with a localization precision up to 5-10 nm for bright organic fluorophores. Wide-field illumination was achieved by focusing the laser beams to the back focal plane of a 100x 1.49 numerical aperture (NA) oil-immersion apochromatic objective lens (Olympus). Data collection was obtained using a module for homogeneous EPI/HiLo/TIRF illumination and two sCMOS Hamamatsu Orca Fusion cameras offering a large field of view and high acquisition speeds. The microscope used is in the M4D imaging platform at the Institut de Biologie Structural (IBS) Grenoble, France. Images were reconstructed using the ThunderSTORM78 Fiji plugin.

RNA sequencing- After validation of the total extracted RNA described previously, RNA paired-end sequencing and stranded library preparation were performed by Novogene sequencing platform (Munich, Germany) from 100 ng total RNA in 10 µL RNase-free water (Thermo). The sequencing depth is of 10M reads per sample PE150 using NovaSeq X Plus Series. The reads were quality-checked by FastQC. Bioinformatic analyses were performed in R using the HTSeq count matrix. Counts were normalized using DESeq2's internal size factor estimation, and dispersion parameters were estimated according to the standard DESeq2 pipeline (Love et al., 2014). Differential expression results were visualized using MA plots and volcano plots, with harmonized axis scales across comparisons to enable direct visual assessment. Given the large dynamic range of transcriptional changes during sporulation, we selected a stringent threshold to define differentially expressed genes. While a cutoff of $|\log2FC| \geq 1$ is commonly used, we applied a more conservative threshold of $|\log2FC| \geq 2$ together with an adjusted p-value (padj) ≤ 0.05, to focus on robust and biologically meaningful changes. Code is naturally available upon request. Gene Ontology (GO) enrichment was performed on RNA-seq count data. For each strain, differential expression between 4 h and 0 h was estimated with DESeq2 using the model

~ time and the contrast 4h vs 0h. The background universe comprised all genes from the same DESeq2 result with finite log_2 fold change and finite adjusted P. GO Biological Process enrichment was tested with clusterProfiler::enrichGO using org.Sc.sgd.db and ORF identifiers; multiple testing was controlled with Benjamini–Hochberg, with nominal P and q value cutoffs of 0.05, and GO term sizes restricted to 10–500 genes; gene lists with fewer than five members were not tested. Results were summarized by strain, direction of change, and the 4 h / 0 h transition. A sporulation progression score was derived from RNA-seq expression profiles by first defining a reference signature in WT control samples only (0 h, 4 h, 8 h). For each gene, a Spearman correlation between expression and time was computed, and genes were ranked by adjusted *P* value and correlation sign. A balanced signature was then built from the top 200 positively time-correlated genes ("up" set) and top 200 negatively time-correlated genes ("down" set). Expression values were log2-transformed normalized counts and standardized gene-wise across all samples (z-scores). For each sample, a raw progression score was calculated as the mean z-score of the upset minus the mean z-score of the down set. To obtain an interpretable scale, scores were linearly calibrated using WT control means, setting WT ctrl 0 h to 0 and WT ctrl 8 h to 1. This yielded a comparable progression index across genotypes and conditions (ctrl and EtOH), where higher values indicate a more advanced sporulation-like transcriptional state.

Nuclei preparation for ATAC and CUT&Tag- Nuclei preparation was adapted and performed as described in Brahma & Henikoff, 2022. For vegetative cells, 500mL of yeast were cultured in YPD at 30°C with shaking at 180 rpm to reach mid-logarithmic phase (OD_{600} ~0.5-0.8). As for spores, 100mL of fresh spores at OD_{600} 2 were recovered and used for the protocol. The cells are centrifuged at 4°C 2700 g for 10 min and the pellets were washed twice with cold ultrapure water. An additional step for spores was added to separate the spores from vegetative contaminants (sporulation efficiency ~80%); this protocol was stated in Jorrit Enserink's lab. The spores are re-suspended in ultrapure water and vortexed for 2 min. The spore wall adheres on Eppendorf 1.5mL tube surface more than vegetative cells due to their hydrophobicity, the remaining solvent is discarded (containing vegetative cells), and the tube's borders were washed with 0.01% NP-40 (Thermo). The tube was vortexed again for 2min allowing the recovery of spores. The spores are washed with ultrapure water then re-suspended in

resuspension buffer (1.2 M Potassium Acetate (Euromedex), 100 mM Potassium phosphate buffer (1M KH_2PO_4 pH4 (Sigma), K_2HPO_4 pH 9 (Sigma)) pH 7.5, 0.5 mM calcium chloride (Sigma), 0.5 mM 2-mercaptoethanol (Sigma)) and incubated for 15 min at 30°C with gentle agitation. They are then spheroplasted using Zymolyase (10 µL of Zymolyase 50 mg/mL) and incubated for 15 min for vegetative cells and 35 min for spores at 37°C. The spheroplasting reaction was monitored using SDS 1% and checking the OD_{600}. Once complete the samples are immediately transferred to ice and centrifuged at 4°C 1000 g for 5 min. The spheroplasts are washed with SPC buffer (1M Potassium Acetate (Euromedex), 20 mM PIPES pH6.5 (Thermo), 0.1 mM calcium chloride (Sigma)) supplemented with 1X Protease Inhibitor Cocktail (Roche 11873580001) twice and resuspended in 0.5 mL SPC without protease inhibitors. 25 mL of cold Ficoll buffer (9% (w/v) Ficoll 400 (Dutscher), 20 mM PIPES pH 6.5 (Thermo), 0.5 mM calcium chloride (Sigma)) and gently agitated at 4°C for 15 min. The samples were the centrifuged at 4°C 6000 g for 10 min and washed twice with SPC buffer with protease inhibitor at 4°C 4200g 10 min. The samples are finally diluted 100X and counted on Neubauer chambre and diluted to reach $1x10^6$ nuclei in 100µL SPC supplemented with protease inhibitor.

ATAC sequencing- Freshly prepared nuclei (see nuclei preparation above) derived from spore or vegetative cells were centrifuged at 4,500 × g for 10 min at 4 °C. The supernatant was removed and replaced with 50 µL tagmentation buffer (10 mM Tris-HCl pH 6.0, 10 mM dimethylformamide, 5 mM $MgCl_2$, 0.33× PBS, 0.1% Tween-20, 0.01% digitonin (Merck, 300410)) containing 0.5 µL Tn5 transposase (Diagenode, C01070012). Nuclei were incubated at 37 °C with shaking at 1,000 rpm for 40 min for spore-derived nuclei and 15 min for vegetative nuclei. Following tagmentation, DNA was purified using the MinElute PCR purification kit (Qiagen, 28204) and eluted in 15 µL elution buffer (1 mM Tris-HCl pH 8.0, 0.1 mM EDTA). DNA fragments were pre-amplified in a 50 µL PCR reaction containing NEBNext HiFi 2× PCR Master Mix (NEB, M0541L), forward primer, and barcoded reverse primer. PCR cycling conditions were: 72 °C for 5 min, 98 °C for 30 s, followed by five cycles of 98 °C for 10 s, 63 °C for 30 s, and 72 °C for 1 min. To determine the optimal number of amplification cycles, 5 µL of the pre-amplified product was subjected to quantitative PCR using SYBR Green, while the remaining 45 µL was kept on ice. The number of additional cycles (N) was calculated as one-quarter of the maximum fluorescence intensity reached during qPCR. The remaining DNA was then amplified

using the same cycling conditions for N cycles. Libraries were purified using AMPure XP beads (Beckman, A63881; 1.1× ratio) and eluted in 25 µL ultrapure water. Library quality and fragment size distribution were assessed using a Bioanalyzer 2100 (Agilent, High Sensitivity DNA kit). Sequencing was performed on an Illumina NextSeq2000 platform (Institut Curie Next Generation Sequencing Platform) to a depth of approximately 20 million paired-end 50 bp reads per sample. Primary bioinformatic processing, including alignment, filtering, and initial coverage generation, was performed on the Galaxy Europe platform (usegalaxy.eu). ATAC-seq reads were aligned to the S. cerevisiae sacCer3/R64-1-1 reference genome using Bowtie2 (v2.5.3) in --very-sensitive mode, with parameters -I 0 -X 2000 --fr --dovetail to preserve subnucleosomal structural resolution. Only high-quality uniquely mapped reads were retained by filtering for MAPQ ≥ 20 using BamTools Filter (v2.5.2). Mitochondrial reads (chrM) were excluded from downstream analyses. Before fragment-size filtering, PCR duplicates were removed using Picard MarkDuplicates (v3.1.1.0) with LENIENT validation stringency. The resulting BAMPE files were retained to preserve paired-end structural information without peak calling. Libraries were partitioned by fragment size using deepTools alignmentSieve (v3.5.4). For global architectural analyses, including V-plots and fragment-size distribution assessments, the full fragment range (0–1000 bp) was retained. Genome-wide coverage tracks were generated with deepTools bamCoverage (v3.5.4) using a 5 bp bin size and CPM normalization. High-resolution two-dimensional structural maps were generated in R using ggplot2 and data.table. Fragment midpoints and lengths were calculated for all fragments located within ±500 bp of the TSS. To reduce technical noise and sequencing artifacts, additional refinement steps were applied. Non-nuclear signals from the mitochondrial genome (chrM) and the highly transcribed ribosomal DNA locus (chrXII: 450,000–491,000) were removed. Technical sequencing spikes were identified using an adaptive notch-filtering approach rather than indiscriminate outlier removal. Specifically, a 15 bp rolling median of fragment-length frequencies was used to define a local biological baseline, and fragment lengths whose raw frequency exceeded this baseline by more than 25% (ratio > 1.25) were classified as technical spikes and proportionally downsampled to the local median. This procedure removed artificial hotspots while preserving a continuous representation of the data. Bins of 4 bp × 4 bp were then smoothed by bilinear interpolation to improve visualization

of nucleosomal V patterns. For direct comparison between conditions, plots were normalized to a shared global density cap corresponding to the 99th percentile across both datasets. To improve the visibility of structural landmarks in lower-recovery libraries, such as the Merck antibody dataset, a square-root transformation was applied to the density scale together with the inferno color palette. Gemini CLI provided computational support for the analysis of and ATAC-seq including data organization, the orchestration of processing workflows on the Galaxy platform, the generation of the high-resolution structural visualization via R.

CUT&Tag sequencing- Freshly prepared nuclei (see nuclei preparation above) were bound to Concanavalin A magnetic beads (Biomag, 86057-10) and recovered using a magnetic rack. Nuclei from spore cells were additionally lysed in lysis buffer (20 mM HEPES pH 7.5, 150 mM NaCl, 0.5 mM spermidine (Sigma, 85558), 1× protease inhibitor cocktail (Roche, 11873580001), 1% BSA (Sigma, A8577), 0.1% NP-40 (Thermo Fisher, 85124), 0.01% digitonin (Merck, 300410)) for 6 min at room temperature. Nuclei were immediately recovered by magnetic separation and resuspended in Dig-Wash buffer (20 mM HEPES pH 7.5, 150 mM NaCl, 0.5 mM spermidine, 1× protease inhibitor cocktail, 1% BSA, 0.01% NP-40, 0.01% digitonin). Nuclei from vegetative cells were directly resuspended in Dig-Wash buffer without lysis. The buffer was replaced by Dig-Wash buffer supplemented with 2 mM EDTA (Invitrogen, AM9260G) using magnetic separation, and antibodies were added as follows: H4ac (Active Motif, 439925, 1:50 dilution or Merck, 06-598, 1:50 dilution), H3K4me3 positive control (Active Motif, 39159, 1:50 dilution), and IgG negative control (Merck, NI01, 1:100 dilution). Samples were incubated overnight at 4 °C with rotation. After incubation, nuclei were recovered using a magnetic rack, the supernatant was removed, and samples were washed once with Dig-Wash buffer. Nuclei were then resuspended in 50 µL Dig-300 buffer (20 mM HEPES pH 7.5, 300 mM NaCl, 0.5 mM spermidine, 1× protease inhibitor cocktail, 1% BSA, 0.1% NP-40, 0.01% digitonin) containing 0.25 µL pA-Tn5 transposase (Diagenode, C01070001) and incubated for 1 h at room temperature with rotation. Nuclei were washed three times in 300 µL Dig-300 buffer, and tagmentation was performed in 100µL Dig-300 buffer supplemented with 10 mM $MgCl_2$ (Invitrogen, AM9530G) at 37 °C for 1 h. The reaction was stopped by adding EDTA to a final concentration of 15 mM. Targeted DNA fragments were released by adding 0.1% SDS and 0.2 mg/mL Proteinase K (Fisher, 25530049), followed by vortexing and incubation at 55 °C for 1 h.

Samples were placed on a magnetic rack, and supernatants containing DNA fragments were transferred to clean microcentrifuge tubes and purified using the MinElute PCR purification kit (Qiagen, 28204). DNA was eluted in 21 µL elution buffer (1 mM Tris-HCl pH 8.0, 0.1 mM EDTA). Library preparation was performed using NEBNext HiFi 2× PCR Master Mix (NEB, M0541L) with 0.4 µM forward primer (AATGATACGGCGACCACCGAGATCTACACTCGTCGGCAGCGTCAGATGTG) and 0.4 µM barcoded reverse primer [CAAGCAGAAGACGGCATACGAGAT (8 bp barcode) GTCTCGTGGGCTCGGAGATGTG]. PCR cycling conditions were: 72 °C for 5 min, 98 °C for 30 s, followed by 17 cycles of 98 °C for 15 s and 63 °C for 20 s, and a final extension at 72 °C for 1 min. Amplified libraries were purified using AMPure XP beads (Beckman, A63881; 0.8× ratio) and eluted in 25 µL ultrapure water. Library quality was assessed using a Bioanalyzer 2100 (Agilent, High Sensitivity DNA kit), and sequencing was performed on an Illumina NextSeq2000 platform (Institut Curie Next Generation Sequencing Platform) to a depth of approximately 20 million paired-end 50 bp reads per histone mark. Primary bioinformatic processing, including alignment, filtering, and initial coverage generation, was performed on the Galaxy Europe platform (usegalaxy.eu). CUT&Tag-seq reads were aligned to the S. cerevisiae sacCer3/R64-1-1 reference genome using Bowtie2 (v2.5.3) in --very-sensitive mode, with parameters -I 0 -X 2000 --fr --dovetail to preserve subnucleosomal structural resolution. Only high-quality uniquely mapped reads were retained by filtering for MAPQ ≥ 20 using BamTools Filter (v2.5.2). Mitochondrial reads (chrM) were excluded from downstream analyses. Before fragment-size filtering, PCR duplicates were removed using Picard MarkDuplicates (v3.1.1.0) with LENIENT validation stringency. The resulting BAMPE files were retained to preserve paired-end structural information without peak calling. Libraries were partitioned by fragment size using deepTools alignmentSieve (v3.5.4). For global architectural analyses, including V-plots and fragment-size distribution assessments, the full fragment range (0–1000 bp) was retained. Genome-wide coverage tracks were generated with deepTools bamCoverage (v3.5.4) using a 5 bp bin size and CPM normalization. Linear multipliers were derived for each sample to anchor the mean signal intensity to 1.0 within a broad regulatory window (-500 bp to +3000 bp relative to the TSS). Scaling factors were averaged within biological replicate groups to preserve natural variance between replicates while equalizing global intensity between conditions. High-

resolution two-dimensional structural maps were generated in R using ggplot2 and data.table. Fragment midpoints and lengths were calculated for all fragments located within ±500 bp of the TSS. To reduce technical noise and sequencing artifacts, additional refinement steps were applied. Non-nuclear signals from the mitochondrial genome (chrM) and the highly transcribed ribosomal DNA locus (chrXII: 450,000–491,000) were removed. Technical sequencing spikes were identified using an adaptive notch-filtering approach rather than indiscriminate outlier removal. Specifically, a 15 bp rolling median of fragment-length frequencies was used to define a local biological baseline, and fragment lengths whose raw frequency exceeded this baseline by more than 25% (ratio > 1.25) were classified as technical spikes and proportionally downsampled to the local median. This procedure removed artificial hotspots while preserving a continuous representation of the data. Bins of 4 bp × 4 bp were then smoothed by bilinear interpolation to improve visualization of nucleosomal V patterns. For direct comparison between conditions, plots were normalized to a shared global density cap corresponding to the 99th percentile across datasets. To improve the visibility of structural landmarks in lower-recovery libraries, such as the Merck antibody dataset, a square-root transformation was applied to the density scale together with the inferno color palette. Gemini CLI provided computational support for the analysis of and CUT&Tag-seq including data organization, the orchestration of processing workflows on the Galaxy platform, the generation of the high-resolution structural visualization via R.

Fluorescence Recovery After Photobleaching (FRAP) assay- Plasmids containing S. cerevisiae Bdf1 and its humanized versions (hBdf1(Brd4) and hBdf1(Brdt)) were generated for this study using GFP-BRD4 (Addgene, 65378) as the backbone and the genomic sequences as the inserts. The genomic DNA was extracted and purified using phenol/chloroform and then amplified by PCR (oligonucleotides found in Table 3). The plasmids were finally assembled by Gibson (NEB HiFi Assembly master mix) respecting a 1:2 backbone: insert ratio at 50°C for 1h. The assembled plasmids were then transformed in Dh5α E. coli and cultured in LB-carbenicillin 1:10000. The plasmids were finally extracted using a mini-prep kit (Macherey-Nagel) following the manufacturer's instructions and then validated by PCR and sanger sequencing. HEK cells were transfected in a 4 well glassbottom Labtek chambers (0,5µg DNA/well) with jetPRIME transfection reagent (Polypuls) according to the manufacture's protocol and 24h after

transfection, the media were changed with DMEM/F-12 supplemented with 10% fetal bovine with and without 1 µM TSA for 4h. Furthermore, TSA treated cells were exposed to 20 µM of JQ1. Cells were then imaged in the M4D Cellular Imaging platform of IBS with a spinning disk confocal microscope (Olympus and Andor) configurated with a Nipkow wheel (Yogokawa CSU-X1) and 6 solid-state lasers for confocal imaging in real time with an Olympus 60X NA 1.42 oil immersion objective. Following bleaching, fluorescence recovery was monitored for 13 sec and images, 120 frames in total, were acquired with an EMCCD camera (Andor iXon ultra). FRAP was achieved using the photoconversion/ photoactivation module. Analysis of the intensity traces were carried out using the easyFRAP software (Rapsomaniki et al., 2012) and corrected for photobleaching and normalized with pre-bleaching intensity for at least 10 cells. The T half and Mobile fractions were calculated by the software after discarding the first 10 fluorescence intensity measurements for each cell and rest of the measured normalized fluorescence intensities for each frame was fitted with the single exponential equation.

Transmission electron microscopy (TEM)- For ultrastructural study, spores were fixed in 1 mL 2% glutaraldehyde-100 mM sodium cacodylate solution containing 0.1% ruthenium red at 4°C overnight. After washing three times in 0.2 M sodium cacodylate buffer, spores were post-fixed with 1% aqueous osmium tetroxide (EMS), containing 1.5% potassium cyanoferrate and 0.1% ruthenium red at RT for 1 h and contrasted with tea Oolong in cacodylate 0.2MpH7.4 (EM grade) for 1 h at RT. After washing three times in 0.2M sodium cacodylate and 1 time in water, they were dehydrated in a graded series of ethanol at RT and embedded in Epon. After polymerization at 60°C for 72h, ultrathin sections (100 nm) were cut on a UC7 (Leica) ultramicrotome and collected on Cupper grids 150 mesh. Sections were stained with lead citrate before observations on a Jeol 1400JEM (Tokyo,Japan) operating at 100kV transmission electron microscope equipped with a cameras in bottom position (Orius 1000) and Digital Micrograph v1.7 (Gatan Inc).

Structural Analysis- For the analysis, the published interaction of Brd4-BD1 with the H4 acetylated on K5 and K8 was used as a model (Miller et al., 2016a). Brdt-BD1, Bdf1-BD1 and Bdf1-BD2 bromodomains were obtained from AlphaFold, RCSB pdb and from C. Petosa's lab at IBS. Structure files were loaded into the PyMol visualization tool (http://pymol.org). Structures were aligned on the Brd4 BD1 model. For better visualization, some loop structures were

simplified. Atom interactions were deduced from the models based on actual H2O positions. For electrostatic continuum rendering, the Adaptive Poisson-Boltzmann Solver (APBS) module of PyMol was used with default settings. The ramp level was set to -3/+3 after APBS calculation. Only the acetyls were made visible on the H4K5acK8ac peptide representation for better visualization.

Sequence alignment- Multiple sequence alignments were generated using Clustal Omega (v1.2.4) at the EMBL-EBI web server (Madeira et al., 2019). Protein sequences of Bdf1 bromodomains and human BET homologs (BRDT/4) were retrieved from UniProt and aligned using default parameters (m=8 iterations, distance metric=Kimura, gap open penalty=6.0). The resulting FASTA alignment was then processed with ESPript 3 (X. Robert & Gouet, 2014) via the IBCP web interface (https://espript.ibcp.fr/) in Experienced mode. Secondary structure elements from PDB structures were incorporated using DSSP files, with conservation shading applied at 70% identity threshold, helical boxes around bromodomain ZA loops, and sequence numbering aligned to S. cerevisiae Bdf1. Output figures were generated as publication-quality PDF.

Chapter 3: Results

Chapter 3: Results

I. Chromatin organization and compaction in yeast spores

To ensure long-term survival, spores encapsulate their genome in a protective state compatible with prolonged quiescence and rapid reactivation. In *Saccharomyces cerevisiae*, post-meiotic differentiation is associated with extensive chromatin reorganization and compaction, as previously reported in (Govin et al., 2010; García-Oliver et al., 2017). This developmental process is initiated by nutrient limitation, specifically nitrogen starvation in the presence of a non-fermentable carbon source, such as acetate (Figure 20A). Progression through sporulation is further coordinated by successive waves of gene expression that ensure proper meiotic division and spore differentiation (Govin & Berger, 2009). Upon the reintroduction of fermentable carbon sources, particularly glucose, spore germination is triggered with a rapid activation of metabolic reprogramming driving the transition from quiescence to vegetative growth (Joseph-Strauss et al., 2007).

Quantitative assessment of nuclear compaction in yeast spores. Reasoning that extensive chromatin compaction would impact global nuclear morphology, we first set out to quantitatively compare nuclear size between vegetative yeast cells and spores. Therefore, we selected nuclear pore complex (NPC) components to mark the nuclear envelope, taking advantage of their status as recognized standards in quantitative microscopy (Thevathasan et al., 2019) and their stable expression during sporulation (Govin et al., 2010; García-Oliver et al., 2017). Several NPC proteins were evaluated according to the stability of their expression during sporulation and compatibility with spore formation (Deutschbauer et al., 2002). To confirm that C-terminal fluorescent tagging did not impair sporulation efficiency, candidate strains from the yeast GFP collection were systematically tested (Huh et al., 2003). Based on these criteria, Nup84 was selected as the most suitable nuclear envelope marker (Figure 20B). A NUP84-GFP fusion was generated in the SK1 background, and its proper localization at the nuclear periphery was validated by confocal fluorescence microscopy comparison with the original collection strain (Figure 20B).

With this reporter validated, we then used confocal fluorescence microscopy to compare nuclear and cellular dimensions between vegetative cells and mature spores (Figure 20C).

Using the Nup84-GFP signal to define nuclear contours, we quantified the nuclear area and estimated total volumes based on a spherical geometry assumption. This analysis demonstrated a reduction in nuclear volume within spores ~1.12 µm³ relative to vegetative cells ~1.7 µm³ (Figure 20D). Moreover, by leveraging cell wall autofluorescence, we estimated the total cellular volumes, finding that spores are substantially smaller than vegetative cells, averaging 18 µm³ and 30 µm³, respectively (Figure 20E). These measurements correspond to a nuclear-to-cellular volume ratio of ~5–6% in vegetative cells and ~6–7% in spores, indicating that despite overall size reduction, the relative nuclear occupancy remains broadly comparable between the two states. These values are consistent with previously reported nuclear and cellular dimensions in *S. cerevisiae* (Jorgensen et al., 2002; Bryan et al., 2010).

Conversely, the small size of spore nuclei imposed intrinsic resolution limits on conventional confocal microscopy, potentially affecting the accuracy of these measurements. To overcome this, in collaboration with Lisa Germain and Guillermo Orsi, we implemented a super-resolution strategy using Stochastic Optical Reconstruction Microscopy (STORM). This technique enables the visualization of subcellular structures beyond the diffraction limit by relying on the stochastic activation of photo-switchable fluorophores. By capturing thousands of individual imaging frames, we were able to reconstruct high-resolution localization maps that surpass the constraints of standard optical systems. (Orsi et al., 2023b)(Figure 20F). I performed all cellular treatments and coverslip preparations; L. Germain and G. Orsi subsequently handled image acquisition and data analysis.

As GFP is not directly compatible with STORM imaging, the Nup84-GFP fusion protein was detected using an anti-GFP antibody coupled to a STORM-compatible fluorophore (e.g., Alexa Fluor 647). Efficient antibody diffusion in fixed yeast required permeabilization of the spore wall. However, the outermost dityrosine layer renders spores resistant to enzymatic digestion. To circumvent this limitation, we disrupted this layer by deleting *DIT1*, thereby enabling zymolyase-mediated digestion (Figure 20G, H) and subsequent antibody access. Under these conditions, Nup84-GFP could be robustly detected by STORM, allowing high-resolution visualization of the nuclear envelope. The overall nuclear morphology was consistent with that observed by confocal microscopy, while exhibiting a markedly improved spatial resolution. Discrete punctate signals corresponding to individual nuclear pore complexes were resolved,

revealing a slightly heterogeneous distribution along the nuclear periphery (Figure 20I). This approach further enabled accurate quantification of nuclear volume based on high-resolution nuclear envelope segmentation demonstrating a five-fold nuclear compaction between vegetative cells and spores (Figure 20J).

Together, these analyses demonstrate a marked nuclear compaction during the transition to the spore state, while preserving a relatively stable nuclear-to-cellular proportion. This structural reorganization highlights the adaptation of yeast spores to long-term quiescence and likely contributes to their capacity for rapid reactivation upon germination.

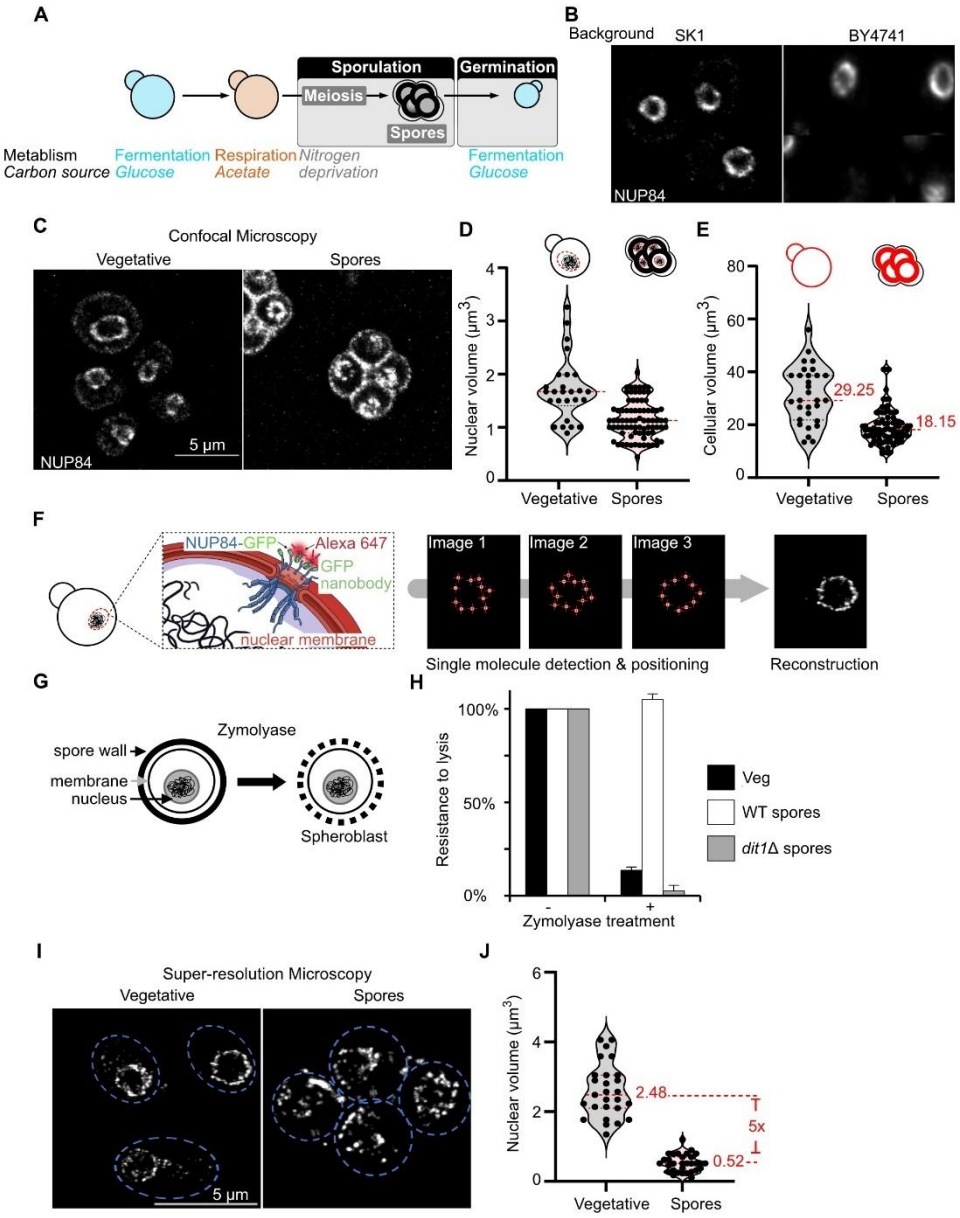

Figure 20: **Quantitative assessment of nuclear compaction in yeast spores. (A)** Schematic representation of sporulation induction following glucose depletion and the switch to acetate-based respiration. Nitrogen starvation triggers meiosis, producing four quiescent haploid spores that remain dormant until favorable conditions induce germination. **(B)** To visualize the NPC architecture, Nup84 was fused to a C-terminal GFP tag. The panel displays classical immunofluorescence in the SK1 background, with the resulting signal validated against published Nup84 distribution patterns in the BY4741 background (right). **(C)** Representative confocal images illustrating the morphology of the nuclear membrane in vegetative cells (right) and mature spores (left). **(D)** Quantitative analysis derived from confocal imaging (~300 cells). Assuming a spherical nuclear geometry, the nuclear volume was calculated based on surface area, revealing a significant reduction in nuclear size in spores compared to vegetative cells. **(E)** Comparative analysis of total cellular volume, demonstrating a marked decrease in the physical dimensions of spore cells relative to their vegetative counterparts. **(F)** Schematic of the labeling strategy for Nup84-GFP: anti-GFP Nanobodies (green) coupled to Alexa 647 fluorophores (red). Upon excitation, the stochastic "blinking" effect of the dye allows for the precise localization of individual molecules and the super-resolution reconstitution of the NPC structure. **(G)** Schematic of the modified spore wall in a dit1Δ background. The removal of the outermost dityrosine layer facilitates effective wall digestion by the Zymolyase enzyme, granting probes access to the interior. **(H)** Analysis confirming the compromised integrity of dit1Δ spores. Sensitivity is measured by cellular death (lysis) following incubation in 1% SDS. **(I)** Super-resolution images of Nup84 distribution, providing a side-by-side structural comparison of the nuclear pore arrangement in vegetative cells and mature spores. **(J)** High-precision volumetric measurements derived from super-resolution imagery (~30 cells) provide a quantitative refinement of the nuclear compaction observed during the vegetative-to-spore transition. Scale bars = 5 µm

Chromatin undergoes extensive compaction and spatial reorganization in spores. To further characterize chromatin organization within the highly compacted spore nucleus, we compared DNA distribution in vegetative cells and spores using confocal microscopy. Cells were fixed with paraformaldehyde, permeabilized, and stained with DAPI. Nuclear DNA volume was estimated using the same strategy as described above.

In vegetative cells, DNA occupied an average volume of ~1.9 μm^3, corresponding to approximately 75% of the total nuclear volume (Figure 21A, B). This estimate is consistent with previous observations indicating that chromatin occupies most of the nuclear space in proliferating yeast cells (Neumann & Nurse, 2007; Fujimoto et al., 2025)

On the other hand, DNA in spores occupied an estimated volume of ~0.12 μm^3, representing an approximately 16-fold reduction relative to vegetative cells (Figure 21 A, B). This DNA volume accounted for only ~24% of the total nuclear volume in spores. This observation was unexpected given the already reduced nuclear size and suggests that chromatin compaction in spores is accompanied by substantial changes in its spatial organization within the nucleus.

However, given the limited resolution of confocal microscopy at this scale as previously mentioned, these measurements likely underestimate chromatin density and structural heterogeneity. This prompted us to employ super-resolution imaging approaches to further resolve chromatin organization in spores. For this reason, we employed STORM with a DNA dye compatible with stochastic fluorophore switching, allowing precise visualization of nuclear DNA organization at high spatial resolution (Figure 21C). Leveraging signal-density analysis of super-resolution data, we further characterized the heterogeneous landscape of the yeast nucleus. In vegetative cells, chromatin is organized into a punctate, non-uniform pattern featuring discrete regions of elevated local density (Figure 21D). Conversely, spores exhibit a pronounced spatial partitioning, where the chromatin mass is consolidated into a primary high-density focus accompanied by a secondary diffuse component (Figure 21D). These findings illustrate a fundamental structural transition in chromatin distribution during sporulation. The sensitivity of this super-resolutive approach enabled the visualization of individual chromatin fibers indicated by red arrows across both developmental stages (Figure 21D). A comparative analysis of signal-density distributions further underscored this transition; while vegetative

nuclei consist primarily of low-density regions, spores are markedly enriched in high-density pixels, reflecting a state of advanced chromatin compaction (Figure 21E). Together, these observations indicate a major redistribution and consolidation of chromatin during spore maturation. Importantly, this subnuclear heterogeneity is consistent with established super-resolution studies of chromatin in other systems (Clément et al., 2018; Orsi et al., 2023), suggesting that these patterns reflect authentic biological structures rather than imaging artifacts.

Finally, super-resolution analysis of Nup84 revealed a five-fold reduction in nuclear volume between vegetative cells and spores. Consistently, DAPI staining showed a 16-fold compaction of chromatin between the two states, while the nuclear-to-cellular proportion remained relatively stable (Figure 21F). Furthermore, signal-density analysis indicated that vegetative cells display a more heterogeneous and low-density chromatin organization, whereas spores exhibit a more compact architecture with a dominant high-density focus. Together, these results indicate that sporulation is accompanied by a major reorganization and compaction of both the nucleus and chromatin.

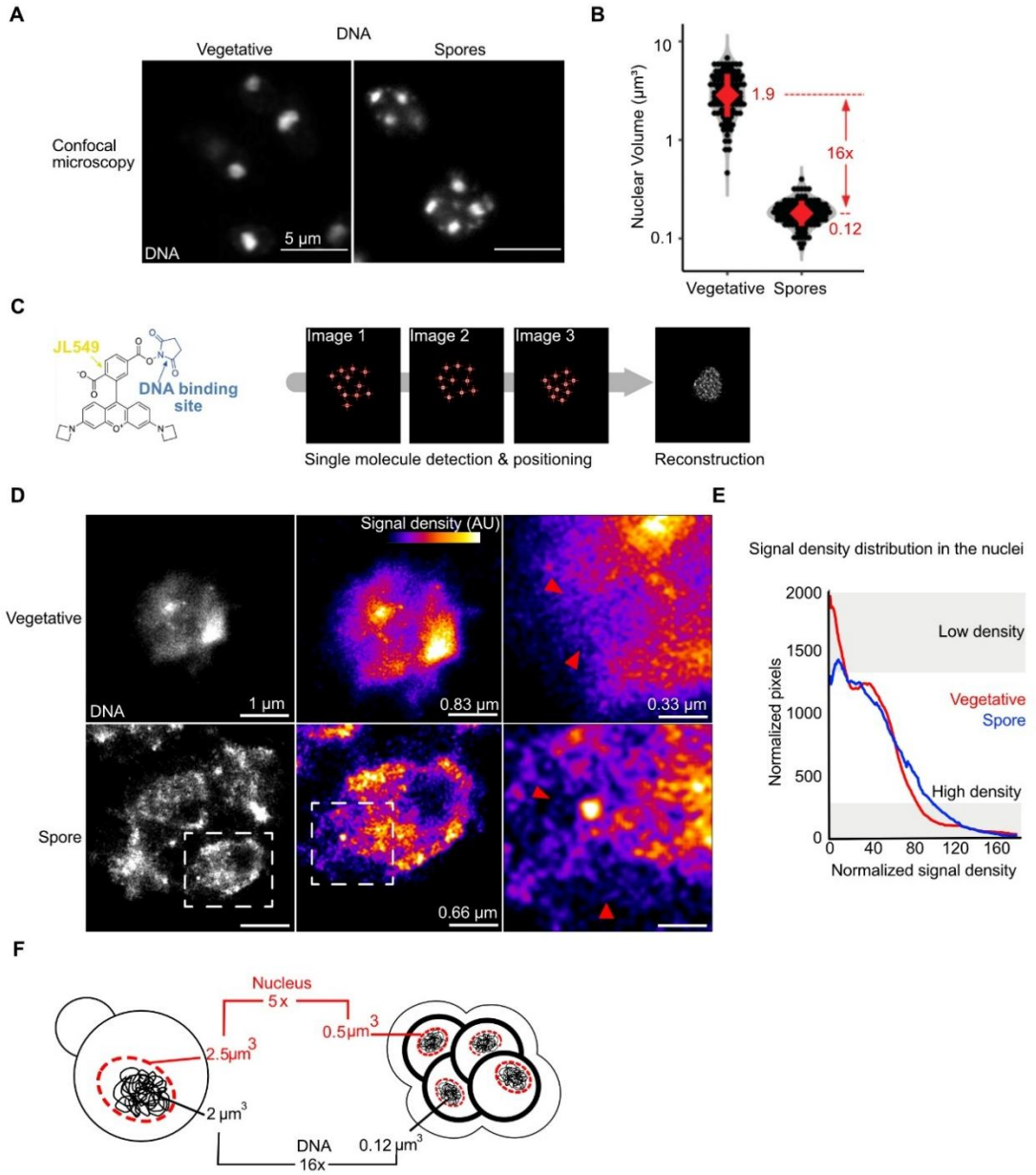

Figure 21: **Comparative spatial organization and compaction of the yeast genome. (A)** Confocal microscopy images of DAPI-stained nuclei illustrating the transition from a broad, nucleoplasm-filling distribution in vegetative cells to a highly restricted and compacted DNA signal in mature spores. Scale bars = 5 µm **(B)** Quantitative assessment of nuclear DNA volume. In vegetative cells, DNA occupies an average of ~1.9 µm³ (~75% of total nuclear volume), consistent with active transcription states. On the other hand, spore DNA collapses to ~0.12 µm³, a 16-fold reduction accounting for only ~24% of the nuclear space. **(C)** Schematic of the STORM approach using a specialized DNA-compatible dye. This method bypasses the diffraction limit of confocal microscopy, utilizing stochastic photo-switching to resolve fine-scale chromatin architecture (as described in Figure I). **(D)** STORM reconstructions of DNA reveal the internal heterogeneity of the genome in vegetative cells and spores. Vegetative chromatin displays a punctate and broadly distributed pattern, whereas spores show a distinct reorganization characterized by a dominant high-density focus and a secondary diffuse signal. Signal-density reconstruction highlights the specific distribution of H4ac and reveals chromatin fibers in spores, indicated by red arrows. **(E)** Preliminary quantitative analysis of signal-density distribution from the super-resolution data provides a precise assessment of nuclear volume reduction. Using refined DNA localization, these measurements confirm strong chromatin compaction during the transition to the spore state, as reflected by the higher proportion of low-density normalized pixels in vegetative cells compared with spores. **(F)** A conceptual model summarizing the dramatic structural changes of the nucleus. The schematic illustrates the transition from a large, transcriptionally active vegetative nucleus, where chromatin occupies ~75% of the space, to the small, compact spore nucleus. This transition is defined by a global decrease in nuclear volume and the ultra-compaction of the genome into a localized, high-density chromatin state.

II. Chromatin accessibility and histone acetylation landscapes in spores

Assessment of chromatin accessibility in spores. Following the observations in chromatin reorganization, we sought to characterize the molecular landscape underlying this DNA spatial heterogeneity. In collaboration with the Epinomics platform at the Institute for Advanced Biosciences (IAB), we investigated chromatin accessibility in both vegetative cells and spores using the Assay for Transposase-Accessible Chromatin with high-throughput sequencing (ATAC-seq). This approach allowed us to determine how the physical compaction observed via microscopy correlates with the global accessibility of the genome during the transition to the dormant spore state. ATAC-seq relies on the hyperactive Tn5 transposase, which inserts sequencing adapters into accessible regions of the genome, enabling genome-wide profiling of chromatin accessibility. The principle of the assay is illustrated in Figure 22A. I conducted the initial cellular preparation and nuclei purification. Subsequent ATAC-seq library preparation was performed by E. Moutaux, followed by computational analysis by M. Mohammed Ali.

Following extensive optimization, we successfully generated and sequenced ATAC-seq libraries of high quality (Figure 22B). The fragment length distribution profiles revealed a globally conserved chromatin organization between vegetative cells and spores, characterized by the expected enrichment of subnucleosomal fragments (~100 bp) and mononucleosomal fragments (~200 bp). These patterns reflect the preferential accessibility of the Tn5 transposase to both nucleosome-free regions (NFRs) and nucleosome-associated DNA. This organizational signature is further supported by V-plots (Figure 22C), which exhibit a robust enrichment of short fragments and a well-defined nucleosomal periodicity, particularly prominent in vegetative cells. These two-dimensional representations display fragment length as a function of genomic position relative to a reference point (here, transcription start sites, TSS) and are commonly used to visualize chromatin organization from sequencing-based assays. The characteristic V-shaped pattern reflects phased nucleosomes flanking accessible regions, with shorter fragments mapping near nucleosome-free regions and longer fragments corresponding to nucleosome-protected DNA.

In vegetative cells, the fragment size distribution indicates high tagmentation efficiency, consistent with established yeast benchmarks. We believe the conditions presented here represent the most robust optimization for ATAC-seq in yeast to date, proving equally

applicable to both vegetative and spore states. While such distributions are characteristic of high-quality ATAC-seq datasets (Buenrostro et al., 2013, 2015), we note that excessive tagmentation or intrinsic enzymatic biases can often shift this balance toward shorter fragments (Schep et al., 2015). This behavior mirrors MNase-seq approaches, which capture nucleosome positioning but remain sensitive to digestion biases (Mieczkowski et al., 2016). Consistent with this interpretation, we successfully detected signals corresponding to fragile nucleosomes within NFRs, matching previously established benchmarks in vegetative cells and confirming the sensitivity of our optimized protocol. IGV (Integrative Genomics Viewer) profiles (Figure 22D) reveal canonical accessibility patterns across both states, although we noted an increased background signal in spores compared to vegetative cells. Furthermore, metagene analysis centered on Transcription Start Sites (TSS) validates the assay's performance, demonstrating clear enrichment at the -1 and +1 nucleosomes (Figure 22E). Notably, we observed a relative decrease in signal within NFRs in spores; this is consistent with a more compacted chromatin architecture and potential over-tagmentation effects, which may alter the recovery of specific fragment populations in the spore state.

Altogether, these data indicate a global reduction in chromatin accessibility in spores (Figure 22E), in agreement with their highly compacted chromatin state. Importantly, the generation of these datasets required extensive optimization, and the current results are based on a single biological replicate. Nevertheless, they demonstrate the feasibility of ATAC-seq in spores, and additional replicates are currently being generated to further validate these observations.

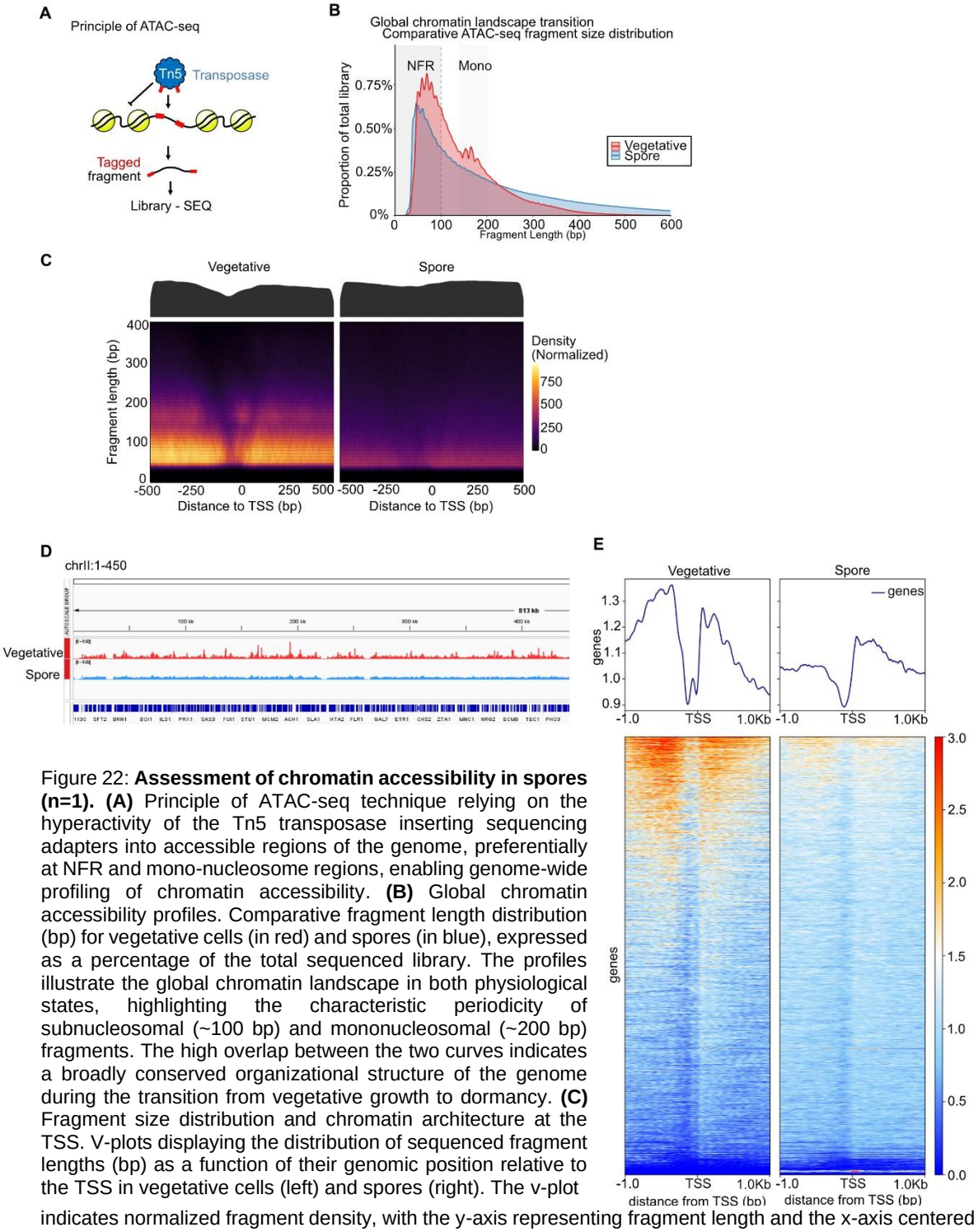

Figure 22: **Assessment of chromatin accessibility in spores (n=1). (A)** Principle of ATAC-seq technique relying on the hyperactivity of the Tn5 transposase inserting sequencing adapters into accessible regions of the genome, preferentially at NFR and mono-nucleosome regions, enabling genome-wide profiling of chromatin accessibility. **(B)** Global chromatin accessibility profiles. Comparative fragment length distribution (bp) for vegetative cells (in red) and spores (in blue), expressed as a percentage of the total sequenced library. The profiles illustrate the global chromatin landscape in both physiological states, highlighting the characteristic periodicity of subnucleosomal (~100 bp) and mononucleosomal (~200 bp) fragments. The high overlap between the two curves indicates a broadly conserved organizational structure of the genome during the transition from vegetative growth to dormancy. **(C)** Fragment size distribution and chromatin architecture at the TSS. V-plots displaying the distribution of sequenced fragment lengths (bp) as a function of their genomic position relative to the TSS in vegetative cells (left) and spores (right). The v-plot indicates normalized fragment density, with the y-axis representing fragment length and the x-axis centered on the TSS. It illustrates the characteristic enrichment of subnucleosomal fragments (<100 bp) within the NFR and the defined V-shaped patterns of mono-nucleosomal fragments (~200 bp) flanking the TSS, reflecting precise nucleosome positioning in both cell states. **(D)** Representative genomic tracks of chromatin accessibility. IGV profiles displaying normalized ATAC-seq signal across the chromosome II for vegetative cells (blue) and spores (red). The tracks illustrate differential accessibility patterns between vegetative cells and spores. **(E)** Metagene analysis of chromatin accessibility centered at TSS. Average ATAC-seq signal density aligned to the TSS for all genes in vegetative cells and spores. Profiles exhibit characteristic enrichment at the −1 and +1 nucleosomes. The spore profile shows a relative decrease in signal intensity at the NFR, consistent with increased chromatin compaction and potential effects of over-tagmentation in this state.

III. Histone acetylation and chromatin compaction in spores

Intriguingly, while the extensive chromatin reorganization and compaction characteristic of sporulation would intuitively suggest an accumulation of repressive, transcriptionally silent epigenetic marks, the opposite occurs. Our team previously demonstrated that this developmental window is instead marked by permissive and active remodeling signatures, specifically the phosphorylation of histone H4 serine 1 (H4S1ph) alongside a prominent wave of histone H4 hyperacetylation at lysine residues K5, K8, K12, and K16, leading to a significant enrichment in the mature spore (Govin et al., 2010).

Distribution of H4 acetylation in yeast spores. We corroborated this striking hyperacetylation through Western blot analysis, confirming that the H4ac signal remains highly concentrated even within the condensed architecture of the spore nucleus (Figure 23A). This observation is particularly intriguing given the highly compacted state of the spore nucleus, as histone acetylation is typically associated with chromatin relaxation. This apparent paradox suggests that H4 acetylation may fulfill a distinct structural or regulatory role in spores, potentially contributing to chromatin organization while preserving the capacity for rapid transcriptional reactivation upon germination.

Building upon our microscopy-based visualization of chromatin architecture, we applied a similar imaging approach to examine the subnuclear localization of H4 acetylation. Using immunofluorescence in vegetative cells and mature spores, confocal microscopy revealed a localized nuclear H4ac signal across both conditions. Intriguingly, we observed clear differences in both the intensity and spatial pattern of H4 acetylation between the two states, highlighting the need for detailed quantitative profiling (Figure 23B-Upper panels).

We next applied super-resolution microscopy to refine the spatial characterization of H4 acetylation. This approach uncovered a heterogeneous nuclear pattern, characterized by discrete foci interspersed with regions of lower signal intensity (Figure 23B-Lower panels). Such subnuclear organization was not detectable using conventional confocal microscopy, highlighting the increased spatial resolution provided by this method. The identity and functional relevance of these H4ac-enriched regions remain to be explored but may reflect localized chromatin domains involved in transcriptional priming or structural organization of

the genome. Further optimization of super-resolution imaging, including dual-color approaches, will be required to assess their spatial relationship with DNA density and chromatin compaction.

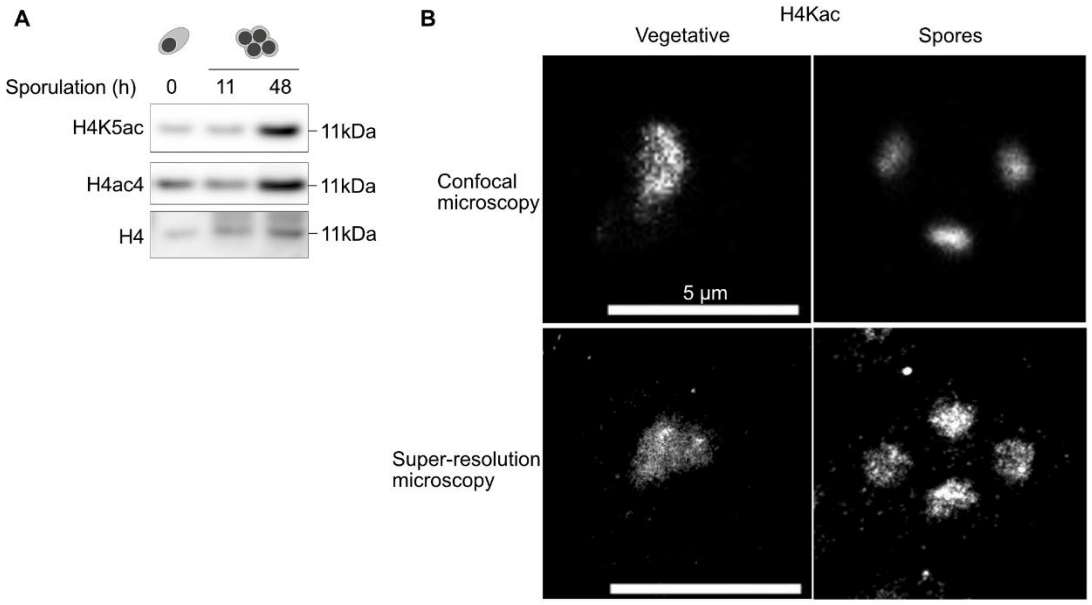

Figure 23: **Distribution of H4ac in yeast spores. (A)** Western blot analysis confirms a significant enrichment of H4ac in mature spores relative to vegetative cells, consistent with previously established benchmarks of sporulation-induced chromatin remodeling (Govin et al., 2010). **(B)** Spatial resolution of H4ac domains. **(Upper panels)** Conventional confocal microscopy shows global nuclear localization of H4ac in both vegetative cells and spores, though with differing signal intensities. **(Lower panels)** Super-resolution imaging reveals a previously uncharacterized, heterogeneous subnuclear architecture. In the highly compacted spore nucleus, H4ac is sequestered into discrete, high-intensity foci. This organized distribution suggests that H4ac may serve a specialized structural role, potentially acting as localized domains for transcriptional priming to facilitate rapid reactivation during germination. Scale bars = 5 µm.

Genome-wide distribution of H4 acetylation by CUT&Tag-seq. While immunofluorescence provided qualitative insights into nuclear localization, determining the precise genomic distribution of H4ac required a high-resolution profiling approach. We therefore conducted CUT&Tag-seq (Cleavage Under Targets and Tagmentation) in both vegetative cells and spores, in collaboration with the Epinomics platform. This targeted profiling approach utilizes a protein A-Tn5 (pA-Tn5) fusion recruited to specific genomic loci via an anti-H4ac antibody. Upon activation, the tethered transposase cleaves the adjacent DNA and simultaneously ligates sequencing adapters, releasing high-resolution fragments of the targeted chromatin (Figure 24A). By leveraging this method, we were able to map H4ac occupancy under native conditions, providing a precise landscape of histone acetylation patterns across the transition

from active growth to dormancy. I conducted the initial cellular preparation and nuclei purification. Subsequent CUT&Tag library preparation was performed by E. Moutaux, followed by computational analysis by M. Mohammed Ali.

This analysis was performed using two independent CUT&Tag-validated antibodies against acetylated histone H4 (pan-H4ac), obtained from Active Motif and Merck, respectively, to ensure reproducibility and specificity in both vegetative cells and spores (Figure 24B). In spores, experiments were performed in a dit1Δ background to allow efficient spore wall digestion and access of reagents to chromatin. Bioanalyzer profiles showed fragment size distributions consistent with previously published CUT&RUN datasets (not shown), indicating successful enrichment and appropriate library complexity. Libraries were subsequently sequenced, enabling genome-wide analysis of H4ac distribution.

To further assess data quality and fragment organization, we generated V-plots. In both vegetative cells and spores, V-plots revealed two main fragment populations: subnucleosomal and nucleosomal fragments (Figure 24C). Based on this distribution, analyses were restricted to fragments in the 140–250 bp range, corresponding to mononucleosome-associated DNA. Following this filtering step, CUT&Tag profiles were aligned at transcription start sites. This analysis revealed a clear enrichment of H4c at the +1 nucleosome downstream of the TSS, consistent with previously reported localization patterns of H4ac in yeast chromatin (Figure 24D).

Unexpectedly, a detectable H4ac signal was also observed upstream of the nucleosome-free region (NFR). Most genome-wide datasets describing H4ac in yeast have been generated following MNase digestion of chromatin and enrichment of individual nucleosomes by ChIP-seq, as in (Weiner et al., 2015). Therefore, this upstream signal should be interpreted with caution, as it may reflect differences inherent to the CUT&Tag approach or to fragment selection and remains under further investigation.

Importantly, the two independent antibodies yielded highly similar genome-wide profiles in vegetative cells (Figure 24D), supporting the robustness of the approach. In spores, overall H4ac distribution patterns were largely conserved, although signal intensity was globally reduced (Figure 24D). This decrease is likely attributable to the highly compacted state of spore

chromatin, which may limit antibody accessibility and transposase activity, rather than reflecting a true loss of histone acetylation.

Sporulation is characterized by extensive and rapid reprogramming of gene expression, involving successive waves of transcriptional activation and repression. In this context, an important question is how H4 acetylation dynamics relate to these transcriptional changes, mainly how long promoter-associated acetylation is maintained following transcriptional shutdown. Sporulation thus represents a powerful model to investigate the temporal coupling between histone acetylation and transcriptional regulation. However, addressing these questions would require a dedicated kinetic analysis and therefore falls beyond the scope of the present work.

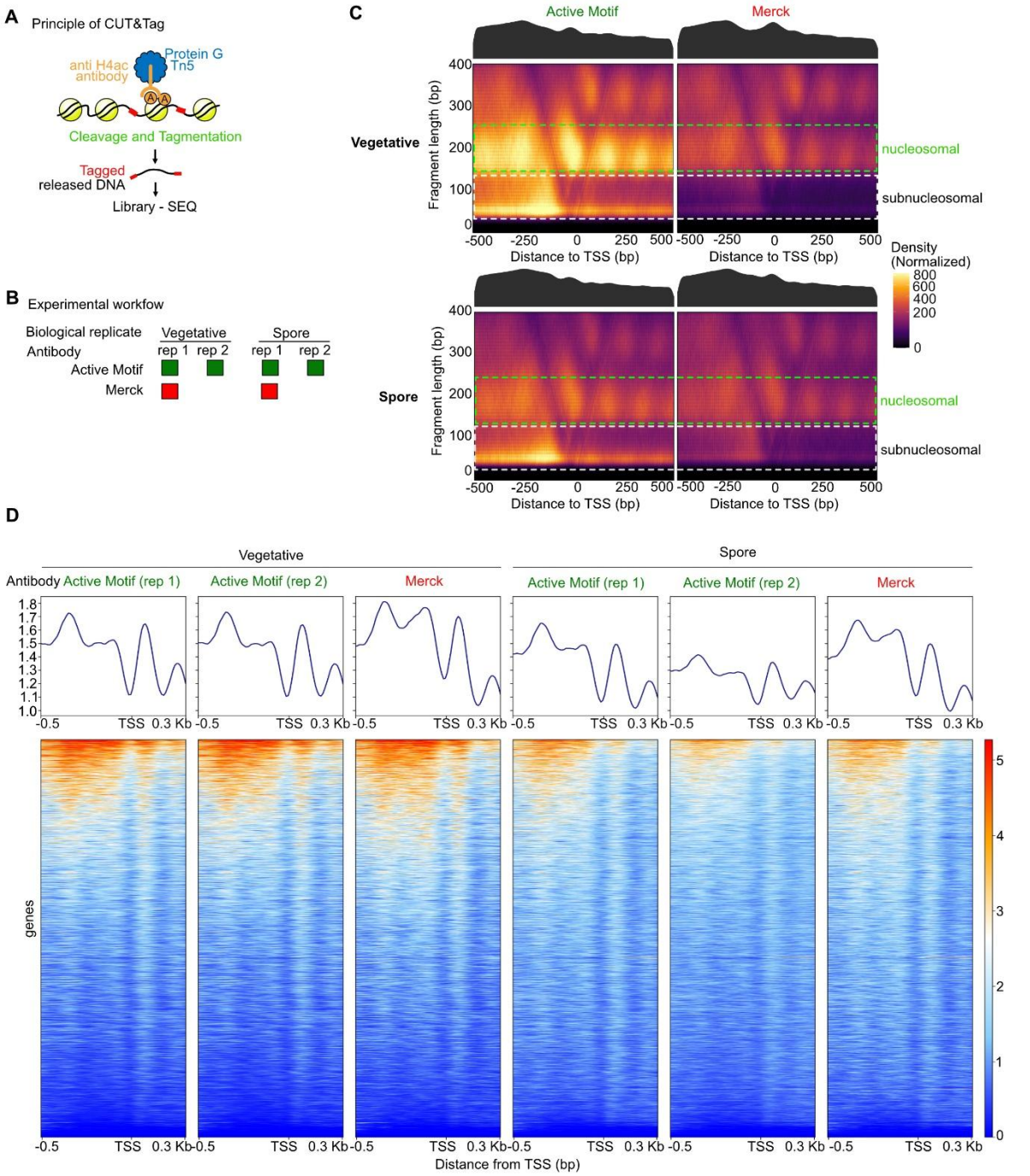

Figure 24: **Genome-wide Profiling of Histone H4 Acetylation via CUT&Tag-seq. (A)** Schematic of the CUT&Tag-seq principle. An anti-H4ac antibody recruits a Protein A-Tn5 (pA-Tn5) fusion protein to acetylated genomic loci. Activation of the tethered transposase results in simultaneous DNA cleavage and adapter ligation, releasing high-resolution fragments for sequencing. This method allows for mapping the H4ac landscape under native conditions during the transition from vegetative growth to dormancy. **(B)** Experimental workflow: Two independent pan-H4ac antibodies (Active Motif and Merck) were utilized across both cell states vegetative and spores to assess proper signalling. **(C)** V-plots generated to assess library organization in vegetative cells and spores. The plots resolve two distinct populations: subnucleosomal (in grey) and nucleosomal fragments (in green). To ensure data specificity, subsequent genome-wide analyses were restricted to the 140–250 bp range, corresponding to DNA protected by a single nucleosome. **(D)** Alignment of filtered CUT&Tag profiles across the yeast genome. Consistent with established yeast chromatin architecture, a robust enrichment of H4ac is observed at the +1 nucleosome directly downstream of the TSS.

IV. Functional analysis of BET bromodomain biology across species

The persistent enrichment of histone H4 acetylation in spores, despite the overall chromatin compaction, raised the question of how this permissive mark is recognized and interpreted within such a dense nuclear environment. Acetylated lysines are typically read by bromodomains, evolutionarily conserved structural modules that recruit downstream regulatory factors to shape chromatin function. Among these, the BET family defines a specialized class of acetylation readers characterized by tandem bromodomains and an extra-terminal domain. In mammals, BET proteins such as BRD4 and BRDT play central roles in transcriptional control and chromatin regulation, including in highly dynamic developmental contexts.

In budding yeast, the BET family is represented by the paralogs Bdf1 and Bdf2. Previous work from the laboratory showed that Bdf1, but not Bdf2, is required for efficient sporulation, and that this requirement specifically depends on bromodomain integrity. These findings strongly suggest that acetylation-dependent chromatin reading by Bdf1 contributes to the execution of the sporulation program.

Cross-species analysis reveals unexpected features of BET bromodomain–chromatin interactions. To investigate the extent to which BET bromodomain functions are conserved across species, we compared yeast Bdf1 bromodomains with their human counterparts from BRD4 and BRDT. Our initial goal was to determine whether human bromodomains could substitute for those of Bdf1 and thereby provide a framework for pharmacological manipulation in yeast. To address this question, we engineered chimeric proteins in which Bdf1 bromodomains were replaced with their human equivalents (Figure 25A). This strategy was motivated by previous work from our laboratory demonstrating the successful implementation of bromodomain-swapping approaches in pathogenic yeasts, including *Candida albicans* and *Candida glabrata* (Wei et al., 2025). Given the close evolutionary relationship between *C. glabrata* and *S. cerevisiae*, we anticipated that this strategy would be transferable to budding yeast.

However, this approach did not provide the expected pharmacological framework. Instead, it uncovered unexpected features of BET bromodomain biology that became a central focus of this work. Building on these observations, we performed a detailed structural comparison

between yeast and human BET bromodomains to identify features that might underlie their functional divergence.

Structural analysis of BET bromodomains in human and yeast. Sequence alignment of the tandem BET bromodomains from yeast Bdf1 and their human counterparts, BRD4 and BRDT, revealed a high degree of evolutionary conservation (Figure 25B). Key structural motifs, particularly the residues essential for acetyl-lysine recognition, remained largely invariant across species, consistent with previous observations in *S. cerevisiae*, *C. albicans*, and *C. glabrata* (García-Oliver et al., 2017; Mietton et al., 2017; Wei et al., 2025). These observations are consistent with the overall preservation of the canonical bromodomain fold and acetyl-lysine binding pocket across species. While the overall architecture of the acetyl-lysine binding pocket remains conserved, we identified two pivotal amino acid substitutions that fundamentally alter the local chemical environment of the BD1 domain. At position 172 of Bdf1 BD1, the positively charged arginine (R172) found in *S. cerevisiae* has been replaced by a neutral, bulky hydrophobic tryptophan (W) in human BRD4 and BRDT (Figure 25B). Concurrently, a second significant divergence occurs at position 237, where the small, uncharged glycine (G237) is substituted by a negatively charged aspartate (D) in the human counterparts (Figure 25B). These coupled transitions, shifting from a basic to a hydrophobic residue at site 172, and from a neutral to an acidic residue at site 237, likely impose significant changes on the electrostatic potential and steric constraints of the binding pocket.

This trend of divergence extends to the BD2 domain, where a tyrosine (Y338) in *S. cerevisiae*, previously identified as a key differential residue, is substituted by a tryptophan (W) in human BETs (García-Oliver et al., 2017). Given the strategic positioning of these three residues within the acetyl-lysine coordination sphere, we hypothesize that these specific substitutions drive a functional divergence between the yeast and human BET proteins by altering their substrate affinity or specificity.

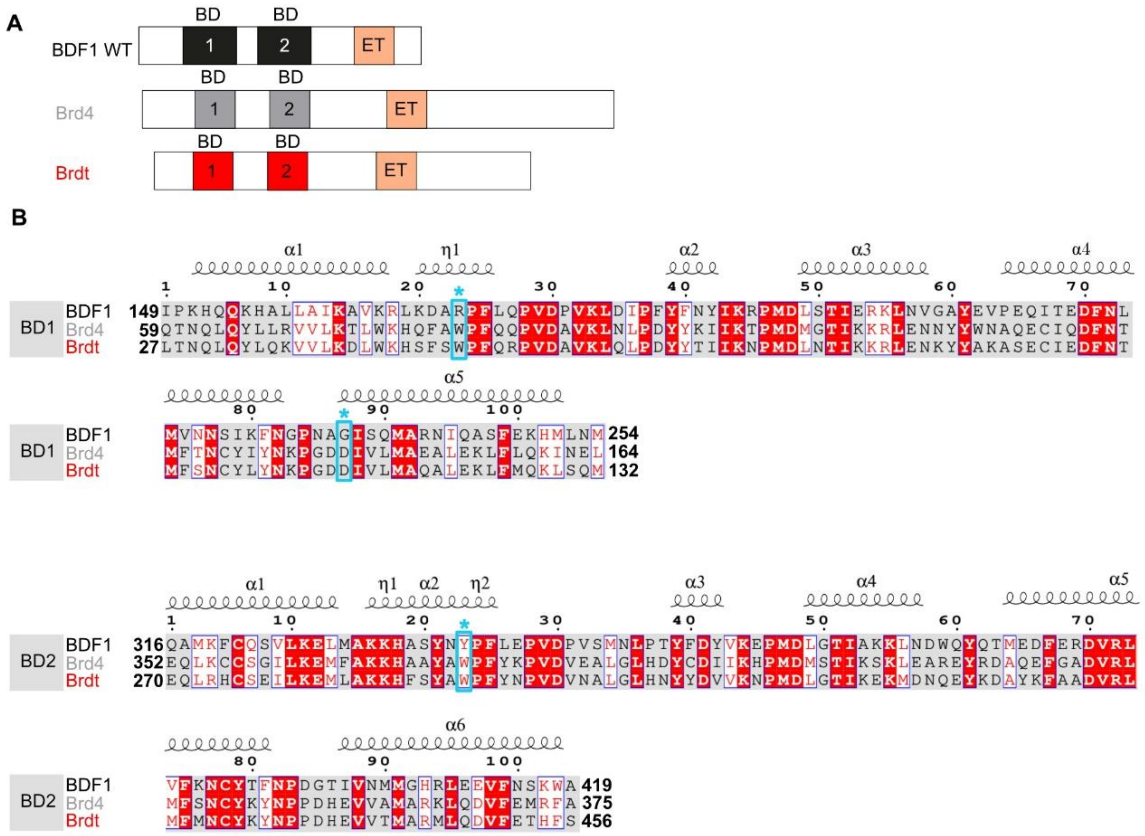

Figure 25: **Structural conservation and chimerization of BET bromodomains. (A)** Schematic representation of the domain-swapping strategy used to replace the tandem bromodomains (BD1 and BD2) of S. cerevisiae Bdf1 (in black) with their human counterparts from BRD4 (in grey) and BRDT (in red). **(B)** Multiple sequence alignment and structural comparison of Bdf1, BRD4, and BRDT bromodomains highlighting in bleu three pivotal amino acid substitutions that could alter the local chemical environment of the Kac-binding sphere.

A comprehensive comparative biochemical analysis of these bromodomains was initially planned in collaboration with the Institut de Biologie Structurale (IBS, Grenoble). However, due to circumstances beyond our control, these experiments could not be completed within the timeframe of this study. Ongoing work is currently focused on pull-down assays using synthetic peptides mimicking the H4 tail in either acetylated or unacetylated form, to test their direct interaction with recombinant bromodomains. At the time of manuscript submission, these results were not yet available.

Although structural conservation is high, our *in vitro* functional assays suggest significant differences in binding kinetics. Specifically, insights from biochemical assays developed for Bdf1 inhibitor discovery in pathogenic yeasts by the host laboratory indicate that the interaction between yeast BET bromodomains and acetylated histone substrates (H4ac) might be weaker than that of their human counterparts (not shown). This is further supported by

previous pull-down assays comparing ScBdf1-BD1 and BRD4-BD1, which demonstrated a markedly higher affinity for the human bromodomain. This trend extends to the BD2 domain, where the evolutionary substitution of tyrosine Y338 for W in the human pocket directly correlates with significantly enhanced binding to acetyl-lysine residues (Figure 26A) (García-Oliver et al., 2017). Such difference in affinity is consistent with the functional divergence highlighted in this study; a shift toward higher-affinity binding in humanized strains may alter the natural residence time of the protein on chromatin, potentially contributing to the differential chromatin-binding properties of BET proteins across species.

We further performed a detailed structural analysis of Bdf1 bromodomains. Notably, the bromodomains 1 and 2 of *S. cerevisiae* Bdf1 have previously been crystallized by the host laboratory, and their atomic structures are available, although not published. These findings were further supported by high-confidence Alpha Fold models, which showed strong agreement with our experimental data (not shown). However, experimentally determined structures remain the gold standard for structural interpretation.

Comparison of these structures with those of human BRD4 BD1 and BRDT BD1 bound to an H4 peptide acetylated on lysine residues K5 and K8 confirm that the molecular principles governing acetyl-lysine recognition are conserved, in agreement with the binding selectivity of Bdf1 bromodomains that we previously reported (García-Oliver et al., 2017).

In addition to acetyl-lysine recognition, bromodomains can exhibit DNA-binding properties through positively charged surface patches, as reported in (Miller et al., 2016b), and can even interact with nucleosomes directly (Zhu et al., 2025). Furthermore, DNA itself may modulate bromodomain recognition of acetylated lysine residues (Kalra et al., 2022). Accordingly, we compared the electrostatic surface potential of the S. cerevisiae Bdf1 bromodomains with those of human BRD4 and BRDT (Figure 26B). Our analysis indicates that the key amino acid substitutions identified earlier, specifically R172W and G237D in BD1, effectively shift the local environment from a basic (positively charged) surface in *S. cerevisiae* to an acidic (negatively charged) surface in the human counterparts (Figure 26B). A similar trend was observed for BD2, where the electrostatic surface shifted from an intermediate surface to a mainly acidic surface, largely driven by the loss of the tyrosine hydroxyl group and changes in the

surrounding loops. These global alterations in the acetyl-binding pocket surface charge suggest significant differences in acetylated lysine interaction capacity.

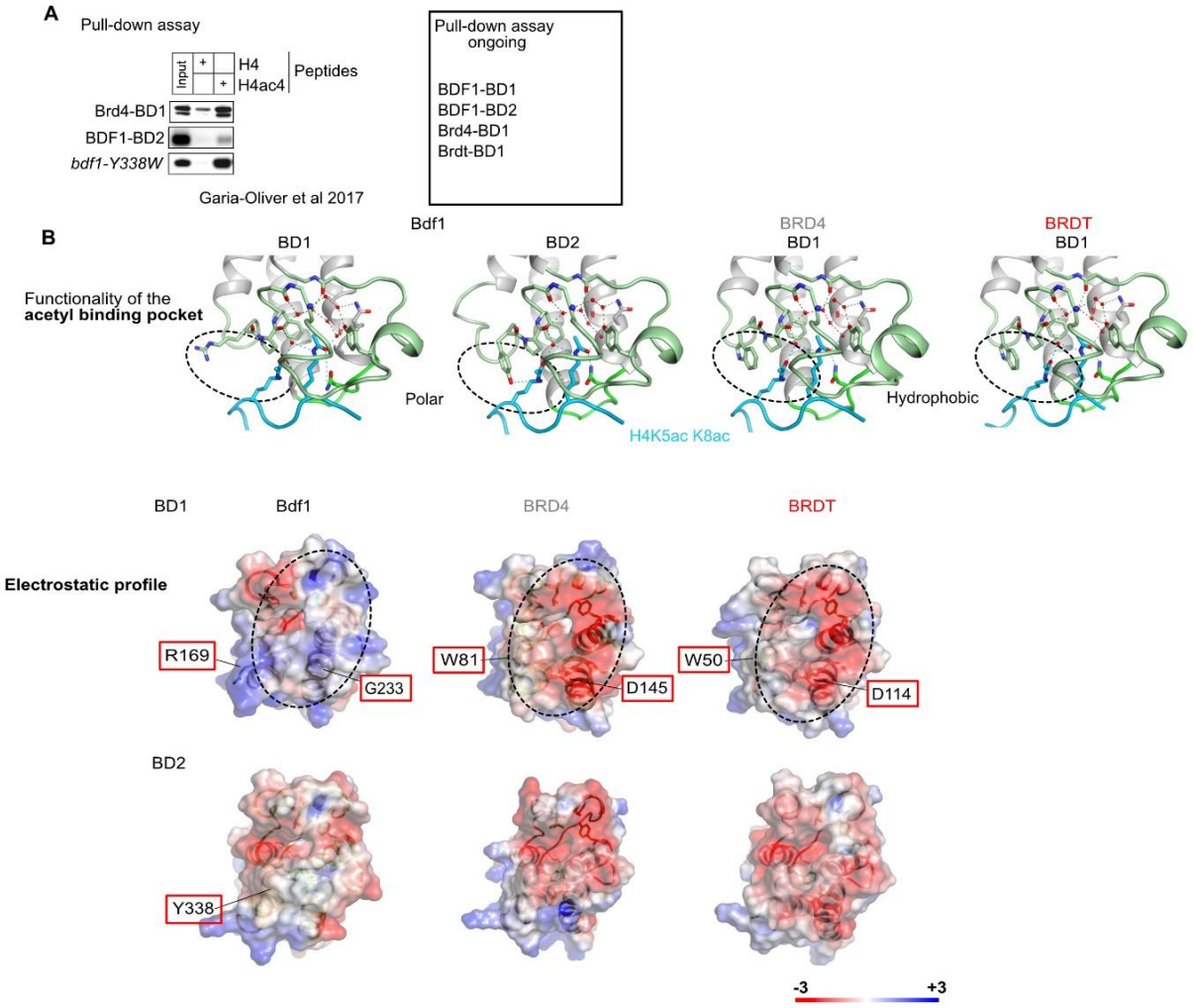

Figure 26: **Comparative structural and electrostatic analysis of yeast and human BET bromodomains. (A)** Pull down assay validating the differential affinity between S. cerevisiae and human bromodomains to acetylated lysine residues. *S. cerevisiae* Bdf1 exhibits inherently weaker interactions with acetylated H4 (H4ac) substrates, human BRD4 and BRDT demonstrate significantly higher affinities. This trend is driven by key substitutions, such as the Y338W mutation in BD2, which enhances binding to acetyl-lysine residues (García-Oliver et al., 2017). **(B) (Upper panels)** Comparison of experimentally determined *S. cerevisiae* Bdf1 structures (unpublished) with human BRD4/BRDT BD1 bound to H4K5acK8ac peptides using AlphaFold2 predictions for Bdf1 and BRDT interactions. The molecular principles of Kac recognition are conserved; however, the yeast binding pocket appears spatially larger potentially altering binding dynamics. **(Lower panels)** Species-specific electrostatic surface potential. Electrostatic maps of Bdf1, BRD4, and BRDT bromodomains are altered due to the evolutionary substitution of specific amino acids identified in red.

V. Bromodomain-dependent regulation of chromatin binding dynamics

Bromodomain-dependent regulation of BET protein mobility revealed by FRAP. To directly assess the functional consequences of bromodomain divergence, we investigated the nuclear mobility of Bdf1 expressed exogenously in human cells as a GFP-tagged fusion protein. Protein dynamics were quantified using fluorescence recovery after photobleaching (FRAP) (Figure 27A). In this approach, a defined nuclear region is selectively photobleached, and the recovery of fluorescence over time reflects the mobility and binding dynamics of the protein of interest, with slower recovery indicating more stable chromatin association. These experiments were conducted in collaboration with Dimitrios Skoufias in the team of Carlo Petosa at IBS. I performed the molecular cloning and generation of the chimeric constructs, while D. Skoufias conducted the subsequent cell culture, transfections, and FRAP experiments, including data acquisition and analysis. We then engineered chimeric Bdf1 proteins in which the endogenous bromodomains were replaced by those of human BRD4 or BRDT (Figure 27B). FRAP analyses revealed that these substitutions markedly alter Bdf1 mobility. Replacement with BRD4 bromodomains led to a significant decrease in mobility, consistent with stronger or more stable association with acetylated chromatin (Figure 27C). In contrast, and somewhat unexpectedly, substitution with BRDT bromodomains resulted in a distinct mobility profile, with a modest but reproducible increase in mobility compared to wild-type (WT) Bdf1 (Figure 27C).

These findings are notable, as they provide direct experimental evidence that BET bromodomains themselves contribute to the dynamic behavior of BET proteins in the nucleus. This has been difficult to assess in human BET proteins, which contain extensive intrinsically disordered regions implicated in biomolecular condensation and liquid–liquid phase separation (Sabari et al., 2018). By isolating the contribution of bromodomains within a simplified chimeric system, our results reveal an intrinsic and differential role of BET bromodomains in modulating chromatin engagement and nuclear dynamics.

In addition, we modulated both histone acetylation levels and the ability of BET bromodomains to engage their substrates using a pharmacological approach. Treatment with Trichostatin A (TSA), a potent inhibitor of class I and II histone deacetylases, leads to global hyperacetylation of histones by preventing the removal of the acetyl groups. Consistent with increased availability of acetylated binding sites, TSA treatment markedly reduced the mobility of Bdf1,

both in its WT form and its chimeric versions containing human bromodomains (Figure 27D-F). This effect was more pronounced for constructs harboring BRD4 or BRDT bromodomains, supporting the notion of stronger engagement of human BET bromodomains with the hyperacetylated chromatin.

We further examined the impact of direct bromodomain inhibition using JQ1, a well-characterized small molecule inhibitor that competitively binds the acetyl-lysine recognition pocket of BET bromodomains (Filippakopoulos et al., 2010). Strikingly, the addition of JQ1 in the presence of TSA partially restored Bdf1 mobility. More specifically, this rescue effect was nearly complete for chimeric proteins containing human bromodomains, whereas reached only ~50% of mobility recovery in the WT Bdf1(Figure 27D-F). This differential response likely reflects a higher affinity of JQ1 for human BET bromodomains compared to their yeast counterparts, consistent with previous observations from the host laboratory using Bdf1 bromodomains from *C. albicans* and *C. glabrata* (Mietton et al., 2017a; Wei et al., 2025).

Complementing the live-cell dynamics, we performed an orthogonal chromatin solubilization assay ito evaluate the biochemical stability of Bdf1–chromatin interactions under increasing ionic strength. Nuclei were purified from the three yeast strains analyzed in this study, WT, hBdf1(Brd4), and hBdf1(Brdt), and subjected to salt extraction to monitor the chromatin association of native and humanized Bdf1 across a gradient of NaCl concentrations. This assay provided an independent biochemical measure of Bdf1–chromatin binding in yeast and allowed us to assess whether bromodomain humanization altered the strength or stability of these interactions. The assay revealed a differential binding capacity for hBdf1(Brd4) (grey) and hBdf1(Brdt) (red) relative to WT across the salt gradient. These salt-dependent release profiles indicate that swapping bromodomain architectures directly modulates chromatin affinity, in agreement with the FRAP measurements. (Figure 27G).

Together, these results provide functional evidence that both histone acetylation levels and intrinsic bromodomain properties critically shape BET protein dynamics on chromatin. To further dissect these contributions, we are currently generating mutants targeting either the acetyl-lysine binding pocket or the putative DNA-interacting surfaces, in both WT and

humanized chimeric contexts. These mutants will allow us to define the respective roles of these bromodomains functions in regulating BET protein mobility.

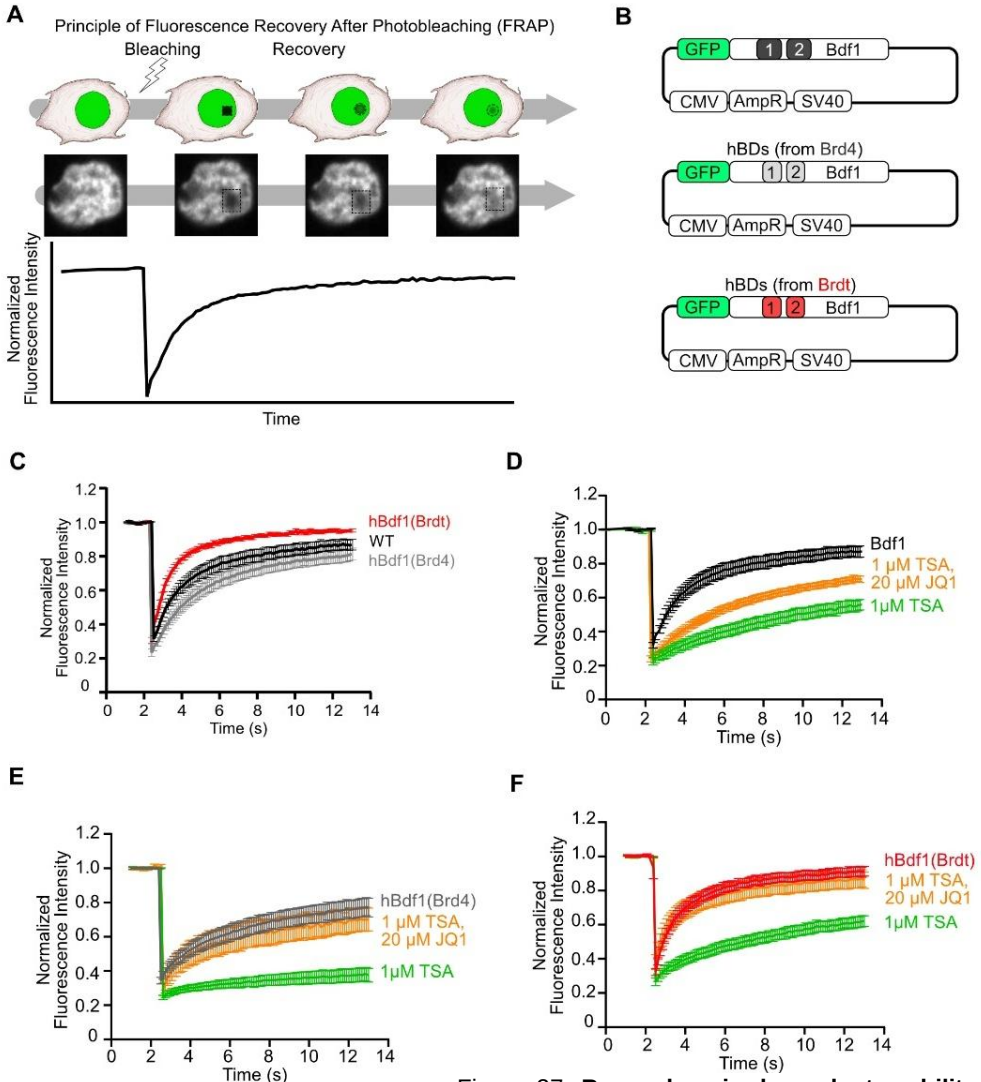

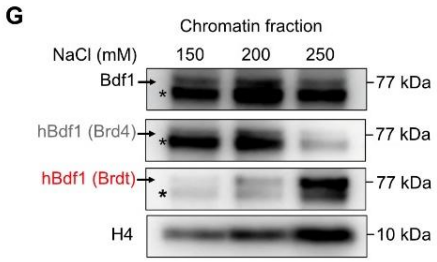

Figure 27: **Bromodomain-dependent mobility of BET proteins. (A)** Schematic representation of the Fluorescence Recovery After Photobleaching (FRAP) experimental setup. The assay was performed in HEK293 cells exogenously expressing fluorescently tagged Bdf1 protein to monitor their real-time diffusion and binding kinetics. **(B)** Schematic representation of the plasmids encoding WT Bdf1, the humanized chimera hBdf1(Brd4), and the humanized chimera hBdf1(Brdt). These constructs were designed on the backbone #65378 to evaluate the functional impact of substituting yeast bromodomains with their human counterparts using FRAP. **(C)** Average fluorescence recovery over time following photobleaching in HEK293 cells. Data represent the mean +/- SEM of at least 10 independent cells per condition. The hBdf1(Brd4) chimera displays a marked reduction in mobility (in grey), consistent with high-affinity chromatin binding, whereas hBdf1(Brdt) shows an increase in recovery rate (in red) compared to WT Bdf1 (in black). **(D-F)** FRAP recovery curves for WT Bdf1 **(D)**, hBdf1(Brd4) **(E)**, and hBdf1(Brdt) **(F)** in the presence of the HDAC inhibitor Trichostatin A (TSA) and the BET inhibitor JQ1. TSA-induced hyperacetylation markedly reduces mobility across all variants by increasing available chromatin binding sites (in green). The subsequent addition of JQ1 competitively restores mobility; notably, this rescue is near-complete for the humanized chimeras but only partial (~50%) for the WT yeast protein (in orange), highlighting differential drug sensitivity between yeast and human bromodomains. **(G)** A chromatin solubilization assay was performed to characterize the binding stability of the humanized Bdf1 variants hBdf1(Brd4) (gray) and hBdf1(Brdt) (red) relative to WT Bdf1. This assay measures the efficiency with which the proteins are released from the chromatin fraction into the supernatant across an increasing gradient of ionic strength (NaCl concentration). (*) corresponds to the non-specific band mentioned in (García-Oliver et al., 2017).

VI. Functional consequences of BET bromodomain humanization in yeast

Engineering endogenous BDF1 bromodomain swaps in a sporulation-competent background. To extend our analysis in a physiological context, we used the SK1 genetic background, optimized for high-efficiency sporulation, to modify the endogenous BDF1 locus. Using a markerless CRISPR-Cas9 genome editing strategy we achieved precise replacement of the native bromodomains without introduction of selection cassettes (Ryan et al., 2014; Horwitz et al., 2015; Jakočiūnas et al., 2016).

Specifically, we engineered strains in which the endogenous Bdf1 bromodomains were replaced by those of human BRD4 or BRDT, mirroring the chimeric constructs used in the FRAP experiments (Figure 28A). This strategy ensures that the modified proteins are expressed under the control of the native promoter and regulatory elements, thereby preserving physiological expression contexts. We first assessed whether these genetic modifications affected BDF1's expression. Transcript analysis indicates that overall mRNA levels remain comparable between WT and engineered strains, although a modest increase in expression is observed in the BRD4-humanized context (Figure 28B). At the protein level, these findings are consistently observed, with a detectable overexpression of Bdf1 in the BRD4 humanized strain and, to a lesser extent, in the BRDT humanized strain (Figure 28C).

This compensatory increase in expression may reflect a partial functional impairment of the humanized bromodomains in the yeast context. Such an adjustment suggests that yeast cells may upregulate Bdf1 levels to maintain sufficient chromatin engagement, supporting the notion of functional divergence between human and yeast BET bromodomains despite their structural conservation.

Physiological impact of bromodomain humanization on growth, mating, and genome stability. Despite the structural and kinetic differences described above, the humanization of Bdf1 bromodomains does not compromise global yeast fitness under standard vegetative conditions. The engineered strains exhibited proliferation rates identical to the WT in both liquid culture (Figure 28D)and on solid media (Figure 28E, left) indicating that the human BRD4 and BRDT bromodomains are broadly compatible with the basal essential functions of Bdf1.

However, we encountered technical constraints when attempting to generate more complex genetic combinations in these humanized strains, suggesting underlying functional limitations. We therefore performed a rapid phenotypic characterization of these strains, focusing on mating efficiency and DNA damage responses.

Yeast mating is a well-characterized process in which haploid cells of opposite mating types (MATa and MATα) undergo pheromone-mediated recognition, cell cycle arrest, polarized growth ("shmoo" formation), and ultimately cell fusion to generate a diploid cell. This process requires coordinated transcriptional reprogramming and chromatin remodeling. Strikingly, humanized strains exhibit a significant reduction in mating efficiency (Figure 28E, right), indicating that substitution of yeast bromodomains alters the regulatory programs required for this developmental transition. We next assessed the ability of these strains to cope with genotoxic stress using three classical agents: methyl methanesulfonate (MMS), which induces DNA alkylation and replication-blocking lesions; hydroxyurea (HU), which depletes deoxyribonucleotide pools and induces replication stress; and camptothecin (CPT), which stabilizes Topo I-DNA cleavage complexes, leading to replication-associated DNA breaks.

Deletion of BDF1 is not strictly lethal in *S. cerevisiae*, but results in a strong growth defect due to partial functional compensation by its paralog BDF2. However, in the presence of genotoxic agents, this compensatory mechanism is insufficient, and bdf1Δ strains fail to grow. In *C. albicans* and *C. glabrata*, mutations that impair acetyl-lysine recognition by Bdf1 bromodomains are lethal (Mietton et al., 2017a; Wei et al., 2025), highlighting a strict dependence on BET bromodomain function in these species. In contrast, this is not the case in *S. cerevisiae*, where partial functional redundancy provided by BDF2 (García-Oliver et al., 2017) allows the cells to tolerate such mutations. In this context, *S. cerevisiae* strains carrying mutations that abolish acetyl-lysine recognition by Bdf1 bromodomains do not display sensitivity to MMS or CPT, consistent with a partial compensation by Bdf2. However, these mutants are sensitive to HU, indicating that replication stress cannot be efficiently buffered by this redundancy and requires Bdf1 functional bromodomain-mediated chromatin interactions. By contrast, Bdf1 bromodomain humanization has a markedly stronger impact. Strains expressing BRD4- or BRDT-derived bromodomains are unable to grow in the presence of MMS, revealing a severe defect in DNA damage tolerance. This phenotype suggests that, although

structurally conserved, human bromodomains cannot functionally substitute for their yeast counterparts in the context of DNA damage responses.

Consistent with the observations made in bromodomain recognition-deficient mutants, HU treatment also impairs the growth of humanized strains, indicating that replication stress represents a common vulnerability when BET bromodomain function is perturbed, regardless of its origin.

Collectively, these results demonstrate that, while dispensable for basal growth, yeast Bdf1 bromodomains play a critical and non-redundant role in chromatin-dependent processes such as mating and the response to DNA damage, and that these functions are not functionally interchangeable with their human BDs BET counterparts.

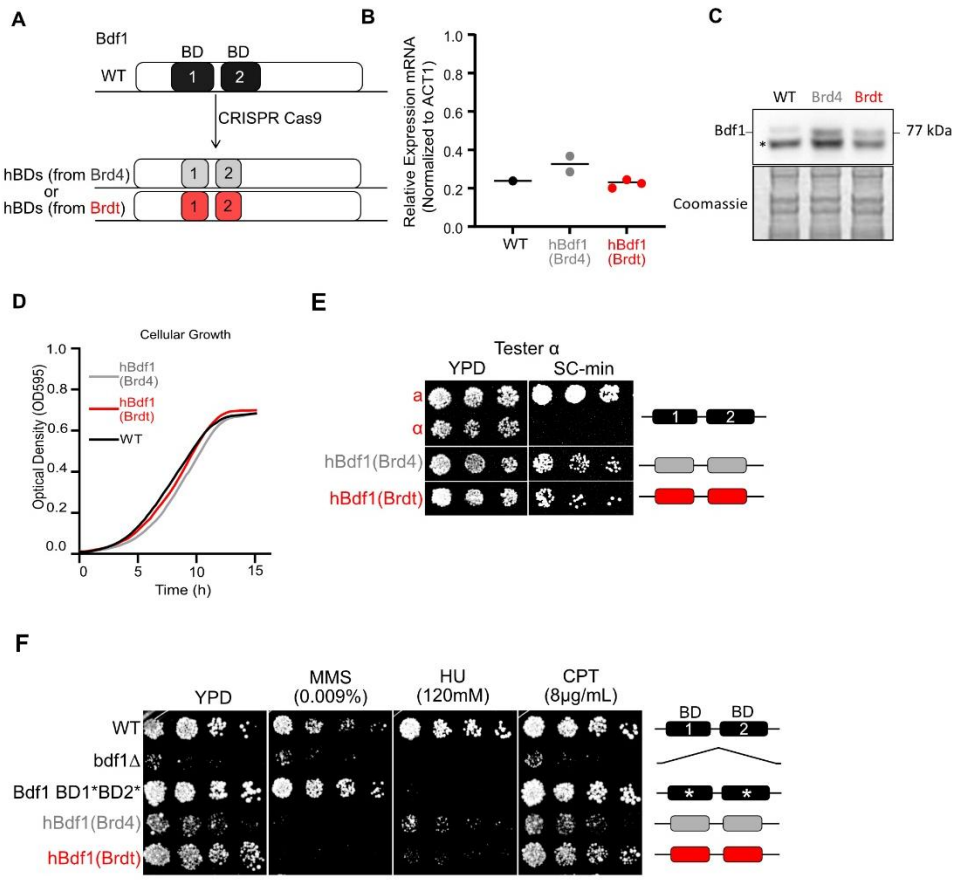

Figure 28: **Impact of BD humanization on growth, mating, and genome stability. (A)** Schematic of the markerless CRISPR-Cas9 genome editing strategy in the SK1 background. Endogenous yeast bromodomains were replaced with human BRD4 or BRDT counterparts. **(B)** mRNA quantification via transcript analysis showing comparable expression levels across strains, with a modest upregulation in the hBdf1(Brd4) context (n=1). **(C)** Western blot analysis of Bdf1 protein levels, revealing a compensatory increase in expression for both humanized chimeras compared to WT (n=3). (*) corresponds to the non-specific band mentioned in (García-Oliver et al., 2017). **(D)** Growth kinetics in liquid culture demonstrating no effect on cellular proliferation (n=4). **(E, left)** Serial dilution spotting assay on solid media, demonstrating that humanized strains maintain basal fitness. **(E, right)** Spotting mating assay showing a significant reduction in diploid formation efficiency for humanized strains compared to WT (n=2). **(F)** Serial dilution assays on YPD-agar plates containing MMS (DNA alkylation), HU (replication stress), and CPT (Topo I inhibition). Humanized chimeras exhibit acute sensitivity to MMS and HU indicating that human BET bromodomains are unable to substitute for Bdf1 in chromatin-mediated DNA damage and replication stress responses (n=2). The Bdf1 BD1 BD2 strain corresponds to the mutant bdf1-Y187F and bdf1-Y354F point mutations described by García-Oliver et al. (2017).

Impact of BET bromodomain humanization on sporulation efficiency and spore morphology.

We next investigated the ability of WT and humanized strains to undergo sporulation. Bromodomain humanization resulted in a modest but reproducible defect, particularly in strains expressing BRD4 bromodomains (Figure 29A). Specifically, sporulation efficiency decreased from ~95% in the WT strain to ~70% in the hBdf1(Brd4) humanized strain. In comparison, strains expressing BRDT bromodomains exhibited an intermediate phenotype, with a sporulation efficiency of approximately ~85%.

However, the morphology of the resulting spores was markedly altered. WT spores appeared properly formed and highly compacted three days post induction (Figure 29B). On the other hand, bromodomain humanization induced pronounced defects in spore formation, affecting ~60% of spores in the hBdf1(Brd4) humanized strain and ~40% in the hBdf1(Brdt) humanized strain (Figure 29C).

These observations were further supported by transmission electron microscopy analyses performed at the CIQLE Platform Lyon-Est (Figure 29D). These experiments confirmed the presence of structural abnormalities in spores derived from the humanization of Bdf1's bromodomains. Due to the recent acquisition of these data, the current ultrastructural description is non-exhaustive. Although a comprehensive ultrastructural characterization is ongoing, initial data show an accumulation of large vacuoles in humanized strains compared to WT. This phenotype is indicative of a heightened cellular stress response, potentially triggered by the humanization of the Bdf1 bromodomains. We hypothesize that the resulting alterations in both acetyl-lysine and DNA-binding affinities disrupt the protein's native dynamicity, leading to the observed cellular dysfunction.

Finally, we evaluated the impact of bromodomain humanization on the terminal stage of the meiotic program by assessing spore viability and germination. In liquid media, humanization resulted in a marked reduction in germination capacity (Figure 29E). This developmental defect was further confirmed through tetrad dissection on solid media, which revealed ~ 70% decrease in overall spore viability for the chimeric strains (Figure 29F, G). The severity of this phenotype was particularly pronounced in the hBdf1(Brd4) strain, where spores were rendered nearly non-viable. While the hBdf1(Brdt) strain also exhibited a significant reduction in survival, it was further characterized by increased phenotypic heterogeneity, with surviving spores displaying highly variable rates of growth resumption. Collectively, these data demonstrate that while human BET bromodomains can support vegetative proliferation, they

are insufficient to sustain the complex chromatin transitions required for successful spore maturation and germination.

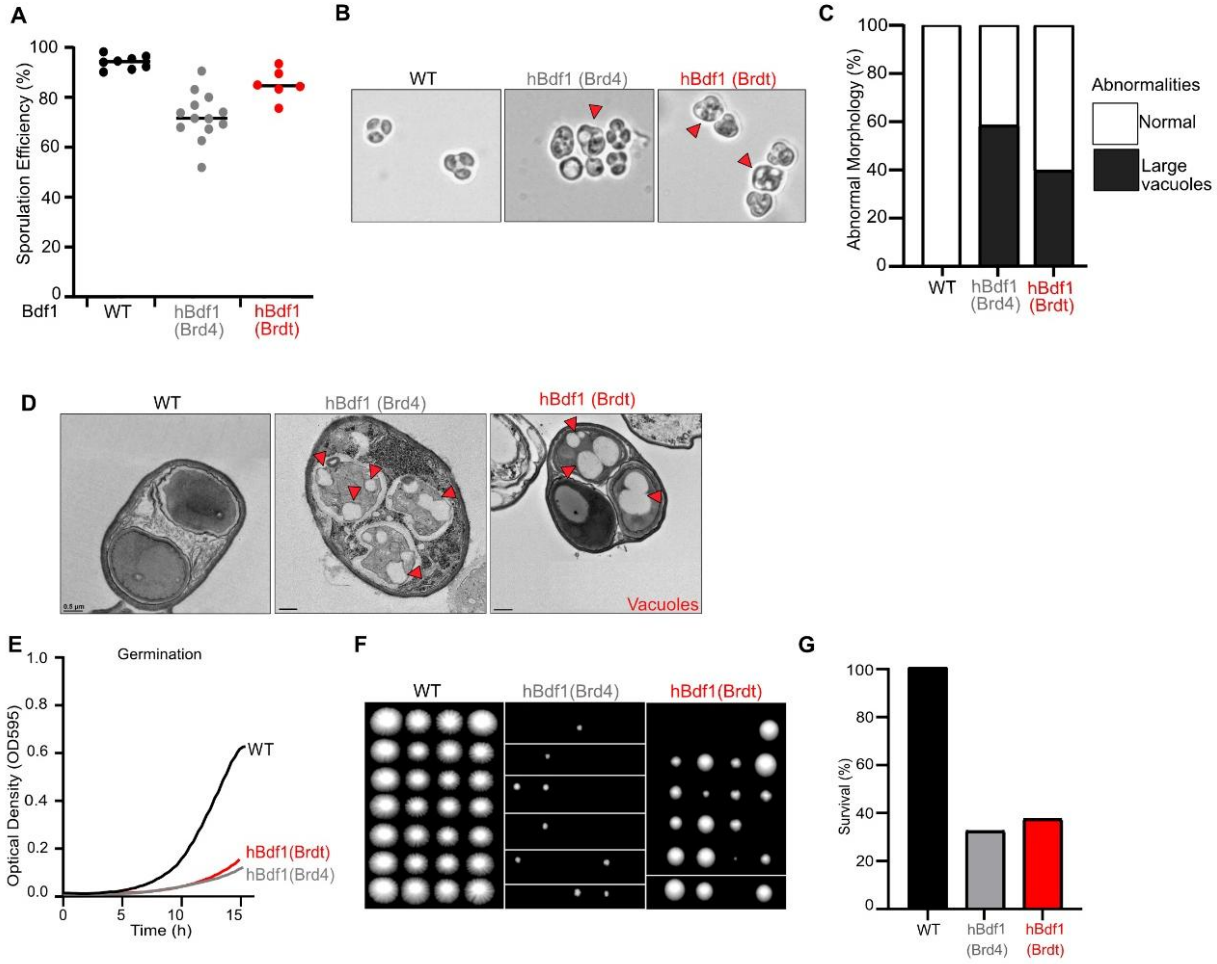

Figure 29: **Impact of BD humanization on sporulation and spores. (A)** Sporulation efficiency represented 72 h post- meiotic induction. WT strains reach ~95% efficiency, while hBdf1(Brd4) (in grey) and hBdf1(Brdt) (in red) strains exhibit modest reductions to ~70% and ~85%, respectively (n=6-13). **(B)** Representative light microscopy images illustrating properly compacted WT asci versus malformed spores in humanized strains. **(C)** Quantification of spores displaying aberrant morphology, with the hBdf1(Brd4) strain showing the most severe defects ~60% (~400 cells were counted). **(D)** Representative transmission electron microscopy (TEM) images (CIQLE Platform, Lyon-Est) revealing structural abnormalities in the humanized strains compared to the highly organized WT spores (pointed with red arrows). **(E)** Germination capacity measured in liquid medium, highlighting a marked reduction in the ability of humanized spores to exit dormancy (n=4). (F) Representative dissection plates and (G) quantification of overall spore viability showing a ~70% decrease in viability for humanized strains compared to WT (n=2).

VII. Distinct BET bromodomains differentially sustain transcriptional program execution

To investigate the mechanical basis of the observed phenotypic abnormalities and cell death, we performed a temporal cytological analysis of meiotic progression. By monitoring the number of nuclei per cell via Hoechst staining, we quantified the kinetics of the meiotic divisions at key timepoints: pre-induction (T0), early meiotic prophase (4 h), to active divisions

(8 h), and the progression through spore maturation (12–72 h) (Figure 30A). Intriguingly, the hBdf1(Brdt) humanized strain exhibited a profound developmental stall. While WT and hBdf1(Brd4) cells progressed through the standard meiotic divisions, the hBdf1(Brdt) cells remained predominantly mononuclear at the 8 h and 12 h timepoints, indicating a significant delay in the meiotic division (Figure 30B).

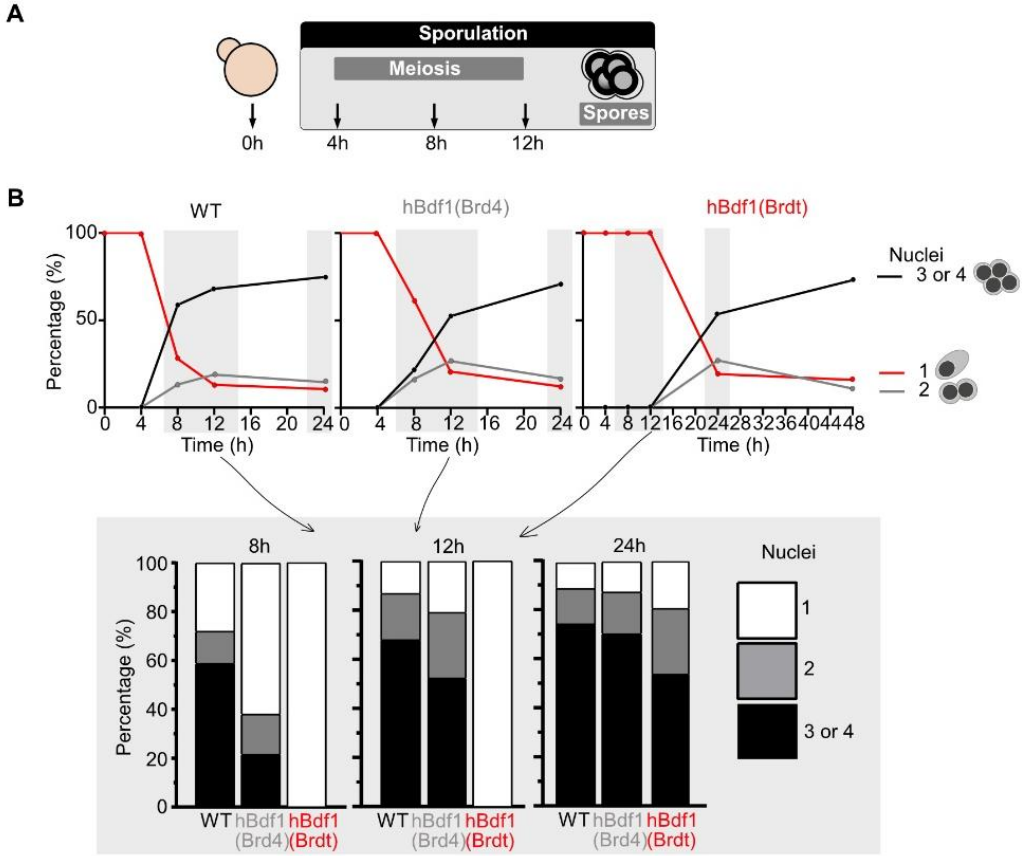

Figure 30: **Impact of Bdf1 BD humanization on the kinetics of meiotic divisions. (A)** Schematic of the sampling intervals used for cytological analysis, ranging from pre-induction (T0) through late spore maturation (72 h). **(B)** Distribution of the number of nuclei per cell, used as a proxy for progression through the meiotic cycle. For each timepoint and condition, ~400 cells were counted and categorized as: mononuclear (prophase I; in red), binuclear (completion of Meiosis I; in grey), or tetranuclear (completion of Meiosis II and sporulation; in black) represented on the graphs (above). The bar graphs (bottom) further illustrate that while WT (in black) and hBdf1(Brd4) (in grey) strains initiate nuclear divisions by 8 h, the hBdf1(Brdt) (in red) strain exhibits a significant developmental delay, remaining mononuclear through the 12 h timepoint.

Transcriptomic profiling reveals delayed meiotic progression in BET-humanized strains. To characterize at the molecular level the delayed sporulation phenotype observed in BET-humanized strains, we performed a transcriptomic time-course analysis during meiosis. WT, BRD4-humanized, and BRDT-humanized strains were sampled in biological triplicates at three key time points: prior to induction (T0), 4 h post-induction, corresponding to early meiotic gene expression prior to the first division, and 8 h post-induction, when meiotic divisions are actively

occurring (Figure 31A). Total RNA was extracted and subjected to high-throughput sequencing following standard quality control procedures. All libraries passed quality metrics and yielded robust sequencing depth of ~11 x 10^6 reads per sample, enabling reliable downstream analyses after normalization.

To assess global transcriptional trajectories and ensure experimental reproducibility, we performed Principal Component Analysis (PCA) on the synchronized meiotic time-course. High reproducibility was observed across all biological replicates, which clustered tightly according to their respective conditions (Figure 31B). The first two principal components (PC1 and PC2) accounted for ~80% of the total variance, successfully capturing the coordinated progression of WT cells through the sporulation program. While hBdf1(Brd4) cells largely mirrored the WT transcriptional trajectory, they exhibited a modest temporal delay first detectable at 8 h post-induction. In contrast, the hBdf1(Brdt) humanized strain showed a more pronounced developmental stall, already apparent by the 4 h milestone. Notably, at 8 h post-induction, the transcriptional profile of hBdf1(Brdt) cells remained positioned near the 4-h WT samples, indicating a ~4-h kinetic lag in the meiotic gene expression program. These results demonstrate that while both humanized variants can navigate the meiotic landscape, the BRDT-bromodomain substitution significantly compromises transcriptional transitions.

Delayed activation of sporulation gene expression programs in BET-humanized strains. Furthermore, we analyzed the most variable genes across all samples, visualized as a heatmap to further resolve the transcriptional differences underlying these altered trajectories (Figure 31C). In WT cells, this revealed the expected sequential reprogramming characteristic of sporulation: the rapid repression of vegetative genes was followed by the highly coordinated, wave-like induction of early and middle meiotic gene cohorts at 4 h and 8 h post-induction, respectively. While this global program was largely preserved in hBdf1(Brd4) cells, consistent with their near-normal progression, closer inspection identified specific failures in the execution of the late-stage program. Specifically, a subset of late-sporulation genes showed reduced or aberrant induction, suggesting that while BRD4 bromodomains support early meiotic transitions, they are not fully interchangeable with yeast Bdf1 for the terminal stages of the developmental program. In contrast, the hBdf1(Brdt) humanized cells display a markedly altered transcriptional profile. While these cells efficiently repressed the vegetative program,

indicating a successful exit from mitosis, they failed to robustly activate the subsequent meiotic waves. At 4 h post-induction, the induction of early meiotic genes was significantly attenuated, a defect that compounded at later stages. By 8 h, neither middle nor late gene programs were properly executed, with the global transcriptome remaining locked in a state reminiscent of early WT timepoints. These data demonstrate that while the BRDT substitution allows for the initiation of sporulation, it stalls the transcriptional dynamics required to drive cells through the meiotic divisions.

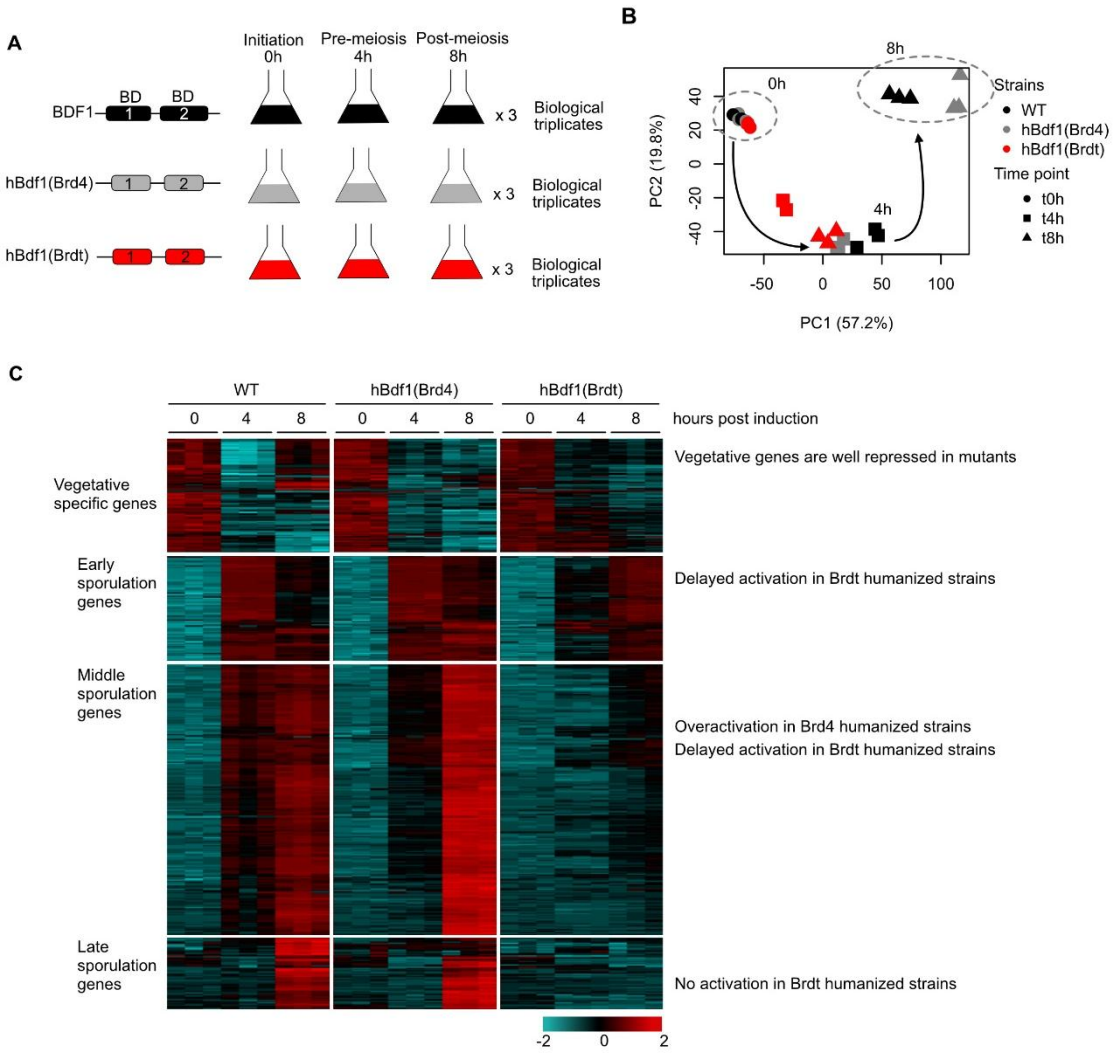

Figure 31: **Global transcriptional landscape of meiotic progression. (A)** Schematic of the sampling intervals used for transcription analysis at three major timepoints, t0h, 4h, and 8h in triplicates. **(B)** PCA of synchronized meiotic time-courses for WT, hBdf1(Brd4), and hBdf1(Brdt) strains. PC1 and PC2 account for ~80% of total variance, capturing the developmental vector from pre-induction (t0) to late sporulation (t8h). Replicates (represented as dots for t0h, squares for t4h, and triangles for t8h) cluster tightly, demonstrating high experimental reproducibility. **(C)** Hierarchical clustering of the most variable genes across the meiotic time-course. The WT program is characterized by a sequential reprogramming cascade: rapid repression of vegetative genes followed by synchronized waves of early, middle, and late sporulation genes.

Gene-level analysis reveals distinct defects in regulatory modules. To further dissect these differences, we examined the expression of key regulators of sporulation (Figure 32). The canonical early meiotic regulators, IME1 and IME2, are robustly induced in both WT and hBdf1(Brd4) cells. In contrast, their induction in hBdf1(Brdt) humanized cells is detectable but significantly attenuated, indicating a functional deficit at the very onset of the meiotic program. A more striking divergence is observed for the middle-phase master transcription factor, NDT80. While properly induced in WT, NDT80 exhibited even higher transcript levels in the hBdf1(Brd4) background, a pattern consistent with the overactivation of specific middle-gene cohorts observed in our global clustering analysis at 8 h. Conversely, hBdf1(Brdt) cells failed to activate NDT80 or its downstream targets at either 4 or 8 h post-induction.

Finally, the late-sporulation genes DIT1 and DIT2, essential for spore wall maturation, showed strong induction in WT and a diminished but present induction in hBdf1(Brd4) cells. This confirms a partial impairment in the terminal differentiation program of the Brd4-humanized strain. In the hBdf1(Brdt) context, however, late gene expression Is essentially absent. Collectively, these results pinpoint a hierarchical latency of the meiotic program in Brdt-humanized cells, characterized by weakened early induction and a total failure to engage the Ndt80-dependent middle and late gene programs at t8h compared to WT and hBdf1(Brd4) strain.

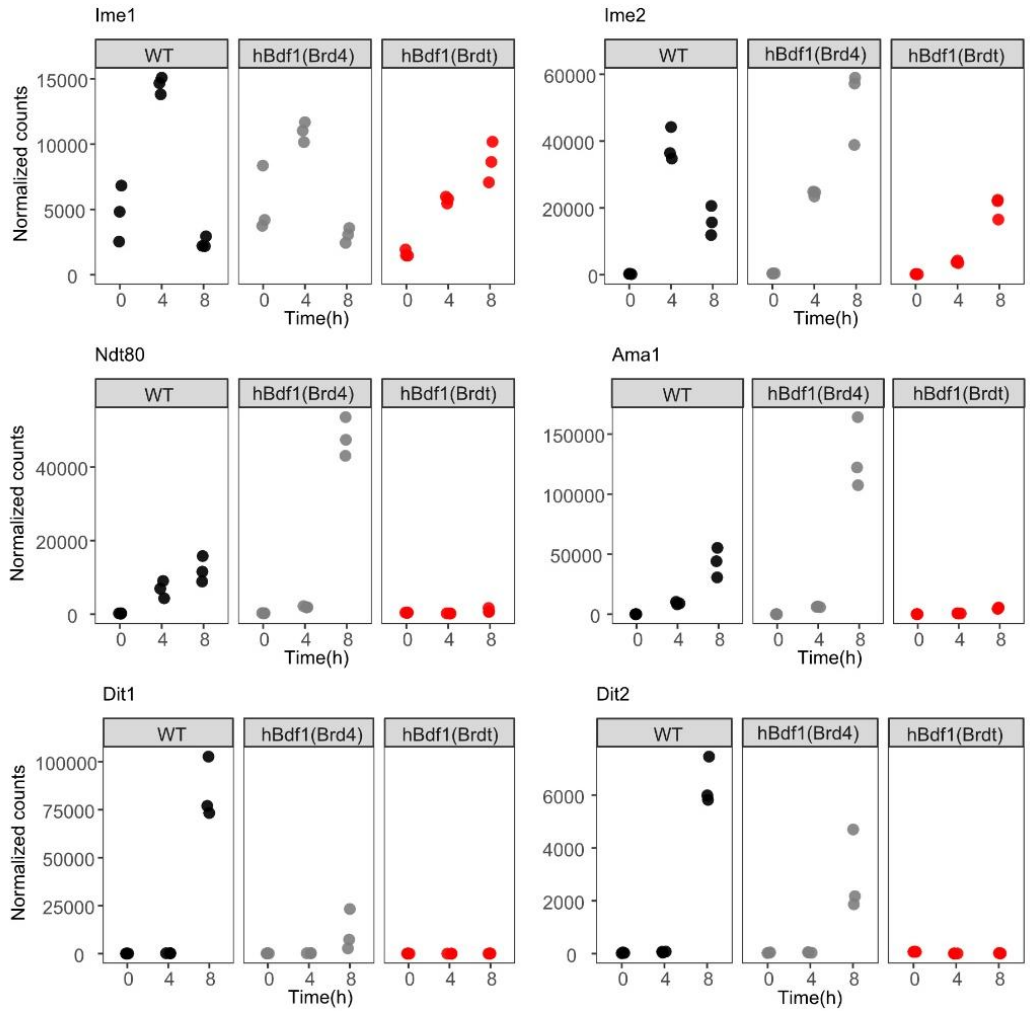

Figure 32: **Transcript levels of canonical genes defining early, middle, and late developmental stages. Early regulators (IME1, IME2):** Induction is robust in WT (in black) and hBdf1(Brd4) (in grey), but significantly attenuated in hBdf1(Brdt) (in red), indicating an early functional deficit. **Middle-phase master regulator (NDT80):** WT levels are maintained in hBdf1(Brd4) (with a compensatory over-induction at 8 h), whereas hBdf1(Brdt) fails to engage the NDT80 circuit at any timepoint. **Late differentiation genes (DIT1, DIT2):** Expression is blunted in hBdf1(Brd4) and abolished in hBdf1(Brdt).

Differential analysis of transcriptional progression. To establish a quantitative reference for transcriptional dynamics during sporulation, we first characterized differential gene expression profiles throughout the WT time course (Figure 33A,B). These dynamics were visualized using MA plots to assess the distribution of changes across the transcriptome and volcano plots to highlight statistical significance. In these MA plots, the $\log_2$ fold change (y-axis) is plotted against the $\log 1_0$ mean of normalized counts (x-axis), demonstrating that the observed transcriptional shifts are consistent across both high- and low-abundance transcripts. Using a threshold of $|\log_2$ fold change$| \geq 2$ and adjusted p-value (padj) ≤ 0.05, we identified 1,018 differentially expressed genes (DEGs) between 0 and 4 h (517 upregulated; 501

downregulated). This robust response reflects the extensive transcriptional reprogramming required for meiotic entry. As sporulation progressed from 4 to 8 h, 698 genes remained dynamically regulated (495 upregulated; 203 downregulated), consistent with the activation of middle- and late-stage meiotic programs. Together, these data confirm that sporulation is driven by a highly dynamic and temporally structured transcriptional cascade. This WT dataset provides a robust framework to interpret the specific transcriptional failures observed in Bdf1-humanized strains.

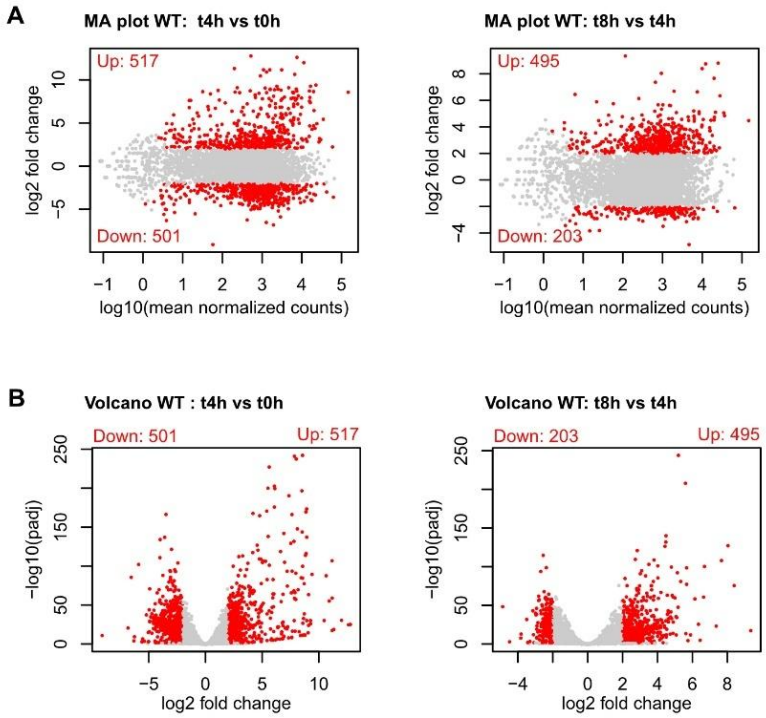

Figure 33: **Dynamics of the WT meiotic program. (A)** MA plots illustrating the transcriptional shifts between key sporulation time points (0 h, 4 h, and 8 h). In the MA plots, the $\log_2$ fold change (y-axis) is plotted against the $\log_{10}$ mean of normalized counts (x-axis), using a stringency threshold of $|\log_2$ fold change$| \geq 2$ and adjusted p-value (padj) ≤ 0.05, and demonstrating that the observed expression changes are representative across a wide range of transcript abundances. **(B)** Volcano plots representing the identified 1,018 DEGs (517 up; 501 down) during the transition to meiotic entry (0–4 h). Continued progression (4–8 h) is characterized by 698 dynamically regulated genes (495 up; 203 down), reflecting the sequential activation of the middle- and late-stage sporulation programs.

BET bromodomains encode distinct functional properties required for transcriptional program execution. We next compared differentially expressed genes between mutants and WT at each time point (Figure 34). At 0 h, only a limited number of genes are deregulated in both mutants (BRD4: 13 up / 10 down; BRDT: 16 up / 10 down), indicating minimal impact under steady-state conditions.

In contrast, upon sporulation induction, a strong and progressive transcriptional defect becomes apparent. In the BRD4-humanized strain, the number of differentially expressed (DE) genes increases from 156 genes at 4 h (75 up / 81 down) to 505 genes at 8 h (243 up / 262

down). This effect is markedly amplified in the BRDT-humanized strain, with 462 DE genes already detected at 4 h (191 up / 271 down), increasing further to 660 genes at 8 hours (162 up / 498 down). Notably, the transcriptional imbalance in BRDT-humanized cells becomes increasingly skewed toward gene repression over time. This trend is consistent with the normal transcriptional dynamics observed in WT cells, where sporulation induction triggers the activation of a large set of sporulation-specific genes, which fail to be properly induced in the BRDT mutant due to its delayed progression.

These observations raise the question of how BET bromodomains contribute to the execution of complex transcriptional programs. Within this framework, humanization of Bdf1 provides a functional assay to probe the intrinsic properties of BET bromodomains. Strikingly, BRD4- and BRDT-derived bromodomains do not support transcriptional reprogramming to the same extent, revealing differential functional capacities.

BRD4-humanized cells largely preserve the temporal structure of the meiotic transcriptional cascade, including proper induction of early and middle genes. However, this progression is accompanied by dysregulation, notably overactivation of middle-phase genes and defective induction of late genes, indicating that BRD4 bromodomains support initiation and progression of the program but are insufficient to ensure its proper resolution.

In contrast, BRDT-humanized cells exhibit a profound defect in transcriptional progression. Although entry into the program is initiated, with repression of vegetative genes and partial activation of early regulators, the transcriptional cascade fails to propagate to middle and late stages. This results in a global and increasingly repressive transcriptional imbalance, consistent with an inability of BRDT bromodomains to sustain dynamic transcriptional transitions in the yeast context.

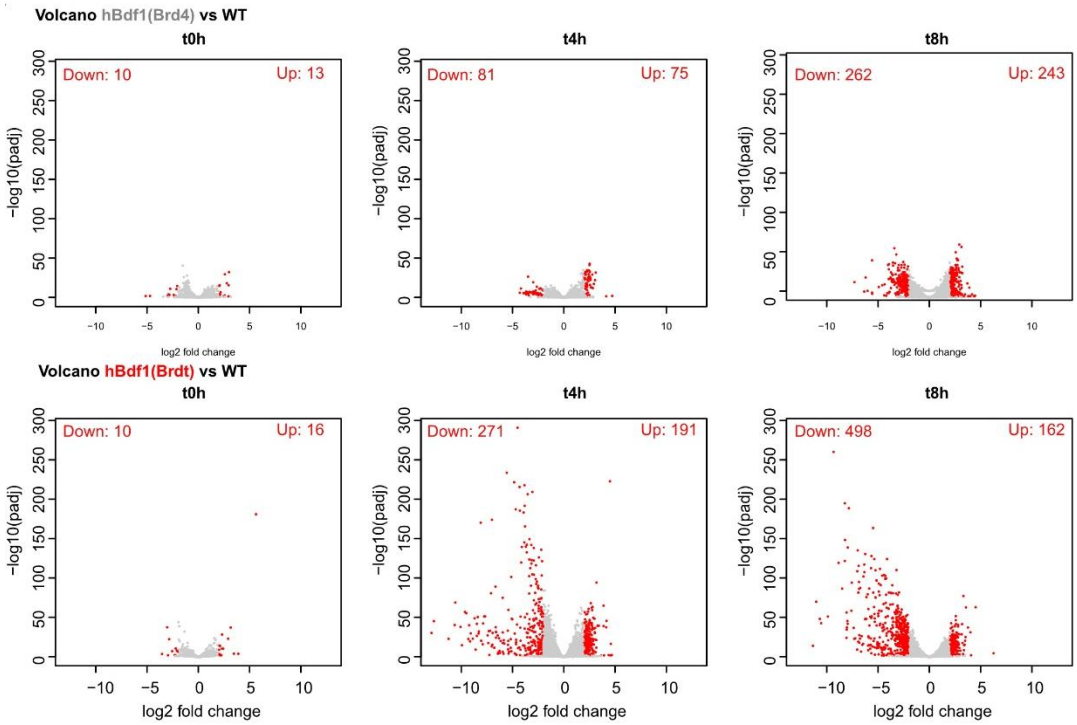

Figure 34: **Comparative transcriptomic analysis of BRD4- and BRDT-humanized strains during sporulation. (A)** Volcano plots and quantitative summaries of differentially expressed genes (DEGs) in humanized strains relative to WT ($|\log_2$ fold change$| \geq 2$ and adjusted p-value (padj) ≤ 0.05). Under steady-state conditions (0 h), both mutants exhibit minimal deregulation. Upon sporulation induction, a progressive transcriptional collapse is observed, with BRDT-humanized strains showing a more rapid and severe imbalance characterized by increasing gene repression over time.

Gene Ontology (GO) enrichment analysis further supports a defect in sporulation progression in both hBdf1(Brd4) and hBdf1(Brdt) humanized strains (Figure 35). For each strain, differentially expressed genes were first identified between 4 h and 0 h post-induction, and these gene sets were subsequently subjected to GO term enrichment analysis. The resulting enriched categories were then compared across WT and mutant strains.

In WT cells, genes differentially expressed at 4 hours are strongly enriched for categories related to meiotic progression, including meiotic cell cycle, meiotic cell cycle progression, reproductive process, sexual reproduction, and reproduction. These enrichments are significantly reduced in the BRD4-humanized strain and are almost completely lost in the BRDT-humanized strain. Altogether, these results indicate that the major transcriptional differences

observed at 4 h between WT and mutant strains primarily reflect an impaired activation of the sporulation program.

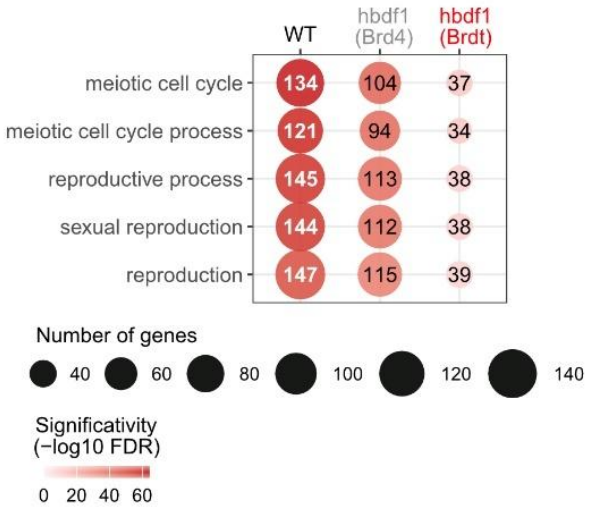

Figure 35: **Comparative Gene Ontology (GO) enrichment.** Dot plot illustrating the enrichment of Biological Process terms for genes differentially expressed between 0 and 4 hours. In WT cells, the transcriptional program is highly enriched for core meiotic categories, including meiotic cell cycle progression, reproductive processes, and sexual reproduction. These functional signatures are markedly attenuated in the BRD4-humanized strain and abolished in the BRDT-humanized strain.

Ongoing analyses aim to determine whether specific gene classes are preferentially affected, for example based on promoter architecture or dependence on distinct transcription factor networks. We are particularly exploring whether differences in chromatin engagement or promoter context may contribute to the differential activity of BRD4 and BRDT bromodomains, although these aspects remain secondary to the primary observation of distinct intrinsic functional capacities.

These differences are especially evident in the context of sporulation, a process involving coordinated genome-wide transcriptional reprogramming of more than 1000 genes through successive waves of activation and repression. While BET proteins are known to broadly regulate RNA polymerase II transcription, our results demonstrate that bromodomain-specific properties become critical in conditions requiring rapid and coordinated transcriptional rewiring.

Together, these findings indicate that BET bromodomains encode intrinsic functional properties that determine transcriptional timing and program execution. More broadly, they

demonstrate that these properties are not fully interchangeable between paralogs and are essential for the proper completion of complex developmental transcriptional programs.

VIII. Functional interplay between Bdf1 and Bdf2 in regulating chromatin acetylation

BDF2 deletion as a strategy to unmask Bdf1 bromodomain function and enable BET inhibitor sensitivity. To investigate the functional role of bromodomains during post-meiotic stages, we sought a strategy to conditionally inhibit Bdf1 after the completion of meiosis. This approach was necessitated by the fact that Bdf1 is essential for meiotic entry, making constitutive deletions unsuitable for studying late-stage sporulation. We focused on the small-molecule inhibitor iBET726, which has been previously shown to exert a potent inhibitory effect on humanized CahBdf1(Brd4) (*C. albicans*) strains, while leaving the WT strain unaffected (Wei et al., 2025) (Figure 36A). Initially, we tested the efficacy of iBET726 in *Saccharomyces cerevisiae* (Sc). Surprisingly, no significant growth defect or inhibitory effect was observed in our Sc humanized strains (Figure 36B). We hypothesized that this lack of sensitivity might be attributed to a compensatory effect by Bdf2, a Bdf1 paralog present in S. cerevisiae but absent in C. albicans. To test this, we engineered a new suite of strains with a bdf2Δ background to eliminate potential functional redundancy. To our surprise, even in the absence of Bdf2, the iBET726 inhibitor failed to impact the growth or viability of either the hBdf1(Brd4) or hBdf1(Brdt) humanized strains in S. cerevisiae (Figure 36C). These results indicate that the observed resistance is not due to the compensatory presence of a paralog. Instead, the lack of effect likely results from physiological differences between the two yeast species, such as the activity of efflux pumps, which may limit the intracellular accumulation of the drug in S. cerevisiae compared to C. albicans. While this pharmacological approach did not provide the intended tool for post-meiotic inhibition, these negative results unlocked new perspectives regarding the deletion of Bdf2 in the humanized backgrounds.

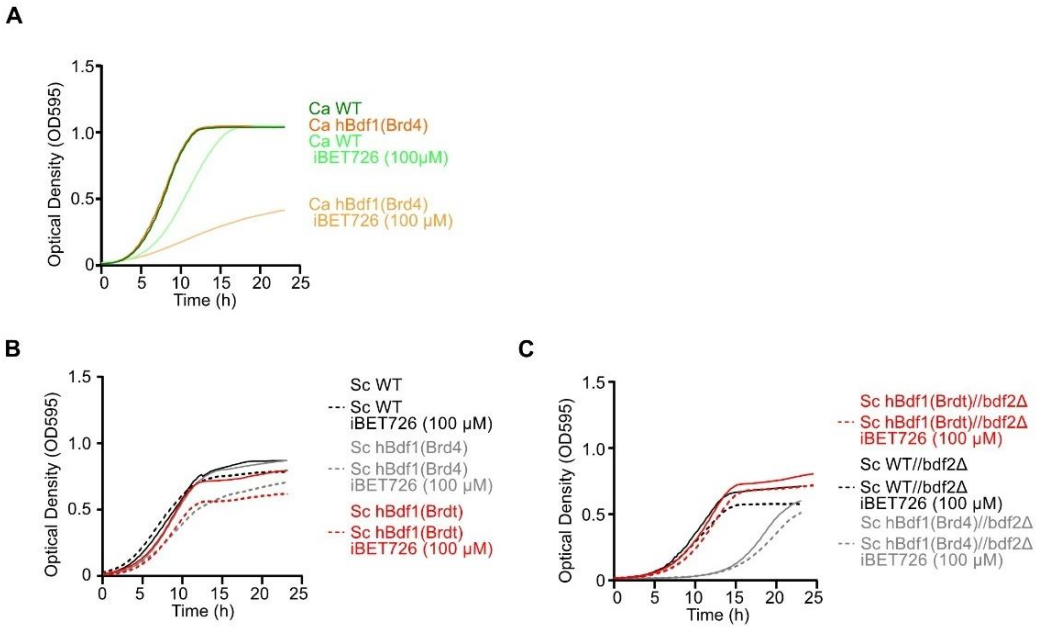

Figure 36: **BDF2 deletion as a strategy to unmask Bdf1 bromodomain function and enable BET inhibitor sensitivity. (A)** Growth assessment results demonstrating that iBET726 selectively inhibits *C. albicans* strains expressing humanized Ca hBdf1(Brd4), while WT strains remain resistant. This assay serves as a control to the function of the drug as previously published (Wei et al., 2025). **(B)** Growth assay data demonstrating that, unlike *C. albicans*, humanized *S. cerevisiae* strains expressing hBdf1(Brd4) (grey) and hBdf1(Brdt) (red) do not exhibit sensitivity to iBET726, likely due to the BET paralog Bdf2. **(C)** The continued lack of inhibition in bdf2Δ strains confirms that the resistance of humanized Sc to iBET726 is not caused by Bdf2-mediated compensation, suggesting a potential role for differential drug efflux or permeability.

Bdf2 loss induces a bromodomain-dependent redistribution of histone H4 acetylation. We therefore deleted *BDF2* in both WT and humanized strains. Unexpectedly, this deletion resulted in a marked alteration of the nuclear distribution of histone H4ac in vegetative cells. Immunofluorescence analyses (Figure 37A) revealed the presence of nuclei displaying an abnormal peripheric redistribution of H4ac signal in bdf2Δ strains. This phenotype was observed in approximately 50% of cells in the WT BDF1 background. Strikingly, its frequency increased to nearly 100% in cells expressing BRD4-humanized bromodomains. In contrast, this altered H4ac distribution was almost completely absent in cells expressing BRDT-humanized bromodomains (Figure 37B).

These observations were further examined by super-resolution microscopy, which provided a more refined view of the subnuclear organization of H4 acetylation. Importantly, this approach revealed a spatial heterogeneity of the H4ac phenotype that is not detectable by low-resolution confocal microscopy (Figure 37C). We thus identified two distinct abnormalities in

the bdf2Δ strain: Abnormal 1, characterized by a peripheral redistribution of H4ac, and Abnormal 2, characterized by a more condensed and tightly compact H4ac signal. Both phenotypes were observed in bdf2 Δ strain, as shown in the figure, although their prevalence differs depending on the human counterpart. In hBdf1 (Brd4) humanized strains, Abnormal 1 is the dominant phenotype, whereas in hBdf1 (Brdt) humanized strains, Abnormal 2 predominates (Figure 37C). Further image acquisition and statistical analysis are ongoing to determine the exact proportion of each phenotype across the different genetic backgrounds. These observations suggest that the difference in the human counterparts bromodomains exert distinct effects on the overall organization of H4Kac.

Together, these results uncover an unexpected functional interplay between Bdf1 and Bdf2 in the control of chromatin acetylation patterns. They further demonstrate that the impact of BDF2 deletion is strongly influenced by the intrinsic properties of the bromodomains present in Bdf1, highlighting a differential capacity of BET bromodomains to interpret or stabilize H4 acetylation landscapes *in vivo*.

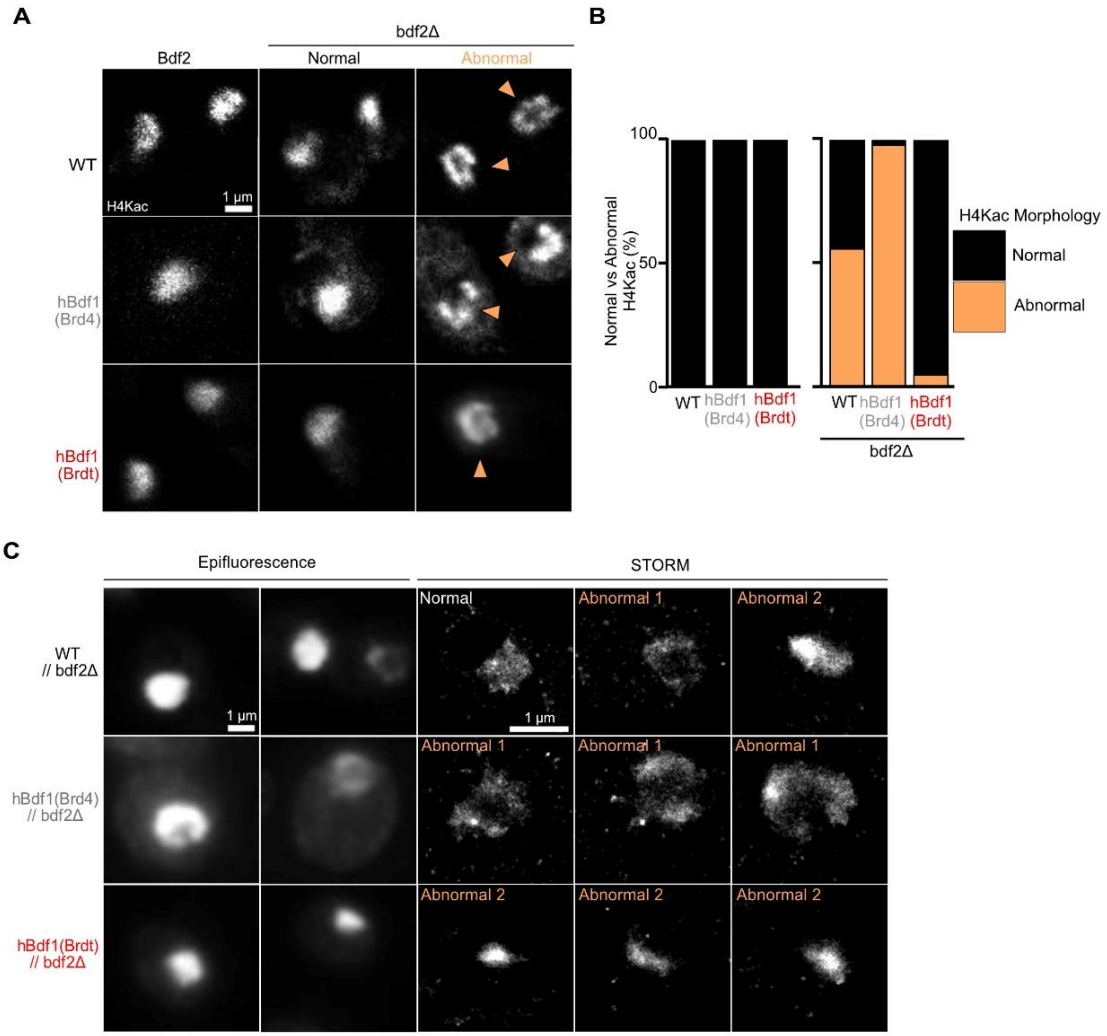

Figure 37: **Bdf2-loss induces H4ac spatial redistribution. (A)** Immunofluorescence images of vegetative cells demonstrating that the loss of Bdf2 induces a significant spatial redistribution of histone H4 acetylation (H4ac). While WT nuclei typically exhibit a defined, localized H4ac signal, bdf2Δ strains display a markedly broader and more diffuse nuclear distribution (pointed with orange arrows). **(B)** Quantitative analysis revealing that the frequency of the diffuse H4ac signal is observed in approximately 50% of WT Bdf1 cells while the frequency of the altered distribution increased to nearly 100% in hBdf1(Brd4) cells (grey) suggesting a high sensitivity to Bdf2 loss. On the other hand, the diffused phenotype is almost entirely absent in hBdf1(Brdt) strains (red), indicating that BRDT-humanized bromodomains may stabilize H4ac patterns independently of Bdf2. **(C)** Super-resolution microscopy reveals a complex subnuclear organization of H4ac that is not resolvable by conventional confocal imaging. In the bdf2Δ background, two distinct abnormal phenotypes were identified: Abnormal 1, a peripheral redistribution of the H4ac signal, and Abnormal 2, a highly condensed and tightly compacted H4ac architecture. The prevalence of these phenotypes is dependent on the humanized counterpart: the hBdf1 (Brd4) strain predominantly displays the peripheral redistribution (Abnormal 1), whereas the hBdf1 (Brdt) strain is characterized by the compacted signal (Abnormal 2). Note: Statistical quantification of phenotype proportions across genetic backgrounds is currently ongoing.

Genome-wide analysis of H4 acetylation profiles across BDF2 deletion and BET-humanized contexts. Based on the heterogeneous distribution of nuclear H4 acetylation observed by immunofluorescence, we next sought to characterize H4ac profiles at the genome-wide level using CUT&Tag. To capture the range of phenotypes observed, we analyzed WT cells, BDF2-deleted WT cells, representing an intermediate phenotype, as well as bdf2Δ strains expressing humanized Bdf1 bromodomains derived from BRD4 or BRDT. These conditions were selected to reflect the distinct nuclear H4ac distributions, ranging from partially diffuse (bdf2Δ WT) to fully diffuse (BRD4-humanized bdf2Δ) and largely preserved patterns (BRDT-humanized bdf2Δ).

CUT&Tag libraries were successfully generated from all conditions and sequenced, enabling comparative analysis of H4 acetylation profiles across these genetic backgrounds. First, deletion of BDF2 resulted in a modest but reproducible global decrease in H4 acetylation levels at transcription start sites (Figure 38A). This observation was unexpected and is currently being further investigated by western blot analyses at the time of manuscript submission.

In parallel, to ensure homogeneous genetic backgrounds when comparing humanized strains, H4ac profiles were assessed in cells combining BDF2 deletion with bromodomain humanization (BRD4 or BRDT). Under these conditions, bromodomain humanization did not significantly alter the overall distribution of H4 acetylation in vegetative cells (Figure 38A), indicating that, at the genome-wide level, H4ac patterns remain largely preserved despite the replacement of endogenous bromodomains.

Altered H4 acetylation landscapes in spores upon BET bromodomain humanization. We next extended our CUT&Tag analyses to spores to determine how Bdf1/Bdf2-dependent regulation of histone acetylation is maintained in a highly compacted chromatin context. In WT and bdf2Δ spores, H4ac profiles were broadly consistent with those described above in vegetative cells. However, we observed an overall reduction in signal intensity, likely reflecting limited accessibility of the antibody to chromatin in this highly compacted nuclear environment rather than a true loss of histone acetylation.

In contrast, spores derived from BET-humanized bdf2Δ strains displayed markedly atypical H4ac profiles. Rather than exhibiting defined enrichment patterns, these samples showed

highly altered and poorly structured signals, suggestive of a profound disruption of chromatin organization. In some cases, the profiles appeared nearly flattened, with a loss of recognizable chromatin features.

These observations are consistent with the severe loss of spore viability described above (Figure 38B), and suggest that bromodomain humanization, in the absence of Bdf2, compromises the establishment or maintenance of proper chromatin architecture during sporulation.

To bridge the observed transcriptional defects with the physical state of the genome, we are currently extending our analysis to the ultrastructural and biochemical levels. Specifically, we are employing immunofluorescence assays to visualize H4ac localization alongside Micrococcal Nuclease (MNase) digestion assays to quantitatively map nucleosome occupancy and positioning in spores. These complementary approaches will provide a high-resolution assessment of the chromatin landscape, allowing us to determine if the humanization of Bdf1 bromodomains, and the resulting shift in binding affinities, manifests as a global alteration of chromatin organization and structure in spores.

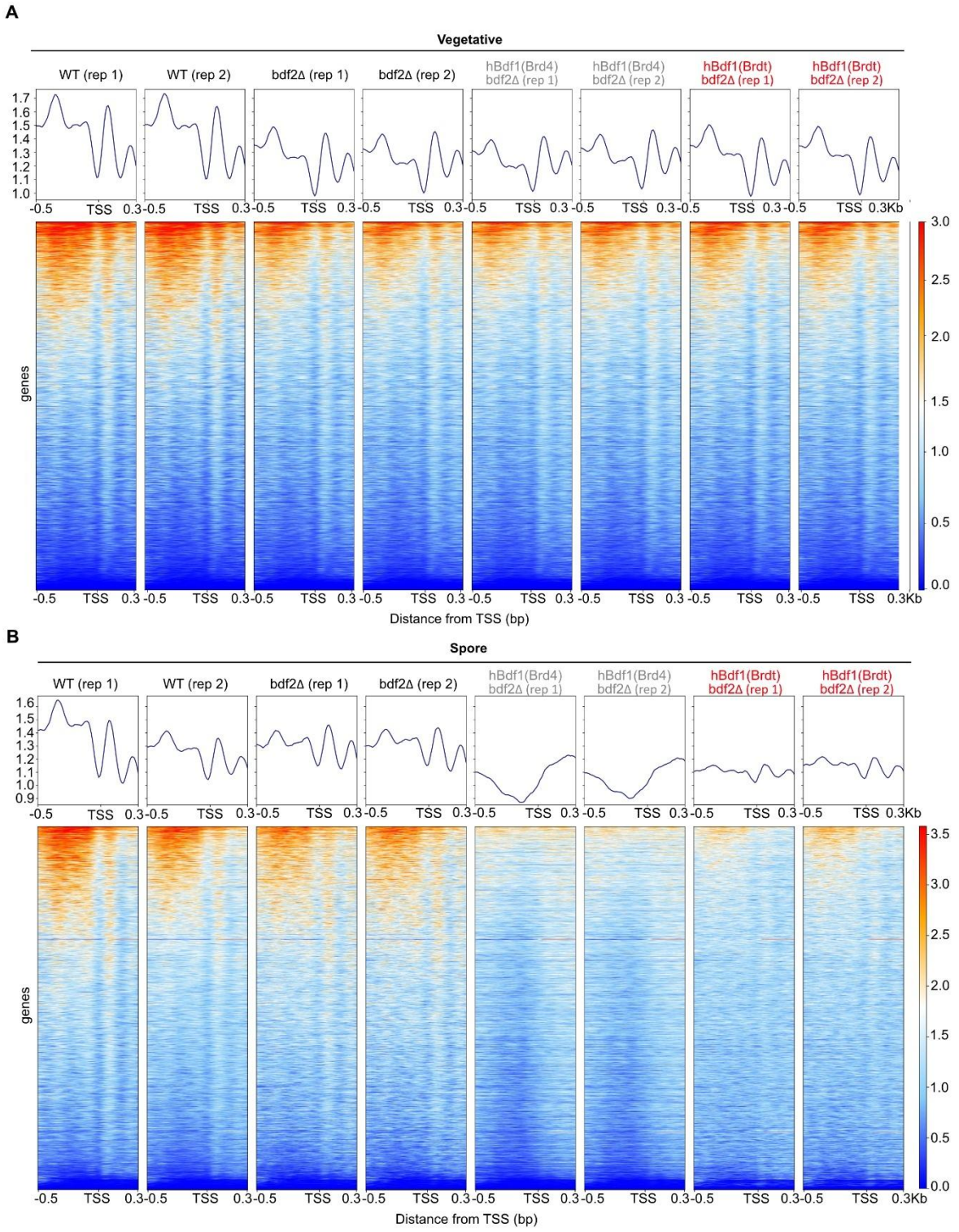

Figure 38: **Genome-wide H4ac profiling via CUT&Tag in vegetative cells and spores. (A)** Genome-wide analysis reveals that the deletion of Bdf2 results in a modest but reproducible global reduction of H4ac at TSS. Comparative analysis of humanized strains in a bdf2Δ background shows that the replacement of endogenous bromodomains with BRD4 or BRDT does not significantly alter the global H4ac distribution in vegetative cells. Despite the distinct nuclear distributions seen by immunofluorescence, the genomic positioning of H4ac remains largely preserved across these backgrounds. **(B)** While WT and bdf2Δ spores maintain recognizable H4ac profiles (with reduced intensity due to chromatin compaction), spores from BET-humanized bdf2Δ strains exhibit profound architectural disruption: signals appear highly altered suggesting that the humanization of Bdf1 bromodomains in the absence of Bdf2 compromises chromatin maintenance during sporulation.

IX. Ethanol exposure reveals a metabolic vulnerability of BET-humanized strains during sporulation

Control solvent conditions uncover a strong sporulation defect in BET-humanized strains. As part of our efforts to pharmacologically target human BET bromodomains in yeast, we tested several inhibitors, including JQ1 and iBET derivatives, under sporulation conditions. All experiments in this section were performed in a BDF2-proficient background, to preserve the endogenous functional redundancy between Bdf1 and Bdf2.

During these experiments, we unexpectedly observed that the solvent control condition used for inhibitor delivery, containing ethanol, had a marked effect on sporulation efficiency. We therefore systematically evaluated the impact of ethanol alone at the concentration present in these conditions (0.8%).

We first confirmed that this concentration does not affect vegetative growth. Cells grown under standard mitotic conditions displayed no detectable growth defect in the presence of ethanol, indicating that this treatment is well tolerated during proliferation (Figure 39A).

BET-humanized strains display strong and differential sensitivity to ethanol during sporulation. In contrast to vegetative growth, ethanol exposure had a pronounced impact on sporulation. While WT cells showed only a moderate reduction in sporulation efficiency, BET-humanized strains exhibited a strong hypersensitivity (Figure 39B, C).

This effect was particularly severe in the BRD4-humanized strain, in which sporulation efficiency dropped to nearly zero. In comparison, the BRDT-humanized strain was less affected, although sporulation efficiency was still significantly reduced to approximately 30%.

These results indicate that, despite the presence of BDF2, humanization of Bdf1 bromodomains generates a strong context-dependent vulnerability that is specifically revealed under sporulation conditions in the presence of ethanol.

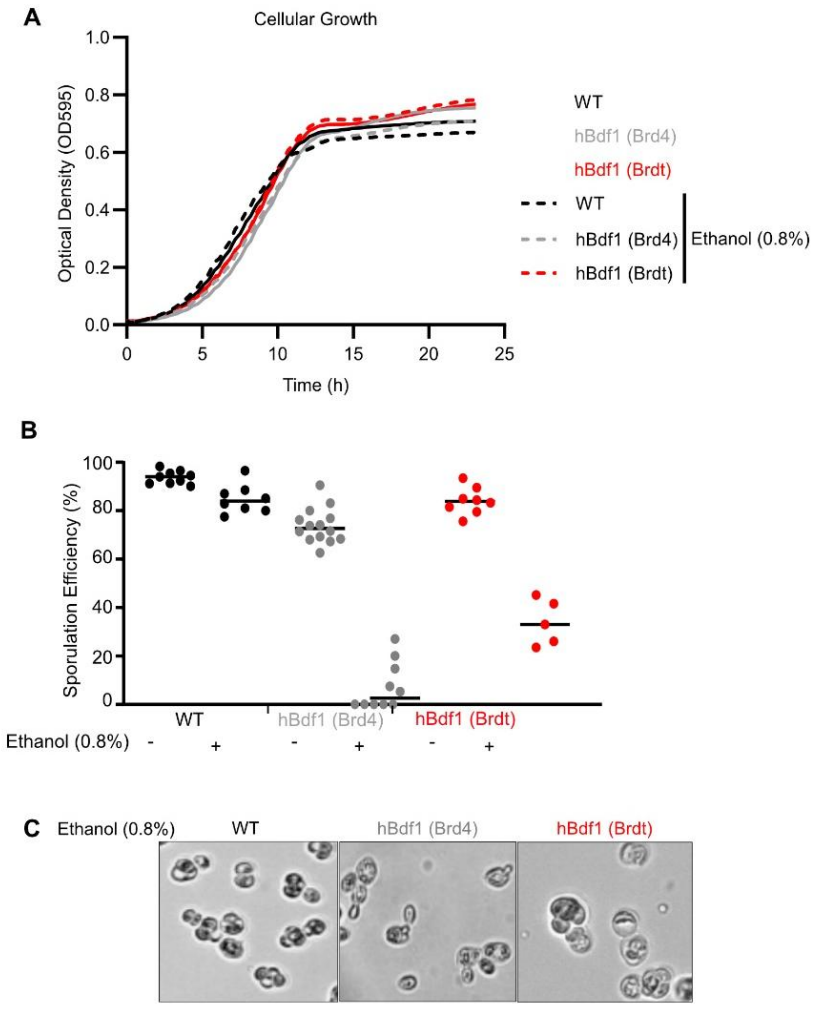

Figure 39: **Ethanol hypersensitivity reveals a hidden functional vulnerability in BET-humanized strains. (A)** Growth analysis of WT, hBdf1(Brd4), and hBdf1(Brdt) strains in the presence of 0.8% ethanol. Under vegetative growth conditions, all strains show equivalent proliferation rates. **(B)** Quantitative assessment of sporulation efficiency in a BDF2 background. Exposure to 0.8% ethanol, induces a profound defect specifically in humanized strains. **(C)** Representative bright-field or phase-contrast microscopy images of WT, hBdf1(BRD4), and hBdf1(BRDT) strains following 72 hours of sporulation induction in the presence of 0.8% ethanol.

Ethanol exposure delays transcriptional progression during sporulation. To assess the impact of ethanol on transcriptional dynamics during sporulation, we performed RNA-seq analyses under the same experimental and analytical framework as described above, in the presence of ethanol.

PCA revealed a clear defect in sporulation progression under ethanol conditions (Figure 40A). As observed under control conditions, vegetative genes are efficiently repressed upon sporulation induction, although to a lesser extent in the presence of ethanol. Early sporulation genes are induced with an approximate extra delay of 4 hours, while middle sporulation genes show markedly reduced expression, and late sporulation genes are almost completely absent in the presence of ethanol (Figure 40B).

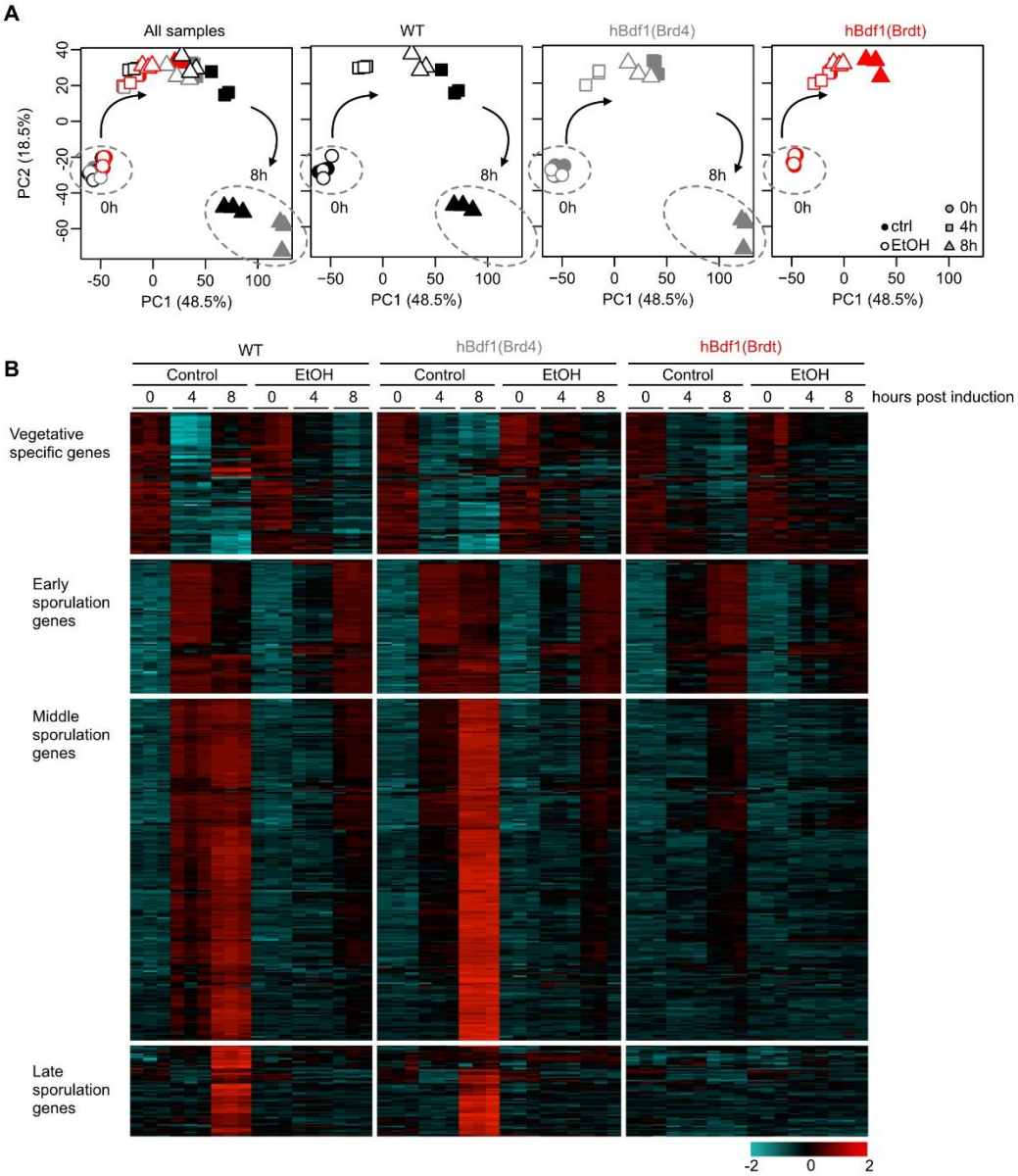

Figure 40: **Impact of ethanol on the temporal dynamics of the sporulation transcriptome. (A)** PCA of RNA-seq profiles for WT and humanized strains in the presence of 0.8% ethanol. High replicate clustering confirms experimental reproducibility. In WT cells, the 4 h time point under ethanol exposure clusters proximal to the control 8 h time point, indicating a significant developmental lag. While BRD4-humanized cells follow a similarly delayed trajectory, BRDT-humanized profiles exhibit substantial overlap across conditions, consistent with a severe and pre-existing kinetic arrest. (B) Heatmap analysis of temporal gene expression patterns confirm a systematic slowdown of the meiotic program. While vegetative gene repression remains largely functional, induction kinetics are profoundly altered.

Analysis of representative genes confirms this phenotype, with little to no induction of key regulators such as NDT80, AMA1, DIT1, and DIT2 (Figure 41A). Importantly, sporulation initiation is not abolished in the presence of ethanol, as evidenced by comparable expression levels of IME1 with and without ethanol (Figure 41A). In contrast, IME2 expression appears delayed, suggesting that ethanol may specifically impact the expression of this master regulator. This raises the possibility that metabolic cues associated with ethanol exposure may influence the expression or activity of key transcriptional regulators.

To quantitatively assess sporulation progression, we developed a transcriptional progression score based on WT dynamics under control conditions (Figure 41B). This score was computed using the 200 most strongly upregulated and 200 most strongly downregulated genes between 0, 4, and 8 hours, normalized to define a continuum from 0 (vegetative state) to 1 (fully progressed sporulation at 8 hours). Application of this metric across all conditions confirms the observed trends. Under control conditions, WT and BRD4-humanized strains display similar progression kinetics, whereas the BRDT-humanized strain exhibits delayed progression, particularly at 8 hours. Strikingly, in the presence of ethanol, all three strains converge toward a similar delayed state, closely resembling the transcriptional profile of the BRDT mutant under control conditions (Figure 41C).

Together, these results demonstrate that ethanol exposure induces a global delay in transcriptional progression during sporulation, phenocopying the defect observed in BRDT-humanized cells and further highlighting the sensitivity of this developmental program to perturbations affecting transcriptional dynamics.

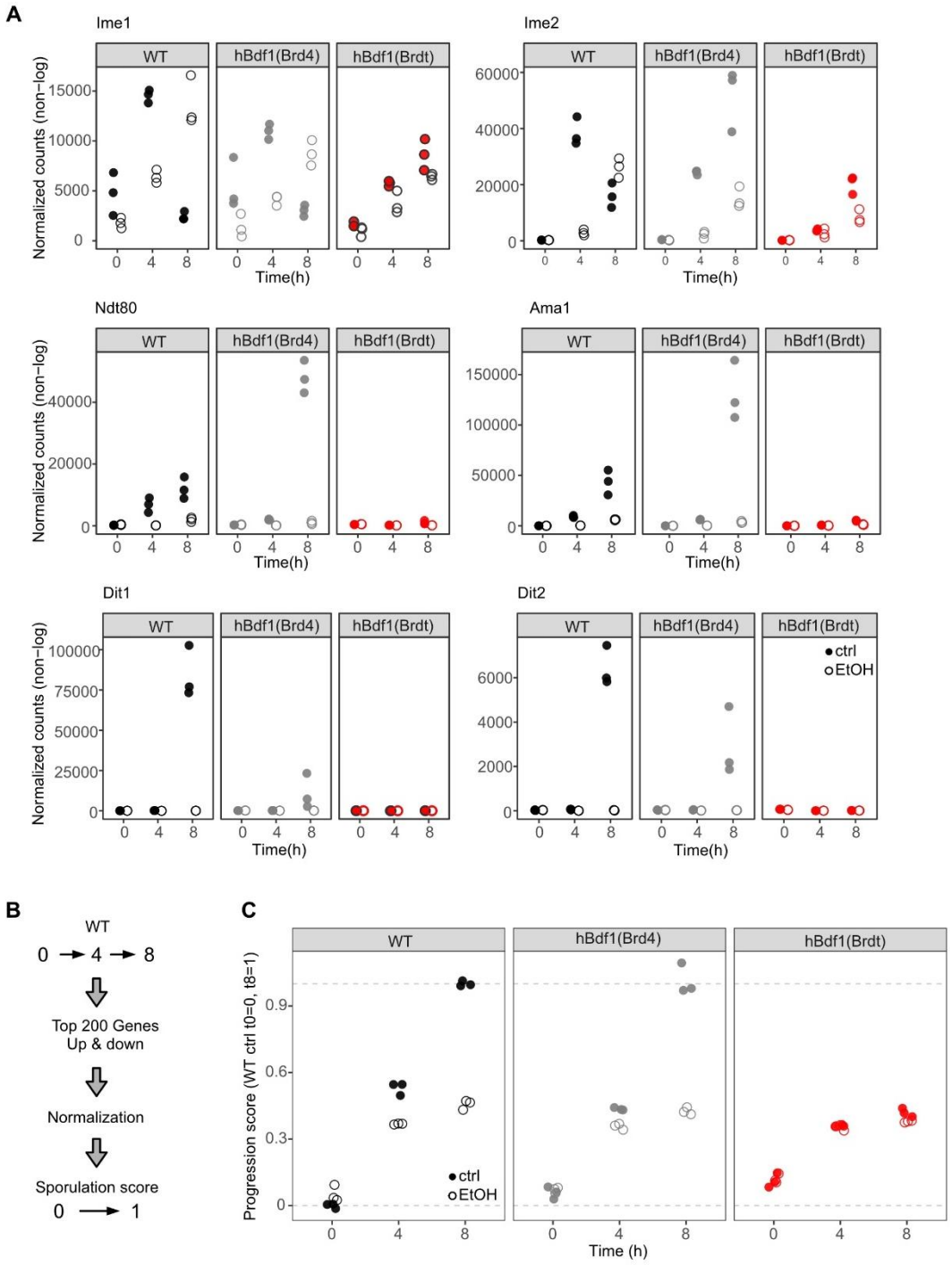

Figure 41: **Quantitative assessment of meiotic progression and the ethanol-induced transcriptional delay**. **(A)** Transcript levels of master regulators and phase-specific genes across the sporulation time course. While IME1 (entry) shows comparable induction across conditions, IME2 (early-middle) displays a significant temporal delay in the presence of ethanol. Downstream middle- and late-phase genes, such as NDT80, AMA1, DIT1, and DIT2, show little to no induction. **(B)** A quantitative metric representing meiotic "velocity" was developed using the 200 most dynamically regulated genes (up/down) in WT control cells. The score defines a continuum from 0 (vegetative state) to 1 (completed 8-hour program). Control Conditions: WT and hBdf1(Brd4) strains follow a similar progression, while hBdf1(Brdt) exhibits a marked kinetic lag. **(C)** These data demonstrate that ethanol exposure acts as a global kinetic suppressor of the meiotic cascade. The fact that ethanol treatment mimics the intrinsic defect of the BRDT-humanized mutant suggests a common susceptibility in the transcriptional program, where minor perturbations to BET-mediated dynamics or metabolic state can arrest the progression toward middle and late sporulation phases.

Ethanol uncouples transcriptional progression from sporulation efficiency in BET-humanized strains. Importantly, these transcriptomic observations must be interpreted considering the phenotypic data presented in Figure 39. In the presence of ethanol, WT, BRD4-humanized, and BRDT-humanized strains display broadly similar transcriptional progression during sporulation. However, extensive experimental replicates consistently demonstrate that sporulation efficiency is markedly different across strains under these conditions.

Ethanol almost completely abolishes spore formation in the BRD4-humanized strain. Thus, despite exhibiting a transcriptional progression profile comparable to WT cells, BRD4-humanized cells are unable to complete sporulation. BRDT-humanized cells also show reduced sporulation efficiency, consistent with their delayed transcriptional progression.

This uncoupling between transcriptional dynamics and phenotypic outcome is especially striking for the BRD4-humanized strain, which, under control conditions, closely follows WT progression. The strong sensitivity of this strain to ethanol therefore suggests that BRD4 bromodomains may be particularly impaired in supporting later stages of sporulation under stress conditions, potentially affecting processes that are not fully captured at the transcriptional level alone.

Ethanol exposure likely perturbs metabolic pathways essential for sporulation. Unlike vegetative growth, sporulation in *S. cerevisiae* occurs under conditions of glucose depletion and relies on non-fermentable carbon sources, particularly acetate. Under these conditions, cellular metabolism is reprogrammed toward respiratory pathways and efficient production of acetyl-CoA, which is required for both energy production and biosynthetic processes supporting meiosis and spore formation. Ethanol is metabolically active in this context and can be oxidized into acetaldehyde and subsequently into acetate through the action of alcohol and aldehyde dehydrogenases. This metabolic conversion feeds into acetyl-CoA production pathways and is coupled to changes in intracellular redox balance through NAD+/NADH interconversion.

As a result, even moderate ethanol concentrations could perturb carbon flux and redox homeostasis during sporulation. Given the central role of acetyl-CoA as a donor for histone acetylation, such metabolic changes may directly influence chromatin regulation.

Strikingly, this phenotype is not observed in WT cells, which remain largely resistant to ethanol under the same conditions, but is strongly exacerbated in BET-humanized strains, particularly in the BRD4-humanized background and, to a lesser extent, in BRDT-humanized cells. This differential sensitivity suggests that yeast BET bromodomains contribute to buffering metabolic fluctuations during sporulation, a function that is impaired upon replacement with human bromodomains.

Ethanol is oxidized into acetaldehyde and subsequently into acetate by Aldehyde Dehydrogenases (ALDs), which is then converted to acetyl-CoA by ACS enzymes (A). Our RNA-seq data provide a molecular basis for this metabolic collapse in the humanized strains. We observed significant deregulation of the ALD gene family (ALD3, ALD5, ALD6) and Acetyl-CoA Synthetases (ACS1, ACS2) in hBdf1(Brd4) and hBdf1(Brdt) compared to WT across the multiple timepoints (Figure 42B). The deregulation of these key players suggests that humanized strains fail to manage the carbon flux and redox imbalances (NAD+/NADH) induced by ethanol. Strikingly, while WT cells remain resistant, this metabolic perturbation is strongly exacerbated in BET-humanized strains, particularly in the BRD4-humanized background. This suggests that native yeast BET bromodomains act as a metabolic-epigenetic buffer, stabilizing transcriptional output despite fluctuations in the acetyl-CoA pool. When replaced by human counterparts, this "buffering" capacity is lost.

In this framework, the strong hypersensitivity of BET-humanized strains indicates that the coupling between metabolic state and chromatin function becomes limiting when bromodomain properties are altered. These results further suggest that distinct human bromodomains differ in their ability to support this coupling, with BRD4 displaying a more pronounced defect than BRDT in the yeast context.

Ethanol exposure reveals a metabolic vulnerability of BET-humanized strains during sporulation. Together, these results reveal that ethanol exposure uncovers a previously unappreciated vulnerability of BET-humanized strains that is not apparent under standard growth conditions. While WT cells efficiently tolerate moderate ethanol levels during sporulation, strains harboring human bromodomains, particularly BRD4, fail to sustain this differentiation program. Given that ethanol metabolism directly feeds into acetate and acetyl-

CoA production while perturbing cellular redox balance, our findings suggest that sporulation requires a tight coordination between metabolic state and chromatin regulation. In this context, yeast BET bromodomains likely contribute to buffering metabolic fluctuations and maintaining transcriptional robustness during large-scale gene expression reprogramming. Their replacement by human counterparts appears to compromise this adaptive capacity, revealing functional differences in how BET bromodomains interpret or respond to dynamic acetylation landscapes.

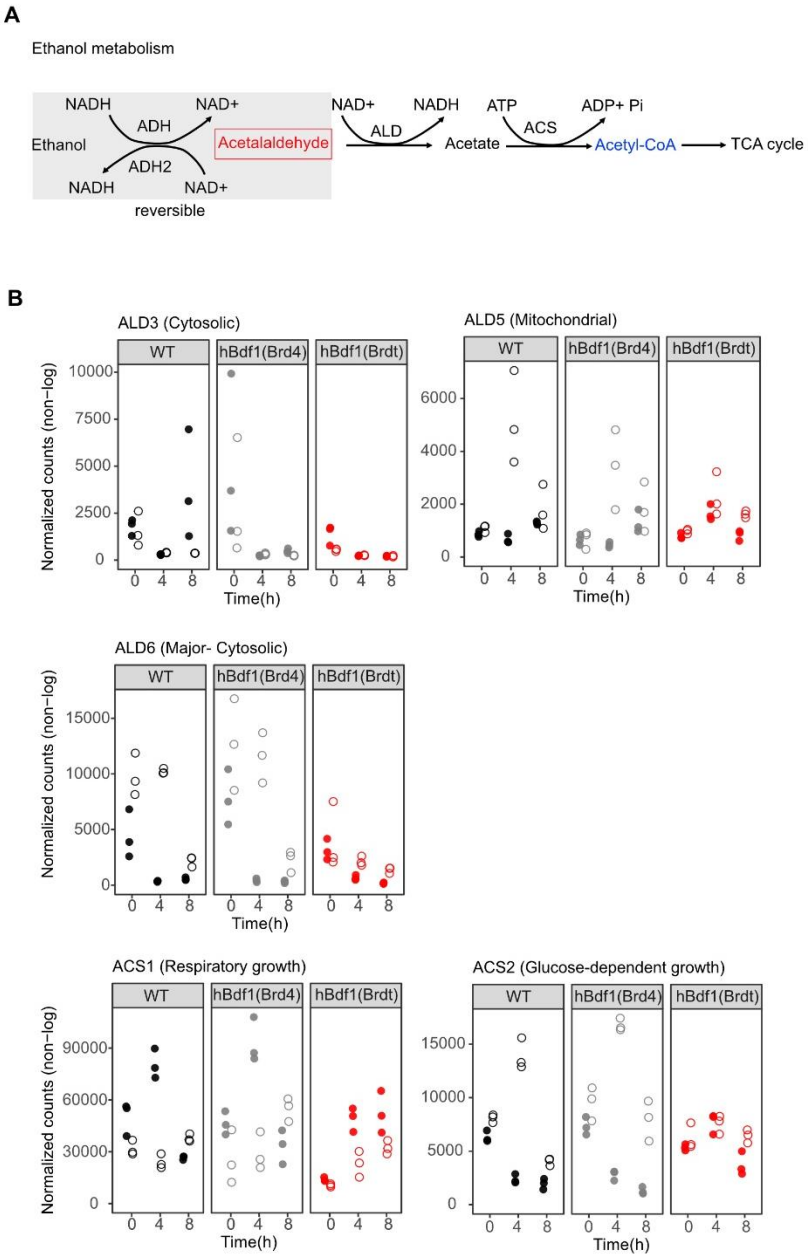

Figure 42: **Transcriptional deregulation of the acetate pathway by ethanol reveals a metabolic-epigenetic vulnerability in humanized strains. (A)** Schematic representation of Ethanol metabolism; Ethanol is catabolized via the Alcohol Dehydrogenase (ADH) pathway, which reversibly oxidizes it into acetaldehyde, a highly toxic intermediate (indicated in red). Acetaldehyde is subsequently converted into acetate by Aldehyde Dehydrogenases (ALD) to prevent cellular damage. The latter is further activated into Acetyl-CoA by Acetyl-CoA Synthetases (ACS). **(B)**Transcript levels of key metabolic enzymes across the sporulation time course. Compared to WT, both hBdf1(Brd4) and hBdf1(Brdt) strains exhibit significant temporal deregulation of Aldehyde Dehydrogenases (ALD3, ALD5, ALD6) and Acetyl-CoA Synthetases (ACS1, ACS2). This highlights a severe defect in managing carbon flux and redox balance (NAD+/NADH) upon ethanol exposure.

X. Summary and concluding remarks of the Results

Collectively, the results presented here establish a comprehensive framework linking chromatin organization, histone acetylation, and BET bromodomain function during yeast sporulation. We first demonstrate that spore differentiation is accompanied by pronounced nuclear remodeling, including reduced nuclear volume, extensive DNA compaction, and a marked reorganization of chromatin spatial distribution. Despite this highly compacted state, histone H4 acetylation remains present and displays a heterogeneous nuclear pattern, suggesting a non-canonical role of this modification in spores.

To understand how this acetylation landscape is interpreted, we investigated the function of BET bromodomains across species. Although yeast and human BET bromodomains share strong structural conservation, our data show that they are not functionally interchangeable. Humanization of Bdf1 bromodomains alters chromatin binding dynamics, as revealed by FRAP, and leads to significant defects in multiple chromatin-dependent processes, including mating, DNA damage response, and sporulation. These phenotypes occur despite largely preserved vegetative growth, indicating that BET bromodomain function becomes particularly critical in contexts requiring large-scale cellular reprogramming.

Consistent with this idea, transcriptomic analyses reveal that BET bromodomains are essential for the timely execution of the meiotic transcriptional program. Humanized strains, especially those carrying BRDT bromodomains, exhibit a pronounced delay in transcriptional reprogramming during sporulation, affecting both global gene expression trajectories and key regulatory pathways.

Our results further uncover a functional interplay between Bdf1 and its paralog Bdf2 in controlling chromatin acetylation. Deletion of BDF2 induces a striking redistribution of H4 acetylation at the nuclear level, which is strongly dependent on the nature of the bromodomains present in Bdf1. Genome-wide analyses indicate that this effect likely reflects a broader reorganization of acetylation landscapes. In spores, the combination of BDF2 deletion and BET bromodomain humanization leads to highly atypical chromatin profiles, consistent with a severe disruption of chromatin architecture and correlating with loss of spore viability.

Finally, we identify an unexpected metabolic vulnerability of BET-humanized strains revealed by ethanol exposure during sporulation. While WT cells tolerate moderate ethanol levels, humanized strains, particularly those expressing BRD4 bromodomains, fail to sustain sporulation under these conditions. Given that ethanol metabolism impacts acetyl-CoA production and redox balance, these findings suggest that BET bromodomains contribute to maintaining the functional coupling between metabolic state and chromatin regulation during differentiation.

Taken together, these results demonstrate that BET bromodomains play a central role in coordinating chromatin structure, transcriptional dynamics, and metabolic adaptation during sporulation. They further reveal that, despite their structural conservation, human BET bromodomains cannot fully recapitulate the functions of their yeast counterparts, highlighting fundamental species-specific differences in how acetylated chromatin is interpreted *in vivo*.

Chapter 4: Discussion

Chapter 4: Discussion

I. Overcoming the technical barriers of the "bunkerized" spore.

A central challenge to analyzing meiotic progression is the "bunkerized" state of the mature spore. This dormancy is achieved through a specialized, multilayered wall built in a hierarchical sequence: an inner mannan-rich layer, a β-glucan layer, a chitosan shell, and finally an outer dityrosine that confers resistance to extreme environmental stress. While essential for survival, this physical robustness creates a critical technical bottleneck, effectively shielding the nucleus and the chromatin from standard epigenomic enzymes, such as transposases, and imaging probes. Standard protocols used to digest and permeabilize vegetative cells, often relying on Zymolyase, are inactivated by the outer dityrosine barrier, preventing enzymatic access to the nucleoplasm (Brettrager et al., 2024). Our study directly addressed these architectural barriers by selectively compromising the wall's integrity. We generated a dit1Δ background to abolish the formation of the outermost dityrosine layer. Thus, by removing this mechanical shield, we bypassed the primary obstacle to Zymolyase digestion, thereby permitting access to the nucleus without destabilizing the underlying developmental framework of the spore.

Managing population heterogeneity to isolate spore-specific signal. Beyond the challenges of physical access, the population heterogeneity of sporulating cultures presented a significant risk of statistical bias. While the humanized strains achieved ~ 80% efficiency, the remaining ~20% contamination of non-sporulating vegetative cells could skew bulk population data. In epigenomic assays such as mapping H4Kac distribution or chromatin accessibility, the highly open architecture of vegetative cells generates a disproportional signal that masks the more cryptic and compacted signatures unique to the spore. To mitigate this risk and ensure our data strictly reflected the "ultracompact" chromatin state of the spore rather than a mixed-population average, we implemented a rigorous purification protocol. This approach exploited the unique surface biophysics of the spore wall, which exhibits significantly greater hydrophobicity and distinct electrostatic properties compared to vegetative cells. By taking advantage of this differential affinity, we utilized DNA-low bind surface treatments on plasticware to selectively capture mature spores while allowing vegetative contamination to be removed, ensuring the purity required for robust epigenomic analysis.

Adapting existing protocols for the compact spore genome. Finally, the inherent size and density of the spore genome demanded a rigorous recalibration of enzymatic assays. We note that while a commercial ATAC-seq kit specifically for yeast was released in late 2023, this occurred after the essential data collection phases of our study had been completed. Consequently, we developed and validated a customized ATAC-seq workflow, optimized for the physical properties of yeast chromatin in collaboration with the Epinomics Platform at IAB. This specialized approach was required because most established epigenomic methodologies are optimized for mammalian systems, which possess genomes roughly 250 times larger and feature a far more open architecture than *S. cerevisiae* (Goffeau et al., 1996; Human Genome Sequencing Consortium, 2004). Directly applying these macro-scale protocols to the small, compact yeast nucleus inevitably results in excess enzyme concentration, favoring massive over fragmentation and experimental noise that masks fine-scale regulatory dynamics. By strictly controlling the titration between transposase kinetics and chromatin density and utilizing adapted lysis conditions, we ensured that our observations of internal chromatin rewiring were robust and accurate representations of the spore's true differentiation state.

II. Nuclear size and chromatin compaction

Cellular and nuclear size. The transition from vegetative growth to sporulation necessitates a profound restructuring of the cell's physical dimensions. Our volumetric analysis reveals a coordinated reduction in both cellular and nuclear size; however, the ratio of nuclear-to-cellular occupancy remains constant (Walters et al., 2019). This isometric scaling suggests that the nuclear and cellular membranes behave as elastic boundaries, acting like a "rubber band" that contracts in response to the total volume of its internal contents.

Impact of ploidy. It is important to note that the observed scale of this reduction is likely influenced by the ploidy of the vegetative populations. In yeast, the volume of a vegetative diploid cell is approximately twice that of a haploid cell (K. C. Chen et al., 2004). Since the vegetative cells in our analysis were haploids, the transition to the haploid spore represents a move between two structurally comparable genomic states. This common ploidy likely explains why the decrease in cellular and nuclear volume was not more drastic thus the scaling down we observed reflects the specific compaction requirements of the spore state.

Chromatin spatial reorganisation. At the chromatin level, the shift is far more extreme than a simple reduction while comparing vegetative diploid cells to spores. We observed a 16-fold DNA compaction within the spore, marking a transition from an expansive, transcriptionally active vegetative state to a hyper-condensed, quiescent architecture. Most striking is the change in global nuclear occupancy: while vegetative chromatin occupies roughly 75% of the nuclear volume, the spore's genome is sequestered into just 24% of the available space. This drastic reduction in occupancy reveals that the nuclear envelope does not shrink in direct proportion to the genome it houses. Instead, the chromatin collapses into a dense, localized cluster, leaving most of the nuclear volume unoccupied by DNA.

III. H4 hyperacetylation in spores

Histone H4ac undergoes extensive remodeling during the transition to the dormant spore state, resulting in a marked enrichment in mature spores (Govin et al., 2010). We confirmed this hyperacetylation by Western blotting, showing that the H4ac signal remains strongly retained even within the highly condensed spore nucleus. This is particularly intriguing because histone acetylation is classically associated with chromatin relaxation; in spores, however, H4 acetylation appears to coexist with a compact nuclear architecture. This apparent paradox suggests that H4 acetylation may have a distinct structural or regulatory function in spores, potentially contributing to chromatin organization while preserving the capacity for rapid transcriptional reactivation upon germination.

We next performed immunofluorescence analyses in vegetative cells and spores. Confocal microscopy revealed a clear nuclear H4ac signal in both conditions, with some differences in signal distribution. But upon using super-resolution microscopy to refine this analysis, we uncovered a heterogeneous intranuclear pattern characterized by discrete H4ac-enriched foci interspersed with regions of lower signal intensity, a level of organization that was not resolved by conventional confocal imaging. The identity and functional relevance of these H4ac-enriched regions remain to be determined, but they may reflect specialized chromatin domains involved in transcriptional priming or structural genome organization. Further optimization of super-resolution imaging, including dual-color approaches, will be necessary to determine their relationship with DNA density and chromatin compaction.

IV. The biology of the bromodomains differs from yeast to human

While bromodomain architecture remains highly conserved across evolution, our findings indicate that structural and functional specializations have emerged. Specifically, we observed a distinct shift in humanized protein dynamicity that correlates with subtle alterations in both the binding pocket affinity and the electrostatic surface properties of the charged patch.

Structural divergence and protein dynamicity. The transition from the specialized yeast readers to their humanized counterparts, BRD4 and BRDT, highlights how evolutionary pressure has tuned these proteins for specific nuclear environments. In our model, the dynamicity of the reader, Bdf1, refers to its residence time on the chromatin and its ability to transition between bound and mobile states. We suggest two primary structural drivers of this differential behavior:

Binding pocket refinement: Variations in the residues lining the acetyl-lysine binding pocket dictate the raw affinity for H4ac (Filippakopoulos et al., 2012). Our data shows that key amino acid differences alter the binding of the polar Bdf1-BD1 bromodomain compared to the hydrophobic acetyl-lysine pocket in the humanized versions.

Enhanced affinity: This hydrophobic shift in the humanized BRD4 version results in a higher affinity for lysine acetylated residues, as directly observed in previously published pull-down assays(García-Oliver et al., 2017). To further strengthen this biochemical correlation within the current model, pull-down assays are further being conducted in this study using BRD4 and BRDT BD1.

The charged patch interface: Beyond the primary binding pocket, the surrounding electrostatic landscape facilitates secondary interactions with the DNA backbone. We identified that the patch interface of binding with DNA changed from a basic patch in Bdf1- BD1 to an acidic charged surface in humanized bromodomains.

Chromatin engagement: Chromatin solubilization assays show a differential lysine interaction between both humanized strains' bromodomains BRD4 and BRDT along with the yeast bromodomains. These biochemical results are complementary to the protein dynamicity observed in FRAP experiments and the high-affinity profiles of Brd4 bromodomains in pull-down assays.

Functional implications of divergence. The structural divergence in both the charged patch interface and the lysine-binding pocket appears to be a key factor in the humanized versions' inability to maintain chromatin architecture during demanding developmental transitions like sporulation. While the humanized bromodomains provide sufficient functionality to support basic growth processes in vegetative cells, they fail to meet the specialized requirements of the yeast spore's extreme nuclear environment. This suggests that the native yeast basic patch and polar pocket are evolutionarily optimized to preserve genomic integrity under high physical compaction, a capacity that is lost in the acidic patch and hydrophobic pocket of the humanized variants. When introduced into the yeast system, these humanized readers either overwhelm the genome with excessive affinity (BRD4) or fail to find their "footing," possibly due to a lack of compatible surface charges (BRDT). Ultimately, these differences suggest that the BET family has evolved not just to recognize acetylation, but to do so with a specific kinetic profile. This suggests that the protein's dynamicity serves as a critical functional filter. It ensures that readers dwell on chromatin just long enough to recruit the necessary downstream effectors, such as the TFIID complex. When this kinetic balance is disrupted, as seen in our humanized strains, the resulting over-tethering or binding instability leads to a cascade of functional failures that ultimately lead to cellular death.

Moreover, this kinetic filtering explains why the conservation of the bromodomain fold is not enough to ensure cross-species compatibility. While the primary structure is preserved, the on/off rates are tailored to the specific complexity and compaction levels of the host genome. In the yeast spore, a system defined by extreme compaction and limited physical space, there is no margin for error. A humanized reader that fails to filter its binding duration effectively turns from a functional coordinator into a lethal architectural defect.

V. Functions of Bdf1 bromodomains in sporulation

Recent findings identify the Bdf1 bromodomains as essential regulators of sporulation entry in S. cerevisiae. The authors demonstrated that altering key amino acids within the lysine-binding pocket completely abolishes the sporulation program (García-Oliver et al., 2017). Beyond this initial requirement for meiotic entry, the team’s previous identification of Bdf1 enrichment on spore chromatin at post-meiotic stages points toward a novel, non-canonical role for Bdf1 in spore maturation and the maintenance of a highly compacted chromatin state. A central

discovery of the current study is the significant divergence in the electrostatic landscape surrounding the bromodomains. We identified that the surface charge of the bromodomains is substantially modified between the native yeast Bdf1-BD1 and its human counterparts, BRD4 and BRDT. Consequently, we next envisage generating specific mutants in this electrostatic patch to determine if modulating these surface charges, independent of the primary binding pocket, is sufficient to alter the sporulation entry capacity and architectural maintenance in yeast.

VI. Bdf1 and chromatin integrity

While autophagy provides the metabolic fuel (Barve & Manjithaya, 2021), Bdf1 provides the regulatory blueprint, ensuring the genome is both transcriptionally and structurally primed for the transition. Bdf1 is essential for driving the expression of NDT80, the master transcription factor that governs the middle sporulation program. The activation of Ndt80 triggers the expression of genes responsible for meiotic divisions and the physical extension of the prospore membrane (PSM) via Sso1-dependent pathways (Chu et al., 1998; Chu & Herskowitz, 1998; Pak & Segall, 2002). This coordination ensures that the internal remodeling of the cell keeps pace with its genetic division. Central to this role is the H4ac signal, where Bdf1 utilizes its bromodomains to specifically sense the surge in H4ac as a critical checkpoint for meiotic commitment. This epigenetic mark serves as a molecular barometer, reflecting the cell's readiness to exit the vegetative cycle and commit to the highly specialized, quiescent spore state.

The central hypothesis of this study is that Bdf1 acts as a critical integrator between nutrient-starvation signals and the physical remodeling of the cell, a coordination that is fundamentally severed upon humanization. This integration breaks down through two specific mechanisms: first, a kinetic mismatch occurs because human BET proteins (BRD4/BRDT) possess altered chromatin residence times, creating a dynamicity gap that could prevent the timely recruitment of the TFIID complex to meiotic promoters and stall the NDT80 program. Second, because autophagy is tightly coupled with vacuolar function, this possible failure to properly regulate meiotic genes leads to the massive collapse and persistent defects such as observed in Figure 27.

VII. Bromodomain specificity and chromatin boundaries

The topographical integrity of the yeast genome depends on a precise balance between Bdf1 and Bdf2, two proteins that have diverged to manage the tension between transcriptional activity and structural boundaries (J. Wang et al., 2013; García-Oliver et al., 2017). This division of labor is essentially a system of "checks and balances" for the physical shape of chromatin.

The division of tasks. Our data shows that when Bdf2 is removed (bdf2Δ), Bdf1 can only manage a 50% "abnormal" profile as observed in Figure 37. This ceiling is quite revealing and suggests that even though Bdf1 can partially step in to help, its promoter-centric design is simply not a substitute for the specialized, boundary-directed function of Bdf2.

By using the bdf2Δ background, we essentially created a "stress test" to see how human bromodomain readers would behave without the native yeast constraints. This revealed two extreme failures in evolutionary calibration: In the Bdf1(Brd4) strain, we saw a dramatic increase in tethering. Because we demonstrated that human BRD4 is highly tethered and promiscuous, it stabilizes acetylated histone clusters in an uncontrolled manner once the native boundaries are gone. The resulting peri-chromatin halos could be the visual footprint of a protein that is over-tethering the genome, expanding acetylated domains into spaces where they do not belong. On the opposite end of the spectrum, the Bdf1(Brdt) strain failed almost entirely to maintain this architecture. BRDT's testis-specific bromodomains would appear to be biologically incompatible with the yeast H4ac landscape. Without the extra scaffolding that Bdf2 normally provides, BRDT bromodomains simply cannot find the requisite affinity to anchor the chromatin.

These observations led us to a model where maintaining the genome's physical limits is not just a side effect of having bromodomains, it requires a precise affinity threshold that is tuned to the local histone environment and that Bdf2 is the essential mechanical "stop" to heterochromatin expansion, a role that human BET proteins either overwhelm through excessive, uncalibrated affinity or fail to fulfill due to a lack of selectivity.

VIII. H4 acetylation genomic pattern

The analysis of H4ac genomic distribution in humanized yeast strains yields a striking contrast between vegetative growth and the sporulation phase, highlighting a potential collapse in

epigenetic maintenance. During vegetative growth, the depletion of Bdf2 in the BRD4 and BRDT humanized strains did not result in a significant shift in the overall genomic organization of H4ac, a finding that stands in apparent contradiction to the spatial heterogeneity observed via IF with the diffused profile in WT and hBdf1(Brd4) strains. This discrepancy suggests that while the spatial localization of acetylated histones might appear altered at a macro-cellular level, the underlying occupancy across specific genomic loci remains relatively stable.

However, this stability vanishes upon entering the developmental stage of sporulation. In humanized spores, the H4ac signal is virtually absent, suggesting a failure in the metabolic or enzymatic pathways required to establish or maintain histone acetylation during the packing of the gametic genome. This loss of H4ac effectively phenocopies the loss of function observed upon Bdf1 depletion (Garabedian et al., 2012b) This profound epigenetic "silencing" correlates directly with the observed phenotype: the spores are non-viable. The loss of H4ac likely prevents the necessary transcriptional activation of the germination program, locking the chromatin in a state that is incompatible with survival. This underscores that while humanized yeast can tolerate certain epigenetic variances during mitosis, the rigorous demands of meiosis and spore formation reveal a critical incompatibility that leads to cellular death.

IX. Coordination of Bdf1 in DNA damage response (DDR)

The process starts when DNA double-strand breaks (DSBs) occur. Whether these are caused by external toxins or the deliberate, programmed action of Spo11 during meiosis, the cell marks these sites with a spike in histone H4 acetylation. Research suggests that by regulating the structure of acetylated chromatin, Bdf1 exerts a significant influence over checkpoint-dependent pathways that protect the genome during replication stress in *S. pombe* (Garabedian et al., 2012b). Moreover, Bdf1 promotes homologous recombination repair of DNA double strand breaks through binding to damage-induced H4ac and facilitate RPA loading on resected single-stranded DNA (Figure 43) (Matangkasombut et al., 2000; H. Peng et al., 2021c). Consequently, Bdf1 functions as a critical molecular coordinator of the DDR. In its absence, the essential recruitment of downstream effectors such as RPA and Rad51 is abrogated, preventing the processing of DNA DSB ends. Without this Bdf1-mediated bridge between the epigenetic recognition of the break and the assembly of the repair complex, the homologous recombination (HR) pathway stalls at the pre-resection stage.

Meiotic integrity checkpoint. During meiosis, the cell intentionally breaks its own DNA via Spo11 to allow for genetic shuffling. This is a high-stakes gamble: the cell must repair these breaks perfectly before it can package the DNA into spores. Bdf1 links these two worlds, repair, and transcription, using a single mechanism. It uses the same H4ac recognition to repair the breaks ensuring the physical genome is intact and activates NDT80 signaling the transcriptional "green light" for the sporulation program (García-Oliver et al., 2017).

Why humanized Bdf1 mutants fail in DDR. The differential sensitivity of humanized strains to genotoxic stress provides a critical window into the evolutionary tuning of bromodomain affinities. While these strains survive CPT treatment that induces relatively isolated double-strand breaks, they exhibit profound lethality when exposed to HU or MMS. This discrepancy likely results from a signal-to-noise crisis during global replication stress. HU and MMS trigger widespread, genome-wide histone acetylation as the cell attempts to stabilize thousands of stalled replication forks simultaneously. In this context, the high intrinsic affinity of human BRD4 bromodomains acts as a tethering trap. Instead of dynamically mobilizing to the specific forks requiring TFIID-mediated stabilization, the reader becomes sequestered at hyperacetylated sites across the chromatin landscape, creating a kinetic bottleneck that prevents the timely recruitment of RPA and Rad51 before forks collapse.

On the other hand, the hBdf1(Brdt) humanized strain fails due to the opposite extreme: a lower residence time on the chromatin compared to native Bdf1. Under the intense pressure of replication stress, BRDT lacks the requisite residence time to serve as a stable scaffold; its binding is too transient to maintain the repair machinery, leading to the same catastrophic fork collapse seen with BRD4. In contrast, the localized nature of CPT-induced damage does not generate a global histone acetylation, thus allowing both high- and low-affinity humanized proteins to successfully navigate and repair isolated lesions. Ultimately, these results suggest that Bdf1's utility relies on a precise affinity and dynamicity threshold that balances stable chromatin recruitment with the mobility necessary to survive a global genotoxic crisis.

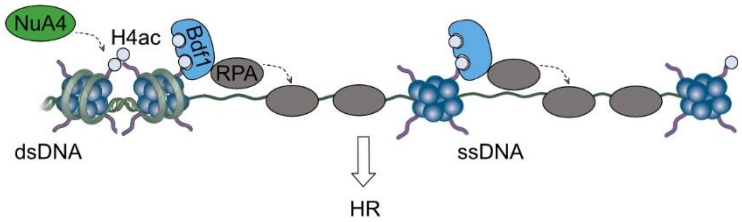

Figure 43: **Bdf1 essential for DNA damage response.** Following double-strand break formation, NuA4-mediated acetylation of histone H4 at break sites recruits Bdf1 through its bromodomains. Bdf1 then engages RPA via its linker and C-terminal regions, enhancing RPA chromatin loading and promoting efficient homologous recombination repair. (Figure adapted from H. Peng et al., 2021c).

X. Possible effect of Bdf1 on mating

While no direct literature connects Bdf1 to yeast mating processes, several testable hypotheses can be formulated based on its known chromatin roles.

A plausible mechanistic bridge between Bdf1 and mating is its role as an acetyl-histone reader that promotes TFIID-associated transcription at promoters. Classical work showed that Bdf1 interacts with Taf subunits and can help localize TFIID to acetylated nucleosomes, while pheromone-responsive genes such as FUS1 and STE2 depend on rapid Ste pathway-driven transcriptional activation (Y. Wang & Dohlman, 2004; Bardwell, 2005; Erdmann et al., 2012). In this framework, reduced mating efficiency in humanized strains could reflect altered bromodomain–chromatin affinity or altered compatibility with the yeast transcription-initiation machinery, but direct evidence for a specific Bdf1–TFIID failure at mating loci is still lacking.

Moreover, research on cryptic promoters indicates that deleting BDF1 does not simply abolish STE11 expression; instead, it alters promoter behavior in a chromatin-context-dependent manner, with Bdf1 acting as a bromodomain reader that supports transcriptional initiation at acetylated promoters (Pattenden et al., 2010). This suggests that Bdf1 functions as a contextual modulator of developmental transcription programs, helping create a permissive chromatin environment for promoter-specific cofactor recruitment rather than acting as a universal switch for DNA accessibility. The reduced mating efficiency of humanized strains could therefore reflect altered sensitivity to chromatin states at mating-regulated loci such as STE11 or FUS1.

XI. The humanization of bromodomains increase sensibility to ethanol

From ethanol to hyperacetylation. During the diauxic shift, yeast oxidizes ethanol through Adh2p to acetaldehyde, which is then converted to acetate by aldehyde dehydrogenases such as Ald6p. Acetate is subsequently converted to acetyl-CoA by Acs2p, a key nuclear-cytosolic acetyl-CoA synthetase that contributes to the acetyl-CoA pool used for chromatin acetylation and biosynthetic processes (de Smidt et al., 2008; Walkey et al., 2012; Bhagwat et al., 2021). Our data suggest that replacing yeast Bdf1 bromodomains with human BRD4/BRDT modules perturbs the transcriptional regulation of ethanol-utilization and acetyl-CoA–producing genes, including ALD and ACS family members. Because Ald6p-dependent acetate production and Acs2p-mediated acetyl-CoA synthesis are central to nucleo-cytosolic acetylation homeostasis, even modest transcriptional deregulation in this pathway could amplify the sensitivity of humanized strains to metabolic and chromatin stress.

Moreover, ethanol exposure fundamentally reshapes the cellular environment. As it is oxidized, the surge in acetate and the shift in the NAD^+/NADH ratio inhibit NAD^+-dependent deacetylases like the SIRT1-like family (Zakhari, 2013; Ghezzi et al., 2017). This inhibition triggers widespread histone hyperacetylation, particularly at H4K16ac (Sabari et al., 2017). In this landscape, the bromodomain reader BRD4 finds itself in a state of competition. The global spike in acetylation increases the protein's affinity for chromatin (Gaub et al., 2020), causing it to be redistributed across the genome (Z. Yang et al., 2008; Slaughter et al., 2021; Lim et al., 2025).

Membrane remodeling and TORC1 inactivation. Beyond the nucleus, ethanol mimics a nutrient-rich environment, which sends a conflicting signal to the cell. It maintains TORC1 activity and prevents the dephosphorylation of Atg13, effectively shutting down the autophagy required for meiotic remodeling (Chang & Neufeld, 2009; Loewith & Hall, 2011; Barve & Manjithaya, 2021). At the same time, ethanol disrupts membrane fluidity. To compensate, the cell activates Npr1 dephosphorylation, which increases vesicle delivery to the plasma membrane and elevates the t-SNARE Sso1 (Oyen et al., 2004; Neiman, 2011). While intended to stabilize the cell surface, this redirection of Sso1 is catastrophic for sporulation; it starves the developing prospore membrane of the materials it needs to extend and fuse, ultimately leading to sporulation abortion (Ben-Ari et al., 2006; Barve & Manjithaya, 2021).

The most striking finding in this study is that humanized Bdf1 strains are significantly more sensitive to ethanol-induced failure than native yeast. We could attribute this to the "kinetic calibration" of the bromodomains as human BET bromodomains (BRD4/BRDT) have a higher intrinsic affinity for acetylated histones. In the presence of ethanol-induced hyperacetylation, they are easily "sequestered" at ectopic stress sites (Filippakopoulos & Knapp, 2014; Donczew & Hahn, 2021b). Suggesting an effectively depleted pool of readers available at essential meiotic promoters like NDT80, amplifying the transcriptional block. On the other hand, the native Bdf1 appears far more resilient. This is likely an evolutionary adaptation where its physical tethering to the TFIID complex acts as a safeguard. This structural "anchor" could help Bdf1 maintain its association with meiotic promoters even when the surrounding acetylation landscape is spiking.

Finally, ethanol forces a cell-fate decision by linking metabolic status directly to genomic occupancy. By shifting the bromodomains from developmental blueprints to stress-response, the cell prioritizes short-term adaptation at the cost of long-term differentiation. This model explains why the humanized bromodomains readers, lacking the evolutionary tuning to resist this redistribution, fail in the yeast system.

XII. Homodimerization of Bdf1 is essential for sporulation entry

In collaboration with Gwanel Rabut's team at IGDR, we identified the spatial interactome of Bdf1 using a NanoLuc-based assay and identified a self-association signal consistent with Bdf1 homodimerization. Subsequent mutational analysis of the homodimerization interface showed that this self-interaction is required for entry into sporulation, revealing an additional structural layer to Bdf1 function during meiotic commitment. The discovery that Bdf1 homodimerizes introduces a critical structural dimension to our understanding of yeast chromatin regulation. This finding shifts the functional paradigm from a simple, one-to-one reader-histone interaction to a multivalent model that mirrors the structural behavior of the human BET protein, BRD2 (Umehara et al., 2010).

Chromatin compaction. We propose that this homodimer architecture allows Bdf1 to function as a molecular clamp, effectively doubling its binding avidity and translating a biochemical recognition event into a mechanical force. By simultaneously engaging multiple acetylated

histones across adjacent nucleosomes, the Bdf1 dimer likely acts as a physical compaction mechanism, decreasing the spatial volume of linker DNA. This localized chromatin condensation is hypothesized to be a prerequisite for the meiotic transition, effectively packaging the genome into an architecture permissive to the meiotic machinery. Consequently, the disruption of this dimerization interface strips the cell of its ability to structurally organize these loci, culminating in the meiotic arrest observed in our homodimerization-deficient mutants.

One of the most interesting aspects of this discovery is that it finally explains why single BD mutants often do not show a strong phenotype. In a monomer, losing a domain is a 50% loss of function. But in a homodimer complex, the remaining functional domains provide a "buffer" or redundancy. Even if one BD is disrupted, its partners in the dimer remain active, maintaining a baseline threshold of chromatin avidity to support partial activity.

Evolutionary conservation of BET dimerization. This structural strategy exhibits striking evolutionary conservation with the human BET paralog BRD2 (PDB: 2DVQ). While previous structural analyses have demonstrated that human BET paralogs such as BRD2 homodimerize via their Motif B interface to achieve high-avidity, multivalent chromatin binding (Umehara et al., 2010; Filippakopoulos et al., 2012), the oligomeric state of yeast Bdf1 has remained uncharacterized. Our discovery that Bdf1 similarly homodimerizes provides a novel structural mechanism that explains the functional redundancy often observed in single bromodomain mutants (García-Oliver et al., 2017). It is highly probable that Bdf1 employs an analogous structural mechanism to stabilize its occupancy at high-demand genomic hubs. Whether tethering repair complexes to DNA double-strand breaks (DSBs) or scaffolding the transcriptional machinery at the NDT80 promoter, the homodimer provides a degree of structural tenacity and affinity that a monomeric reader fundamentally cannot achieve. Finally, this multivalent capability appears to be an evolutionarily conserved requisite for BET proteins to serve as robust, high-fidelity integrators of the epigenetic landscape.

Bibliographic References

Bibliographic References

Aguillon, R., Rinsky, M., Simon-Blecher, N., Doniger, T., Appelbaum, L., & Levy, O. (2024). CLOCK evolved in cnidaria to synchronize internal rhythms with diel environmental cues. *eLife*, *12*, RP89499. https://doi.org/10.7554/eLife.89499

Ajmal, M., Hussain, A., Ali, A., Chen, H., & Lin, H. (2023). Strategies for Controlling the Sporulation in Fusarium spp. *Journal of Fungi*, *9*(1), 10. https://doi.org/10.3390/jof9010010

Akishina, A. A., Kuvaeva, E. E., Vorontsova, Y. E., & Simonova, O. B. (2020). NAP Family Histone Chaperones: Characterization and Role in Ontogenesis. *Russian Journal of Developmental Biology*, *51*(6), 343–355. https://doi.org/10.1134/S1062360420060028

Albulescu, L.-O., Sabet, N., Gudipati, M., Stepankiw, N., Bergman, Z. J., Huffaker, T. C., & Pleiss, J. A. (2012). A Quantitative, High-Throughput Reverse Genetic Screen Reveals Novel Connections between Pre–mRNA Splicing and 5′ and 3′ End Transcript Determinants. *PLOS Genetics*, *8*(3), e1002530. https://doi.org/10.1371/journal.pgen.1002530

Ali, H. A., Li, Y., Bilal, A. H. M., Qin, T., Yuan, Z., & Zhao, W. (2022). A Comprehensive Review of BET Protein Biochemistry, Physiology, and Pathological Roles. *Frontiers in Pharmacology*, *13*. https://doi.org/10.3389/fphar.2022.818891

Allshire, R. C., & Ekwall, K. (2015). Epigenetic Regulation of Chromatin States in Schizosaccharomyces pombe. *Cold Spring Harbor Perspectives in Biology*, *7*(7), a018770. https://doi.org/10.1101/cshperspect.a018770

Altaf, M., Auger, A., Monnet-Saksouk, J., Brodeur, J., Piquet, S., Cramet, M., Bouchard, N., Lacoste, N., Utley, R. T., Gaudreau, L., & Côté, J. (2010). NuA4-dependent Acetylation of Nucleosomal Histones H4 and H2A Directly Stimulates Incorporation of H2A.Z by the SWR1 Complex. *The Journal of Biological Chemistry*, *285*(21), 15966–15977. https://doi.org/10.1074/jbc.M110.117069

Anderson, S. F., Steber, C. M., Esposito, R. E., & Coleman, J. E. (1995). UME6, a negative regulator of meiosis in Saccharomyces cerevisiae, contains a C-terminal Zn2Cys6 binuclear cluster that

binds the URS1 DNA sequence in a zinc-dependent manner. *Protein Science: A Publication of the Protein Society*, *4*(9), 1832–1843. https://doi.org/10.1002/pro.5560040918

Arents, G., & Moudrianakis, E. N. (1995). The histone fold: A ubiquitous architectural motif utilized in DNA compaction and protein dimerization. *Proceedings of the National Academy of Sciences of the United States of America*, *92*(24), 11170–11174. https://doi.org/10.1073/pnas.92.24.11170

Arimbasseri, A. G., Shukla, A., Pradhan, A. K., & Bhargava, P. (2024). Increased histone acetylation is the signature of repressed state on the genes transcribed by RNA polymerase III. *Gene*, *893*, 147958. https://doi.org/10.1016/j.gene.2023.147958

Arrowsmith, C. H., Bountra, C., Fish, P. V., Lee, K., & Schapira, M. (2012). Epigenetic protein families: A new frontier for drug discovery. *Nature Reviews Drug Discovery*, *11*(5), 384–400. https://doi.org/10.1038/nrd3674

Aryal, S. C., Zia, S., Rodgers, S., Shen, Y., Perry, K., & Yuan, L. (2022). BRD3-NUTM1-expressing NUT carcinoma of lung on endobronchial ultrasound-guided transbronchial needle aspiration cytology, a diagnostic pitfall. *Diagnostic Cytopathology*, *50*(2), E47–E53. https://doi.org/10.1002/dc.24885

August, M. D. (n.d.). *Lithium acetate transformation of yeast*.

Ausió, J. (2006). Histone variants—The structure behind the function. *Briefings in Functional Genomics & Proteomics*, *5*(3), 228–243. https://doi.org/10.1093/bfgp/ell020

Baek, S. H. (2011). When Signaling Kinases Meet Histones and Histone Modifiers in the Nucleus. *Molecular Cell*, *42*(3), 274–284. https://doi.org/10.1016/j.molcel.2011.03.022

Bardwell, L. (2005). A walk-through of the yeast mating pheromone response pathway. *Peptides*, *26*(2), 339–350. https://doi.org/10.1016/j.peptides.2004.10.002

Barral, S., Morozumi, Y., Tanaka, H., Montellier, E., Govin, J., Dieuleveult, M. de, Charbonnier, G., Couté, Y., Puthier, D., Buchou, T., Boussouar, F., Urahama, T., Fenaille, F., Curtet, S., Héry, P., Fernandez-Nunez, N., Shiota, H., Gérard, M., Rousseaux, S., … Khochbin, S. (2017). Histone

Variant H2A.L.2 Guides Transition Protein-Dependent Protamine Assembly in Male Germ Cells. *Molecular Cell*, *66*(1), 89-101.e8. https://doi.org/10.1016/j.molcel.2017.02.025

Bartholomew, B. (2014). ISWI Chromatin Remodeling: One primary actor or a coordinated effort? *Current Opinion in Structural Biology*, *24*, 150–155. https://doi.org/10.1016/j.sbi.2014.01.010

Barve, G., & Manjithaya, R. (2021). Cross-talk between autophagy and sporulation in Saccharomyces cerevisiae. *Yeast*, *38*(7), 401–413. https://doi.org/10.1002/yea.3556

Basiony, M., Yang, Y., Liu, G., Gao, X.-D., & Nakanishi, H. (2020). Studies on the Properties of the Sporulation Specific Protein Dit1 and Its Product Formyl Tyrosine. *Journal of Fungi*, *6*(2), 77. https://doi.org/10.3390/jof6020077

Bast, J., Jaron, K. S., Schuseil, D., Roze, D., & Schwander, T. (2019). Asexual reproduction reduces transposable element load in experimental yeast populations. *eLife*, *8*, e48548. https://doi.org/10.7554/eLife.48548

Becker, P. B., & Workman, J. L. (2013). Nucleosome Remodeling and Epigenetics. *Cold Spring Harbor Perspectives in Biology*, *5*(9), a017905. https://doi.org/10.1101/cshperspect.a017905

Ben-Ari, G., Zenvirth, D., Sherman, A., David, L., Klutstein, M., Lavi, U., Hillel, J., & Simchen, G. (2006). Four Linked Genes Participate in Controlling Sporulation Efficiency in Budding Yeast. *PLOS Genetics*, *2*(11), e195. https://doi.org/10.1371/journal.pgen.0020195

Berger, S. L. (2002). Histone modifications in transcriptional regulation. *Current Opinion in Genetics & Development*, *12*(2), 142–148. https://doi.org/10.1016/S0959-437X(02)00279-4

Berger, S. L., Kouzarides, T., Shiekhattar, R., & Shilatifard, A. (2009). An operational definition of epigenetics. *Genes & Development*, *23*(7), 781–783. https://doi.org/10.1101/gad.1787609

Berkovits, B. D., Wang, L., Guarnieri, P., & Wolgemuth, D. J. (2012). The testis-specific double bromodomain-containing protein BRDT forms a complex with multiple spliceosome components and is required for mRNA splicing and 3′-UTR truncation in round spermatids. *Nucleic Acids Research*, *40*(15), 7162–7175. https://doi.org/10.1093/nar/gks342

Bernardes, N. E., & Chook, Y. M. (2020). Nuclear import of histones. *Biochemical Society Transactions*, *48*(6), 2753–2767. https://doi.org/10.1042/BST20200572

Bhagwat, M., Nagar, S., Kaur, P., Jassar, S., Vancurova, I., & Vancura, A. (2021). Synthesis of nucleocytosolic acetyl-CoA regulates mitochondrial respiration and ATP synthesis in budding yeast. *Biochimica et Biophysica Acta. Molecular Cell Research*, *1868*(7), 119025. https://doi.org/10.1016/j.bbamcr.2021.119025

Bi, X. (2025). Parental Histone Recycling During Chromatin Replication. *Biomolecules*, *16*(1), 13. https://doi.org/10.3390/biom16010013

Bieluszewski, T., Prakash, S., Roulé, T., & Wagner, D. (2023). The Role and Activity of SWI/SNF Chromatin Remodelers. *Annual Review of Plant Biology*, *74*(Volume 74, 2023), 139–163. https://doi.org/10.1146/annurev-arplant-102820-093218

Biermann, K., & Steger, K. (2007). Epigenetics in Male Germ Cells. *Journal of Andrology*, *28*(4), 466–480. https://doi.org/10.2164/jandrol.106.002048

Biterge, B., & Schneider, R. (2014). Histone variants: Key players of chromatin. *Cell and Tissue Research*, *356*(3), 457–466. https://doi.org/10.1007/s00441-014-1862-4

Bonasio, R., Lecona, E., & Reinberg, D. (2010). MBT domain proteins in development and disease. *Seminars in Cell & Developmental Biology*, *21*(2), 221–230. https://doi.org/10.1016/j.semcdb.2009.09.010

Bonazzi, D., Julien, J.-D., Romao, M., Seddiki, R., Piel, M., Boudaoud, A., & Minc, N. (2014a). Symmetry Breaking in Spore Germination Relies on an Interplay between Polar Cap Stability and Spore Wall Mechanics. *Developmental Cell*, *28*(5), 534–546. https://doi.org/10.1016/j.devcel.2014.01.023

Bonazzi, D., Julien, J.-D., Romao, M., Seddiki, R., Piel, M., Boudaoud, A., & Minc, N. (2014b). Symmetry Breaking in Spore Germination Relies on an Interplay between Polar Cap Stability and Spore Wall Mechanics. *Developmental Cell*, *28*(5), 534–546. https://doi.org/10.1016/j.devcel.2014.01.023

Borg, M., & Berger, F. (2015). Chromatin remodelling during male gametophyte development. *The Plant Journal: For Cell and Molecular Biology*, *83*(1), 177–188. https://doi.org/10.1111/tpj.12856

Borg, M., Jiang, D., & Berger, F. (2021). Histone variants take center stage in shaping the epigenome. *Current Opinion in Plant Biology, Epigenetics*, *61*, 101991. https://doi.org/10.1016/j.pbi.2020.101991

Boussouar, F., Rousseaux, S., & Khochbin, S. (2008). A new insight into male genome reprogramming by histone variants and histone code. *Cell Cycle*, *7*(22), 3499–3502. https://doi.org/10.4161/cc.7.22.6975

Bradley, A. I., Marsh, N. M., Borror, H. R., Mostoller, K. E., Gama, A. I., & Gardner, R. G. (2021). Acute ethanol stress induces sumoylation of conserved chromatin structural proteins in Saccharomyces cerevisiae. *Molecular Biology of the Cell*, *32*(11), 1121–1133. https://doi.org/10.1091/mbc.E20-11-0715

Brahma, S., & Henikoff, S. (2022). CUT&RUN Profiling of the Budding Yeast Epigenome. In F. Devaux (Ed.), *Yeast Functional Genomics* (Vol. 2477, pp. 129–147). Springer US. https://doi.org/10.1007/978-1-0716-2257-5_9

Breeden, L. L. (2003). Periodic Transcription: A Cycle within a Cycle. *Current Biology*, *13*(1), R31–R38. https://doi.org/10.1016/S0960-9822(02)01386-6

Brettrager, E. J., Frederick, A. J., & van Waardenburg, R. C. A. M. (2024). Zymolyase Treatment of Saccharomyces cerevisiae Affects Cellular Proteins and Degrades Tyrosyl-DNA Phosphodiesterase I. *DNA and Cell Biology*, *43*(7), 353–361. https://doi.org/10.1089/dna.2024.0062

Bryan, A. K., Goranov, A., Amon, A., Manalis, S. R., & Kirschner, M. W. (2010). Measurement of Mass, Density, and Volume during the Cell Cycle of Yeast. *Proceedings of the National Academy of Sciences of the United States of America*, *107*(3), 999–1004.

Bryant, J. M., Govin, J., Zhang, L., Donahue, G., Pugh, B. F., & Berger, S. L. (2012). The Linker Histone Plays a Dual Role during Gametogenesis in Saccharomyces cerevisiae. *Molecular and Cellular Biology*, *32*(14), 2771–2783. https://doi.org/10.1128/MCB.00282-12

Budovskaya, Y. V., Stephan, J. S., Reggiori, F., Klionsky, D. J., & Herman, P. K. (2004). The Ras/cAMP-dependent Protein Kinase Signaling Pathway Regulates an Early Step of the Autophagy Process in Saccharomyces cerevisiae. *The Journal of Biological Chemistry*, *279*(20), 20663–20671. https://doi.org/10.1074/jbc.M400272200

Buenrostro, J. D., Giresi, P. G., Zaba, L. C., Chang, H. Y., & Greenleaf, W. J. (2013). Transposition of native chromatin for fast and sensitive epigenomic profiling of open chromatin, DNA-binding proteins and nucleosome position. *Nature Methods*, *10*(12), 1213–1218. https://doi.org/10.1038/nmeth.2688

Buenrostro, J. D., Wu, B., Litzenburger, U. M., Ruff, D., Gonzales, M. L., Snyder, M. P., Chang, H. Y., & Greenleaf, W. J. (2015). Single-cell chromatin accessibility reveals principles of regulatory variation. *Nature*, *523*(7561), 486–490. https://doi.org/10.1038/nature14590

Buitrago, D., Labrador, M., Arcon, J. P., Lema, R., Flores, O., Esteve-Codina, A., Blanc, J., Villegas, N., Bellido, D., Gut, M., Dans, P. D., Heath, S. C., Gut, I. G., Brun Heath, I., & Orozco, M. (2021). Impact of DNA methylation on 3D genome structure. *Nature Communications*, *12*(1), 3243. https://doi.org/10.1038/s41467-021-23142-8

Bungard, D., Reed, M., & Winter, E. (2004). RSC1 and RSC2 Are Required for Expression of Mid-Late Sporulation-Specific Genes in Saccharomyces cerevisiae. *Eukaryotic Cell*, *3*(4), 910–918. https://doi.org/10.1128/EC.3.4.910-918.2004

Burgess, R. J., & Zhang, Z. (2013). Histone chaperones in nucleosome assembly and human disease. *Nature Structural & Molecular Biology*, *20*(1), 14–22. https://doi.org/10.1038/nsmb.2461

Burgess, S. M., Powers, T., & Mell, J. C. (2017). *Budding Yeast Saccharomyces Cerevisiae as a Model Genetic Organism*. 1–12. https://doi.org/10.1002/9780470015902.a0000821.pub2

Burton, D. R., Butler, M. J., Hyde, J. E., Phillips, D., Skidmore, C. J., & Walker, I. O. (1978). The interaction of core histones with DNA: Equilibrium binding studies. *Nucleic Acids Research*, *5*(10), 3643–3663. https://doi.org/10.1093/nar/5.10.3643

Buttress, T., He, S., Wang, L., Zhou, S., Saalbach, G., Vickers, M., Li, G., Li, P., & Feng, X. (2022). Histone H2B.8 compacts flowering plant sperm through chromatin phase separation. *Nature*, *611*(7936), 614–622. https://doi.org/10.1038/s41586-022-05386-6

Buttress, T., He, S., Wang, L., Zhou, S., Sun, L., Saalbach, G., Vickers, M., Li, P., & Feng, X. (2021). *A histone variant condenses flowering plant sperm via chromatin phase separation* (p. 2021.09.14.460326). bioRxiv. https://doi.org/10.1101/2021.09.14.460326

Cahn, J., Lloyd, J. P. B., Karemaker, I. D., Jansen, P. W. T. C., Pflueger, J., Duncan, O., Petereit, J., Bogdanovic, O., Millar, A. H., Vermeulen, M., & Lister, R. (2023). *Characterization of DNA methylation reader proteins of Arabidopsis thaliana* (p. 2023.12.05.570080). bioRxiv. https://doi.org/10.1101/2023.12.05.570080

Cal-Kayitmazbatir, S., Francey, L. J., Lee, Y., Liu, A. C., & Hogenesch, J. B. (2023). PSMD11 modulates circadian clock function through PER and CRY nuclear translocation. *PloS One*, *18*(3), e0283463. https://doi.org/10.1371/journal.pone.0283463

Capuano, F., Mülleder, M., Kok, R., Blom, H. J., & Ralser, M. (2014a). Cytosine DNA Methylation Is Found in Drosophila melanogaster but Absent in Saccharomyces cerevisiae, Schizosaccharomyces pombe, and Other Yeast Species. *Analytical Chemistry*, *86*(8), 3697–3702. https://doi.org/10.1021/ac500447w

Capuano, F., Mülleder, M., Kok, R., Blom, H. J., & Ralser, M. (2014b). Cytosine DNA Methylation Is Found in Drosophila melanogaster but Absent in Saccharomyces cerevisiae, Schizosaccharomyces pombe, and Other Yeast Species. *Analytical Chemistry*, *86*(8), 3697–3702. https://doi.org/10.1021/ac500447w

Carlberg, C., & Molnár, F. (2018). The Histone Code. In C. Carlberg & F. Molnár (Eds), *Human Epigenomics* (pp. 75–88). Springer. https://doi.org/10.1007/978-981-10-7614-5_5

Caron, C., Govin, J., Rousseaux, S., & Khochbin, S. (2005). How to Pack the Genome for a Safe Trip. In P. Jeanteur (Ed.), *Epigenetics and Chromatin* (pp. 65–89). Springer. https://doi.org/10.1007/3-540-27310-7_3

Catoni, M., Lechon Gomez, T., & Probst, A. V. (2025). Plant epigenetics: Controlling genome expression to integrate developmental and environmental cues. *Journal of Experimental Botany*, *76*(9), 2389–2393. https://doi.org/10.1093/jxb/eraf134

Cejka, P., & Jiricny, J. (2008). Interplay of DNA Repair Pathways Controls Methylation Damage Toxicity in Saccharomyces cerevisiae. *Genetics*, *179*(4), 1835–1844. https://doi.org/10.1534/genetics.108.089979

Chambers, A. L., Ormerod, G., Durley, S. C., Sing, T. L., Brown, G. W., Kent, N. A., & Downs, J. A. (2012). The INO80 chromatin remodeling complex prevents polyploidy and maintains normal chromatin structure at centromeres. *Genes & Development*, *26*(23), 2590–2603. https://doi.org/10.1101/gad.199976.112

Chang, Y.-Y., & Neufeld, T. P. (2009). An Atg1/Atg13 Complex with Multiple Roles in TOR-mediated Autophagy Regulation. *Molecular Biology of the Cell*, *20*(7), 2004–2014. https://doi.org/10.1091/mbc.E08-12-1250

Chen, K. C., Calzone, L., Csikasz-Nagy, A., Cross, F. R., Novak, B., & Tyson, J. J. (2004). Integrative analysis of cell cycle control in budding yeast. *Molecular Biology of the Cell*, *15*(8), 3841–3862. https://doi.org/10.1091/mbc.e03-11-0794

Chen, L., Wang, M., Hou, J., Liu, L., Fu, J., Shen, Y., Zhang, Z., & Bao, X. (2014). Regulation of *Saccharomyces cerevisiae MEF1* by Hda1p affects salt resistance of *bdf1Δ* mutant. *FEMS Yeast Research*, *14*(4), 575–585. https://doi.org/10.1111/1567-1364.12144

Chen, P., Zhao, J., & Li, G. (2013). Histone variants in development and diseases. *Journal of Genetics and Genomics = Yi Chuan Xue Bao*, *40*(7), 355–365. https://doi.org/10.1016/j.jgg.2013.05.001

Chen, Y., Guo, P., & Dong, Z. (2024). The role of histone acetylation in transcriptional regulation and seed development. *Plant Physiology*, *194*(4), 1962–1979. https://doi.org/10.1093/plphys/kiad614

Chen, Y., Sprung, R., Tang, Y., Ball, H., Sangras, B., Kim, S. C., Falck, J. R., Peng, J., Gu, W., & Zhao, Y. (2007). Lysine Propionylation and Butyrylation Are Novel Post-translational Modifications in Histones *. *Molecular & Cellular Proteomics*, *6*(5), 812–819. https://doi.org/10.1074/mcp.M700021-MCP200

Chen, Z., Zang, J., Kappler, J., Hong, X., Crawford, F., Wang, Q., Lan, F., Jiang, C., Whetstine, J., Dai, S., Hansen, K., Shi, Y., & Zhang, G. (2007). Structural Basis of the Recognition of a Methylated Histone Tail by JMJD2A. *Proceedings of the National Academy of Sciences of the United States of America*, *104*(26), 10818–10823.

Cheung, K. L., Kim, C., & Zhou, M.-M. (2021). The Functions of BET Proteins in Gene Transcription of Biology and Diseases. *Frontiers in Molecular Biosciences*, *8*. https://doi.org/10.3389/fmolb.2021.728777

Cheung, W. L., Turner, F. B., Krishnamoorthy, T., Wolner, B., Ahn, S.-H., Foley, M., Dorsey, J. A., Peterson, C. L., Berger, S. L., & Allis, C. D. (2005). Phosphorylation of Histone H4 Serine 1 during DNA Damage Requires Casein Kinase II in S. cerevisiae. *Current Biology*, *15*(7), 656–660. https://doi.org/10.1016/j.cub.2005.02.049

Chigweshe, L., MacQueen, A. J., & Holmes, S. G. (2022). Histone variant H2A.Z promotes meiotic chromosome axis organization in Saccharomyces cerevisiae. *G3 Genes|Genomes|Genetics*, *12*(8), jkac128. https://doi.org/10.1093/g3journal/jkac128

Chiou, J.-G., Balasubramanian, M. K., & Lew, D. J. (2017). Cell Polarity in Yeast. *Annual Review of Cell and Developmental Biology*, *33*, 77–101. https://doi.org/10.1146/annurev-cellbio-100616-060856

Chowdhury, R., Abboud, M. I., Wiley, J., Tumber, A., Markolovic, S., & Schofield, C. J. (2022). Conservation of the unusual dimeric JmjC fold of JMJD7 from Drosophila melanogaster to humans. *Scientific Reports*, *12*(1), 6065. https://doi.org/10.1038/s41598-022-10028-y

Chromodomain—An overview | ScienceDirect Topics. (n.d.). Retrieved 12 August 2025, from https://www.sciencedirect.com/topics/biochemistry-genetics-and-molecular-biology/chromodomain

Chu, S., DeRisi, J., Eisen, M., Mulholland, J., Botstein, D., Brown, P. O., & Herskowitz, I. (1998). The transcriptional program of sporulation in budding yeast. *Science (New York, N.Y.)*, *282*(5389), 699–705. https://doi.org/10.1126/science.282.5389.699

Chu, S., & Herskowitz, I. (1998). Gametogenesis in yeast is regulated by a transcriptional cascade dependent on Ndt80. *Molecular Cell*, *1*(5), 685–696. https://doi.org/10.1016/s1097-2765(00)80068-4

Chua, P., & Roeder, G. S. (1995). Bdf1, a yeast chromosomal protein required for sporulation. *Molecular and Cellular Biology*, *15*(7), 3685–3696. https://doi.org/10.1128/mcb.15.7.3685

Church, M. C., & Workman, J. L. (2024). The SWI/SNF chromatin remodeling complex: A critical regulator of metabolism. *Biochemical Society Transactions*, *52*(3), 1327–1337. https://doi.org/10.1042/BST20231141

Clément, C., Orsi, G. A., Gatto, A., Boyarchuk, E., Forest, A., Hajj, B., Miné-Hattab, J., Garnier, M., Gurard-Levin, Z. A., Quivy, J.-P., & Almouzni, G. (2018). High-resolution visualization of H3 variants during replication reveals their controlled recycling. *Nature Communications*, *9*(1), 3181. https://doi.org/10.1038/s41467-018-05697-1

Coluccio, A., Bogengruber, E., Conrad, M. N., Dresser, M. E., Briza, P., & Neiman, A. M. (2004). Morphogenetic Pathway of Spore Wall Assembly in Saccharomyces cerevisiae. *Eukaryotic Cell*, *3*(6), 1464–1475. https://doi.org/10.1128/EC.3.6.1464-1475.2004

Contreras, J., Vichier-Guerre, S., Dugué, L., Bonhomme, F., Jallet, C., Nguyen, M.-H., Vitorge, B., Feoli, A., Sbardella, G., Guijarro, J. I., & Arimondo, P. B. (2025). In Quest of Chemical Probes for DNA

Methylation Reader Proteins: Nucleoside and Dimer Analogues of 5-Methylcytosine Interact with MBD2. *Angewandte Chemie International Edition*, *64*(26), e202425599. https://doi.org/10.1002/anie.202425599

Cook, A. J. L., Gurard-Levin, Z. A., Vassias, I., & Almouzni, G. (2011). A specific function for the histone chaperone NASP to fine-tune a reservoir of soluble H3-H4 in the histone supply chain. *Molecular Cell*, *44*(6), 918–927. https://doi.org/10.1016/j.molcel.2011.11.021

Corpet, A., & Almouzni, G. (2009). Making copies of chromatin: The challenge of nucleosomal organization and epigenetic information. *Trends in Cell Biology*, *19*(1), 29–41. https://doi.org/10.1016/j.tcb.2008.10.002

Corujo, D., & Buschbeck, M. (2018). Post-Translational Modifications of H2A Histone Variants and Their Role in Cancer. *Cancers*, *10*(3), 59. https://doi.org/10.3390/cancers10030059

Cribbs, A. P., Filippakopoulos, P., Philpott, M., Wells, G., Penn, H., Oerum, H., Valge-Archer, V., Feldmann, M., & Oppermann, U. (2021). Dissecting the Role of BET Bromodomain Proteins BRD2 and BRD4 in Human NK Cell Function. *Frontiers in Immunology*, *12*. https://doi.org/10.3389/fimmu.2021.626255

Cui, J. Y., Fu, Z. D., & Dempsey, J. (2019). Chapter 1-2—The Role of Histone Methylation and Methyltransferases in Gene Regulation. In S. D. McCullough & D. C. Dolinoy (Eds), *Toxicoepigenetics* (pp. 31–84). Academic Press. https://doi.org/10.1016/B978-0-12-812433-8.00002-2

Dalal, Y., Wang, H., Lindsay, S., & Henikoff, S. (2007). Tetrameric Structure of Centromeric Nucleosomes in Interphase Drosophila Cells. *PLOS Biology*, *5*(8), e218. https://doi.org/10.1371/journal.pbio.0050218

de Smidt, O., du Preez, J. C., & Albertyn, J. (2008). The alcohol dehydrogenases of Saccharomyces cerevisiae: A comprehensive review. *FEMS Yeast Research*, *8*(7), 967–978. https://doi.org/10.1111/j.1567-1364.2008.00387.x

Delaney, K., Tan, M., Zhu, Z., Gao, J., Dai, L., Kim, S., Ding, J., He, M., Halabelian, L., Yang, L., Nagarajan, P., Parthun, M. R., Lee, S., Khochbin, S., Zheng, Y. G., & Zhao, Y. (2021). Histone lysine methacrylation is a dynamic post-translational modification regulated by HAT1 and SIRT2. *Cell Discovery*, *7*(1), 122. https://doi.org/10.1038/s41421-021-00344-4

Delaney, K., Weiss, N., & Almouzni, G. (2023). The cell-cycle choreography of H3 variants shapes the genome. *Molecular Cell*, *83*(21), 3773–3786. https://doi.org/10.1016/j.molcel.2023.08.030

Demetriadou, C., & Kirmizis, A. (2017). Histone Acetyltransferases in Cancer: Guardians or Hazards? *Critical Reviews™ in Oncogenesis*, *22*(3–4). https://doi.org/10.1615/CritRevOncog.2017024506

Deng, L., Nagasawa, J., Ono, Y., Ishikawa, Y., Kakihara, T., Fukuda, R., & Ohta, A. (2008). Manipulation of Major Membrane Lipid Synthesis and Its Effects on Sporulation in *Saccharomyces cerevisiae*. *Bioscience, Biotechnology, and Biochemistry*, *72*(9), 2362–2368. https://doi.org/10.1271/bbb.80265

DeRan, M., Pulvino, M., Greene, E., Su, C., & Zhao, J. (2008). Transcriptional Activation of Histone Genes Requires NPAT-Dependent Recruitment of TRRAP-Tip60 Complex to Histone Promoters during the G1/S Phase Transition. *Molecular and Cellular Biology*, *28*(1), 435–447. https://doi.org/10.1128/MCB.00607-07

Deutschbauer, A. M., Williams, R. M., Chu, A. M., & Davis, R. W. (2002a). Parallel phenotypic analysis of sporulation and postgermination growth in Saccharomyces cerevisiae. *Proceedings of the National Academy of Sciences*, *99*(24), 15530–15535. https://doi.org/10.1073/pnas.202604399

Deutschbauer, A. M., Williams, R. M., Chu, A. M., & Davis, R. W. (2002b). Parallel phenotypic analysis of sporulation and postgermination growth in Saccharomyces cerevisiae. *Proceedings of the National Academy of Sciences*, *99*(24), 15530–15535. https://doi.org/10.1073/pnas.202604399

Devaiah, B. N., Singh, A. K., Mu, J., Chen, Q., Meerzaman, D., & Singer, D. S. (2024). Phosphorylation by JNK switches BRD4 functions. *Molecular Cell*, *84*(22), 4282-4296.e7. https://doi.org/10.1016/j.molcel.2024.09.030

Dhar, S., Thota, A., & Rao, M. R. S. (2012). Insights into Role of Bromodomain, Testis-specific (Brdt) in Acetylated Histone H4-dependent Chromatin Remodeling in Mammalian Spermiogenesis. *The Journal of Biological Chemistry*, *287*(9), 6387–6405. https://doi.org/10.1074/jbc.M111.288167

Dimitrova, E., Turberfield, A. H., & Klose, R. J. (2015). Histone demethylases in chromatin biology and beyond. *EMBO Reports*, *16*(12), 1620–1639. https://doi.org/10.15252/embr.201541113

Ding, D., Nguyen, T. T., Pang, M. Y. H., & Ishibashi, T. (2020). Primate-specific histone variants1. *Genome*. (1840 Woodward Drive, Suite 1, Ottawa, ON K2C 0P7). https://doi.org/10.1139/gen-2020-0094

Doenecke, D. (2014). Chromatin dynamics from S-phase to mitosis: Contributions of histone modifications. *Cell and Tissue Research*, *356*(3), 467–475. https://doi.org/10.1007/s00441-014-1873-1

Donaldson, A. D. (2000). The yeast mitotic cyclin Clb2 cannot substitute for S phase cyclins in replication origin firing. *EMBO Reports*, *1*(6), 507–512. https://doi.org/10.1093/embo-reports/kvd108

Donczew, R., & Hahn, S. (2021a). BET family members Bdf1/2 modulate global transcription initiation and elongation in Saccharomyces cerevisiae. *eLife*, *10*, e69619. https://doi.org/10.7554/eLife.69619

Donczew, R., & Hahn, S. (2021b). BET family members Bdf1/2 modulate global transcription initiation and elongation in Saccharomyces cerevisiae. *eLife*, *10*, e69619. https://doi.org/10.7554/eLife.69619

Dong, Y., Isono, K., Ohbo, K., Endo, T. A., Ohara, O., Maekawa, M., Toyama, Y., Ito, C., Toshimori, K., Helin, K., Ogonuki, N., Inoue, K., Ogura, A., Yamagata, K., Kitabayashi, I., & Koseki, H. (2017).

EPC1/TIP60-Mediated Histone Acetylation Facilitates Spermiogenesis in Mice. *Molecular and Cellular Biology*, *37*(19), e00082-17. https://doi.org/10.1128/MCB.00082-17

Driks, A., & Eichenberger, P. (2016). The Spore Coat. *Microbiology Spectrum*, *4*(2). https://doi.org/10.1128/microbiolspec.TBS-0023-2016

Duan, Z., Andronescu, M., Schutz, K., McIlwain, S., Kim, Y. J., Lee, C., Shendure, J., Fields, S., Blau, C. A., & Noble, W. S. (2010). A three-dimensional model of the yeast genome. *Nature*, *465*(7296), 363–367. https://doi.org/10.1038/nature08973

Durant, M., Mucelli, X., & Huang, L. S. (2024). Meiotic Cytokinesis in Saccharomyces cerevisiae: Spores That Just Need Closure. *Journal of Fungi*, *10*(2), 132. https://doi.org/10.3390/jof10020132

Durant, M., & Pugh, B. F. (2006). Genome-Wide Relationships between TAF1 and Histone Acetyltransferases in Saccharomyces cerevisiae. *Molecular and Cellular Biology*, *26*(7), 2791–2802. https://doi.org/10.1128/MCB.26.7.2791-2802.2006

Erb, M. A. (2023). Small-molecule tools for YEATS domain proteins. *Current Opinion in Chemical Biology*, *77*, 102404. https://doi.org/10.1016/j.cbpa.2023.102404

Erdel, F., Schubert, T., Marth, C., Längst, G., & Rippe, K. (2010). Human ISWI chromatin-remodeling complexes sample nucleosomes via transient binding reactions and become immobilized at active sites. *Proceedings of the National Academy of Sciences*, *107*(46), 19873–19878. https://doi.org/10.1073/pnas.1003438107

Erdmann, S., Freihorst, D., Raudaskoski, M., Schmidt-Heck, W., Jung, E.-M., Senftleben, D., & Kothe, E. (2012). Transcriptome and Functional Analysis of Mating in the Basidiomycete Schizophyllum commune. *Eukaryotic Cell*, *11*(5), 571–589. https://doi.org/10.1128/EC.05214-11

ERKMANN, J. A., SÀNCHEZ, R., TREICHEL, N., MARZLUFF, W. F., & KUTAY, U. (2005). Nuclear export of metazoan replication-dependent histone mRNAs is dependent on RNA length and is mediated by TAP. *RNA*, *11*(1), 45–58. https://doi.org/10.1261/rna.7189205

Eustermann, S., Schall, K., Kostrewa, D., Lakomek, K., Strauss, M., Moldt, M., & Hopfner, K.-P. (2018). Structural basis for ATP-dependent chromatin remodelling by the INO80 complex. *Nature*, *556*(7701), 386–390. https://doi.org/10.1038/s41586-018-0029-y

Fan, J., Baeza, J., & Denu, J. M. (2016). Chapter Six—Investigating Histone Acetylation Stoichiometry and Turnover Rate. In R. Marmorstein (Ed.), *Methods in Enzymology* (Vol. 574, pp. 125–148). Academic Press. https://doi.org/10.1016/bs.mie.2016.01.007

Fang, J., Cheng, J., Wang, J., Zhang, Q., Liu, M., Gong, R., Wang, P., Zhang, X., Feng, Y., Lan, W., Gong, Z., Tang, C., Wong, J., Yang, H., Cao, C., & Xu, Y. (2016). Hemi-methylated DNA opens a closed conformation of UHRF1 to facilitate its histone recognition. *Nature Communications*, *7*(1), 11197. https://doi.org/10.1038/ncomms11197

Feierman, E. R., Louzon, S., Prescott, N. A., Biaco, T., Gao, Q., Qiu, Q., Choi, K., Palozola, K. C., Voss, A. J., Mehta, S. D., Quaye, C. N., Lynch, K. T., Fuccillo, M. V., Wu, H., David, Y., & Korb, E. (2024). Histone variant H2BE enhances chromatin accessibility in neurons to promote synaptic gene expression and long-term memory. *bioRxiv: The Preprint Server for Biology*, 2024.01.29.575103. https://doi.org/10.1101/2024.01.29.575103

Felsenfeld, G. (2014). A Brief History of Epigenetics. *Cold Spring Harbor Perspectives in Biology*, *6*(1), a018200. https://doi.org/10.1101/cshperspect.a018200

Felsenfeld, G., Camerini-Otero, R. D., & Sollner-Webb, B. (1976). THE STRUCTURE OF CHROMATIN AND ITS RECONSTRUCTION. In D. P. Nierlich, W. J. Rutter, & C. F. Fox (Eds), *Molecular Mechanisms in the Control of Gene Expression* (pp. 1–6). Academic Press. https://doi.org/10.1016/B978-0-12-518550-9.50004-4

Feng, S., Gui, Y., Yin, S., Xiong, X., Liu, K., Li, J., Dong, J., Ma, X., Zhou, S., Zhang, B., Yang, S., Wang, F., Wang, X., Jiang, X., & Yuan, S. (2024). Histone demethylase KDM2A recruits HCFC1 and E2F1 to orchestrate male germ cell meiotic entry and progression. *The EMBO Journal*, *43*(19), 4197–4227. https://doi.org/10.1038/s44318-024-00203-4

Feng, Y., Endo, M., & Sugiyama, H. (2021a). Nucleosomes and Epigenetics from a Chemical Perspective. *ChemBioChem*, *22*(4), 595–612. https://doi.org/10.1002/cbic.202000332

Feng, Y., Endo, M., & Sugiyama, H. (2021b). Nucleosomes and Epigenetics from a Chemical Perspective. *ChemBioChem*, *22*(4), 595–612. https://doi.org/10.1002/cbic.202000332

Ferguson, L., Ellis, P. J. I., & Affara, N. A. (2009). Two novel mouse genes mapped to chromosome Yp are expressed specifically in spermatids. *Mammalian Genome*, *20*(4), 193–206. https://doi.org/10.1007/s00335-009-9175-8

Ferri, E., Petosa, C., & McKenna, C. E. (2016). Bromodomains: Structure, function and pharmacology of inhibition. *Biochemical Pharmacology*, *106*, 1–18. https://doi.org/10.1016/j.bcp.2015.12.005

Filippakopoulos, P., & Knapp, S. (2014). Targeting bromodomains: Epigenetic readers of lysine acetylation. *Nature Reviews. Drug Discovery*, *13*(5), 337–356. https://doi.org/10.1038/nrd4286

Filippakopoulos, P., Picaud, S., Mangos, M., Keates, T., Lambert, J.-P., Barsyte-Lovejoy, D., Felletar, I., Volkmer, R., Müller, S., Pawson, T., Gingras, A.-C., Arrowsmith, C. H., & Knapp, S. (2012). Histone Recognition and Large-Scale Structural Analysis of the Human Bromodomain Family. *Cell*, *149*(1), 214–231. https://doi.org/10.1016/j.cell.2012.02.013

Filippakopoulos, P., Qi, J., Picaud, S., Shen, Y., Smith, W. B., Fedorov, O., Morse, E. M., Keates, T., Hickman, T. T., Felletar, I., Philpott, M., Munro, S., McKeown, M. R., Wang, Y., Christie, A. L., West, N., Cameron, M. J., Schwartz, B., Heightman, T. D., … Bradner, J. E. (2010). Selective inhibition of BET bromodomains. *Nature*, *468*(7327), 1067–1073. https://doi.org/10.1038/nature09504

Fischer, G., Liti, G., & Llorente, B. (2021). The budding yeast life cycle: More complex than anticipated? *Yeast*, *38*(1), 5–11. https://doi.org/10.1002/yea.3533

Flipphi, M., Harispe, M. L., Hamari, Z., Kocsubé, S., Scazzocchio, C., & Ramón, A. (2024). An ascomycete H4 variant with an unknown function. *Royal Society Open Science*, *11*(2), 231705. https://doi.org/10.1098/rsos.231705

Flury, V., Reverón-Gómez, N., Alcaraz, N., Stewart-Morgan, K. R., Wenger, A., Klose, R. J., & Groth, A. (2023). Recycling of modified H2A-H2B provides short-term memory of chromatin states. *Cell*, *186*(5), 1050-1065.e19. https://doi.org/10.1016/j.cell.2023.01.007

Franklin, K. A., Shields, C. E., & Haynes, K. A. (2022). Beyond the marks: Reader-effectors as drivers of epigenetics and chromatin engineering. *Trends in Biochemical Sciences*, *47*(5), 417–432. https://doi.org/10.1016/j.tibs.2022.03.002

Franklin, R. E., & Gosling, R. G. (1953). Molecular Configuration in Sodium Thymonucleate. *Nature*, *171*(4356), 740–741. https://doi.org/10.1038/171740a0

Freitag, M., Hickey, P. C., Khlafallah, T. K., Read, N. D., & Selker, E. U. (2004). HP1 is essential for DNA methylation in neurospora. *Molecular Cell*, *13*(3), 427–434. https://doi.org/10.1016/s1097-2765(04)00024-3

French, C. A., Miyoshi, I., Kubonishi, I., Grier, H. E., Perez-Atayde, A. R., & Fletcher, J. A. (2003). BRD4-NUT fusion oncogene: A novel mechanism in aggressive carcinoma. *Cancer Research*, *63*(2), 304–307.

Fujimoto, T., Watanabe, S., Imamura, Y., Mizunuma, M., & Kume, K. (2025). Nuclear enlargement induced by overexpression of nuclear export signal is associated with abnormal nuclear division in Schizosaccharomyces pombe. *Biology Open*, *14*(11), bio062331. https://doi.org/10.1242/bio.062331

Gan, B., Chen, S., Liu, H., Min, J., & Liu, K. (2019). Structure and function of eTudor domain containing TDRD proteins. *Critical Reviews in Biochemistry and Molecular Biology*, *54*(2), 119–132. https://doi.org/10.1080/10409238.2019.1603199

Ganesan, A. (2018). Epigenetics: The first 25 centuries. *Philosophical Transactions of the Royal Society B: Biological Sciences*, *373*(1748), 20170067. https://doi.org/10.1098/rstb.2017.0067

Gao, G., Bracken, A. P., Burkard, K., Pasini, D., Classon, M., Attwooll, C., Sagara, M., Imai, T., Helin, K., & Zhao, J. (2003). NPAT expression is regulated by E2F and is essential for cell cycle progression. *Molecular and Cellular Biology*, *23*(8), 2821–2833. https://doi.org/10.1128/MCB.23.8.2821-2833.2003

Garabedian, M. V., Noguchi, C., Ziegler, M. A., Das, M. M., Singh, T., Harper, L. J., Leman, A. R., Khair, L., Moser, B. A., Nakamura, T. M., & Noguchi, E. (2012a). The Double-Bromodomain Proteins Bdf1 and Bdf2 Modulate Chromatin Structure to Regulate S-Phase Stress Response in Schizosaccharomyces pombe. *Genetics*, *190*(2), 487–500. https://doi.org/10.1534/genetics.111.135459

Garabedian, M. V., Noguchi, C., Ziegler, M. A., Das, M. M., Singh, T., Harper, L. J., Leman, A. R., Khair, L., Moser, B. A., Nakamura, T. M., & Noguchi, E. (2012b). The Double-Bromodomain Proteins Bdf1 and Bdf2 Modulate Chromatin Structure to Regulate S-Phase Stress Response in Schizosaccharomyces pombe. *Genetics*, *190*(2), 487–500. https://doi.org/10.1534/genetics.111.135459

García-Oliver, E., Ramus, C., Perot, J., Arlotto, M., Champleboux, M., Mietton, F., Battail, C., Boland, A., Deleuze, J.-F., Ferro, M., Couté, Y., & Govin, J. (2017). Bdf1 Bromodomains Are Essential for Meiosis and the Expression of Meiotic-Specific Genes. *PLOS Genetics*, *13*(1), e1006541. https://doi.org/10.1371/journal.pgen.1006541

Gaub, A., Sheikh, B. N., Basilicata, M. F., Vincent, M., Nizon, M., Colson, C., Bird, M. J., Bradner, J. E., Thevenon, J., Boutros, M., & Akhtar, A. (2020). Evolutionary conserved NSL complex/BRD4 axis controls transcription activation via histone acetylation. *Nature Communications*, *11*(1), 2243. https://doi.org/10.1038/s41467-020-16103-0

Gaucher, J., Boussouar, F., Montellier, E., Curtet, S., Buchou, T., Bertrand, S., Hery, P., Jounier, S., Depaux, A., Vitte, A.-L., Guardiola, P., Pernet, K., Debernardi, A., Lopez, F., Holota, H., Imbert, J., Wolgemuth, D. J., Gérard, M., Rousseaux, S., & Khochbin, S. (2012). Bromodomain-

dependent stage-specific male genome programming by Brdt. *The EMBO Journal*, *31*(19), 3809–3820. https://doi.org/10.1038/emboj.2012.233

Geijer, C., Pirkov, I., Vongsangnak, W., Ericsson, A., Nielsen, J., Krantz, M., & Hohmann, S. (2012). Time course gene expression profiling of yeast spore germination reveals a network of transcription factors orchestrating the global response. *BMC Genomics*, *13*, 554. https://doi.org/10.1186/1471-2164-13-554

Georgieva, M., Roguev, A., Balashev, K., Zlatanova, J., & Miloshev, G. (2012). Hho1p, the linker histone of Saccharomyces cerevisiae, is important for the proper chromatin organization in vivo. *Biochimica Et Biophysica Acta*, *1819*(5), 366–374. https://doi.org/10.1016/j.bbagrm.2011.12.003

Ghezzi, A., Li, X., Lew, L. K., Wijesekera, T. P., & Atkinson, N. S. (2017). Alcohol-Induced Neuroadaptation Is Orchestrated by the Histone Acetyltransferase CBP. *Frontiers in Molecular Neuroscience*, *10*, 103. https://doi.org/10.3389/fnmol.2017.00103

Gietz, R. D., & Schiestl, R. H. (2007). High-efficiency yeast transformation using the LiAc/SS carrier DNA/PEG method. *Nature Protocols*, *2*(1), 31–34. https://doi.org/10.1038/nprot.2007.13

Giunta, S., Hervé, S., White, R. R., Wilhelm, T., Dumont, M., Scelfo, A., Gamba, R., Wong, C. K., Rancati, G., Smogorzewska, A., Funabiki, H., & Fachinetti, D. (2021). CENP-A chromatin prevents replication stress at centromeres to avoid structural aneuploidy. *Proceedings of the National Academy of Sciences of the United States of America*, *118*(10), e2015634118. https://doi.org/10.1073/pnas.2015634118

Goffeau, A., Barrell, B. G., Bussey, H., Davis, R. W., Dujon, B., Feldmann, H., Galibert, F., Hoheisel, J. D., Jacq, C., Johnston, M., Louis, E. J., Mewes, H. W., Murakami, Y., Philippsen, P., Tettelin, H., & Oliver, S. G. (1996). Life with 6000 genes. *Science*, *274*(5287), 546, 563–567. https://doi.org/10.1126/science.274.5287.546

González, C. R., Perez Lujan, C., Vitullo, A. D., & González, B. (2022). *Transcriptome Profiling of Histone Acetylation and Methylation Writers and Erasers Families Across Male Germ Cell Development*

and Pre-Cleavage Zygote (SSRN Scholarly Paper No. 4052009). Social Science Research Network. https://doi.org/10.2139/ssrn.4052009

González-Arranz, S., Cavero, S., Morillo-Huesca, M., Andújar, E., Pérez-Alegre, M., Prado, F., & San-Segundo, P. (2018). Functional Impact of the H2A.Z Histone Variant During Meiosis in Saccharomyces cerevisiae. *Genetics*, *209*(4), 997–1015. https://doi.org/10.1534/genetics.118.301110

Gordon, S. J. V., Perner, F., MacPherson, L., Fennell, K. A., Wenge, D. V., Bourgeois, W., Klaus, T., Plenge, T., Murat, A., Petrovic, J., Horvath, J., Cao, J. Q., Lapek, J. D., Uryu, S., White, J. R., Lam, E. Y., Mu, X. J., Chan, Y.-C., Gillespie, A., … Dawson, M. A. (2025). Catalytic inhibition of KAT6/KAT7 enhances the efficacy and overcomes primary and acquired resistance to Menin inhibitors in MLL leukaemia. *Cancer Discovery*. https://doi.org/10.1158/2159-8290.CD-24-1517

Gothwal, S. K., Refaat, A. M., Nakata, M., Stanlie, A., Honjo, T., & Begum, N. A. (2024). BRD2 promotes antibody class switch recombination by facilitating DNA repair in collaboration with NIPBL. *Nucleic Acids Research*, *52*(8), 4422–4439. https://doi.org/10.1093/nar/gkae204

Goudarzi, A., Shiota, H., Rousseaux, S., & Khochbin, S. (2014). Genome-Scale Acetylation-Dependent Histone Eviction during Spermatogenesis. *Journal of Molecular Biology, Emerging Concepts in Epigenetic Signaling*, *426*(20), 3342–3349. https://doi.org/10.1016/j.jmb.2014.02.023

Govin, J., & Berger, S. L. (2009). Genome reprogramming during sporulation. *The International Journal of Developmental Biology*, *53*(2–3), 425–432. https://doi.org/10.1387/ijdb.082687jg

Govin, J., Escoffier, E., Rousseaux, S., Kuhn, L., Ferro, M., Th�venon, J., Catena, R., Davidson, I., Garin, J., Khochbin, S., & Caron, C. (2007). Pericentric Heterochromatin Reprogramming by New Histone Variants during Mouse Spermiogenesis. *The Journal of Cell Biology*, *176*(3), 283–294.

Govin, J., Lestrat, C., Caron, C., Pivot-Pajot, C., Rousseaux, S., & Khochbin, S. (2006). Histone acetylation-mediated chromatin compaction during mouse spermatogenesis. *Ernst Schering Research Foundation Workshop*, (57), 155–172. https://doi.org/10.1007/3-540-37633-x_9

Govin, J., Schug, J., Krishnamoorthy, T., Dorsey, J., Khochbin, S., & Berger, S. L. (2010). Genome-wide mapping of histone H4 serine-1 phosphorylation during sporulation in Saccharomyces cerevisiae. *Nucleic Acids Research*, *38*(14), 4599–4606. https://doi.org/10.1093/nar/gkq218

Grimanelli, D., & Ingouff, M. (2020). DNA Methylation Readers in Plants. *Journal of Molecular Biology, Reading DNA Modifications*, *432*(6), 1706–1717. https://doi.org/10.1016/j.jmb.2019.12.043

Gujral, P., Mahajan, V., Lissaman, A. C., & Ponnampalam, A. P. (2020). Histone acetylation and the role of histone deacetylases in normal cyclic endometrium. *Reproductive Biology and Endocrinology*, *18*(1), 84. https://doi.org/10.1186/s12958-020-00637-5

Hakim, S. (2018, March 20). *Saccharomyces cerevisiae | Viticulture and Enology*. https://wineserver.ucdavis.edu/industry-info/enology/wine-microbiology/yeast-mold/saccharomyces-cerevisiae

Halabelian, L., & Barsyte-Lovejoy, D. (2021). Structure and Function of Protein Arginine Methyltransferase PRMT7. *Life*, *11*(8), Article 8. https://doi.org/10.3390/life11080768

Hammond, C. M., Strømme, C. B., Huang, H., Patel, D. J., & Groth, A. (2017). Histone chaperone networks shaping chromatin function. *Nature Reviews. Molecular Cell Biology*, *18*(3), 141–158. https://doi.org/10.1038/nrm.2016.159

Handy, D. E., Castro, R., & Loscalzo, J. (2011). Epigenetic Modifications: Basic Mechanisms and Role in Cardiovascular Disease. *Circulation*, *123*(19), 2145–2156. https://doi.org/10.1161/CIRCULATIONAHA.110.956839

Hao, F., Kale, S., Dimitrov, S., & Hayes, J. J. (2021). Unraveling Linker Histone Interactions in Nucleosomes. *Current Opinion in Structural Biology*, *71*, 87–93. https://doi.org/10.1016/j.sbi.2021.06.001

Happel, N., & Doenecke, D. (2009). Histone H1 and its isoforms: Contribution to chromatin structure and function. *Gene*, *431*(1), 1–12. https://doi.org/10.1016/j.gene.2008.11.003

Hashimoto, M., Masuda, T., Nakano, Y., Tobo, T., Saito, H., Koike, K., Takahashi, J., Abe, T., Ando, Y., Ozato, Y., Hosoda, K., Higuchi, S., Hisamatsu, Y., Toshima, T., Yonemura, Y., Hata, T., Uemura,

M., Eguchi, H., Doki, Y., … Mimori, K. (2024). Tumor suppressive role of the epigenetic master regulator BRD3 in colorectal cancer. *Cancer Science*, *115*(6), 1866–1880. https://doi.org/10.1111/cas.16129

Hashimoto, T., Conti, S. F., & Naylor, H. B. (1958). FINE STRUCTURE OF MICROORGANISMS: III. Electron Microscopy of Resting and Germinating Ascospores of *Saccharomyces cerevisiae*. *Journal of Bacteriology*, *76*(4), 406–416. https://doi.org/10.1128/jb.76.4.406-416.1958

He, R., Dantas, A., & Riabowol, K. (2021). Histone Acetyltransferases and Stem Cell Identity. *Cancers*, *13*(10), 2407. https://doi.org/10.3390/cancers13102407

He, S., Yu, Y., Wang, L., Zhang, J., Bai, Z., Li, G., Li, P., & Feng, X. (2024). Linker histone H1 drives heterochromatin condensation via phase separation in Arabidopsis. *The Plant Cell*, *36*(5), 1829–1843. https://doi.org/10.1093/plcell/koae034

He, Z., Chen, K., Ye, Y., & Chen, Z. (2021). Structure of the SWI/SNF complex bound to the nucleosome and insights into the functional modularity. *Cell Discovery*, *7*(1), 28. https://doi.org/10.1038/s41421-021-00262-5

Heasley, L. R., Singer, E., Cooperman, B. J., & McMurray, M. A. (2021). Saccharomyces spores are born prepolarized to outgrow away from spore–spore connections and penetrate the ascus wall. *Yeast*, *38*(1), 90–101. https://doi.org/10.1002/yea.3540

Hegazy, Y. A., Dhahri, H., Osmani, N. E., George, S., Chandler, D. P., & Fondufe-Mittendorf, Y. N. (2025). Histone variants: The bricks that fit differently. *Journal of Biological Chemistry*, *301*(1). https://doi.org/10.1016/j.jbc.2024.108048

Heideker, J., Perry, J. J. P., & Boddy, M. N. (2009). Genome stability roles of SUMO-targeted ubiquitin ligases. *DNA Repair, Ubiquitin, SUMO and the Maintenance of Genome Stability*, *8*(4), 517–524. https://doi.org/10.1016/j.dnarep.2009.01.010

Hergeth, S. P., & Schneider, R. (2015). The H1 linker histones: Multifunctional proteins beyond the nucleosomal core particle. *EMBO Reports*, *16*(11), 1439–1453. https://doi.org/10.15252/embr.201540749

Herman, P. K., & Rine, J. (1997). Yeast spore germination: A requirement for Ras protein activity during re-entry into the cell cycle. *The EMBO Journal*, *16*(20), 6171–6181. https://doi.org/10.1093/emboj/16.20.6171

Hilton, T. L., Li, Y., Dunphy, E. L., & Wang, E. H. (2005). TAF1 Histone Acetyltransferase Activity in Sp1 Activation of the Cyclin D1 Promoter. *Molecular and Cellular Biology*, *25*(10), 4321–4332. https://doi.org/10.1128/MCB.25.10.4321-4332.2005

Hoghoughi, N., Barral, S., Vargas, A., Rousseaux, S., & Khochbin, S. (2018). Histone variants: Essential actors in male genome programming. *Journal of Biochemistry*, *163*(2), 97–103. https://doi.org/10.1093/jb/mvx079

Honda, S., & Selker, E. U. (2008). Direct Interaction between DNA Methyltransferase DIM-2 and HP1 Is Required for DNA Methylation in Neurospora crassa. *Molecular and Cellular Biology*, *28*(19), 6044–6055. https://doi.org/10.1128/MCB.00823-08

Honer, M. A., Ferman, B. I., Gray, Z. H., Bondarenko, E. A., & Whetstine, J. R. (2024). Epigenetic modulators provide a path to understanding disease and therapeutic opportunity. *Genes & Development*, *38*(11–12), 473–503. https://doi.org/10.1101/gad.351444.123

Hong, H., Li, Y.-M., Meng, X.-M., Deng, T., & Zhu, B.-M. (2022). [Histone methylation and diabetic cardiomyopathy]. *Sheng Li Xue Bao: [Acta Physiologica Sinica]*, *74*(3), 461–468.

Horard, B., Sapey-Triomphe, L., Bonnefoy, E., & Loppin, B. (2018). ASF1 is required to load histones on the HIRA complex in preparation of paternal chromatin assembly at fertilization. *Epigenetics Chromatin*, *11*, 19.

Horwitz, A. A., Walter, J. M., Schubert, M. G., Kung, S. H., Hawkins, K., Platt, D. M., Hernday, A. D., Mahatdejkul-Meadows, T., Szeto, W., Chandran, S. S., & Newman, J. D. (2015). Efficient Multiplexed Integration of Synergistic Alleles and Metabolic Pathways in Yeasts via CRISPR-Cas. *Cell Systems*, *1*(1), 88–96. https://doi.org/10.1016/j.cels.2015.02.001

Hou, X., Xu, M., Zhu, C., Gao, J., Li, M., Chen, X., Sun, C., Nashan, B., Zang, J., Zhou, Y., Guang, S., & Feng, X. (2023). Systematic characterization of chromodomain proteins reveals an

H3K9me1/2 reader regulating aging in C. elegans. *Nature Communications*, *14*(1), 1254. https://doi.org/10.1038/s41467-023-36898-y

House, N. C., Polleys, E. J., Quasem, I., De la Rosa Mejia, M., Joyce, C. E., Takacsi-Nagy, O., Krebs, J. E., Fuchs, S. M., & Freudenreich, C. H. (2019). Distinct roles for S. cerevisiae H2A copies in recombination and repeat stability, with a role for H2A.1 threonine 126. *eLife*, *8*, e53362. https://doi.org/10.7554/eLife.53362

Hu, F. (2025). DOT1L suppressed the proliferation of osteosarcoma cell line via modulating SYK/EGFR/P53 and SHP2-induced STING-NLRP3-pyroptosis signaling. *Scientific Reports*, *15*(1), 23187. https://doi.org/10.1038/s41598-025-05221-8

Huang, F., Shao, W., Fujinaga, K., & Peterlin, B. M. (2018). Bromodomain-containing protein 4–independent transcriptional activation by autoimmune regulator (AIRE) and NF-κB. *The Journal of Biological Chemistry*, *293*(14), 4993–5004. https://doi.org/10.1074/jbc.RA117.001518

Huang, H., Strømme, C. B., Saredi, G., Hödl, M., Strandsby, A., González-Aguilera, C., Chen, S., Groth, A., & Patel, D. J. (2015). A unique binding mode enables MCM2 to chaperone histones H3–H4 at replication forks. *Nature Structural & Molecular Biology*, *22*(8), 618–626. https://doi.org/10.1038/nsmb.3055

Huh, W.-K., Falvo, J. V., Gerke, L. C., Carroll, A. S., Howson, R. W., Weissman, J. S., & O'Shea, E. K. (2003). Global analysis of protein localization in budding yeast. *Nature*, *425*(6959), 686–691. https://doi.org/10.1038/nature02026

Human Genome Sequencing Consortium, I. (2004). Finishing the euchromatic sequence of the human genome. *Nature*, *431*(7011), 931–945. (14764724). https://doi.org/10.1038/nature03001

Hutchison, E. A., Miller, D. A., & Angert, E. R. (2014). Sporulation in Bacteria: Beyond the Standard Model. *Microbiology Spectrum*, *2*(5), 10.1128/microbiolspec.tbs-0013–2012. https://doi.org/10.1128/microbiolspec.tbs-0013-2012

Hwang, J. W., Cho, Y., Bae, G.-U., Kim, S.-N., & Kim, Y. K. (2021). Protein arginine methyltransferases: Promising targets for cancer therapy. *Experimental & Molecular Medicine*, *53*(5), 788–808. https://doi.org/10.1038/s12276-021-00613-y

Ibrahim, S. Y., Carter, J., & Bagchi, R. A. (2025). Histone Deacetylases in Metabolism: The Known and the Unexplored. *Physiology*, *40*(3), 247–257. https://doi.org/10.1152/physiol.00044.2024

Ibrahim, Z., Wang, T., Destaing, O., Salvi, N., Hoghoughi, N., Chabert, C., Rusu, A., Gao, J., Feletto, L., Reynoird, N., Schalch, T., Zhao, Y., Blackledge, M., Khochbin, S., & Panne, D. (2022). Structural insights into p300 regulation and acetylation-dependent genome organisation. *Nature Communications*, *13*(1), 7759. https://doi.org/10.1038/s41467-022-35375-2

Iñiguez-Lluhí, J. A. (2006). For a Healthy Histone Code, a Little SUMO in the Tail Keeps the Acetyl Away. *ACS Chemical Biology*, *1*(4), 204–206. https://doi.org/10.1021/cb600188m

Ishiguro, K., Kitajima, H., Niinuma, T., Maruyama, R., Tsukahara, T., Hirohashi, Y., Takaya, A., Kumegawa, K., Yoshido, A., Sekiguchi, S., Sasaki, H., Yorozu, A., Toyota, M., Kai, M., Torigoe, T., Nakase, H., & Suzuki, H. (2025). DOT1L inhibition reprograms innate immunity to potentiate immunomodulatory drug responses in multiple myeloma. *Cancer Letters*, *631*, 217941. https://doi.org/10.1016/j.canlet.2025.217941

Islam, M. S., Markoulides, M., Chowdhury, R., & Schofield, C. J. (2022). Structural analysis of the 2-oxoglutarate binding site of the circadian rhythm linked oxygenase JMJD5. *Scientific Reports*, *12*(1), 20680. https://doi.org/10.1038/s41598-022-24154-0

Iwase, M., Luo, J., Nagaraj, S., Longtine, M., Kim, H. B., Haarer, B. K., Caruso, C., Tong, Z., Pringle, J. R., & Bi, E. (2006). Role of a Cdc42p Effector Pathway in Recruitment of the Yeast Septins to the Presumptive Bud Site. *Molecular Biology of the Cell*, *17*(3), 1110–1125. https://doi.org/10.1091/mbc.e05-08-0793

Jain, K., Fraser, C. S., Marunde, M. R., Parker, M. M., Sagum, C., Burg, J. M., Hall, N., Popova, I. K., Rodriguez, K. L., Vaidya, A., Krajewski, K., Keogh, M.-C., Bedford, M. T., & Strahl, B. D. (2020).

Characterization of the plant homeodomain (PHD) reader family for their histone tail interactions. *Epigenetics & Chromatin*, *13*(1), 3. https://doi.org/10.1186/s13072-020-0328-z

Jaiswal, D., Jezek, M., Quijote, J., Lum, J., Choi, G., Kulkarni, R., Park, D., & Green, E. M. (2017). Repression of Middle Sporulation Genes in Saccharomyces cerevisiae by the Sum1-Rfm1-Hst1 Complex Is Maintained by Set1 and H3K4 Methylation. *G3: Genes|Genomes|Genetics*, *7*(12), 3971–3982. https://doi.org/10.1534/g3.117.300150

Jakočiūnas, T., Jensen, M. K., & Keasling, J. D. (2016). CRISPR/Cas9 advances engineering of microbial cell factories. *Metabolic Engineering*, *34*, 44–59. https://doi.org/10.1016/j.ymben.2015.12.003

Ji, Y., Chen, W., & Wang, X. (2024). Bromodomain and Extraterminal Domain Protein 2 in Multiple Human Diseases. *The Journal of Pharmacology and Experimental Therapeutics*, *389*(3), 277–288. https://doi.org/10.1124/jpet.123.002036

Jiang, S., Liu, Y., Wang, A., Qin, Y., Luo, M., Wu, Q., Boeke, J. D., & Dai, J. (2017). Construction of comprehensive dosage-matching core histone mutant libraries for Saccharomyces cerevisiae. *Genetics*, *207*(4), 1263–1273. https://doi.org/10.1534/genetics.117.300450

Jiménez, J., Bru, S., Ribeiro, M. P., & Clotet, J. (2015). Live fast, die soon: Cell cycle progression and lifespan in yeast cells. *Microbial Cell*, *2*(3), 62–67. https://doi.org/10.15698/mic2015.03.191

Jorgensen, P., Nishikawa, J. L., Breitkreutz, B.-J., & Tyers, M. (2002). Systematic identification of pathways that couple cell growth and division in yeast. *Science*, *297*(5580), 395–400. https://doi.org/10.1126/science.1070850

Joseph, F. M., & Young, N. L. (2023). Histone Variant-Specific Post-Translational Modifications. *Seminars in Cell & Developmental Biology*, *135*, 73–84. https://doi.org/10.1016/j.semcdb.2022.02.012

Joseph-Strauss, D., Zenvirth, D., Simchen, G., & Barkai, N. (2007a). Spore germination in Saccharomyces cerevisiae: Global gene expression patterns and cell cycle landmarks. *Genome Biology*, *8*(11), R241. https://doi.org/10.1186/gb-2007-8-11-r241

Joseph-Strauss, D., Zenvirth, D., Simchen, G., & Barkai, N. (2007b). Spore germination in Saccharomyces cerevisiae: Global gene expression patterns and cell cycle landmarks. *Genome Biology*, *8*(11), R241. https://doi.org/10.1186/gb-2007-8-11-r241

Joseph-Strauss, D., Zenvirth, D., Simchen, G., & Barkai, N. (2007c). Spore germination in Saccharomyces cerevisiae: Global gene expression patterns and cell cycle landmarks. *Genome Biology*, *8*(11), R241. https://doi.org/10.1186/gb-2007-8-11-r241

Joseph-Strauss, D., Zenvirth, D., Simchen, G., & Barkai, N. (2007d). Spore germination in Saccharomyces cerevisiae: Global gene expression patterns and cell cycle landmarks. *Genome Biology*, *8*(11), R241. https://doi.org/10.1186/gb-2007-8-11-r241

Jullien, J., Miyamoto, K., Pasque, V., Allen, G. E., Bradshaw, C. R., Garrett, N. J., Halley-Stott, R. P., Kimura, H., Ohsumi, K., & Gurdon, J. B. (2014). Hierarchical Molecular Events Driven by Oocyte-Specific Factors Lead to Rapid and Extensive Reprogramming. *Molecular Cell*, *55*(4), 524–536. https://doi.org/10.1016/j.molcel.2014.06.024

Kaimori, J.-Y., Maehara, K., Hayashi-Takanaka, Y., Harada, A., Fukuda, M., Yamamoto, S., Ichimaru, N., Umehara, T., Yokoyama, S., Matsuda, R., Ikura, T., Nagao, K., Obuse, C., Nozaki, N., Takahara, S., Takao, T., Ohkawa, Y., Kimura, H., & Isaka, Y. (2016). Histone H4 lysine 20 acetylation is associated with gene repression in human cells. *Scientific Reports*, *6*(1), 24318. https://doi.org/10.1038/srep24318

Kaitera, J., Hiltunen, R., Kauppila, T., & Hantula, J. (2017). Five plant families support natural sporulation of Cronartium ribicola and C. flaccidum in Finland. *European Journal of Plant Pathology*, *149*(2), 367–383. https://doi.org/10.1007/s10658-017-1188-7

Kales, S. C., & Simeonov, A. (n.d.). *Histone Demethylases*. Retrieved 31 July 2025, from https://books.rsc.org/books/edited-volume/2227/chapter/8160895/Histone-Demethylases

Kalra, P., Zahid, H., Ayoub, A., Dou, Y., & Pomerantz, W. C. K. (2022). Alternative Mechanisms for DNA Engagement by BET Bromodomain-Containing Proteins. *Biochemistry*, *61*(13), 1260–1272. https://doi.org/10.1021/acs.biochem.2c00157

Karki, G. (2017, November 18). Yeast: Morphology and life cycle. *Online Biology Notes*. https://www.onlinebiologynotes.com/yeast-morphology-life-cycle/

Kassir, Y., & Simchen, G. (1976). REGULATION OF MATING AND MEIOSIS IN YEAST BY THE MATING-TYPE REGION. *Genetics*, *82*(2), 187–206. https://doi.org/10.1093/genetics/82.2.187

Kayikci, Ö., & Magwene, P. M. (2018). *Divergent Roles for cAMP–PKA Signaling in the Regulation of Filamentous Growth in Saccharomyces cerevisiae and Saccharomyces bayanus* (p. 311415). bioRxiv. https://doi.org/10.1101/311415

Keiten-Schmitz, J., Schunck, K., & Müller, S. (2020). SUMO Chains Rule on Chromatin Occupancy. *Frontiers in Cell and Developmental Biology*, *7*. https://doi.org/10.3389/fcell.2019.00343

Keogh, M.-C., Kim, J.-A., Downey, M., Fillingham, J., Chowdhury, D., Harrison, J. C., Onishi, M., Datta, N., Galicia, S., Emili, A., Lieberman, J., Shen, X., Buratowski, S., Haber, J. E., Durocher, D., Greenblatt, J. F., & Krogan, N. J. (2006). A phosphatase complex that dephosphorylates gammaH2AX regulates DNA damage checkpoint recovery. *Nature*, *439*(7075), 497–501. https://doi.org/10.1038/nature04384

Kerrigan, L. A., & Kadonaga, J. T. (1992). Periodic binding of individual core histones to DNA: Inadvertent purification of the core histone H2B as a putative enhancer-binding factor. *Nucleic Acids Research*, *20*(24), 6673–6680. https://doi.org/10.1093/nar/20.24.6673

Khadka, J., Pesok, A., & Grafi, G. (2020). Plant Histone HTB (H2B) Variants in Regulating Chromatin Structure and Function. *Plants*, *9*(11), Article 11. https://doi.org/10.3390/plants9111435

Khochbin, S. (2011). In the Heart of a Dynamic Chromatin. *Chemistry & Biology*, *18*(4), 410–412. https://doi.org/10.1016/j.chembiol.2011.04.001

Kilichowska, M., & Kotliński, M. (2022). Histon H1 – struktura i funkcja. *Postępy Biochemii*. https://doi.org/10.18388/pb.2021_466

Kirkiz, E., Meers, O., Grebien, F., & Buschbeck, M. (2023). Histone Variants and Their Chaperones in Hematological Malignancies. *HemaSphere*, *7*(8), e927. https://doi.org/10.1097/HS9.0000000000000927

Kloimwieder, A., & Winston, F. (2011). A Screen for Germination Mutants in Saccharomyces cerevisiae. *G3 Genes|Genomes|Genetics*, *1*(2), 143–149. https://doi.org/10.1534/g3.111.000323

Kong, Y., Olejar, K. J., On, S. L. W., Winefield, C., Wescombe, P. A., Brennan, C. S., Hider, R. N., & Chelikani, V. (2022). Epigenetic Changes in Saccharomyces cerevisiae Alters the Aromatic Profile in Alcoholic Fermentation. *Applied and Environmental Microbiology*. (1752 N St., N.W., Washington, DC). https://doi.org/10.1128/aem.01528-22

Kouzminova, E., & Selker, E. U. (2001). Dim-2 encodes a DNA methyltransferase responsible for all known cytosine methylation in Neurospora. *The EMBO Journal*, *20*(15), 4309–4323. https://doi.org/10.1093/emboj/20.15.4309

Kozminski, K. G., Chen, A. J., Rodal, A. A., & Drubin, D. G. (2000). Functions and Functional Domains of the GTPase Cdc42p. *Molecular Biology of the Cell*, *11*(1), 339–354. https://doi.org/10.1091/mbc.11.1.339

Krapp, A., Collin, P., Cokoja, A., Dischinger, S., Cano, E., & Simanis, V. (2006). The Schizosaccharomyces pombe septation initiation network (SIN) is required for spore formation in meiosis. *Journal of Cell Science*, *119*(14), 2882–2891. https://doi.org/10.1242/jcs.03025

Krishnamoorthy, T., Chen, X., Govin, J., Cheung, W. L., Dorsey, J., Schindler, K., Winter, E., Allis, C. D., Guacci, V., Khochbin, S., Fuller, M. T., & Berger, S. L. (2006). Phosphorylation of histone H4 Ser1 regulates sporulation in yeast and is conserved in fly and mouse spermatogenesis. *Genes & Development*, *20*(18), 2580–2592. https://doi.org/10.1101/gad.1457006

Kubota, S., Takeo, I., Kume, K., Kanai, M., Shitamukai, A., Mizunuma, M., Miyakawa, T., Shimoi, H., Iefuji, H., & Hirata, D. (2004). Effect of Ethanol on Cell Growth of Budding Yeast: Genes That Are Important for Cell Growth in the Presence of Ethanol. *Bioscience, Biotechnology, and Biochemistry*, *68*(4), 968–972. https://doi.org/10.1271/bbb.68.968

Kurat, C. F., Lambert, J.-P., Petschnigg, J., Friesen, H., Pawson, T., Rosebrock, A., Gingras, A.-C., Fillingham, J., & Andrews, B. (2014). Cell cycle-regulated oscillator coordinates core histone

gene transcription through histone acetylation. *Proceedings of the National Academy of Sciences of the United States of America*, *111*(39), 14124–14129. https://doi.org/10.1073/pnas.1414024111

Lacoste, N., & Côté, J. (2003). Le code épigénétique des histones. *médecine/sciences*, *19*(10), 955–959. https://doi.org/10.1051/medsci/20031910955

Ladurner, A. G., Inouye, C., Jain, R., & Tjian, R. (2003a). Bromodomains Mediate an Acetyl-Histone Encoded Antisilencing Function at Heterochromatin Boundaries. *Molecular Cell*, *11*(2), 365–376. https://doi.org/10.1016/S1097-2765(03)00035-2

Ladurner, A. G., Inouye, C., Jain, R., & Tjian, R. (2003b). Bromodomains mediate an acetyl-histone encoded antisilencing function at heterochromatin boundaries. *Molecular Cell*, *11*(2), 365–376. https://doi.org/10.1016/s1097-2765(03)00035-2

Lai, P. M., & Chan, K. M. (2024). Roles of Histone H2A Variants in Cancer Development, Prognosis, and Treatment. *International Journal of Molecular Sciences*, *25*(6), 3144. https://doi.org/10.3390/ijms25063144

Lai, P. M., Gong, X., & Chan, K. M. (2024). Roles of Histone H2B, H3 and H4 Variants in Cancer Development and Prognosis. *International Journal of Molecular Sciences*, *25*(17), Article 17. https://doi.org/10.3390/ijms25179699

Lamm, E., Harman, O., & Veigl, S. J. (2020). Before Watson and Crick in 1953 Came Friedrich Miescher in 1869. *Genetics*, *215*(2), 291–296. https://doi.org/10.1534/genetics.120.303195

Landsman, D. (1996). Histone H1 inSaccharomyces cerevisiae: A double mystery solved? *Trends in Biochemical Sciences*, *21*(8), 287–288. https://doi.org/10.1016/s0968-0004(96)30030-3

Lee, J.-H., & Skalnik, D. G. (2021). Transcription | Chromatin: Methyl-CpG-Binding Proteins☆. In J. Jez (Ed.), *Encyclopedia of Biological Chemistry III (Third Edition)* (pp. 390–396). Elsevier. https://doi.org/10.1016/B978-0-12-819460-7.00213-9

Lei, B., & Berger, F. (2020). H2A Variants in Arabidopsis: Versatile Regulators of Genome Activity. *Plant Communications*, *1*(1). https://doi.org/10.1016/j.xplc.2019.100015

Lennartsson, A., & Ekwall, K. (2009). Histone modification patterns and epigenetic codes. *Biochimica et Biophysica Acta (BBA) - General Subjects, Epigenetic Control of Gene Expression*, *1790*(9), 863–868. https://doi.org/10.1016/j.bbagen.2008.12.006

Li, G. (2024). Chapter 13—Post-translational modification of proteins. In G. Li (Ed.), *Chemical Theory and Multiscale Simulation in Biomolecules* (pp. 243–254). Elsevier. https://doi.org/10.1016/B978-0-323-95917-9.00013-4

Li, K., & Wang, Z. (2021). Histone crotonylation-centric gene regulation. *Epigenetics & Chromatin*, *14*(1), 10. https://doi.org/10.1186/s13072-021-00385-9

Li, Q., Burgess, R., & Zhang, Z. (2012). All roads lead to chromatin: Multiple pathways for histone deposition. *Biochimica et Biophysica Acta*, *1819*(0), 238–246. https://doi.org/10.1016/j.bbagrm.2011.06.013

Li, X., & Li, X. D. (2021). Integrative Chemical Biology Approaches to Deciphering the Histone Code: A Problem-Driven Journey. *Accounts of Chemical Research*, *54*(19), 3734–3747. https://doi.org/10.1021/acs.accounts.1c00463

Li, X., Xiong, H., Mou, X., Huang, C., Thomas, E. R., Yu, W., Jiang, Y., & Chen, Y. (2024). Androgen receptor cofactors: A potential role in understanding prostate cancer. *Biomedicine & Pharmacotherapy = Biomedecine & Pharmacotherapie*, *173*, 116338. https://doi.org/10.1016/j.biopha.2024.116338

Li, Y., Chen, X., & Lu, C. (2021). The interplay between DNA and histone methylation: Molecular mechanisms and disease implications. *EMBO Reports*, *22*(5), e51803. https://doi.org/10.15252/embr.202051803

Li, Z., Hua, X., Serra-Cardona, A., Xu, X., Gan, S., Zhou, H., Yang, W.-S., Chen, C., Xu, R.-M., & Zhang, Z. (2020). DNA polymerase α interacts with H3-H4 and facilitates the transfer of parental histones to lagging strands. *Science Advances*, *6*(35), eabb5820. https://doi.org/10.1126/sciadv.abb5820

Libuda, D. E., & Winston, F. (2006). Amplification of histone genes by circular chromosome formation in Saccharomyces cerevisiae. *Nature*, *443*(7114), 1003–1007. https://doi.org/10.1038/nature05205

Lim, J. R., Chae, C. W., Yoon, J. H., Cho, J. H., Park, J. Y., Han, S. J., Chang, H. S., Kim, S. Y., Kim, H. J., Jung, Y. H., & Han, H. J. (2025). Recovery of FAM134A-mediated ER-phagy through BRD4 inhibition alleviates ethanol-induced neurodegeneration. *International Journal of Biological Sciences*, *21*(12), 5167–5184. https://doi.org/10.7150/ijbs.116673

Lin, Z., Li, Z., Guo, Z., Cao, Y., Li, J., Liu, P., & Li, Z. (2022). Epigenetic Reader Bromodomain Containing Protein 2 Facilitates Pathological Cardiac Hypertrophy via Regulating the Expression of Citrate Cycle Genes. *Frontiers in Pharmacology*, *13*. https://doi.org/10.3389/fphar.2022.887991

Liu, J., Jin, Y., Zuo, S., Mu, C., Wang, B., Huang, D., Liu, Q., Zhang, K., Song, J., Xuan, C., Zhang, J., & Yu, Y. (2025). Dot1L Promotes Stress-Induced Cardiac Hypertrophy in Mice via Tbx6. *Circulation Research*, *137*(4), 496–512. https://doi.org/10.1161/CIRCRESAHA.124.324940

Liu, K., Xu, C., Lei, M., Yang, A., Loppnau, P., Hughes, T. R., & Min, J. (2018). Structural basis for the ability of MBD domains to bind methyl-CG and TG sites in DNA. *The Journal of Biological Chemistry*, *293*(19), 7344–7354. https://doi.org/10.1074/jbc.RA118.001785

Liu, L., Liu, L., Deng, S., Zou, L., He, Y., Zhu, X., Li, H., Hu, Y., Chu, W., & Wang, X. (2024). Circadian Rhythm Alteration of the Core Clock Genes and the Lipid Metabolism Genes Induced by High-Fat Diet (HFD) in the Liver Tissue of the Chinese Soft-Shelled Turtle (Trionyx sinensis). *Genes*, *15*(2), 157. https://doi.org/10.3390/genes15020157

Liu, M., Li, W., Zheng, X., Yuan, Z., Zhou, Y., Yang, J., Mao, Y., Wang, D., Wu, Q., He, Y., He, L., Zong, D., & Chen, J. (2024). Genome-Wide Identification and Expression Analysis of the PHD Finger Gene Family in Pea (Pisum sativum). *Plants*, *13*(11), 1489. https://doi.org/10.3390/plants13111489

Liu, R., Wu, J., Guo, H., Yao, W., Li, S., Lu, Y., Jia, Y., Liang, X., Tang, J., & Zhang, H. (2023). Post-translational modifications of histones: Mechanisms, biological functions, and therapeutic targets. *MedComm*, *4*(3), e292. https://doi.org/10.1002/mco2.292

Liu, X., Yang, H., Zhang, X., Liu, L., Lei, M., Zhang, Z., & Bao, X. (2009). Bdf1p deletion affects mitochondrial function and causes apoptotic cell death under salt stress. *FEMS Yeast Research*, *9*(2), 240–246. https://doi.org/10.1111/j.1567-1364.2008.00469.x

Liu, Y., Liu, Y., Zhu, Y., Hu, D., Nie, H., Xie, Y., Sun, R., He, J., Zhang, H., & Lu, F. (2025). KDM2A and KDM2B protect a subset of CpG islands from DNA methylation. *Journal of Genetics and Genomics*, *52*(1), 39–50. https://doi.org/10.1016/j.jgg.2024.10.012

Liu, Y., Wood, N. E., Marchand, A. J., Arguello-Miranda, O., & Doncic, A. (2020). Functional interrelationships between carbohydrate and lipid storage, and mitochondrial activity during sporulation in Saccharomyces cerevisiae. *Yeast*, *37*(3), 269–279. https://doi.org/10.1002/yea.3460

Loewith, R., & Hall, M. N. (2011). Target of rapamycin (TOR) in nutrient signaling and growth control. *Genetics*, *189*(4), 1177–1201. https://doi.org/10.1534/genetics.111.133363

Long, M., Sun, X., Shi, W., Yanru, A., Leung, S. T. C., Ding, D., Cheema, M. S., MacPherson, N., Nelson, C. J., Ausio, J., Yan, Y., & Ishibashi, T. (2019). A novel histone H4 variant H4G regulates rDNA transcription in breast cancer. *Nucleic Acids Research*, *47*(16), 8399–8409. https://doi.org/10.1093/nar/gkz547

Lopes, M., Lund, P. J., & Garcia, B. A. (2024). Optimized and Robust Workflow for Quantifying the Canonical Histone Ubiquitination Marks H2AK119ub and H2BK120ub by LC–MS/MS. *Journal of Proteome Research*, *23*(12), 5405–5420. https://doi.org/10.1021/acs.jproteome.4c00519

Louzon, S., Feierman, E. R., Qiu, Q., Maroni, M. J., Quaye, C. N., Perez-Tremble, R., Wu, H., & Korb, E. (2025). Age- and cell-type-specific effects of histone variant H2BE in the brain. *Cell Reports*, *44*(12), 116655. https://doi.org/10.1016/j.celrep.2025.116655

Lu, R., & Wang, G. G. (2013). Tudor: A versatile family of histone methylation 'readers'. *Trends in Biochemical Sciences*, *38*(11), 10.1016/j.tibs.2013.08.002. https://doi.org/10.1016/j.tibs.2013.08.002

Luger, K., Dechassa, M. L., & Tremethick, D. J. (2012). New insights into nucleosome and chromatin structure: An ordered state or a disordered affair? *Nature Reviews. Molecular Cell Biology*, *13*(7), 436–447. https://doi.org/10.1038/nrm3382

Lygerou, Z., Conesa, C., Lesage, P., Swanson, R. N., Ruet, A., Carlson, M., Sentenac, A., & Séraphin, B. (1994). The yeast BDF1 gene encodes a transcription factor involved in the expression of a broad class of genes including snRNAs. *Nucleic Acids Research*, *22*(24), 5332–5340. https://doi.org/10.1093/nar/22.24.5332

Madeira, F., Park, Y. mi, Lee, J., Buso, N., Gur, T., Madhusoodanan, N., Basutkar, P., Tivey, A. R. N., Potter, S. C., Finn, R. D., & Lopez, R. (2019). The EMBL-EBI search and sequence analysis tools APIs in 2019. *Nucleic Acids Research*, *47*(W1), W636–W641. https://doi.org/10.1093/nar/gkz268

Mahmood, N., & Rabbani, S. A. (2019). DNA Methylation Readers and Cancer: Mechanistic and Therapeutic Applications. *Frontiers in Oncology*, *9*. https://doi.org/10.3389/fonc.2019.00489

Malvezzi, F., Stubbs, C. J., Jowitt, T. A., Dale, I. L., Guo, X., DeGnore, J. P., Degliesposti, G., Skehel, J. M., Bannister, A. J., & McAlister, M. S. (2021). Phosphorylation-dependent BRD4 dimerization and implications for therapeutic inhibition of BET family proteins. *Communications Biology*, *4*(1), 1273. https://doi.org/10.1038/s42003-021-02750-6

Mann, M., Fu, Y., Xu, X., Roberts, D. S., Li, Y., Zhou, J., Ge, Y., & Brasier, A. R. (2023). *Bromodomain-containing Protein 4 Regulates Innate Inflammation in Airway Epithelial Cells via Modulation of Alternative Splicing* (p. 2023.01.17.524257). bioRxiv. https://doi.org/10.1101/2023.01.17.524257

Manterola, M., Brown, T. M., Oh, M. Y., Garyn, C., Gonzalez, B. J., & Wolgemuth, D. J. (2018). BRDT is an essential epigenetic regulator for proper chromatin organization, silencing of sex

chromosomes and crossover formation in male meiosis. *PLOS Genetics*, *14*(3), e1007209. https://doi.org/10.1371/journal.pgen.1007209

Map of Second Genetic Code, the 'Epigenome,' Is Unveiled. (n.d.). Scientific American. Retrieved 25 March 2026, from https://www.scientificamerican.com/article/map-of-second-genetic-code-the-epigenome-is-unveiled/

Marabita, F., Tegnér, J., & Gomez-Cabrero, D. (2015). Introduction to Data Types in Epigenomics. In A. E. Teschendorff (Ed.), *Computational and Statistical Epigenomics* (pp. 3–34). Springer Netherlands. https://doi.org/10.1007/978-94-017-9927-0_1

Mariño-Ramírez, L., Kann, M. G., Shoemaker, B. A., & Landsman, D. (2005). Histone structure and nucleosome stability. *Expert Review of Proteomics*, *2*(5), 719–729. https://doi.org/10.1586/14789450.2.5.719

Markolovic, S., Zhuang, Q., Wilkins, S. E., Eaton, C. D., Abboud, M. I., Katz, M. J., McNeil, H. E., Leśniak, R. K., Hall, C., Struwe, W. B., Konietzny, R., Davis, S., Yang, M., Ge, W., Benesch, J. L., Kessler, B. M., Ratcliffe, P. J., Cockman, M. E., Fischer, R., … Schofield, C. J. (2018). The Jumonji-C oxygenase JMJD7 catalyzes (3S)-lysyl hydroxylation of TRAFAC GTPases. *Nature Chemical Biology*, *14*(7), 688–695. https://doi.org/10.1038/s41589-018-0071-y

Marmorstein, R., & Trievel, R. C. (2009). Histone Modifying Enzymes: Structures, Mechanisms, and Specificities. *Biochimica et Biophysica Acta*, *1789*(1), 58–68. https://doi.org/10.1016/j.bbagrm.2008.07.009

Marzluff, W. F., & Duronio, R. J. (2002). Histone mRNA expression: Multiple levels of cell cycle regulation and important developmental consequences. *Current Opinion in Cell Biology*, *14*(6), 692–699. https://doi.org/10.1016/S0955-0674(02)00387-3

Matangkasombut, O., Buratowski, R. M., Swilling, N. W., & Buratowski, S. (2000). Bromodomain factor 1 corresponds to a missing piece of yeast TFIID. *Genes & Development*, *14*(8), 951–962.

Matangkasombut, O., & Buratowski, S. (2003a). Different Sensitivities of Bromodomain Factors 1 and 2 to Histone H4 Acetylation. *Molecular Cell*, *11*(2), 353–363. https://doi.org/10.1016/S1097-2765(03)00033-9

Matangkasombut, O., & Buratowski, S. (2003b). Different Sensitivities of Bromodomain Factors 1 and 2 to Histone H4 Acetylation. *Molecular Cell*, *11*(2), 353–363. https://doi.org/10.1016/S1097-2765(03)00033-9

Matthews, H. R., & Huebner, V. D. (1984). Nuclear protein kinases. *Molecular and Cellular Biochemistry*, *59*(1), 81–99. https://doi.org/10.1007/BF00231306

Mattiroli, F., D'Arcy, S., & Luger, K. (2015). The right place at the right time: Chaperoning core histone variants. *EMBO Reports*, *16*(11), 1454–1466. https://doi.org/10.15252/embr.201540840

Maunakea, A. K., Chepelev, I., & Zhao, K. (2010). Epigenome Mapping in Normal and Disease States. *Circulation Research*, *107*(3), 327–339. https://doi.org/10.1161/CIRCRESAHA.110.222463

Mazur, P. K., Reynoird, N., Khatri, P., Jansen, P. W. T. C., Wilkinson, A. W., Liu, S., Barbash, O., Van Aller, G. S., Huddleston, M., Dhanak, D., Tummino, P. J., Kruger, R. G., Garcia, B. A., Butte, A. J., Vermeulen, M., Sage, J., & Gozani, O. (2014). SMYD3 links lysine methylation of MAP3K2 to Ras-driven cancer. *Nature*, *510*(7504), 283–287. (96445522). https://doi.org/10.1038/nature13320

Mbuyane, L. L., Bauer, F. F., & Divol, B. (2021). The metabolism of lipids in yeasts and applications in oenology. *Food Research International*, *141*, 110142. https://doi.org/10.1016/j.foodres.2021.110142

McCord, R., Pierce, M., Xie, J., Wonkatal, S., Mickel, C., & Vershon, A. K. (2003). Rfm1, a Novel Tethering Factor Required To Recruit the Hst1 Histone Deacetylase for Repression of Middle Sporulation Genes. *Molecular and Cellular Biology*, *23*(6), 2009–2016. https://doi.org/10.1128/MCB.23.6.2009-2016.2003

McCullough, L., Connell, Z., Petersen, C., & Formosa, T. (2015). The Abundant Histone Chaperones Spt6 and FACT Collaborate to Assemble, Inspect, and Maintain Chromatin Structure in

Saccharomyces cerevisiae. *Genetics*, *201*(3), 1031–1045. https://doi.org/10.1534/genetics.115.180794

McLay, D. W., & Clarke, H. J. (2003). Remodelling the paternal chromatin at fertilization in mammals. *Reproduction (Cambridge, England)*, *125*(5), 625–633. https://doi.org/10.1530/rep.0.1250625

Mell, J. C., & Burgess, S. M. (2003). Yeast as a Model Genetic Organism. In Wiley, *Encyclopedia of Life Sciences* (1st edn). Wiley. https://doi.org/10.1038/npg.els.0000821

Mendiratta, S., Ray-Gallet, D., Lemaire, S., Gatto, A., Forest, A., Kerlin, M. A., & Almouzni, G. (2024). Regulation of replicative histone RNA metabolism by the histone chaperone ASF1. *Molecular Cell*, *84*(4), 791-801.e6. https://doi.org/10.1016/j.molcel.2023.12.038

Méteignier, L.-V. (2022). A chromatin modification at the crossroads of cell fates in pollen. *The Plant Cell*, *34*(8), 2823–2824. https://doi.org/10.1093/plcell/koac145

Mieczkowski, J., Cook, A., Bowman, S. K., Mueller, B., Alver, B. H., Kundu, S., Deaton, A. M., Urban, J. A., Larschan, E., Park, P. J., Kingston, R. E., & Tolstorukov, M. Y. (2016). MNase titration reveals differences between nucleosome occupancy and chromatin accessibility. *Nature Communications*, *7*(1), 11485. https://doi.org/10.1038/ncomms11485

Mietton, F., Ferri, E., Champleboux, M., Zala, N., Maubon, D., Zhou, Y., Harbut, M., Spittler, D., Garnaud, C., Courçon, M., Chauvel, M., d'Enfert, C., Kashemirov, B. A., Hull, M., Cornet, M., McKenna, C. E., Govin, J., & Petosa, C. (2017a). Selective BET bromodomain inhibition as an antifungal therapeutic strategy. *Nature Communications*, *8*(1), 15482. https://doi.org/10.1038/ncomms15482

Mietton, F., Ferri, E., Champleboux, M., Zala, N., Maubon, D., Zhou, Y., Harbut, M., Spittler, D., Garnaud, C., Courçon, M., Chauvel, M., d'Enfert, C., Kashemirov, B. A., Hull, M., Cornet, M., McKenna, C. E., Govin, J., & Petosa, C. (2017b). Selective BET bromodomain inhibition as an antifungal therapeutic strategy. *Nature Communications*, *8*(1), 15482. https://doi.org/10.1038/ncomms15482

Milazzo, G., Mercatelli, D., Di Muzio, G., Triboli, L., De Rosa, P., Perini, G., & Giorgi, F. M. (2020). Histone Deacetylases (HDACs): Evolution, Specificity, Role in Transcriptional Complexes, and Pharmacological Actionability. *Genes*, *11*(5), 556. https://doi.org/10.3390/genes11050556

Miller, T. C. R., Simon, B., Rybin, V., Grötsch, H., Curtet, S., Khochbin, S., Carlomagno, T., & Müller, C. W. (2016a). A bromodomain-DNA interaction facilitates acetylation-dependent bivalent nucleosome recognition by the BET protein BRDT. *Nature Communications*, *7*, 13855. https://doi.org/10.1038/ncomms13855

Miller, T. C. R., Simon, B., Rybin, V., Grötsch, H., Curtet, S., Khochbin, S., Carlomagno, T., & Müller, C. W. (2016b). A bromodomain–DNA interaction facilitates acetylation-dependent bivalent nucleosome recognition by the BET protein BRDT. *Nature Communications*, *7*(1), 13855. https://doi.org/10.1038/ncomms13855

Miron, E., Oldenkamp, R., Brown, J. M., Pinto, D. M. S., Xu, C. S., Faria, A. R., Shaban, H. A., Rhodes, J. D. P., Innocent, C., de Ornellas, S., Hess, H. F., Buckle, V., & Schermelleh, L. (2020). Chromatin arranges in chains of mesoscale domains with nanoscale functional topography independent of cohesin. *Science Advances*, *6*(39), eaba8811. https://doi.org/10.1126/sciadv.aba8811

Mizuguchi, G., Shen, X., Landry, J., Wu, W.-H., Sen, S., & Wu, C. (2004). ATP-Driven Exchange of Histone H2AZ Variant Catalyzed by SWR1 Chromatin Remodeling Complex. *Science*, *303*(5656), 343–348. https://doi.org/10.1126/science.1090701

Moens, P. B. (1971). Fine structure of ascospore development in the yeast Saccharomyces cerevisiae. *Canadian Journal of Microbiology*, *17*(4), 507–510. https://doi.org/10.1139/m71-084

Moindrot, B. (2012). *Organisation de la chromatine et son lien avec la réplication de l'ADN* [These de doctorat, Lyon, École normale supérieure]. https://theses.fr/2012ENSL0728

Molaro, A., Wood, A. J., Janssens, D., Kindelay, S. M., Eickbush, M. T., Wu, S., Singh, P., Muller, C. H., Henikoff, S., & Malik, H. S. (2020). Biparental contributions of the H2A.B histone variant control embryonic development in mice. *PLoS Biology*, *18*(12), e3001001. https://doi.org/10.1371/journal.pbio.3001001

Molaro, A., Young, J. M., & Malik, H. S. (2018). Evolutionary origins and diversification of testis-specific short histone H2A variants in mammals. *Genome Research*, *28*(4), 460–473. https://doi.org/10.1101/gr.229799.117

Monteiro, F. L., Baptista, T., Amado, F., Vitorino, R., Jerónimo, C., & Helguero, L. A. (2014). Expression and functionality of histone H2A variants in cancer. *Oncotarget*, *5*(11), 3428–3443. https://doi.org/10.18632/oncotarget.2007

Montellier, E., Boussouar, F., Rousseaux, S., Zhang, K., Buchou, T., Fenaille, F., Shiota, H., Debernardi, A., Héry, P., Curtet, S., Jamshidikia, M., Barral, S., Holota, H., Bergon, A., Lopez, F., Guardiola, P., Pernet, K., Imbert, J., Petosa, C., … Khochbin, S. (2013). Chromatin-to-nucleoprotamine transition is controlled by the histone H2B variant TH2B. *Genes & Development*, *27*(15), 1680–1692. https://doi.org/10.1101/gad.220095.113

Montellier, E., Rousseaux, S., Zhao, Y., & Khochbin, S. (2012). Histone crotonylation specifically marks the haploid male germ cell gene expression program: Post-meiotic male-specific gene expression. *BioEssays*, *34*(3), 187–193. https://doi.org/10.1002/bies.201100141

Moore, L. D., Le, T., & Fan, G. (2013). DNA Methylation and Its Basic Function. *Neuropsychopharmacology*, *38*(1), 23–38. https://doi.org/10.1038/npp.2012.112

Mousavi, N., & Yang, X.-J. (2025). Lysine Acetyltransferase 6 Complexes in Neurodevelopmental Disorders and Different Types of Cancer. *Results and Problems in Cell Differentiation*, *75*, 391–410. https://doi.org/10.1007/978-3-031-91459-1_14

Movilla Miangolarra, A., Saxton, D. S., Yan, Z., Rine, J., & Howard, M. (2024). Two-way feedback between chromatin compaction and histone modification state explains Saccharomyces cerevisiae heterochromatin bistability. *Proceedings of the National Academy of Sciences*, *121*(16), e2403316121. https://doi.org/10.1073/pnas.2403316121

Mühlen, D., Li, X., Dovgusha, O., Jäckle, H., & Günesdogan, U. (2023). Recycling of parental histones preserves the epigenetic landscape during embryonic development. *Science Advances*, *9*(5), eadd6440. https://doi.org/10.1126/sciadv.add6440

N, M. (2016, October 17). Reproduction in Yeast (With Diagram) | Fungi. *Biology Discussion*. https://www.biologydiscussion.com/yeasts/reproduction-in-yeast-with-diagram-fungi/58223

Nagae, F., Murayama, Y., & Terakawa, T. (2024). Molecular mechanism of parental H3/H4 recycling at a replication fork. *Nature Communications*, *15*(1), 9485. https://doi.org/10.1038/s41467-024-53187-4

Nagarajan, P., Ge, Z., Sirbu, B., Doughty, C., Garcia, P. A. A., Schlederer, M., Annunziato, A. T., Cortez, D., Kenner, L., & Parthun, M. R. (2013). Histone Acetyl Transferase 1 Is Essential for Mammalian Development, Genome Stability, and the Processing of Newly Synthesized Histones H3 and H4. *PLOS Genetics*, *9*(6), e1003518. https://doi.org/10.1371/journal.pgen.1003518

Nathan, D., Ingvarsdottir, K., Sterner, D. E., Bylebyl, G. R., Dokmanovic, M., Dorsey, J. A., Whelan, K. A., Krsmanovic, M., Lane, W. S., Meluh, P. B., Johnson, E. S., & Berger, S. L. (2006). Histone sumoylation is a negative regulator in Saccharomyces cerevisiae and shows dynamic interplay with positive-acting histone modifications. *Genes & Development*, *20*(8), 966–976. https://doi.org/10.1101/gad.1404206

Neiman, A. M. (1998). Prospore Membrane Formation Defines a Developmentally Regulated Branch of the Secretory Pathway in Yeast. *Journal of Cell Biology*, *140*(1), 29–37. https://doi.org/10.1083/jcb.140.1.29

Neiman, A. M. (2011). Sporulation in the Budding Yeast Saccharomyces cerevisiae. *Genetics*, *189*(3), 737–765. https://doi.org/10.1534/genetics.111.127126

Neumann, F. R., & Nurse, P. (2007). Nuclear size control in fission yeast. *The Journal of Cell Biology*, *179*(4), 593–600. https://doi.org/10.1083/jcb.200708054

Nicholson, J. M., Wood, C. M., Reynolds, C. D., Brown, A., Lambert, S. J., Chantalat, L., & Baldwin, J. P. (2004). Histone Structures: Targets for Modifications by Molecular Assemblies. *Annals of the New York Academy of Sciences*, *1030*(1), 644–655. https://doi.org/10.1196/annals.1329.075

Nicholson, T. B., Veland, N., & Chen, T. (2015). Chapter 3—Writers, Readers, and Erasers of Epigenetic Marks. In S. G. Gray (Ed.), *Epigenetic Cancer Therapy* (pp. 31–66). Academic Press. https://doi.org/10.1016/B978-0-12-800206-3.00003-3

Nihozeko, F. (2023). Abstract 4751: The function of bromodomain containing protein 4 (BRD44) in hematopoiesis. *Cancer Research*, *83*(7_Supplement), 4751. https://doi.org/10.1158/1538-7445.AM2023-4751

Ntorla, A., & Burgoyne, J. R. (2021). The Regulation and Function of Histone Crotonylation. *Frontiers in Cell and Developmental Biology*, *9*. https://doi.org/10.3389/fcell.2021.624914

Oberdoerffer, P., & Miller, K. M. (2023). Histone H2A variants: Diversifying chromatin to ensure genome integrity. *Seminars in Cell & Developmental Biology*, *135*, 59–72. https://doi.org/10.1016/j.semcdb.2022.03.011

Ohkuni, K., Levy-Myers, R., Warren, J., Au, W.-C., Takahashi, Y., Baker, R. E., & Basrai, M. A. (2018). N-terminal Sumoylation of Centromeric Histone H3 Variant Cse4 Regulates Its Proteolysis To Prevent Mislocalization to Non-centromeric Chromatin. *G3: Genes|Genomes|Genetics*, *8*(4), 1215–1223. https://doi.org/10.1534/g3.117.300419

Ohtomo, H., Kurita, J., Sakuraba, S., Li, Z., Arimura, Y., Wakamori, M., Tsunaka, Y., Umehara, T., Kurumizaka, H., Kono, H., & Nishimura, Y. (2021). The N-terminal Tails of Histones H2A and H2B Adopt Two Distinct Conformations in the Nucleosome with Contact and Reduced Contact to DNA. *Journal of Molecular Biology*, *433*(15), 167110. https://doi.org/10.1016/j.jmb.2021.167110

O'Kane, C. J., & Hyland, E. M. (2019). Yeast epigenetics: The inheritance of histone modification states. *Bioscience Reports*, *39*(5), BSR20182006. https://doi.org/10.1042/BSR20182006

Okumura, Y., Nakamura, T. S., Tanaka, T., Inoue, I., Suda, Y., Takahashi, T., Nakanishi, H., Nakamura, S., Gao, X.-D., & Tachikawa, H. (2015). The Dysferlin Domain-Only Protein, Spo73, Is Required for Prospore Membrane Extension in Saccharomyces cerevisiae. *mSphere*, *1*(1), 10.1128/msphere.00038-15. https://doi.org/10.1128/msphere.00038-15

Omari, N. E., Bakrim, S., Bakha, M., Balahbib, A., Bouyahya, A., Ardianto, C., Ming, L. C., & Ser, H. L. (2025). DNA Methylation: Its Role and Interaction with Epigenetic Modifications in Cancer. *Progress In Microbes & Molecular Biology*, *8*(1), Article 1. https://doi.org/10.36877/pmmb.a0000458

Ono, K., Kusano, O., Shimotakahara, S., Shimizu, M., Yamazaki, T., & Shindo, H. (2003). The linker histone homolog Hho1p from Saccharomyces cerevisiae represents a winged helix–turn–helix fold as determined by NMR spectroscopy. *Nucleic Acids Research*, *31*(24), 7199–7207. https://doi.org/10.1093/nar/gkg931

Orsi, G. A., Tortora, M. M. C., Horard, B., Baas, D., Kleman, J.-P., Bucevičius, J., Lukinavičius, G., Jost, D., & Loppin, B. (2023a). Biophysical ordering transitions underlie genome 3D re-organization during cricket spermiogenesis. *Nature Communications*, *14*(1), 4187. https://doi.org/10.1038/s41467-023-39908-1

Orsi, G. A., Tortora, M. M. C., Horard, B., Baas, D., Kleman, J.-P., Bucevičius, J., Lukinavičius, G., Jost, D., & Loppin, B. (2023b). Biophysical ordering transitions underlie genome 3D re-organization during cricket spermiogenesis. *Nature Communications*, *14*(1), 4187. https://doi.org/10.1038/s41467-023-39908-1

Ortega, M. A., De Leon-Oliva, D., Garcia-Montero, C., Fraile-Martinez, O., Boaru, D. L., del Val Toledo Lobo, M., García-Tuñón, I., Royuela, M., García-Honduvilla, N., Bujan, J., Guijarro, L. G., Alvarez-Mon, M., & Alvarez-Mon, M. Á. (2023). Understanding HAT1: A Comprehensive Review of Noncanonical Roles and Connection with Disease. *Genes*, *14*(4), 915. https://doi.org/10.3390/genes14040915

Oyen, M., Jäntti, J., Keränen, S., & Ronne, H. (2004). Mapping of sporulation-specific functions in the yeast syntaxin gene SSO1. *Current Genetics*, *45*(2), 76–82. https://doi.org/10.1007/s00294-003-0462-8

Ozonov, E. A., & Nimwegen, E. van. (2013). Nucleosome Free Regions in Yeast Promoters Result from Competitive Binding of Transcription Factors That Interact with Chromatin Modifiers. *PLOS Computational Biology*, *9*(8), e1003181. https://doi.org/10.1371/journal.pcbi.1003181

Pak, J., & Segall, J. (2002). Regulation of the premiddle and middle phases of expression of the NDT80 gene during sporulation of Saccharomyces cerevisiae. *Molecular and Cellular Biology*, *22*(18), 6417–6429. https://doi.org/10.1128/MCB.22.18.6417-6429.2002

Panday, A., & Grove, A. (2016). Yeast HMO1: Linker Histone Reinvented. *Microbiology and Molecular Biology Reviews : MMBR*, *81*(1), e00037-16. https://doi.org/10.1128/MMBR.00037-16

Panek, A. D., & Bernardes, E. J. (1983). Trehalose: Its role in germination of Saccharomyces cerevisiae. *Current Genetics*, *7*(5), 393–397. https://doi.org/10.1007/BF00445880

Parapouli, M., Vasileiadis, A., Afendra, A.-S., & Hatziloukas, E. (2020). Saccharomyces cerevisiae and its industrial applications. *AIMS Microbiology*, *6*(1), 1–31. https://doi.org/10.3934/microbiol.2020001

Pardal, A. J., Fernandes-Duarte, F., & Bowman, A. J. (2019). The histone chaperoning pathway: From ribosome to nucleosome. *Essays in Biochemistry*, *63*(1), 29–43. https://doi.org/10.1042/EBC20180055

Pascal, C., Zonszain, J., Hameiri, O., Gargi-Levi, C., Lev-Maor, G., Tammer, L., Levy, T., Tarabeih, A., Roy, V. R., Ben-Salmon, S., Elbaz, L., Eid, M., Hakim, T., Rabe'a, S. A., Shalev, N., Jordan, A., Meshorer, E., & Ast, G. (2023). Human histone H1 variants impact splicing outcome by controlling RNA polymerase II elongation. *Molecular Cell*, *83*(21), 3801-3817.e8. https://doi.org/10.1016/j.molcel.2023.10.003

Pattenden, S. G., Gogol, M. M., & Workman, J. L. (2010). Features of Cryptic Promoters and Their Varied Reliance on Bromodomain-Containing Factors. *PLOS ONE*, *5*(9), e12927. https://doi.org/10.1371/journal.pone.0012927

Patterton, H. G., Landel, C. C., Landsman, D., Peterson, C. L., & Simpson, R. T. (1998). The Biochemical and Phenotypic Characterization of Hho1p, the Putative Linker Histone H1 of Saccharomyces

cerevisiae. *Journal of Biological Chemistry*, *273*(13), 7268–7276. https://doi.org/10.1074/jbc.273.13.7268

Peng, H., Zhang, S., Peng, Y., Zhu, S., Zhao, X., Zhao, X., Yang, S., Liu, G., Dong, Y., Gan, X., Li, Q., Zhang, X., Pei, H., & Chen, X. (2021a). Yeast Bromodomain Factor 1 and Its Human Homolog TAF1 Play Conserved Roles in Promoting Homologous Recombination. *Advanced Science*, *8*(15), 2100753. https://doi.org/10.1002/advs.202100753

Peng, H., Zhang, S., Peng, Y., Zhu, S., Zhao, X., Zhao, X., Yang, S., Liu, G., Dong, Y., Gan, X., Li, Q., Zhang, X., Pei, H., & Chen, X. (2021b). Yeast Bromodomain Factor 1 and Its Human Homolog TAF1 Play Conserved Roles in Promoting Homologous Recombination. *Advanced Science*, *8*(15), 2100753. https://doi.org/10.1002/advs.202100753

Peng, H., Zhang, S., Peng, Y., Zhu, S., Zhao, X., Zhao, X., Yang, S., Liu, G., Dong, Y., Gan, X., Li, Q., Zhang, X., Pei, H., & Chen, X. (2021c). Yeast Bromodomain Factor 1 and Its Human Homolog TAF1 Play Conserved Roles in Promoting Homologous Recombination. *Advanced Science*, *8*(15), 2100753. https://doi.org/10.1002/advs.202100753

Peng, Y., Li, S., Onufriev, A., Landsman, D., & Panchenko, A. R. (2021). Binding of regulatory proteins to nucleosomes is modulated by dynamic histone tails. *Nature Communications*, *12*(1), 5280. https://doi.org/10.1038/s41467-021-25568-6

Piekarska, I., Rytka, J., & Rempola, B. (1970). Regulation of sporulation in the yeast Saccharomyces cerevisiae. *Acta Biochimica Polonica*, *57*(3). https://doi.org/10.18388/abp.2010_2401

Pienkowski, T., Kowalczyk, T., Cysewski, D., Kretowski, A., & Ciborowski, M. (2023). Glioma and post-translational modifications: A complex relationship. *Biochimica et Biophysica Acta (BBA) - Reviews on Cancer*, *1878*(6), 189009. https://doi.org/10.1016/j.bbcan.2023.189009

Piggot, P. J., & Hilbert, D. W. (2004). Sporulation of *Bacillus subtilis*. *Current Opinion in Microbiology, Growth and Development*, *7*(6), 579–586. https://doi.org/10.1016/j.mib.2004.10.001

Pivot-Pajot, C., Caron, C., Govin, J., Vion, A., Rousseaux, S., & Khochbin, S. (2003). Acetylation-dependent chromatin reorganization by BRDT, a testis-specific bromodomain-containing

protein. *Molecular and Cellular Biology*, *23*(15), 5354–5365. https://doi.org/10.1128/MCB.23.15.5354-5365.2003

Plante, S., Moon, K.-M., Lemieux, P., Foster, L. J., & Landry, C. R. (n.d.). *Exit of spore dormancy transforms the yeast cytoplasm and the solubility of its proteome*.

Plante, S., Moon, K.-M., Lemieux, P., Foster, L. J., & Landry, C. R. (2023a). Breaking spore dormancy in budding yeast transforms the cytoplasm and the solubility of the proteome. *PLOS Biology*, *21*(4), e3002042. https://doi.org/10.1371/journal.pbio.3002042

Plante, S., Moon, K.-M., Lemieux, P., Foster, L. J., & Landry, C. R. (2023b). Breaking spore dormancy in budding yeast transforms the cytoplasm and the solubility of the proteome. *PLOS Biology*, *21*(4), e3002042. https://doi.org/10.1371/journal.pbio.3002042

Primig, M., Williams, R. M., Winzeler, E. A., Tevzadze, G. G., Conway, A. R., Hwang, S. Y., Davis, R. W., & Esposito, R. E. (2000). The core meiotic transcriptome in budding yeasts. *Nature Genetics*, *26*(4), 415–423. https://doi.org/10.1038/82539

Pringle, J. R., Bi, E., Harkins, H. A., Zahner, J. E., Virgilio, C. D., Chant, J., Corrado, K., & Fares, H. (1995). Establishment of Cell Polarity in Yeast. *Cold Spring Harbor Symposia on Quantitative Biology*, *60*, 729–744. https://doi.org/10.1101/SQB.1995.060.01.079

Pruyne, D., Gao, L., Bi, E., & Bretscher, A. (2004). Stable and Dynamic Axes of Polarity Use Distinct Formin Isoforms in Budding Yeast. *Molecular Biology of the Cell*, *15*(11), 4971–4989. https://doi.org/10.1091/mbc.E04-04-0296

Puttalingaiah, S., Greeshma, M. V., Kuruburu, M. G., Bovilla, V. R., & Madhunapantula, S. V. (2022). Naturally Occurring Histone Deacetylase (HDAC) Inhibitors in the Treatment of Cancers. In *Medicinal Plants for Cosmetics, Health and Diseases*. CRC Press.

Qin, S., & Min, J. (2014). Structure and function of the nucleosome-binding PWWP domain. *Trends in Biochemical Sciences*, *39*(11), 536–547. https://doi.org/10.1016/j.tibs.2014.09.001

Quan, W., Chan, Z., Wei, P., Mao, Y., Bartels, D., & Liu, X. (2023). PHD finger proteins function in plant development and abiotic stress responses: An overview. *Frontiers in Plant Science*, *14*. https://doi.org/10.3389/fpls.2023.1297607

Ragusa, D., & Vagnarelli, P. (2023). Contribution of histone variants to aneuploidy: A cancer perspective. *Frontiers in Genetics*, *14*. https://doi.org/10.3389/fgene.2023.1290903

Raisner, R. M., Hartley, P. D., Meneghini, M. D., Bao, M. Z., Liu, C. L., Schreiber, S. L., Rando, O. J., & Madhani, H. D. (2005). Histone variant H2A.Z marks the 5' ends of both active and inactive genes in euchromatin. *Cell*, *123*(2), 233–248. https://doi.org/10.1016/j.cell.2005.10.002

Rajender, S., Avery, K., & Agarwal, A. (2011). Epigenetics, spermatogenesis and male infertility. *Mutation Research*, *727*(3), 62–71. https://doi.org/10.1016/j.mrrev.2011.04.002

Raman, P., Rominger, M. C., Young, J. M., Molaro, A., Tsukiyama, T., & Malik, H. S. (2022). Novel Classes and Evolutionary Turnover of Histone H2B Variants in the Mammalian Germline. *Molecular Biology and Evolution*, *39*(2), msac019. https://doi.org/10.1093/molbev/msac019

Ranjan, A., Elalaoui, E., Tang, X., Cha, J., Louder, R. K., Nguyen, K., Ye, J., Bennani, M., Gardner, A. M., Liu, D., Pugh, B. F., & Wu, C. (2025). Histone acetylation readers Bdf1 and Yaf9 direct SWR1 remodeler to +1 nucleosome. *Science Advances*, *11*(32), eadt2002. https://doi.org/10.1126/sciadv.adt2002

Ren, R., Horton, J. R., Hong, S., & Cheng, X. (2022). Recent Advances on DNA Base Flipping: A General Mechanism for Writing, Reading, and Erasing DNA Modifications. In A. Jeltsch & R. Z. Jurkowska (Eds), *DNA Methyltransferases—Role and Function* (pp. 295–315). Springer International Publishing. https://doi.org/10.1007/978-3-031-11454-0_12

Ren, R., Liu, H., Wang, W., Wang, M., Yang, N., Dong, Y., Gong, W., Lehmann, R., & Xu, R.-M. (2014). Structure and domain organization of Drosophila Tudor. *Cell Research*, *24*(9), 1146–1149. https://doi.org/10.1038/cr.2014.63

Ren, W., Wang, C., Wang, Q., Zhao, D., Zhao, K., Sun, D., Liu, X., Han, C., Hou, J., Li, X., Zhang, Q., Cao, X., & Li, N. (2017). Bromodomain protein Brd3 promotes Ifnb1 transcription via enhancing

IRF3/p300 complex formation and recruitment to Ifnb1 promoter in macrophages. *Scientific Reports*, *7*(1), 39986. https://doi.org/10.1038/srep39986

Reynoird, N., Schwartz, B. E., Delvecchio, M., Sadoul, K., Meyers, D., Mukherjee, C., Caron, C., Kimura, H., Rousseaux, S., Cole, P. A., Panne, D., French, C. A., & Khochbin, S. (2010). Oncogenesis by sequestration of CBP/p300 in transcriptionally inactive hyperacetylated chromatin domains. *The EMBO Journal*, *29*(17), 2943–2952. https://doi.org/10.1038/emboj.2010.176

Rizzardi, L. F., Dorn, E. S., Strahl, B. D., & Cook, J. G. (2012). DNA Replication Origin Function Is Promoted by H3K4 Di-methylation in Saccharomyces cerevisiae. *Genetics*, *192*(2), 371–384. https://doi.org/10.1534/genetics.112.142349

Rizzo, J. F., Shah, M. P., Krasniqi, D., Lu, Y. R., Sinclair, D. A., & Ksander, B. R. (2024). The Role of Epigenetics in Accelerated Aging: A Reconsideration of Later-Life Visual Loss After Early Optic Neuropathy. *Journal of Neuro-Ophthalmology: The Official Journal of the North American Neuro-Ophthalmology Society*, *44*(1), 16–21. https://doi.org/10.1097/WNO.0000000000002041

Robert, F., Pokholok, D. K., Hannett, N. M., Rinaldi, N. J., Chandy, M., Rolfe, A., Workman, J. L., Gifford, D. K., & Young, R. A. (2004). Global Position and Recruitment of HATs and HDACs in the Yeast Genome. *Molecular Cell*, *16*(2), 199–209. https://doi.org/10.1016/j.molcel.2004.09.021

Robert, X., & Gouet, P. (2014). Deciphering key features in protein structures with the new ENDscript server. *Nucleic Acids Research*, *42*(W1), W320–W324. https://doi.org/10.1093/nar/gku316

Robertson, K. D. (2005). DNA methylation and human disease. *Nature Reviews. Genetics*, *6*(8), 597–610. https://doi.org/10.1038/nrg1655

Rona, G. B., Eleutherio, E. C. A., & Pinheiro, A. S. (2016). PWWP domains and their modes of sensing DNA and histone methylated lysines. *Biophysical Reviews*, *8*(1), 63–74. https://doi.org/10.1007/s12551-015-0190-6

Roque, A., Iloro, I., Ponte, I., Arrondo, J. L. R., & Suau, P. (2005). DNA-induced Secondary Structure of the Carboxyl-terminal Domain of Histone H1. *Journal of Biological Chemistry*, *280*(37), 32141–32147. https://doi.org/10.1074/jbc.m505636200

Rossetto, D., Avvakumov, N., & Côté, J. (2012). Histone phosphorylation: A chromatin modification involved in diverse nuclear events. *Epigenetics*, *7*(10), 1098–1108. https://doi.org/10.4161/epi.21975

Roth, S. Y., Denu, J. M., & Allis, C. D. (2001). Histone Acetyltransferases. *Annual Review of Biochemistry*, *70*(Volume 70, 2001), 81–120. https://doi.org/10.1146/annurev.biochem.70.1.81

Rountree, M. R., & Selker, E. U. (2010). DNA methylation and the formation of heterochromatin in Neurospora crassa. *Heredity*, *105*(1), 38–44. https://doi.org/10.1038/hdy.2010.44

Rousseaux, S., Reynoird, N., & Khochbin, S. (2022). NUT Is a Driver of p300-Mediated Histone Hyperacetylation: From Spermatogenesis to Cancer. *Cancers*, *14*(9), 2234. https://doi.org/10.3390/cancers14092234

Ruault, M., De Meyer, A., Loïodice, I., & Taddei, A. (2011). Clustering heterochromatin: Sir3 promotes telomere clustering independently of silencing in yeast. *Journal of Cell Biology*, *192*(3), 417–431. https://doi.org/10.1083/jcb.201008007

Ryan, O. W., Skerker, J. M., Maurer, M. J., Li, X., Tsai, J. C., Poddar, S., Lee, M. E., DeLoache, W., Dueber, J. E., Arkin, A. P., & Cate, J. H. (2014). Selection of chromosomal DNA libraries using a multiplex CRISPR system. *eLife*, *3*, e03703. https://doi.org/10.7554/eLife.03703

Ryu, H.-Y., Zhao, D., Li, J., Su, D., & Hochstrasser, M. (2020). Histone sumoylation promotes Set3 histone-deacetylase complex-mediated transcriptional regulation. *Nucleic Acids Research*, *48*(21), 12151–12168. https://doi.org/10.1093/nar/gkaa1093

Sabari, B. R., Dall'Agnese, A., Boija, A., Klein, I. A., Coffey, E. L., Shrinivas, K., Abraham, B. J., Hannett, N. M., Zamudio, A. V., Manteiga, J. C., Li, C. H., Guo, Y. E., Day, D. S., Schuijers, J., Vasile, E., Malik, S., Hnisz, D., Lee, T. I., Cisse, I. I., … Young, R. A. (2018). Coactivator condensation at

super-enhancers links phase separation and gene control. *Science (New York, N.Y.)*, *361*(6400), eaar3958. https://doi.org/10.1126/science.aar3958

Sabari, B. R., Zhang, D., Allis, C. D., & Zhao, Y. (2017). Metabolic regulation of gene expression through histone acylations. *Nature Reviews. Molecular Cell Biology*, *18*(2), 90–101. https://doi.org/10.1038/nrm.2016.140

Sáenz, D. A., Chianelli, M. S., Stella, C. A., Mattoon, J. R., & Ramos, E. H. (1997). RAS2/PKA pathway activity is involved in the nitrogen regulation of l-leucine uptake in *Saccharomyces cerevisiae*. *The International Journal of Biochemistry & Cell Biology*, *29*(3), 505–512. https://doi.org/10.1016/S1357-2725(96)00102-1

Saintilnord, W. N., Hegazy, Y. A., Chesnutt, K., Eckstein, M., Cassidy, R. N., Dhahri, H., Bennett, R. L., Melters, D. P., Lopes, E., Fu, Z., Lau, K., Chandler, D. P., Poirier, M. G., Dalal, Y., Licht, J. D., & Fondufe-Mittendorf, Y. (2024). Aberrant expression of histone H2B variants reshape chromatin and alter oncogenic gene expression programs. *bioRxiv*, 2024.11.18.624207. https://doi.org/10.1101/2024.11.18.624207

Salinas-Pena, M., Rebollo, E., & Jordan, A. (2024). Imaging analysis of six human histone H1 variants reveals universal enrichment of H1.2, H1.3, and H1.5 at the nuclear periphery and nucleolar H1X presence. *eLife*, *12*, RP91306. https://doi.org/10.7554/eLife.91306

Sanchez, K. M., Addagarla, M., Judd, H., Wang, X., & Maupin-Furlow, J. (2025). Dynamic acetylation of a conserved lysine impacts glycerol kinase activity and abundance in the haloarchaeon Haloferax volcanii. *bioRxiv: The Preprint Server for Biology*, 2025.07.03.662939. https://doi.org/10.1101/2025.07.03.662939

Santoro, S. W., & Dulac, C. (2012). The activity-dependent histone variant H2BE modulates the life span of olfactory neurons. *eLife*, *1*, e00070. https://doi.org/10.7554/eLife.00070

Sawa, C., Nedea, E., Krogan, N., Wada, T., Handa, H., Greenblatt, J., & Buratowski, S. (2004). Bromodomain Factor 1 (Bdf1) Is Phosphorylated by Protein Kinase CK2. *Molecular and Cellular Biology*, *24*(11), 4734–4742. https://doi.org/10.1128/MCB.24.11.4734-4742.2004

Schep, A. N., Buenrostro, J. D., Denny, S. K., Schwartz, K., Sherlock, G., & Greenleaf, W. J. (2015). Structured nucleosome fingerprints enable high-resolution mapping of chromatin architecture within regulatory regions. *Genome Research*, *25*(11), 1757–1770. https://doi.org/10.1101/gr.192294.115

Schwab, M., Lutum, A. S., & Seufert, W. (1997). Yeast Hct1 Is a Regulator of Clb2 Cyclin Proteolysis. *Cell*, *90*(4), 683–693. https://doi.org/10.1016/S0092-8674(00)80529-2

Selker, E. U., Freitag, M., Kothe, G. O., Margolin, B. S., Rountree, M. R., Allis, C. D., & Tamaru, H. (2002). Induction and maintenance of nonsymmetrical DNA methylation in Neurospora. *Proceedings of the National Academy of Sciences*, *99*(suppl_4), 16485–16490. https://doi.org/10.1073/pnas.182427299

Setlow, P. (2014). Spore Resistance Properties. *Microbiology Spectrum*, *2*(5). https://doi.org/10.1128/microbiolspec.TBS-0003-2012

Shahid, Z., Simpson, B., Miao, K. H., & Singh, G. (2026). Genetics, Histone Code. In *StatPearls*. StatPearls Publishing. http://www.ncbi.nlm.nih.gov/books/NBK538477/

Shao, Z., Lu, J., Khudaverdyan, N., & Song, J. (2024). Multi-layered heterochromatin interaction as a switch for DIM2-mediated DNA methylation. *Nature Communications*, *15*(1), 6815. https://doi.org/10.1038/s41467-024-51246-4

Shaw, W. M., Yamauchi, H., Mead, J., Gowers, G.-O. F., Bell, D. J., Öling, D., Larsson, N., Wigglesworth, M., Ladds, G., & Ellis, T. (2019). Engineering a Model Cell for Rational Tuning of GPCR Signaling. *Cell*, *177*(3), 782-796.e27. https://doi.org/10.1016/j.cell.2019.02.023

Shiio, Y., & Eisenman, R. N. (2003). Histone sumoylation is associated with transcriptional repression. *Proceedings of the National Academy of Sciences*, *100*(23), 13225–13230. https://doi.org/10.1073/pnas.1735528100

Shimizu, M., Li, W., Covitz, P. A., Hara, M., Shindo, H., & Mitchell, A. P. (1998). Genomic footprinting of the yeast zinc finger protein Rme1p and its roles in repression of the meiotic activator IME1. *Nucleic Acids Research*, *26*(10), 2329–2336. https://doi.org/10.1093/nar/26.10.2329

Shimizu, M., Li, W., Shindo, H., & Mitchell, A. P. (1997). Transcriptional repression at a distance through exclusion of activator binding in vivo. *Proceedings of the National Academy of Sciences of the United States of America*, *94*(3), 790–795. https://doi.org/10.1073/pnas.94.3.790

Shin, K.-J., Lee, D., & Kim, A. (2024). Acetylation of Histones in Chromatin and Its Functions in Gene Transcription. *Biomedical Science Letters*, *30*(4), 199–208. https://doi.org/10.15616/BSL.2024.30.4.199

Shinagawa, T., Takagi, T., Tsukamoto, D., Tomaru, C., Huynh, L. M., Sivaraman, P., Kumarevel, T., Inoue, K., Nakato, R., Katou, Y., Sado, T., Takahashi, S., Ogura, A., Shirahige, K., & Ishii, S. (2014). Histone Variants Enriched in Oocytes Enhance Reprogramming to Induced Pluripotent Stem Cells. *Cell Stem Cell*, *14*(2), 217–227. https://doi.org/10.1016/j.stem.2013.12.015

Simithy, J., Sidoli, S., Yuan, Z.-F., Coradin, M., Bhanu, N. V., Marchione, D. M., Klein, B. J., Bazilevsky, G. A., McCullough, C. E., Magin, R. S., Kutateladze, T. G., Snyder, N. W., Marmorstein, R., & Garcia, B. A. (2017). Characterization of histone acylations links chromatin modifications with metabolism. *Nature Communications*, *8*(1), 1141. https://doi.org/10.1038/s41467-017-01384-9

Simpson, R. T. (1978). Structure of the chromatosome, a chromatin particle containing 160 base pairs of DNA and all the histones. *Biochemistry*, *17*(25), 5524–5531. https://doi.org/10.1021/bi00618a030

Simpson-Lavy, K., & Kupiec, M. (2019). Carbon Catabolite Repression in Yeast is Not Limited to Glucose. *Scientific Reports*, *9*(1), 6491. https://doi.org/10.1038/s41598-019-43032-w

Singla, N., Thapa, R., Kulshrestha, R., Bhat, A. A., Gupta, S., Purohit, M., Singh, S. K., & Gupta, G. (2023). Introduction to Epigenetics. In G. Gupta, B. G. Oliver, K. Dua, M. K. Ali, & P. Dave (Eds), *Targeting Epigenetics in Inflammatory Lung Diseases* (pp. 17–41). Springer Nature. https://doi.org/10.1007/978-981-99-4780-5_2

Skalnik, D. G. (2004). Methyl-CpG-Binding Proteins. In W. J. Lennarz & M. D. Lane (Eds), *Encyclopedia of Biological Chemistry* (pp. 672–675). Elsevier. https://doi.org/10.1016/B0-12-443710-9/00170-8

Skene, P. J., & Henikoff, S. (2013). Histone variants in pluripotency and disease. *Development*, *140*(12), 2513–2524. https://doi.org/10.1242/dev.091439

Slaughter, M. J., Shanle, E. K., Khan, A., Chua, K. F., Hong, T., Boxer, L. D., Allis, C. D., Josefowicz, S. Z., Garcia, B. A., Rothbart, S. B., Strahl, B. D., & Davis, I. J. (2021). HDAC inhibition results in widespread alteration of the histone acetylation landscape and BRD4 targeting to gene bodies. *Cell Reports*, *34*(3), 108638. https://doi.org/10.1016/j.celrep.2020.108638

Smith, S. G., & Zhou, M.-M. (2016). The Bromodomain: A New Target in Emerging Epigenetic Medicine. *ACS Chemical Biology*, *11*(3), 598–608. https://doi.org/10.1021/acschembio.5b00831

Soloaga, A., Thomson, S., Wiggin, G. R., Rampersaud, N., Dyson, M. H., Hazzalin, C. A., Mahadevan, L. C., & Arthur, J. S. C. (2003). MSK2 and MSK1 mediate the mitogen- and stress-induced phosphorylation of histone H3 and HMG-14. *The EMBO Journal*, *22*(11), 2788–2797. https://doi.org/10.1093/emboj/cdg273

Song, Q., Johnson, C., Wilson, T. E., & Kumar, A. (2014). Pooled Segregant Sequencing Reveals Genetic Determinants of Yeast Pseudohyphal Growth. *PLoS Genetics*, *10*(8), e1004570. https://doi.org/10.1371/journal.pgen.1004570

Spellman, P. T., Sherlock, G., Zhang, M. Q., Iyer, V. R., Anders, K., Eisen, M. B., Brown, P. O., Botstein, D., & Futcher, B. (1998). Comprehensive Identification of Cell Cycle–regulated Genes of the Yeast Saccharomyces cerevisiae by Microarray Hybridization. *Molecular Biology of the Cell*, *9*(12), 3273–3297. https://doi.org/10.1091/mbc.9.12.3273

Spencer, J. F. T., & Spencer, D. M. (1997). The Yeasts: Sex and Nonsex. Life Cycles, Sporulation and Genetics. In J. F. T. Spencer & D. M. Spencer (Eds), *Yeasts in Natural and Artificial Habitats* (pp. 133–152). Springer. https://doi.org/10.1007/978-3-662-03370-8_9

Stein, G. S., Stein, J. L., Van Wijnen, A. J., & Lian, J. B. (1996). Transcriptional control of cell cycle progression: The histone gene is a paradigm for the G1/S phase and proliferation/differentiation transitions. *Cell Biology International*, *20*(1), 41–49. https://doi.org/10.1006/cbir.1996.0007

Stepanić, V., Kujundžić, R. N., Trošelj, K. G., Stepanić, V., Kujundžić, R. N., & Trošelj, K. G. (2014). Epigenome, Cancer Prevention and Flavonoids and Curcumin. In *Epigenetics and Epigenomics*. IntechOpen. https://doi.org/10.5772/58247

Stewart-Ornstein, J., Chen, S., Bhatnagar, R., Weissman, J. S., & El-Samad, H. (2017). Model-guided optogenetic study of PKA signaling in budding yeast. *Molecular Biology of the Cell*, *28*(1), 221–227. https://doi.org/10.1091/mbc.e16-06-0354

Stragier, P., & Losick, R. (1996). MOLECULAR GENETICS OF SPORULATION IN BACILLUS SUBTILIS. *Annual Review of Genetics*, *30*(Volume 30, 1996), 297–341. https://doi.org/10.1146/annurev.genet.30.1.297

Strahl, B. D., Ohba, R., Cook, R. G., & Allis, C. D. (1999). Methylation of histone H3 at lysine 4 is highly conserved and correlates with transcriptionally active nuclei in Tetrahymena. *Proceedings of the National Academy of Sciences of the United States of America*, *96*(26), 14967–14972. https://doi.org/10.1073/pnas.96.26.14967

Strich, R., Surosky, R. T., Steber, C., Dubois, E., Messenguy, F., & Esposito, R. E. (n.d.). *UME6 !s a key regulator of nitrogen repression and meiotic development*.

Sun, Q.-Y., Gao, D., Li, C., Liu, S. Y., Lin, X. T., Tan, Y. P., Gao, F. M., Yi, L. T., Zhang, J. V., Ma, J. Y., Meng, T.-G., Yeung, W. S. B., Liu, K., Ou, X. H., & Su, R. (2023). *P300 Regulates Histone Crotonylation and Preimplantation Embryo Development*. Research Square. https://doi.org/10.21203/rs.3.rs-3281941/v1

Sundrani, D., Khot, V., & Joshi, S. (2016). Chapter 18—DNA Methylation for Prediction of Adverse Pregnancy Outcomes. In J. L. García-Giménez (Ed.), *Epigenetic Biomarkers and Diagnostics* (pp. 351–376). Academic Press. https://doi.org/10.1016/B978-0-12-801899-6.00018-8

Sweet, M. T., & Allis, C. D. (1993). Phosphorylation of linker histones by cAMP-dependent protein kinase in mitotic micronuclei of Tetrahymena. *Chromosoma*, *102*(9), 637–647. https://doi.org/10.1007/BF00352312

Tachiwana, H., Osakabe, A., Shiga, T., Miya, Y., Kimura, H., Kagawa, W., & Kurumizaka, H. (2011). Structures of human nucleosomes containing major histone H3 variants. *Acta Crystallographica Section D Biological Crystallography*, *67*(6), 578–583. https://doi.org/10.1107/S0907444911014818

Tagami, H., Ray-Gallet, D., Almouzni, G., & Nakatani, Y. (2004). Histone H3.1 and H3.3 Complexes Mediate Nucleosome Assembly Pathways Dependent or Independent of DNA Synthesis. *Cell*, *116*(1), 51–61. https://doi.org/10.1016/S0092-8674(03)01064-X

Taguchi, H., Xie, Y., Horikoshi, N., Maehara, K., Harada, A., Nogami, J., Sato, K., Arimura, Y., Osakabe, A., Kujirai, T., Iwasaki, T., Semba, Y., Tachibana, T., Kimura, H., Ohkawa, Y., & Kurumizaka, H. (2017). Crystal Structure and Characterization of Novel Human Histone H3 Variants, H3.6, H3.7, and H3.8. *Biochemistry*, *56*(16), 2184–2196. https://doi.org/10.1021/acs.biochem.6b01098

Talbert, P. B., & Henikoff, S. (2021). Histone variants at a glance. *Journal of Cell Science*, *134*(6), jcs244749. https://doi.org/10.1242/jcs.244749

Tamanoi, F. (2011). Ras Signaling in Yeast. *Genes & Cancer*, *2*(3), 210–215. https://doi.org/10.1177/1947601911407322

Tamborrini, D., & Piatti, S. (n.d.). Septin clearance from the division site triggers cytokinesis in budding yeast. *Microbial Cell*. Retrieved 20 January 2026, from https://pubmed.ncbi.nlm.nih.gov/31172014/

Tang, L., Nogales, E., & Ciferri, C. (2010). Structure and Function of SWI/SNF Chromatin Remodeling Complexes and Mechanistic Implications for Transcription. *Progress in Biophysics and Molecular Biology*, *102*(2–3), 122–128. https://doi.org/10.1016/j.pbiomolbio.2010.05.001

Tang, M., Shen, H., Jin, Y., Lin, T., Cai, Q., Pinard, M. A., Biswas, S., Tran, Q., Li, G., Shenoy, A. K., Tongdee, E., Lin, S., Gu, Y., Law, B. K., Zhou, L., Mckenna, R., Wu, L., & Lu, J. (2013). The Malignant Brain Tumor (MBT) Domain Protein SFMBT1 Is an Integral Histone Reader Subunit of the LSD1 Demethylase Complex for Chromatin Association and Epithelial-to-mesenchymal Transition. *The Journal of Biological Chemistry*, *288*(38), 27680–27691. https://doi.org/10.1074/jbc.M113.482349

Tang, Y., Gao, X.-D., Wang, Y., Yuan, B.-F., & Feng, Y.-Q. (2012). Widespread Existence of Cytosine Methylation in Yeast DNA Measured by Gas Chromatography/Mass Spectrometry. *Analytical Chemistry*, *84*(16), 7249–7255. https://doi.org/10.1021/ac301727c

Taniguchi, Y. (2016). *The Bromodomain and Extra-Terminal Domain (BET) Family: Functional Anatomy of BET Paralogous Proteins* (No. 2016100100). Preprints. https://doi.org/10.20944/preprints201610.0100.v1

Tessadori, F., Duran, K., Knapp, K., Fellner, M., Smithson, S., Meireles, A. B., Elting, M. W., Waisfisz, Q., O'Donnell-Luria, A., Nowak, C., Douglas, J., Ronan, A., Brunet, T., Kotzaeridou, U., Svihovec, S., Saenz, M. S., Thiffault, I., Viso, F. D., Devine, P., … Haaften, G. van. (2022). Recurrent de novo missense variants across multiple histone H4 genes underlie a neurodevelopmental syndrome. *The American Journal of Human Genetics*, *109*(4), 750–758. https://doi.org/10.1016/j.ajhg.2022.02.003

Tewary, S. K., Zheng, Y. G., & Ho, M.-C. (2019). Protein arginine methyltransferases: Insights into the enzyme structure and mechanism at the atomic level. *Cellular and Molecular Life Sciences*, *76*(15), 2917–2932. https://doi.org/10.1007/s00018-019-03145-x

Thevathasan, J. V., Kahnwald, M., Cieśliński, K., Hoess, P., Peneti, S. K., Reitberger, M., Heid, D., Kasuba, K. C., Hoerner, S. J., Li, Y., Wu, Y.-L., Mund, M., Matti, U., Pereira, P. M., Henriques, R., Nijmeijer, B., Kueblbeck, M., Sabinina, V. J., Ellenberg, J., & Ries, J. (2019). Nuclear pores as versatile reference standards for quantitative superresolution microscopy. *Nature Methods*, *16*(10), 1045–1053. https://doi.org/10.1038/s41592-019-0574-9

Torchy, M. P., Hamiche, A., & Klaholz, B. P. (2015). Structure and function insights into the NuRD chromatin remodeling complex. *Cellular and Molecular Life Sciences: CMLS*, *72*(13), 2491–2507. https://doi.org/10.1007/s00018-015-1880-8

Tóth, D. M., Szeri, F., Ashaber, M., Muazu, M., Székvölgyi, L., & Arányi, T. (2025). Tissue-specific roles of de novo DNA methyltransferases. *Epigenetics & Chromatin*, *18*(1), 5. https://doi.org/10.1186/s13072-024-00566-2

Tsui, K., Simon, L., & Norris, D. (1997). Progression into the First Meiotic Division Is Sensitive to Histone H2a-H2b Dimer Concentration in Saccharomyces Cerevisiae. *Genetics*, *145*(3), 647–659. https://doi.org/10.1093/genetics/145.3.647

Ullmann, R., Chien, C. D., Avantaggiati, M. L., & Muller, S. (2012). An Acetylation Switch Regulates SUMO-Dependent Protein Interaction Networks. *Molecular Cell*, *46*(6), 759–770. https://doi.org/10.1016/j.molcel.2012.04.006

Umehara, T., Nakamura, Y., Jang, M. K., Nakano, K., Tanaka, A., Ozato, K., Padmanabhan, B., & Yokoyama, S. (2010). Structural Basis for Acetylated Histone H4 Recognition by the Human BRD2 Bromodomain. *The Journal of Biological Chemistry*, *285*(10), 7610–7618. https://doi.org/10.1074/jbc.M109.062422

Ushinsky, S. C., Bussey, H., Ahmed, A. A., Wang, Y., Friesen, J., Williams, B. A., & Storms, R. K. (1997). Histone H1 inSaccharomyces cerevisiae. *Yeast*, *13*(2), 151–161. https://doi.org/10.1002/(sici)1097-0061(199702)13:2%3C151::aid-yea94%3E3.0.co;2-5

Utley, R. T., Lacoste, N., Jobin-Robitaille, O., Allard, S., & Côté, J. (2005). Regulation of NuA4 Histone Acetyltransferase Activity in Transcription and DNA Repair by Phosphorylation of Histone H4. *Molecular and Cellular Biology*, *25*(18), 8179–8190. https://doi.org/10.1128/MCB.25.18.8179-8190.2005

vanLieshout, T. L., Bonafiglia, J. T., Gurd, B. J., & Ljubicic, V. (2019). Protein arginine methyltransferase biology in humans during acute and chronic skeletal muscle plasticity. *Journal of Applied Physiology*, *127*(3), 867–880. https://doi.org/10.1152/japplphysiol.00142.2019

Varga, J., Korbai, S., Neller, A., Zsindely, N., & Bodai, L. (2019). Hat1 acetylates histone H4 and modulates the transcriptional program in Drosophila embryogenesis. *Scientific Reports*, *9*(1), 17973. https://doi.org/10.1038/s41598-019-54497-0

Veis, J., Klug, H., Koranda, M., & Ammerer, G. (2007). Activation of the G2/M-Specific Gene CLB2 Requires Multiple Cell Cycle Signals. *Molecular and Cellular Biology*, *27*(23), 8364–8373. https://doi.org/10.1128/MCB.01253-07

Vinayak, V., Lakadamyali, M., & Shenoy, V. B. (2026). Architecture and regulation of nanoscale chromatin domains. *Nature Communications*, *17*(1), 4682. https://doi.org/10.1038/s41467-026-71213-5

Vollmuth, F., Blankenfeldt, W., & Geyer, M. (2009). Structures of the Dual Bromodomains of the P-TEFb-activating Protein Brd4 at Atomic Resolution. *The Journal of Biological Chemistry*, *284*(52), 36547–36556. https://doi.org/10.1074/jbc.M109.033712

Voss, A. J., & Korb, E. (2025). The ABCs of the H2Bs: The histone H2B sequences, variants, and modifications. *Trends in Genetics*, *41*(6), 506–521. https://doi.org/10.1016/j.tig.2025.01.003

Walkey, C. J., Luo, Z., Madilao, L. L., & Vuuren, H. J. J. van. (2012). The Fermentation Stress Response Protein Aaf1p/Yml081Wp Regulates Acetate Production in Saccharomyces cerevisiae. *PLOS ONE*, *7*(12), e51551. https://doi.org/10.1371/journal.pone.0051551

Walters, A. D., Amoateng, K., Wang, R., Chen, J.-H., McDermott, G., Larabell, C. A., Gadal, O., & Cohen-Fix, O. (2019). Nuclear envelope expansion in budding yeast is independent of cell growth and does not determine nuclear volume. *Molecular Biology of the Cell*, *30*(1), 131–145. https://doi.org/10.1091/mbc.E18-04-0204

Wang, A. Y., Schulze, J. M., Skordalakes, E., Gin, J. W., Berger, J. M., Rine, J., & Kobor, M. S. (2009). Asf1-like structure of the conserved Yaf9 YEATS domain and role in H2A.Z deposition and acetylation. *Proceedings of the National Academy of Sciences*, *106*(51), 21573–21578. https://doi.org/10.1073/pnas.0906539106

Wang, H., Lin, A., Gu, W., Huan, L., Gao, S., & Wang, G. (2016). The sporulation of the green alga Ulva prolifera is controlled by changes in photosynthetic electron transport chain. *Scientific Reports*, *6*(1), 24923. https://doi.org/10.1038/srep24923

Wang, J., Tadeo, X., Hou, H., Tu, P. G., Thompson, J., Yates, J. R., & Jia, S. (2013). Epe1 recruits BET family bromodomain protein Bdf2 to establish heterochromatin boundaries. *Genes & Development*, *27*(17), 1886–1902. https://doi.org/10.1101/gad.221010.113

Wang, L., Zhao, L., Lan, X., Zhu, M., Tan, Y., Luo, H., & Wu, D. (2025). Lysine Acetyltransferase 8: A Target for Natural Compounds in Cancer Therapy. *International Journal of Molecular Sciences*, *26*(11), 5257. https://doi.org/10.3390/ijms26115257

Wang, X., Kutschat, A. P., Yamada, M., Prokakis, E., Böttcher, P., Tanaka, K., Doki, Y., Hamdan, F. H., & Johnsen, S. A. (2021). Bromodomain protein BRDT directs ΔNp63 function and super-enhancer activity in a subset of esophageal squamous cell carcinomas. *Cell Death & Differentiation*, *28*(7), 2207–2220. https://doi.org/10.1038/s41418-021-00751-w

Wang, Y., & Dohlman, H. G. (2004). Pheromone Signaling Mechanisms in Yeast: A Prototypical Sex Machine. *Science*, *306*(5701), 1508–1509.

Wang, Y., Fischle, W., Cheung, W., Jacobs, S., Khorasanizadeh, S., & Allis, C. D. (2004). Beyond the Double Helix: Writing and Reading the Histone Code. In G. Bock & J. Goode (Eds), *Novartis Foundation Symposia* (1st edn, Vol. 259, pp. 3–21). Wiley. https://doi.org/10.1002/0470862637.ch2

Wang, Y., Zhai, B., Tan, T., Yang, X., Zhang, J., Song, M., Tan, Y., Yang, X., Chu, T., Zhang, S., Wang, S., & Zhang, L. (2021). ESA1 regulates meiotic chromosome axis and crossover frequency via acetylating histone H4. *Nucleic Acids Research*, *49*(16), 9353–9373. https://doi.org/10.1093/nar/gkab722

Wang, Z., Liu, Z., Lv, M., Luan, Z., Li, T., & Hu, J. (2025). Novel histone modifications and liver cancer: Emerging frontiers in epigenetic regulation. *Clinical Epigenetics*, *17*(1), 30. https://doi.org/10.1186/s13148-025-01838-8

Wang, Z.-Q., Zhang, Z.-C., Wu, Y.-Y., Pi, Y.-N., Lou, S.-H., Liu, T.-B., Lou, G., & Yang, C. (2023). Bromodomain and extraterminal (BET) proteins: Biological functions, diseases and targeted therapy. *Signal Transduction and Targeted Therapy*, *8*(1), 420. https://doi.org/10.1038/s41392-023-01647-6

Watanabe, S., Tan, D., Lakshminarasimhan, M., Washburn, M. P., Erica Hong, E.-J., Walz, T., & Peterson, C. L. (2015). Structural analyses of the chromatin remodelling enzymes INO80-C and SWR-C. *Nature Communications*, *6*(1), 7108. https://doi.org/10.1038/ncomms8108

Watson, N. A., & Higgins, J. M. G. (2016). Chapter 4—Histone Kinases and Phosphatases. In O. Binda & M. E. Fernandez-Zapico (Eds), *Chromatin Signaling and Diseases* (pp. 75–94). Academic Press. https://doi.org/10.1016/B978-0-12-802389-1.00004-6

Weake, V. M., & Workman, J. L. (2010). Chapter 292—Histone Ubiquitination. In R. A. Bradshaw & E. A. Dennis (Eds), *Handbook of Cell Signaling (Second Edition)* (pp. 2449–2460). Academic Press. https://doi.org/10.1016/B978-0-12-374145-5.00292-8

Weber, K. R., Novillo, B., & Maupin-Furlow, J. A. (2025). Revisiting synthetic lethality of Gcn5-related N-acetyltransferase (GNAT) family mutations in Haloferax volcanii. *Microbiology Spectrum*, *13*(8), e0122925. https://doi.org/10.1128/spectrum.01229-25

Wei, K., Arlotto, M., Overhulse, J. M., Dinh, T.-A., Zhou, Y., Dupper, N. J., Yang, J., Kashemirov, B. A., Dawi, H., Garnaud, C., Bourgine, G., Mietton, F., Champleboux, M., Larabi, A., Hayat, Y., Indorato, R.-L., Noirclerc-Savoye, M., Skoufias, D., Cornet, M., … Govin, J. (2025). Humanized Candida and NanoBiT Assays Expedite Discovery of Bdf1 Bromodomain Inhibitors With Antifungal Potential. *Advanced Science*, *12*(10), 2404260. https://doi.org/10.1002/advs.202404260

Weiner, A., Hsieh, T.-H. S., Appleboim, A., Chen, H. V., Rahat, A., Amit, I., Rando, O. J., & Friedman, N. (2015). High-Resolution Chromatin Dynamics during a Yeast Stress Response. *Molecular Cell*, *58*(2), 371–386. https://doi.org/10.1016/j.molcel.2015.02.002

Werner, M. T., Wang, H., Hamagami, N., Hsu, S. C., Yano, J. A., Stonestrom, A. J., Behera, V., Zong, Y., Mackay, J. P., & Blobel, G. A. (2020). Comparative structure-function analysis of bromodomain and extraterminal motif (BET) proteins in a gene-complementation system. *The Journal of Biological Chemistry*, *295*(7), 1898–1914. https://doi.org/10.1074/jbc.RA119.010679

West, M. H. P., & Bonner, W. M. (1980). Histone 2A, a heteromorphous family of eight protein species. *Biochemistry*, *19*(14), 3238–3245. https://doi.org/10.1021/bi00555a022

Wu, C. -t., & Morris, J. R. (2001). Genes, Genetics, and Epigenetics: A Correspondence. *Science*, *293*(5532), 1103–1105.

Wu, H., Zeng, H., Lam, R., Tempel, W., Amaya, M. F., Xu, C., Dombrovski, L., Qiu, W., Wang, Y., & Min, J. (2011). Structural and Histone Binding Ability Characterizations of Human PWWP Domains. *PLOS ONE*, *6*(6), e18919. https://doi.org/10.1371/journal.pone.0018919

Xiao, B., Jing, C., Wilson, J. R., Walker, P. A., Vasisht, N., Kelly, G., Howell, S., Taylor, I. A., Blackburn, G. M., & Gamblin, S. J. (2003). Structure and catalytic mechanism of the human histone methyltransferase SET7/9. *Nature*, *421*(6923), 652–656. https://doi.org/10.1038/nature01378

Xiao, W., Chow, B. L., & Rathgeber, L. (1996). The repair of DNA methylation damage in Saccharomyces cerevisiae. *Current Genetics*, *30*(6), 461–468. https://doi.org/10.1007/s002940050157

Xie, J., Pierce, M., Gailus-Durner, V., Wagner, M., Winter, E., & Vershon, A. K. (1999). Sum1 and Hst1 repress middle sporulation-specific gene expression during mitosis in Saccharomyces cerevisiae. *The EMBO Journal*, *18*(22), 6448–6454. https://doi.org/10.1093/emboj/18.22.6448

Xie, W., Ling, T., Zhou, Y., Feng, W., Zhu, Q., Stunnenberg, H. G., Grummt, I., & Tao, W. (2012). The chromatin remodeling complex NuRD establishes the poised state of rRNA genes characterized by bivalent histone modifications and altered nucleosome positions.

Proceedings of the National Academy of Sciences, *109*(21), 8161–8166. https://doi.org/10.1073/pnas.1201262109

Xie, Z., Zhang, D., Chung, D., Tang, Z., Huang, H., Dai, L., Qi, S., Li, J., Colak, G., Chen, Y., Xia, C., Peng, C., Ruan, H., Kirkey, M., Wang, D., Jensen, L. M., Kwon, O. K., Lee, S., Pletcher, S. D., … Zhao, Y. (2016). Metabolic Regulation of Gene Expression by Histone Lysine β-Hydroxybutyrylation. *Molecular Cell*, *62*(2), 194–206. https://doi.org/10.1016/j.molcel.2016.03.036

Xiong, C., Wen, Z., & Li, G. (2016). Histone Variant H3.3: A versatile H3 variant in health and in disease. *Science China. Life Sciences*, *59*(3), 245–256. https://doi.org/10.1007/s11427-016-5006-9

Xue, B., Zhao, J., Feng, P., Xing, J., Wu, H., & Li, Y. (2019). Epigenetic mechanism and target therapy of UHRF1 protein complex in malignancies. *OncoTargets and Therapy*, *12*, 549–559. https://doi.org/10.2147/OTT.S192234

Yamaguchi, K., Chen, X., Rodgers, B., Miura, F., Bashtrykov, P., Bonhomme, F., Salinas-Luypaert, C., Haxholli, D., Gutekunst, N., Aygenli, B. Ö., Ferry, L., Kirsh, O., Laisné, M., Scelfo, A., Ugur, E., Arimondo, P. B., Leonhardt, H., Kanemaki, M. T., Bartke, T., … Defossez, P.-A. (2024). Non-canonical functions of UHRF1 maintain DNA methylation homeostasis in cancer cells. *Nature Communications*, *15*, 2960. https://doi.org/10.1038/s41467-024-47314-4

Yan, L., Geng, Q., Cao, Z., Liu, B., Li, L., Lu, P., Lin, L., Wei, L., Tan, Y., He, X., Li, L., Zhao, N., & Lu, C. (2023). Insights into DNMT1 and programmed cell death in diseases. *Biomedicine & Pharmacotherapy*, *168*, 115753. https://doi.org/10.1016/j.biopha.2023.115753

Yan, L., Wu, H., Li, X., Gao, N., & Chen, Z. (2019). Structures of the ISWI–nucleosome complex reveal a conserved mechanism of chromatin remodeling. *Nature Structural & Molecular Biology*, *26*(4), 258–266. https://doi.org/10.1038/s41594-019-0199-9

Yang, A. Y., Kim, H., Li, W., & Kong, A.-N. T. (n.d.). Natural compound-derived epigenetic regulators targeting epigenetic readers, writers and erasers. *Current Topics in Medicinal Chemistry*, *16*(7), 697–713. https://doi.org/10.2174/1568026615666150826114359

Yang, Z., He, N., & Zhou, Q. (2008). Brd4 recruits P-TEFb to chromosomes at late mitosis to promote G1 gene expression and cell cycle progression. *Molecular and Cellular Biology*, *28*(3), 967–976. https://doi.org/10.1128/MCB.01020-07

Yao, W., Hu, X., & Wang, X. (2024). Crossing epigenetic frontiers: The intersection of novel histone modifications and diseases. *Signal Transduction and Targeted Therapy*, *9*(1), 232. https://doi.org/10.1038/s41392-024-01918-w

Yin, F., Hu, Y., Cao, X., Xiao, X., Zhang, M., Xiang, Y., Wang, L., Yao, Y., Sui, M., & Shi, W. (2024). JmjC domain-containing histone demethylase gene family in Chinese cabbage: Genome-wide identification and expressional profiling. *PLOS ONE*, *19*(11), e0312798. https://doi.org/10.1371/journal.pone.0312798

Yin, X., Zeng, D., Liao, Y., Tang, C., & Li, Y. (2024). The Function of H2A Histone Variants and Their Roles in Diseases. *Biomolecules*, *14*(8), 993. https://doi.org/10.3390/biom14080993

Yu, L., Myers, G., Ku, C.-J., Schneider, E., Wang, Y., Singh, S. A., Jearawiriyapaisarn, N., White, A., Moriguchi, T., Khoriaty, R., Yamamoto, M., Rosenfeld, M. G., Pedron, J., Bushweller, J. H., Lim, K.-C., & Engel, J. D. (2021). *The epigenetic eraser LSD1 lies at the apex of a reversible erythroid to myeloid cell fate decision* (p. 2021.01.13.426552). bioRxiv. https://doi.org/10.1101/2021.01.13.426552

Yuan, B., Das, S. K., Wang, W., Camacho, G., Kumar, A., Hayes, J. J., & Lee, T.-H. (2026). Conformations of Linker Histone H1 Bound to Nucleosome Arrays. *Journal of Molecular Biology*, *438*(6), 169655. https://doi.org/10.1016/j.jmb.2026.169655

Zakhari, S. (2013). Alcohol Metabolism and Epigenetics Changes. *Alcohol Research : Current Reviews*, *35*(1), 6–16. https://doi.org/10.35946/arcr.v35.1.02

Zentner, G. E., & Henikoff, S. (2013). Regulation of nucleosome dynamics by histone modifications. *Nature Structural & Molecular Biology*, *20*(3), 259–266. https://doi.org/10.1038/nsmb.2470

Zhang, B., Dong, Q., Su, H., Birchler, J. A., & Han, F. (2014). Histone Phosphorylation: Its Role during Cell Cycle and Centromere Identity in Plants. *Cytogenetic and Genome Research*, *143*(1–3), 144–149. https://doi.org/10.1159/000360435

Zhang, J., Tan, D., DeRose, E. F., Perera, L., Dominski, Z., Marzluff, W. F., Tong, L., & Hall, T. M. T. (2014). Molecular mechanisms for the regulation of histone mRNA stem-loop–binding protein by phosphorylation. *Proceedings of the National Academy of Sciences*, *111*(29), E2937–E2946. https://doi.org/10.1073/pnas.1406381111

Zhang, K., Needleman, L., Zhou, S., & Neiman, A. M. (2017). A Novel Assay Reveals a Maturation Process during Ascospore Wall Formation. *Journal of Fungi*, *3*(4), 54. https://doi.org/10.3390/jof3040054

Zhang, W., Cao, X., Wu, H., Zhong, X., Shi, Y., & Sun, Z. (2024). Function of Steroid Receptor Coactivators in T Cells and Cancers: Implications for Cancer Immunotherapy. *Critical Reviews in Immunology*, *44*(6), 111–126. https://doi.org/10.1615/CritRevImmunol.2024051613

Zhang, X., Zhou, L., & Cheng, X. (2000). Crystal structure of the conserved core of protein arginine methyltransferase PRMT3. *The EMBO Journal*, *19*(14), 3509–3519. https://doi.org/10.1093/emboj/19.14.3509

Zheng, S., Barczak, W., Liu, G., & Thangue, N. L. (n.d.). *Histone Deacetylases*. Retrieved 11 August 2025, from https://books.rsc.org/books/edited-volume/2227/chapter/8160492/Histone-Deacetylases

Zheng, Y.-C., Ma, J.-L., Liu, Y., & Liu, H. M. (n.d.). Writers and Erasers of Histone Lysine methylation with Clinically Applied Modulators: Promising Target for Cancer Therapy. *Current Pharmaceutical Design*, *22*(39), 5943–5947. https://doi.org/10.2174/1381612822666160715125417

Zhou, W., Zhu, P., Wang, J., Pascual, G., Ohgi, K. A., Lozach, J., Glass, C. K., & Rosenfeld, M. G. (2008). Histone H2A Monoubiquitination Represses Transcription by Inhibiting RNA Polymerase II

Transcriptional Elongation. *Molecular Cell*, *29*(1), 69–80. https://doi.org/10.1016/j.molcel.2007.11.002

Zhu, J., Leith, E. M., O'Donnell, E. N., Manzano, B. P., Wu, S.-Y., Chiang, C.-M., Armache, J.-P., & Tan, S. (2025). BRD4 binds the nucleosome via both histone and DNA interactions. *bioRxiv: The Preprint Server for Biology*, 2025.05.29.656846. https://doi.org/10.1101/2025.05.29.656846

Żukowska, A., & Perła-Kaján, J. (2024). Linker histones H1 in human disease. *Postępy Biochemii*, *70*(3), 336–347. https://doi.org/10.18388/pb.2021_561

Abstract

Sporulation in *Saccharomyces cerevisiae* is accompanied by profound nuclear remodeling and extensive transcriptional reprogramming, providing a powerful model to study how chromatin state supports cellular differentiation. In this work, we show that spore formation is associated with reduced nuclear volume, strong DNA compaction, and a striking redistribution of chromatin within the nucleus. Despite this highly compacted architecture, histone H4 acetylation persists in spores and exhibits a heterogeneous nuclear pattern, suggesting that this mark may have non-canonical functions during differentiation.

To uncover new functions of bromodomains, with a particular focus on BET readers across species, we took advantage of the highly demanding sporulation process. We unraveled that, although yeast and human BET bromodomains are structurally conserved, they are not functionally interchangeable. Replacing the yeast bromodomains with their human counterparts BRD4 and BRDT alters chromatin-binding dynamics and causes defects in mating, DNA damage response, and sporulation, while largely preserving vegetative growth. These phenotypes indicate that BET bromodomain function becomes especially important in contexts requiring extensive cellular reprogramming.

Transcriptomic analyses further show that BET bromodomains are required for timely execution of the meiotic transcriptional program. Particularly, strains carrying BRDT bromodomains display a pronounced delay in transcriptional reprogramming during sporulation, affecting both global expression trajectories and key regulatory pathways. In parallel, we uncover a functional interplay between Bdf1 and its paralog Bdf2 in shaping chromatin acetylation. Loss of BDF2 leads to a marked spatial redistribution of H4 acetylation, and this effect depends strongly on the bromodomain composition of Bdf1. In spores, combining BDF2 deletion with bromodomain humanization produces highly abnormal chromatin profiles, consistent with severe disruption of chromatin architecture and loss of spore viability.

Finally, we identify an unexpected metabolic vulnerability of humanized strains during ethanol exposure. Whereas WT cells tolerate low ethanol levels, humanized strains, especially those expressing BRD4 bromodomains, fail to sustain sporulation under these conditions. Because ethanol metabolism affects acetyl-CoA availability and redox balance, these findings suggest that bromodomains help maintain the coupling between metabolic state and chromatin regulation during differentiation.

Together, these results establish BET bromodomains as central regulators of chromatin organization, transcriptional dynamics, and metabolic adaptation during yeast sporulation. They also demonstrate that human bromodomains cannot fully replace their yeast counterparts, revealing species-specific differences in the *in vivo* interpretation of acetylated chromatin.

Résumé

La sporulation chez *Saccharomyces cerevisiae* s'accompagne d'un remodelage nucléaire profond et d'une reprogrammation transcriptionnelle massive, ce qui en fait un modèle puissant pour étudier la manière dont l'état de la chromatine régule la différenciation cellulaire. Dans ce travail, nous montrons que la formation des spores est associée à une diminution du volume nucléaire, à une forte compaction de l'ADN et à une redistribution marquée de la chromatine au sein du noyau. Malgré cette architecture fortement compactée, l'acétylation de l'histone H4 persiste dans les spores et présente un profil nucléaire hétérogène, suggérant que cette marque pourrait exercer des fonctions non canoniques au cours de la différenciation.

Pour découvrir de nouvelles fonctions des bromodomaines, en particulier des lecteurs BET à travers les espèces, nous avons exploité le processus de sporulation, particulièrement exigeant. Nos travaux ont démontré que bien que les bromodomaines BET de la levure et de l'humain soient structurellement conservés, ils ne sont pas fonctionnellement interchangeables. Le remplacement des bromodomaines de levure par leurs homologues humains BRD4 et BRDT modifie la dynamique de liaison à la chromatine et entraîne des défauts de croisement, de réponse aux dommages de l'ADN et de sporulation, tout en préservant largement la croissance végétative. Ces phénotypes indiquent que la fonction des bromodomaines devient particulièrement importante dans les contextes nécessitant une reprogrammation cellulaire accrue.

Les analyses transcriptomiques indiquent que les bromodomaines BET sont indispensables à l'établissement correct du programme transcriptionnel méiotique. En particulier, les souches portant les bromodomaines BRDT présentent un retard marqué dans la reprogrammation transcriptionnelle au cours de la sporulation, affectant à la fois les trajectoires d'expression globales et des voies régulatrices clés. Parallèlement, nous avons mis en évidence une interaction fonctionnelle entre Bdf1 et son paralogue Bdf2 dans l'organisation de l'acétylation de la chromatine. En conséquence, la perte de BDF2 entraîne une redistribution spatiale nette de l'acétylation de H4, et cet effet dépend fortement de la composition en bromodomaines de Bdf1. Dans les spores, la combinaison de la délétion de BDF2 et de l'humanisation des bromodomaines BET produit des profils de chromatine fortement aberrants, compatibles avec une perturbation sévère de l'architecture chromatinienne et une perte de viabilité des spores.

Enfin, nous identifions une vulnérabilité métabolique inattendue des souches humanisées lors de l'exposition à l'éthanol. Tandis que les cellules de type sauvage tolèrent des concentrations faibles d'éthanol, les souches humanisées, en particulier celles exprimant les bromodomaines BRD4, ne parviennent pas à maintenir la sporulation dans ces conditions. Comme le métabolisme de l'éthanol influence la disponibilité en acétyl-CoA et l'équilibre rédox, ces résultats suggèrent que les bromodomaines contribuent à maintenir le couplage entre l'état métabolique et la régulation de la chromatine au cours de la différenciation.

L'ensemble de ces résultats établit les bromodomaines BET comme des régulateurs centraux de l'organisation de la chromatine, de la dynamique transcriptionnelle et de l'adaptation métabolique au cours de la sporulation chez la levure. Ils montrent également que les bromodomaines humains ne peuvent pas entièrement remplacer leurs homologues de levure, révélant ainsi des différences spécifiques à l'espèce dans l'interprétation *in vivo* de la chromatine acétylée.